DOCTORAL THESIS

Stabilization-Solidification of High Water Content Dredged Sediments

Strength, Compressibility and Durability Evaluations

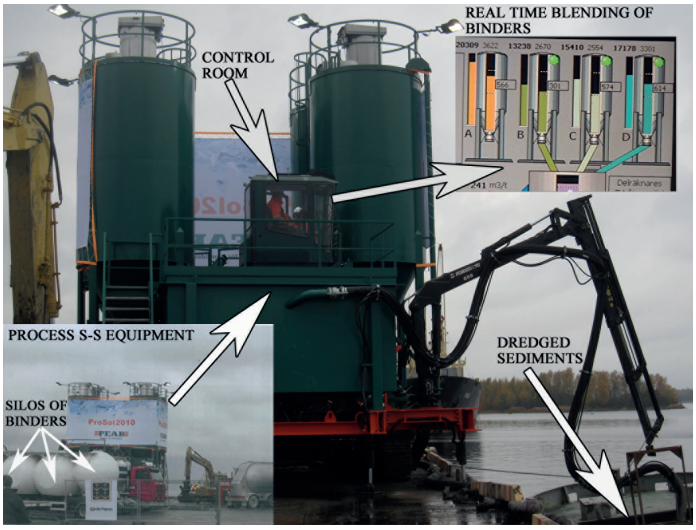

Gregory Paul Makusa

LULEÅ UNIVERSITY OF TECHNOLOGY

LULEÅ
UNIVERSITY
OF TECHNOLOGY

Stabilization-Solidification of High Water Content Dredged Sediments

Strength, Compressibility and Durability Evaluations

Gregory Paul Makusa

Submitted in Partial Fulfillment of the Requirements for the Degree of
Doctor of Philosophy in Geotechnical Engineering

Division of Mining and Geotechnical Engineering
Department of Civil, Environmental and Natural Resources Engineering
Luleå University of Technology
Luleå, Sweden

Cover Picture: *Process Stabilization-Solidification of Dredged Sediments for Structural Backfill at a Large–Scale Field Test, Port of Gävle, Sweden.*

Printed by Luleå University of Technology, Graphic Production 2015

ISSN 1402-1544
ISBN 978-91-7583-437-5 (print)
ISBN 978-91-7583-438-2 (pdf)

Luleå 2015

www.ltu.se

To my children:
Jessica and Lisa

"For soils stabilized with lime or cement, it is still not possible to predict the strength of in-situ mixed soil with a reasonable level of accuracy. As a consequence of this fundamental deficiency, which we are challenged to overcome, it is believed that the development of shallow mixing will be continued along a somewhat erratic experimental path, and will be to a large extent dependent on accumulated experiences." M. Topolnicki (2004)

Preface

Sustainable Management of Contaminated Sediments (SMOCS) project was funded by the EU within the Baltic Sea regional program for the period 2007–2013. The project strived to establish guidelines for beneficial reuse of dredged sediments. SMOCS in collaboration with Port of Gävle in Sweden identified stabilization-solidification technology as potential treatment method for handling both clean and contaminated high water content dredged sediments.

Process stabilization–solidification is an emerging technology for blending high water content dredged sediments with binder. Stabilized dredged material can have improved strength and reduced compressibility while encapsulating the contaminants to be less mobile. These properties can make the stabilized dredged material suitable for use in engineering applications.

Acceptance of new materials technology requires justifications with regard to short and long term field performance. Thus, understanding the mechanical properties (e.g. strength and compressibility) and durability of stabilized dredged sediments has become important. Therefore, the focus of this doctoral thesis was to evaluate strength, compressibility and durability of high water content stabilized dredged material.

Acknowledgements

Many people and organizations have contributed to the accomplishment of this work. First of all, I am obliged to thank SMOCS project for financial support along with the Port of Gävle in collaboration with Luleå University of Technology and Swedish Geotechnical Institute (SGI). The University of Dar es Salaam in Tanzania is hereby appreciated for extended study leave.

In geotechnical engineering perspective, this work would not be appreciable without help of my supervisors and fellow researchers. I would therefore, like to recognize and acknowledge Prof. Sven Knutsson, who was not only my main supervisor, but also my role model and father figure who sees and gives best things to his children. You gave me an opportunity to learn and acquire this knowledge. However, as the saying goes *"Excellence is not a skill but an attitude."* This work was done persistently with a lot of love. Assistant supervisor Dr. Hans Mattsson is hereby accredited for his useful discussions and challenges, which helped me to grow both professionally and personally. Dr. Josef Mácsik and Mr. Göran Holm are hereby appreciated for their contributions to my work. Fellow researchers, Sabrina Bradshaw, Erin Berns, and supervisor Prof. Craig Benson are hereby acknowledged for rewarding summer school at the University of Wisconsin-Madison, USA. Dr. Peter Robertson at Greggdrilling, New Port Beach, California, USA is hereby recognized for his expertise on cone penetration test and interpretations.

I would also like to thank individual persons within various organizations who have directly contributed to this work. Mr. Jonas Rahm and Ms. Linda Astner (Port of Gävle); Mr. Göran Holm and Tekn. Lic. Bo Svedberg (SMOCS); Mr. Per-Evert Bengstsson (SGI). Mr. Mats-Johan Rostman (FriGeo Company); Mr. Seth Mueller (Boliden Mineral AB). I would like to thank geotechnical senior researcher, Kerstin Pousette and laboratory technicians, Mr. Thomas Forsberg and Mr. Ulf Stenamn at Luleå University of Technology for useful skill and endless technical support. I would like to extend my appreciations to all my colleagues and staff members at the division of mining and geotechnical engineering and LTU at large for friendly support. In a special way, I would like to thank Mr. Pocorni, J. and Mwanga, A. for valuable comments and suggestions.

Special thanks remain to my beloved wife Agness Mgasa for moral support, an endless love and care throughout my studies. This journey would not be possible without the initiative of my late father Paul Fr. Makusa (1933-2010). Although we could not travel together to this end but, with a pride and moral support of my mother, sisters and brothers, I could still find courage to continue tirelessly.

Makusa, G.P.

November, 2015

Abstract

Dredging activities at ports and harbors are inevitable for safe navigation of ships and vessels. The outcomes of dredging are huge volumes of dredged materials, which can range from very fine and contaminated sediments to sands and gravels. The coarse sands and gravels can be directly used in civil engineering applications. The fine dredged sediments (DS) are usually associated with high water content, low shear strength, high compressibility and presence of contaminants. However, these unfavorable properties do not exclude the suitability of fined dredged sediments for use in geotechnical applications.

Stabilization-solidification technology provides a comprehensive treatment method for improving strength, reducing the compressibility and mobilizing the contaminants to be less mobile. These properties make the stabilized fine dredged material (SDM) suitable for use in civil engineering applications (e.g. road embankment or structural backfill in land reclamation). However, stabilization-solidification is not a magic wand by which every geotechnical property is improved for better. In cold region climates, repetitive freeze–thaw cycles have detrimental effects to the strength and hydraulic properties of the SDM. Consequently, the applications and long term performance of the SDM under repetitive freeze-thaw cycles are still uncertain.

Successful stabilization–solidification of the DS and the performance of the SDM depend on stabilization methods and materials. Process stabilization-solidification (PSS) is convenient technology for amending high water content DS with binders. The use of composite binders for stabilization–solidification of the DS is increasing due to increased artificial pozzolanas that can be used as supplementary cementitious materials (SCM). Primary binders such as cement can be supplemented with SCM (e.g. fly ash and ground granulated blast furnace slag). Cement hydration is a complex process with a complex series of unknown chemical reactions. The hydration of cement incorporating SCM is more complicated due to the co–existence of cement hydration and the pozzolanic reactions of the SCM. The fabric of dredged sediments formed under different physicochemical environments affects the reactivity of binders. The physicochemical interactions between binders and the DS that influences the strength, compressibility and durability of high water content stabilized dredged sediment are examined and presented in this thesis.

The findings of this study show that the use of fly ash (FA) and ground granulated blast furnace slag (GGBS) delays strength development of composite binder (CB)-treated DS. Irrespective of the amounts of CB, the improved strength depends on the amount of cement in the blend. The unconfined compressive strength increases with increasing the cement quantity.

Three phases of hydration mechanisms determine the compressibility behaviour of the SDM during curing. These are induction phase (IP), nucleation and crystallization phase (NCP), and hardening phase (HP). The IP occurs immediately after mixing. A protective layer is formed on the particle surface of binders, which prevent further penetration of water and then increases resistance to deformations. The evaluated tangent modulus increases to maximum value followed by abrupt drop to lower values at effective vertical stress, which is equals to preconsolidation stress. NCP follows when the protective layer changes to a more permeable membrane, which permits inward flow of water molecules, and outward migration of calcium ion and silicate ions. The tangent modulus of the SDM in NCP is small and increases linearly with effective vertical stress. The SDM in NCP is characterized by loss in apparent preconsolidation stress and tangent modulus. HP occurs as a result of increased thickness and stiffness of the protective layer. The compressibility of the SDM in HP is reduced significantly due to increased apparent preconsolidation pressure and tangent modulus. It is concluded that the maximum tangent modulus of untreated DS determines the maximum deformation of the SDM in all phases of hydration processes.

Healing of the damaged SDM due to repetitive freeze-thaw action depend on the type of binder. The inclusion of SCM on one hand increases the healing of the SDM with reduced strength. This occurs during thaw consolidation. On the other hand, inclusion of SCM causes increased HC of the SDM. Considering healing potential on the damaged SDM with reduced strength, increased hydraulic conductivity causes increased rate of dissipation of excess pore pressure, reduced undrained conditions, and improved strength (enhanced outcome). In order to maintain its strength and hydraulic conductivity, the SDM requires protection from severe damage of repetitive freeze–thaw cycles. It can be beneficial to place the SDM below frost depth or use protective cover of geosythetic clay liners (GCL).

Symbols and abbreviations

u_0	Hydrostatic pore water
ψ	Dilatancy angle
f_t	Corrected friction ratio
q_t	Corrected total cone resistance
c'	Effective cohesion
φ'	Effective friction angle
ν'	Effective Poisson's ratio
E'	Effective Young's modulus
B_q	Normalized pore pressure
δ_c	Settlement of compressible layer
G	Shear modulus
f_c	Sleeve friction
I_c	Soil behavior type index
q_c	Total cone resistance
ν_u	Undrained Poisson's ratio
s_u	Undrained shear strength
N_{kt}	Cone tip factor
$\Delta\sigma'$	Consolidation stress
M	Constrained modulus
α_m	Constrained modulus cone factor
σ'_{CPT}	CPT induced effective vertical stress
Δu_2	Excess pore pressure
σ'_{vf}	Final effective vertical stress
σ'_{vo}	Initial effective vertical stress
Q_{t1}	Normalized cone resistance for clay
F_R	Normalized friction ratio
E_{oed}	Oedometer modulus
σ'_c	Preconsolidation stress
σ_{vo}	Total initial vertical stress
E_u	Undrained Young's modulus
r_σ	Total stress reduction factor
$C_{c/r}$	Compression or recompression index
CPT	Cone Penetration Test
DFS	Dredged sediments
F-T	Freeze-thaw
GCL	Geosynthetic clay liner
HC	Hydraulic conductivity
HP	Hardening phase
IP	Induction phase
NCP	Nucleation and crystallization phase
PSS	Process stabilization solidification
s/c	Solid/cement ratio
SDM	Stabilized dredged material
SMOCS	Sustainable management of contaminated sediments
TC	Thaw consolidation
TW	Thaw weakening
UCS	Unconfined compressive strength
w/c	Water/cement ratio
wc	Water content

Terminologies

Term	*Description/Definition*
Beneficial use	Any use of dredged fine sediments other than merely disposal (PIANC, 2009).
Binder	Hydraulic or non-hydraulic materials that when in contact with water or in presence of pozzolanic minerals reacts with water to form cementitious composite materials (Sherwood, 1993).
Cation exchange capacity	A measure of net negative charge on the soil particle, resulting from isormophous substitution and broken bonds at the boundaries (Terzaghi et al., 1996; Mitchell and Soga, 2005).
Compressibility	Property of a soil pertaining to its susceptibility to decrease in volume when subjected to load (ASTM D 653).
Constitutive model	A mathematical description on how material responds to various loading.
Curing (cure)	The change in properties of stabilized material, which occur with time under favorable condition. Curing time is the period of time elapsed from subjecting the stabilized materials to curing conditions to the end of pozzolanic or hydration reactions (ASTM D 653).
Dredging	The art of removing underwater soils or sediments (dredged material) for the purpose of increasing or maintaining the depth, widening or cleaning the navigation channels.
Flocculants (flocs)	Loose, open-structured soil mass formed in a suspension by the aggregation of minute particles (ASTM D 653).
Freeze-thaw cycle	The completely freezing of a material followed by completely thawing of the same (ASTM D 653).
Grace period	A period of time allotted to a thawed soil sample before subjecting to subsequent freezing.
Hardening phase	Hydration stage of binder that occurs as a result of increased thickness and stiffness of protective layer, which glue soil particles together.
Hydration reaction	The process under which cement or pozzolanic reactions takes place.
Hydraulic conductivity	The volume of fluid passing through a unit cross-section in unit time under the action of a unit hydraulic potential gradient (ASTM D 653).
High water content dredged sediments	Dredged sediments with weight of water greater than weight of solids per given unit weight.
Induction phase	Hydration stage of binder which occur as a result of formation of protective layer on surface of binder, which delay fully hydration of binder.
Land reclamation	The art of obtaining dry land from the Sea or water bodies.

Term	*Description/Definition*
Lyotropic series	The arrangement of anions and cations according to their ability to modify the properties of other solutes (Cammack et al., 2006).
Mechanical properties	The properties of a material that reveal its elastic and inelastic behavior when subjected to load for mechanical applications. For example, modulus of elasticity or shear strength.
Nucleation and crystallization phase	Hydration stage of binder which occur as a result of change from impermeable to permeable protective layer, which cause fully hydration of binder and decreased plasticity of stabilized mass.
Pozzolanas	Natural (e.g. clay minerals) or artificial (e.g. ashes) siliceous and aluminous materials, which in itself possess little or no cementitious value, but will, in finely divided form and in the presence of moisture chemically react with calcium hydroxide at ordinarily temperature to form compound possessing cementious property (ASTM D 653).
Preconsolidation pressure	The greatest effective pressure to which the soil has been subjected. The maximum pressure that may be applied to the soil without causing large deformation (Crawford, 1986; Terzaghi et al., 1996).
Soil stabilization	Chemical or mechanical treatment designed to increase or maintain the stability of a mass of soil or otherwise to improve its engineering properties (ASTM D 653).
Solidification	Refers to the process that binds a contaminated media with reagents, changing its physical properties by increasing the compressive strength, decreasing its permeability and encapsulating the contaminants to form a solid material (USEPA, 1993).
Stabilization	Refers to the process, which involves chemical reactions that reduce the reachability of contaminants. The contaminants are chemically immobilized and its solubility is reduced, hence, the contaminants become less mobile (USEPA, 1993).
Stiffness	The ratio of change of force (or torque) to the corresponding change in translational (or rotational) deflection of an elastic element (ASTM D 653).
Strain	The change in length per unit length in a given direction.
Strength	The maximum stress, which a material (including soil mass) can resist without failure for any given type of loading (ASTM D 653).
Stress	The force per unit area acting within the body (including soil mass).
Sediments	Fragmented materials that originate from weathering and erosion of rocks or unconsolidated deposits and are transported by, suspended in, or deposited by water (USEPA, 1993).

Term	*Description/Definition*
Tangent modulus	Slope of the tangent to the stress-strain curve at a given stress value. Generally, it is taken at a stress equal to half the compressive strength (ASTM D 653).
Thaw consolidation	Refers to the process by which the density increases due to the escape of water under the weight of soil itself or an applied load (ASTM D7099).
Thaw weakening	Refers to a reduction in shear strength due to the decrease in effective stress (ASTM D7099).
Void ratio	The ratio of volume of voids to the volume of solids (Terzaghi et al., 1996).

Table of contents

PART II..... Appended papers and co-authorship

This work was carried out by Gregory Makusa under main supervision of Prof. Sven Knutsson. Bradshaw, S. and Bern, E. carried out cation exchange capacity experiment, analysis and interpretations of test result. All other laboratory experiments works, evaluations and interpretations of test results were conducted by Gregory Makusa. The featured coauthors assisted in preparation of final papers. The findings, and conclusions expressed in these papers are those of the authors and do not necessarily represent the view of SMOCS or Luleå University of technology.

Paper I

Makusa, G.P., Mácsik, J., Holm, G., and Knusson, S. (Submitted). Process stabilization-solidification and physicochemical factors influencing strength development of treated dredged sediments (Submitted: *Geo-Chicago 2016: Sustainability, Energy and Geoenviroment conference*)

Paper II

Makusa, G.P. and Knusson, S. (Submitted). Influence of hydration phases on compressibility behaviour of high water content stabilized dredged sediments: an oedometer test study (Submitted to Canadian Geotechnical Journal).

Paper III

Makusa, G.P., Mácsik, J., Holm, G., and Knusson, S. A laboratory test study on effect of freeze–thaw cycles on strength and hydraulic conductivity of stabilized dredged sediments (Submitted: *Canadian Geotechnical Journal*)

Paper IV

Makusa, G.P., Mattsson, H., and Knusson, S. (2013). Investigation of increased hydraulic conductivity of silty till subjected to freeze–thaw cycles. *ASTM International: Selected technical paper STP 1568, Mechanical Properties of frozen soils*.

Paper V

Makusa, G.P., Bradshaw, S., Bern, E., Benson, C.H., and Knusson, S. (2014). Freeze-thaw cycling concurrent with cation exchange and the hydraulic conductivity of geosynthetic clay liners. *Canadian Geotechnical Journal.*

Paper VI

Makusa, G.P., Mattsson, H., and Knusson, S. (2012). Verification of field settlement of in-situ stabilized dredged sediments using CPT data. *Electronic Journal of Geotechnical Engineering.*

Paper VII

Makusa, G.P., Mattsson, H., and Knusson, S. (2014). Shear strength evaluation of preloaded stabilized dredged sediments using CPT. *3rd International symposium on cone penetration testing, Las Vegas, Nevada, USA-2014*.

PART I *Thesis*

1. Introduction

Dredging is the art of removing underwater sediments and debris for the purpose of widening, maintaining or increasing the depth of navigational channels or waterways. Thus, dredging activities at ports, harbors and navigational channels are inevitable for safe navigations of ships and vessels. Dredged sediments may range from clean gravels and sands to clean or contaminated fine sediments. While gravels and sands can directly be utilized as construction materials, contaminated fine sediments may pose high risks to human health and the environment. In Sweden, sea disposal of dredged sediments is banned; high taxes associated with land disposal, scarcity of landfill and constant demand for dredging have given rise to the need for finding beneficial use of fine and contaminated dredged sediments.

The Sustainable Management of Contaminated Sediments (SMOCS) project was funded by the EU within the Baltic Sea regional program for the period 2007–2013. The project established a guideline for beneficial use of contaminated fine dredged sediments. SMOCS in collaboration with Port of Gävle in Sweden identified stabilization–solidification technology as potential method for amending and improving the geoenvironmental properties of the fine dredged sediments for civil engineering applications such as road embankments and structural backfill. However, the geotechnical design process, which includes evaluations of mechanical properties, loading conditions and constitutive model of stabilized dredged material (SDM) can be uncertain (Makusa 2013b).

Stiffness and strength properties which are obtained from laboratory tests results are utilized to predict in–situ performance of the SDM (EuroSoilStab, 2002). Oedometer and unconfined compression tests are the most utilized laboratory tests for evaluation of deformation and strength properties of soils, respectively. These tests have remained popular because of their simplicity in obtaining data for evaluation of stiffness and strength parameters for use in design analysis. For instance, by interpreting the stress-strain curves from oedometer test, compressibility parameters such as preconsolidation pressure and tangent modulus can be obtained. According to Grozic et al. (2003), the preconsolidation stress (σ_c') interpreted from oedometer tests provide important information on the stress history of the soil, which in turn can be correlated to many behavioural properties. However, the apparent preconsolidation pressure for stabilized soils is brought by cementation action. The cementation process and consolidation stress applied during curing greatly affect the apparent preconsolidation stress. This pressure is strongly linked to the strength of the stabilized mass and has considerable influence on its deformation behaviour Åhnberg (2007).

Bemben (1986) suggested that for cemented soils, the relevant apparent preconsolidation stress is the only stress existing at the time of cementation.

Laboratory properties evaluated on the SDM may differ significantly from those attained during the in-situ stabilization (Makusa, 2013b; Forsman et al., 2008; Andersson et al., 2000; Jelisic and Leppänen, 1999). Several factors may contribute to these discrepancies. Some of which occur as a result of physicochemical interactions between binders and stabilized materials. Other factors are due to laboratory sample preparations and curing conditions, evaluations and interpretations of test results. It is important that appropriate in–situ stiffness and strength parameters be utilized in a suitable constitutive model during design and analysis to predict the long term performance of geotechnical structures found in the SDM.

Cone penetration test (CPT) is one of the most used in-situ tests for the determination of in-situ soil stratigraphy, identification of soil behaviour type and evaluation of in-situ mechanical properties. According to EuroSoilStab (2002), common CPT is very suitable for testing stabilized mass if the undrained shear strength is between 50 kPa and 1000 kPa. Seemingly, there are no observed CPT correlations proposed specifically for evaluation of mechanical properties of the SDM. Consequently, CPT empirical relationships that were developed for use in typical soils are utilized for evaluation of stiffness and strength parameters of the SDM.

Generally, stabilization-solidification is not a magic wand by which every geotechnical properties can be improved for better (Ingles and Metcafe, 1972). Literature has shown that in cold regions climate, repetitive freeze–thaw cycles have detrimental effect on strength and hydraulic properties of the SDM. Frozen moisture in stabilized mass generates expansive forces, which causes (i) the stabilized mass to increase in volume and (ii) formation of cracks and micro-cracks. While the former is reported to cause permanent loss of strength due to some bond breakage (Maher et al., 2006), the later may cause increased hydraulic conductivity due to increasing hydraulic paths. However, the healing potential of the SDM with damaged mechanical properties due to repetitive freeze-thaw is unclear under current assessments of the impact of freeze-thaw cycling.

Acceptance of new materials technology requires justifications with regard to short and long term field performance. The majority of researches on mechanical properties of the SDM have been carried out on compacted stabilized soils with low water content. Little information is available regarding the strength, compressibility and durability of uncompacted high water content stabilized dredged sediment, which are utilized in structural backfill in cold region climates. In this study, high water content dredged sediment is defined as sediments with the amount of water greater than the amount of solids. Based on the laboratory and field test study, the present thesis examines

physicochemical factors influencing strength development, compressibility properties, hydraulic conductivity and resistance of the high water content SDM to repetitive freeze–thaw cycles.

1.1 Problem statement and research questions

Laboratory tests studies on the possibility to improve the mechanical properties of high water content dredged sediments (DS) were carried out by Fossenstrand (2009) and Lagerlund (2010a, 2010b). Lagerlund (2010b) utilized typical dredged sediments from the Port of Gävle with average water content of 450%. Byggcement (BC), Bio fly ash (BFA) and ground granulated blast furnace slag (GGBS) were used. The BFA and GGBS were obtained from Vattenfall power plant and Merox AB, respectively. BFA and GGBS were utilized as supplementary cementing material (Holm et al., 2012). Treatability study was carried out using different recipes with different amount of composite (ternary) binder. The desired unconfined compressive strength (UCS) and hydraulic conductivity (HC) were 140 kPa and 10^{-9} m/s, respectively after 91 days of curing. A design recipe comprised of BC/BFA/GGBS at ratio of 40%/40%/20%, respectively by total weight of binder. It was concluded that a binder dosage of 150 kg/m^3 of the DS would meet the desired UCS and HC values. The design recipe and amount of binder were selected based on cost analysis. The minimum undrained shear strength of 70 kPa (i.e. UCS of 140 kPa) was considered to be sufficient for most of the Port of Gävle activities at Granudden terminal. The targeted maximum hydraulic conductivity of 10^{-9} m/s was desired for waste containments. Stabilized dredged materials (SDM) were utilized as structural backfill during port expansion. Cone penetration test (CPT) was utilized for quality assurance, determination of geotechnical properties and classification of soil behaviour. Results from the large-scale field test indicated excessive deformation of the SDM under preloading weight. The evaluated shear strength values were below expected values. The measured field settlement of the SDM under applied preloading weight varied from 0.2 m to 1.20 m. The average undrained shear strength of 50 kPa (equivalent to the average UCS value of 100 kPa) was measured after 250 days of curing. Thus, the predicted UCS value could not be achieved. Consequently, the following research questions were raised:

- What factors contributed to the differences between the anticipated and achieved UCS values or observed variations of field settlement?
- In absence of CPT empirical correlations established for use in stabilized mass, what are the limitations of using conventional CPT empirical correlations in the stabilized dredged material?

1.2 Objectives of the research work

The primary objectives of the present thesis work were to:

1. Verify strength and compressibility behaviour at the large-field test.
2. Exemplify factors that contributed to the achieved strength and observed settlement at the large-scale field test.

In order to fulfill these objectives, the following specific tasks were carried out:

i. laboratory investigations on how:
   - physicochemical interactions between binders and high water content dredged sediments affect strength development and compressibility behaviour of the SDM during curing.
   - the effect of freeze–thaw cycles on durability of the SDM.

ii. To demonstrate the validity and limitations in using conventional CPT empirical correlations for evaluations of geotechnical properties of the SDM.

1.3 Scope of the research work

The findings of the present study are limited to the following methods and materials:

- ***Stabilization methods***: process stabilization-solidification.
- ***Dredged Materials***: high initial water content dredged sediments (DS), which was defined as follows: for a given unit weight of the DS, the weight of water is greater than the weight of solids.
- ***Binders:*** Byggcement, fly ash and ground granulated blast furnace slag.
- ***Tests methods***: In-situ tests using cone penetration test. Laboratory test using oedometer test, unconfined compression tests, and hydraulic conductivity test.

1.4 Layout of the thesis

This thesis is divided into two parts, *part I* and *part II*. Part I of the thesis consists of the introduction, stabilization-solidification, geotechnical properties and durability evaluations, conclusions and ideas for future work. Part II consists of seven appended papers. Part I can be viewed as a synthesis of the appended papers in part II.

2. **Stabilization-solidification**

USEPA (1993) describes stabilization solidification (SS) technology as a combination of two distinct technologies, namely; stabilization and solidification. *Stabilization* refers to the process, which involves chemical reactions that reduces leachability of contaminants. Chemically the contaminants are immobilized and its solubility and mobility reduced. *Solidification* refers to the process that binds contaminated media with reagent. Stabilization-solidification results in improved compressive strength, reduced compressibility and permeability. In geotechnical perspective, the improved physical properties can allow the structure to be found on shallow footing without soil replacement or deep foundation (Garbin et al., 2011; Maher et al., 2004; Holm et al., 2005).

Application of stabilization–solidification technology for soil improvement is a site-specific technique. There are no general rules for mix designs to achieve a certain strength, stiffness, hydraulic conductivity and durability. However, the aforementioned mechanical properties are the governing criteria used to characterize the mix design for treatment of variety of weak soils and sediments (Ingles and Metcalf, 1972; Al-Tabbaa and Evans, 1998; Topolnicki, 2004; Rekik and Boutouil, 2009).

The purpose of in-situ soil stabilization-solidification for geotechnical application is to produce the stabilized soil mass that can interact with native soil. The objective is not to produce too stiffly stabilized soil mass (like a rigid pile wall), which may independently carry out the design load (EuroSoilStab 2002). If the stabilized soil will behave like a rigid body in relation to the surrounding soil, its external stability can be evaluated under failure mode similar to gravity structures such as sliding, overturning and bearing capacity (Topolnicki, 2004). Åhnberg (2007) and Yu et al. (1997) showed that failure features of soil–cement under triaxial tests are different from those under unconfined condition. The confining stress highly contributes to increased axial stress at failure resulting into plastic shear failure mode. As confining pressure increases the stress–strain of cement-treated soil increases, while initial stiffness modulus shows small changes. The stress–strain relations changes from strain–softening to strain–hardening and volumetric strain change from dilation to contraction. On the other hand, soil–cement sample under unconfined condition experiences brittle failure such as crushing (Yu et al., 1997). Yu et al. concluded that it might be suitable to describe the strength of stabilized soil mass with Mohr–Coulomb (MC) failure criteria. The Mohr failure is concerned with stress conditions on potential rupture planes within the geomaterial. The MC criterion states that failure of a soil mass will occur if the induced stress exceeds the available strength. Consequently, literature (Topolnicki, 2004; EuroSoilStab, 2002) has

shown that any safe designs will require that the stresses inside the stabilized soil body do not exceed the capacity of soil–binder material.

The improved strength and reduced compressibility of stabilized dredged material (SDM) become important in the search of good proportions and mix ingredient of binders. The achieved geotechnical properties and durability of the SDM depend on stabilization methods and materials (Makusa, 2013a).

2.1 Stabilization methods

Dredged sediments and soft soils at high initial water contents can be treated with binder by either mass stabilization–solidification (MSS) or process stabilization–solidification (PSS). These techniques offer a cost–effective solution for ground improvement. However, the achieved geotechnical properties under these two methods can vary significantly.

2.1.1 Mass stabilization-solidification

Mass stabilization solidification refers to soil improvement technology, in which the entire volume of soft soil or sediments can be stabilized and solidified to a prescribed depth. The technique offers a cost–effective solution for ground improvement work, and is highly suited for treatment of high water content brownfield, soft clays, peat, organic soils and waste sludge in a confined disposal facility as shown in Fig. 2.1 (Topolnicki, 2004; EuroSoilStab, 2002; Garbin et al., 2011; Pousette et al., 1999). The blending of the soil mass may be achieved by either use of excavator mounted mixing tool with unique shuttles pneumatically delivering the binder to the head of the mixing tool and into the mix zone or by self-injection of binder into a rotating auger or mixing head and the soil (Fig. 2.1). The mixer rotates and simultaneously moves vertically and horizontally while mixing the soil block with selected binder. The diameter of mixing tool normally lies between 600 mm to 800 mm, with rotation speed between 80 and 100 rpm. Usually, the soil is stabilized in a sequence of a block, which is defined as the operating range of the machine. The typical range is 8–10 m^2 in plan and 1.5 to 3 m in depth (i.e. 2 m wide x 5 m long x 3 m deep) with production rate between 200 and 300 m^3 of stabilized soft soil per shift. The amount of binder is in a typical range of 100–400 kg/m^3 and the minimum targeted shear strength is 50 kPa (Massarsch and Topolnicki, 2005; EuroSoilStab, 2002). Thus, the outcome of mass stabilization solidification will mainly depend on the workmanship. Prior to the initial set of the stabilized mass, a geo–membrane separator is placed on top of stabilized soil on which a selected preloading weight is placed as shown in Fig. 2.1b.

Fig. 2.1: Mass stabilization solidification at (a) Fort Point Channel in Boston, USA: excavator mounted on a special floater, which is dragged horizontally by winches (Topolnicki, 2004). (b) Vuosaari Harbor in Finland (Photo: courtesy of ALLU).

Based on literature (Garbin et al., 2011; Åhnberg et al., 2001; EuroSoilStab, 2002), the primary purposes of the preloading weight is to serve as a working platform, while compressing the stabilized volume. This helps to remove air entrapped during mixing and bring soil particles close together for effective hydration. The secondary aim of preloading weight is to consolidate the stabilized mass for higher load than self-weight.

2.1.2 Process stabilization-solidification

Process stabilization–solidification (PSS) is an emerging technology for blending high water content dredged sediments (DS) with binder. The PSS equipment comprises of a chassis that carries pugmills and silos of up to four binders. Primary binders such as cement (C) can be blended with supplementary cementitious materials (SCM) such as fly ash (FA) and granulated blast furnace slag (GGBS). The mixing process is controlled from a control room. The proportionality of the amounts of selected binder and the DS are regulated and checked while maneuvering the position of the pumps that transports the DS from the barge to the pugmill. The mixture is finally discharged at their final destination by using discharge tube connected to the pugmill. The stabilized material is finally preloaded and left to cure. ProSol2010 (Fig. 2.2) is an example of PSS equipment that was developed by PEAB, a Swedish construction company. It is environmentally friendly, quiet and dustless equipment which can mix more than 300 m^3 of sediments per hour (Holm et al., 2012). The PSS method utilizes constant amount of binder at varying initial water content of the dredged materials. Thus, the geotechnical properties under PSS technology will depend on uniformity of water content of the dredged sediments, which depends on the dredging methods.

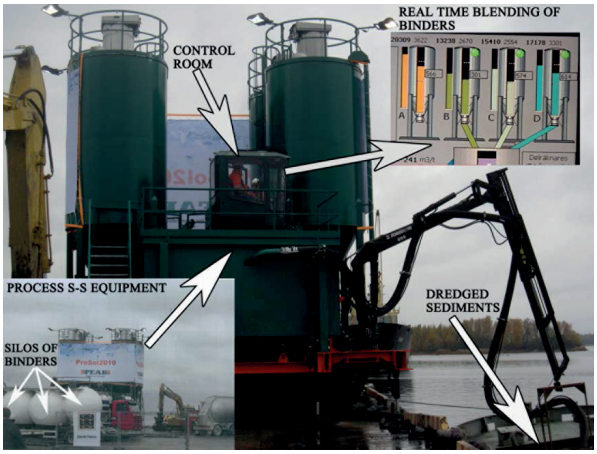

Fig. 2.2. Process stabilization-solidification of high water content dredged sediments at Port of Gävle, Sweden (Photo: Courtesy of Port of Gävle, Sweden; ALLU, Finland).

2.2 Stabilization materials

Most of stabilization–solidification work has to be undertaken in a variety of weak soils and sediments with moderate to high initial water content (e.g. silty, clayey, peat or organic soils, and dredged fine sediments) using either single or composite binder.

2.2.1 Soils and sediments

Fine–grained granular materials are the easiest to stabilize due to their large surface area in relation to their particle diameters. For instance, clay soils compared to others has a large surface area due to flat and elongated particle shapes. On the other hand, silty materials can be sensitive to small change in moisture and, therefore, may prove difficult during stabilization-solidification (Sherwood, 1993). Peat soils and organic soils are rich in water content of up to 2000% (Pousette et al., 1999). These soils are characterized by high porosity and organic content. The consistency of peat soil can vary from muddy to fibrous. In most cases, the deposit is shallow but in worst cases, it can extend to several meters below the surface (Pousette et al., 1999; Cortellazzo and Cola, 1999; Åhnberg and Holm, 1999). Organic soils have high cation exchange capacity. These soils can hinder the hydration process by retaining the calcium ions liberated during the hydration of calcium silicate and calcium aluminate in the cement to satisfy the exchange capacity. In such soils, successful stabilization–solidification has to depend on the proper selection of binder and amounts of binder (Hebib and Farrell, 1999; Lahtinen and Jyrävä, 1999, Åhnberg et al, 2003).

2.2.2 Binders

Binders are hydraulic (primary binders) or non–hydraulic (secondary binders) materials that when in contact with water or in the presence of pozzolanic materials reacts with water to form cementitious composite materials. Primary binders can be utilized alone to bring the required effect, whereas secondary binder may require an activator to initiate their latent hydraulic behaviour. Cement and lime are generally considered as primary binder while, natural and artificial pozzolanas materials are secondary binders.

2.2.2.1 Cement

Cement is a well-known primary binder existing in different form depending on percentage mineral constituents. The major phases of modern cement typically consists of an alite (C_3S), belite (C_2S), aluminate (C_3A) and Ferrite (C_4AF) (Taylor, 1997; Lee et al., 2013). Taylor (1997) described each phase and its influence on strength development as follows: Alite is the major constituent of normal Portland cement (PC) clinker. It reacts relatively quickly with water, and is the most important PC constituent phase for strength development at ages up to 28 days. Belite reacts slowly with water, thus contributing little to the strength during the first 28 days. However, belite contributes substantially to further increase in strength that occurs at later ages. Generally, under comparable conditions, by one year, the strengths obtained from pure alite and pure belite is about the same. Aluminate reacts rapidly with water, and may cause undesirable rapid setting. A reaction of ferrite with water appears to be somewhat variable, but generally is high initially and low or very low at later ages.

The reaction of cement with water forms various hydrates. Calcium hydroxide (CH) and calcium silicate hydrate (CSH) or calcium aluminate hydrate (CAH) are the end products of cement hydration. In presence of calcium and alkaline condition, silica and alumina are the main elements required for formation of the CSH and CAH, respectively. The main principal binding phases in all calcium silicate and aluminate–based pastes are the CSH and CAH gels, respectively (Richardson and Grove, 1997; Taylor, 1997; Kamon and Nontanandh, 1991; Chrysochoous et al., 2010). Reaction of CH describes an increase in strength produced by cation exchange capacity rather than by cementing effect brought by pozzolanic reaction (Sherwood, 1993).

2.2.2.2 Pozzolanas

ASTM C595 defines pozzolanas as siliceous and aluminous materials, which in itself possess little or no cementitious values. However, in finely divided form and in the presence of moisture it reacts with an activator such as calcium hydroxide (CH) at ordinary temperature to form compounds

possessing cementitious properties. Clay minerals such as kaolinite, smectite, illite and mica are pozzolanic in nature whereas, ashes are artificial pozzolanas materials. On the other hand, blast furnace slag has chemical composition similar to that of Portland cement. It is, however, not cementitious by itself, but it possesses latent hydraulic properties which can develop in cementitious product when dissolved in an activator.

2.2.2.3 Composite binder

The use of composite binders for stabilization–solidification of the dredged sediments (DS) is increasing due to increased artificial pozzolanas materials that can be utilized as supplementary cementing materials (SCM). Primary binders such as cement can be partially supplemented with pozzolanas materials such as fly ash (FA) and granulated blast furnace slag (GGBS). Cement hydration is a complex process with a complex series of not well known chemical reactions (Taylor, 1997). The hydration of cement incorporating supplementary cementitious material is even more complicated due to the co–existence of cement hydration and the pozzolanic reactions of mineral admixtures (Wang and Lee, 2009). Richardson and Groves (1997) observed that regardless of composition of GGBS or FA, the main hydration products and principal binding phases in all calcium silicate–based pastes are the CSH gels. Thus, other mechanical properties of the stabilized dredged sediments become important in the search of good proportions and mix ingredient (e.g. inclusion of SCM), which will ensure other desired engineering properties are achieved without compromising the required strength of the stabilized dredged material (SDM).

2.3 Geotechnical parameters

In classical theory of soil mechanics, lays simple elastic and rigid plastic models that lead to concentration of site investigation efforts on seeking the strength and the stiffness of the soil (Muir Wood, 1990; Atkinson, 2007). Like in conventional soils, the geotechnical parameters assessed on stabilized weak soils and sediments for design purposes include strength, stiffness, and durability.

2.3.1 Strength

The unconfined compressive strength (UCS) is the key parameter for the current design practice. The UCS is used to estimate the undrained shear strength of stabilized soil (Åhnberg, 2006; Åhnberg, 2007). The undrained shear strength is considered to be equal to half the UCS values. Thus, it is common practice that advance tests be conducted in the laboratory to obtain adequate data concerning the UCS values of the stabilized dredged materials before a full scale project can take over (EuroSoilStab, 2002).

Significant discrepancies have been reported between laboratory and in–situ achieved strength values. Jelisic and Leppänen (1999) reported laboratory shear strength between 30 kPa and 140 kPa. Contrary, the field shear strength measured by cone penetration test (CPT) indicated values between 5 kPa and 60 kPa. Table 2.1 presents other similar projects showing the discrepancies between predicted and achieved field strength values. There can be several factors contributing to the differences between laboratory and field strength values. The most probable causes are physicochemical interactions associated with binders and stabilized materials.

The fabric of soft sediments formed under different physicochemical environments is strongly dependent on the clay mineralogy. The volume change undergone by kaolinitic soils during settling and sediment formation is controlled by shearing resistance at the particle level. The volume change for montmorillonitic/smectitic soils is governed by the diffuse double layer repulsion. Therefore, any factor contributing to increased attractive force and reduction in repulsive force will accelerate the formation of flocculants fabric (i.e. higher sediment volume and void ratio) for case of kaolinitic soils. Likewise, any factor causing decreased attractive forces and increased repulsive forces will end up increasing sediment volume of montmorillonitic soils (Sridharan and Prakash 1999).

The effect of binder(s) on strength development may depend on the main hydration products, cation exchange, and principal binding phases. Rajasekaran and Rao (2002) observed that addition supply and higher adsorption of divalent ions (e.g. calcium Ca^{2+}) by the soil particles as a result of cation exchange phenomena improves the shear strength of fine particles compared to addition supply of monovalent ions (e.g. sodium ion, Na^{+}). Quang and Chai (2015) observed that increased concentrations of Ca^{2+} result in a thinner diffusive double layer and vice versa. Thinner diffuse double layer can be associated with improved strength due to increased shearing resistance.

Table 2.1: Some of evaluated shear strength values from laboratory tests results relative to the achieved in-situ values.

Case study	**Target (kPa)**	**Measured (CPT) (kPa)**	**CP (days, d)**	**Soil**	**Source**
Veittostensuo, Finland	50	40–150	30	Peat	Jelisic and Leppänen (1999)
Sundsvägen-Råneå (road no. 601), Sweden	50	40–185	30	Peat	Jelisic and Leppänen (1999)
Enånger trial embankment, Sweden	200	5–60	90	gyttja	Jelisic and Leppänen (1999)
Road 255 Sodertalje, Sweden	50	50	28	Peat/gyttja	Topolnicki (2004)
Florida School for the Deaf and Blind (FSDB), USA	105	200 1300	14 28	Organic clay	Garbin et al. (2011)
Port of Hamina, Finland	-	30–120	30	DS	Andersson et al. (2000)
Park at Sörnäinen, Finland	30	120	28	DS	Forsman et al. (2008)

2.3.2 Compressibility

Compressibility of soil mass can be explained as the change in volume due to the change in effective stress. This phenomenon depends on the extent to which the soil structure impedes the movement of the pore fluid. In untreated soft soils, when the consolidation pressure increment is applied, the consolidating layer is compressed and excess pore water pressure is dissipated. During consolidation process, the quantity of water leaving consolidating soil is larger than the quantity of water entering it (Terzaghi et al., 1996). Thus, when a soil is deformed, significant and often–irreversible changes in volume occur as the relative positions of the particles changes. In order for this change to occur, fluid in the voids must flow through the soil (Muir Wood, 1990).

Like conventional soils, compressibility of the stabilized dredged material (SDM) is the measure of its consolidation under sustained vertical load owing to dissipation of pore water. It can be assessed by examining the extent to which the stabilized mass structure impedes the movement of pore water. The obstruction of pore water in the SDM during consolidation can occur because of two reasons. Firstly, the existing pore water can be lodged in due to cementation action (Bemben, 1986). Secondly, the initial pore water in the specimen is utilized during on–going hydration reactions. While the first possibility may prevent a change in void ratio, the latter may cause decreased initial water content and hydraulic conductivity of the SDM. Thus, the whole process of loading may respond differently from that of conventional soft soils. It may be difficult to define the boundaries between the region of small and large deformation in $e - log\sigma_v^{'}$ as shown Fig. 2.3, where e is the void ratio, $\sigma_c^{'}$ is the preconsolidation stress and $\sigma_v^{'}$ is the applied effective vertical stress. As a result, conventional approach for evaluation of stiffness properties may not apply.

2.3.3 Hydraulic conductivity

Hydraulic conductivity (HC) presents engineering problems, of which the chief cause is associated with flow of water or pore pressure dissipation (Ingles and Metcalf, 1972). The HC of stabilized dredged material (SDM) dictates its strength and compressibility. Inadequate pore pressure dissipation due to low hydraulic conductivity may lead to undrained condition and incompressibility, which is associated with low strength. Researchers (Vappalli et al., 1999; Benson and Othman, 1990; Quang and Chai, 2015; Viklander, 1998) have shown that the hydraulic conductivity of soils is a function of microstructure of pores (size and distributions) and properties of pore water (permeant).

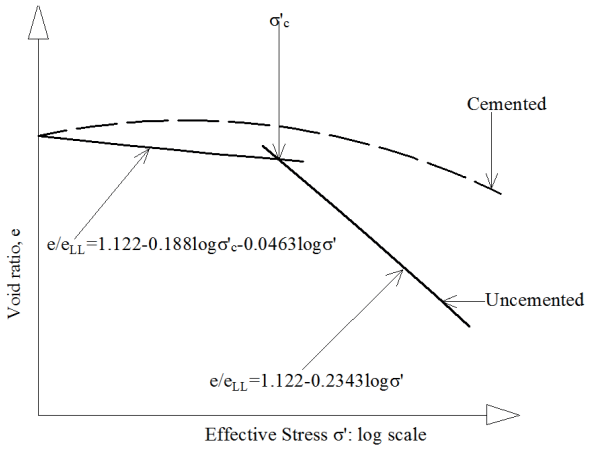

Fig. 2.3: Comparison of possible compressive behavior of cemented overconsolidated soil with that predicted based on physical state identification (Boone and Lutenegger, 1997).

Formation of aluminosulphate in cement stabilized soil cured under water may cause expansion in volume of hydrated paste and hydration products filling the pores and cavities, thereby, reducing the hydraulic conductivity (USEPA, 1993; Sing et al., 2008; Topolnicki, 2004; Åhnberg et al., 2003; Maher et al., 2004). On the other hand, clay stabilized with lime increases in hydraulic conductivities up to several times compared to the native clay. Formation of floccules of highly porous nature may be considered as a reason for an increased hydraulic conductivity of lime treated soil. The change in the initial dispersed orientation particles due to flocculation increases the void ratio and hydraulic conductivity (Rajasekaran and Rao, 2002; Cássia de Brito Galvão et al., 2004). Addition of cement to soils agglomerates several small aggregates into a large one. Large pores are associated with high hydraulic conductivity. Likewise, increased concentration of Ca^{2+} results in thinner diffusive double layer, which tend to exhibit a higher hydraulic conductivity compared to thicker diffusive double layer (Quang and Chai 2015).

2.3.4 Durability

The term durability refers to the resistance of the material to the processes of weathering, erosion and traffic usage (Ingles and Metcalf, 1972). In cold regions climates, the ability to withstand the freeze–thaw cycles is the most important factor for long term performance of stabilized soil mass. Repetitive freeze–thaw cycling may have detrimental effect on stabilized soils (Sparrevik et al., 2008; Al-Tabbaa and Evans, 1998; Jamshidi and Lake, 2015; Maher et al., 2006).

Research has been carried out to investigate the impact of repetitive freeze–thaw cycles on the durability of treated and untreated natural soft soils (Al-Tabbaa and Evans, 1998; Topolnicki, 2004; Maher et al., 2006; Jamshidi et al., 2014; Jamshidi and lake, 2015). These studies have shown that freeze–thaw cycles have detrimental effects on the strength and the hydraulic conductivity of stabilized materials. Frozen moisture in stabilized materials produces expansive forces, which cause the increase in volume and some bond breakage. This results in permanent loss of strength and increased hydraulic conductivity.

Durability assessment of construction material is the most difficult parameter an engineer must meet during design process (Ingles and Metcalf, 1972). The current practice for assessing the resistance to repetitive freeze-thaw cycles of compacted cement-treated soils utilizes percentage dry mass loss as performance indicator (ASTM D560). However, mass loss does not correspond to internal structures that control for instance, the hydraulic conductivity and strength of cement–treated soil (Jamshidi et al., 2014; Jamshidi and Lake, 2015). In addition, the use of percentage dry mass loss criteria on uncompacted–treated soft soils may be unsuitable due to high water content and low to moderate strength. In Sweden, the change in the hydraulic conductivity or unconfined compressive strength of stabilized soils subjected to freeze-thaw cycles are normally utilized as performance indicator.

Although literature has shown that stabilized weak soils are susceptible to freeze-thaw cycling, in truth, the healing potential of affected stabilized dredged material (SDM) is unclear or not investigated at all. Understanding the healing likely of the SDM with damaged geotechnical properties provides a comprehensive assessment of the SDM for long term performance in cold regions climates.

2.4 Evaluations of geotechnical parameters

Determination of soil parameters for geotechnical design depends mainly on the type of design and method of analysis. Settlement and stability calculations are the two common design calculations that are carried out in geotechnical engineering. Settlement calculations are concerned with stiffness of soil mass under applied load. The stress–strain curve is assumed to be linear and elastic under working load. Stability analysis focuses on complete failure of the soil masses with large deformation occurring in rupture planes. This may lead to ultimate failure of geotechnical structures for which the stress–strain behavior become rigid and perfectly plastic (Muir Wood, 1990). Geotechnical design parameters can be obtained based on either laboratory or field tests.

2.4.1 Laboratory evaluations

Oedometer and unconfined compression tests are common laboratory tests used for evaluation of deformation and strength properties of the stabilized dredged material (SDM), respectively. These tests have remained popular because of their simplicity in obtaining data for evaluation of stiffness and strength parameters of soils for use in design analysis. For instance, a primary objective of the consolidation test is to estimate the maximum pressure (i.e. preconsolidation stress) that may be applied to the soil without causing large deformation (Crawford 1986). Thus, preconsolidation stress is the maximum effective vertical stress that natural soil deposit has experienced during geological time. Contrary, the preconsolidation pressure of stabilized soils mass is brought by cementation action. The cementation process and consolidation stress applied during curing greatly affect the apparent preconsolidation stress. This pressure is strongly linked to the undrained strength of the stabilized mass and has considerable influence on its deformation behaviour (Åhnberg, 2007). Bemben (1986) suggests that for cemented soils, the relevant apparent preconsolidation pressure is the only one existing at the time of cementation. Consequently, the term apparent preconsolidation stress is utilized throughout this thesis to avoid confusion with conventional preconsolidation stress.

By interpreting the stress-strain curves from oedometer tests, compressibility parameters such as preconsolidation pressure and tangent modulus can be obtained. According to Grozic et al. (2003), the preconsolidation stress (σ_c') interpreted from oedometer tests provides important information on the stress history of the soil, which in turn can be correlated to many behavioural properties. However, the accuracy in evaluating the preconsolidation stress $\sigma_c^{'}$ depends on the shape of compression curves. A well-known Casagrande method (ASTM D 2435) or Sällfors (1975) are the fast techniques for obtaining the $\sigma_c^{'}$ provided there is a well-defined break in the $e - log\sigma_v^{'}$ curve or $\varepsilon - log\sigma_v^{'}$ curve (e.g. $e - log\sigma_v^{'}$ for uncemented soil in Fig. 2.3.

Tangent modulus is preferred as a standard measure for the compressibility characteristics for all types of soil (Janbu, 1967). Soil specimen during oedometer test will have a relatively stiff response at stresses below preconsolidation stress (σ_c') and a soft response at stresses above σ_c'. The constrained modulus is expected to drop to minimum value at stress near σ_c' and then increase with increasing stress values above σ_c' (Janbu, 1963; Janbu 1998; Karlsrud and Hernandez-Martinez, 2013; Crawford, 1986; Sällfors, 1975). Topolnicki (2004) observed that the stiffness modulus of stabilized soil is highly dependent on the strain level. As a result, it may be appropriate to use the initial stiffness (tangent) modulus rather than secant modulus in settlement analysis. This is because the latter may be unrealistic small, which in turn can result into over estimation of deformations.

According to EuroSoilStab (2002), settlements within the stabilized mass are calculated by assuming the stabilized volume to behave as linear elastic perfectly plastic layer with the entire load being carried by stabilized mass. The geotechnical parameters evaluated from the laboratory tests can be utilized to estimate the field settlements of stabilized volume by

$$\delta_m = \sum \Delta h . \frac{\sigma'}{M} \tag{1}$$

where:

δ_m = settlement in the stabilized mass, m

Δh = thickness of sublayer, m,

q = effective load on stabilized mass, kPa,

M = tangent modulus of stabilized soil mass, kPa.

The tangent modulus M varies with effective vertical stress σ_v' and all variations could be accounted by:

$$M = m p_a \left[\frac{\sigma_v'}{p_a} \right]^{(1-n)} \tag{2}$$

where:

m = the constrained modulus number,

p_a = the atmospheric pressure, kPa,

n = the stress exponent.

Janbu (1998) suggested the following steps for obtaining the preconsolidation stress σ_c' and modulus number m:

- obtain the tangent modulus from $\mathrm{M} = \Delta\sigma_\mathrm{v}'/\Delta\varepsilon$ for each load step.
- plot M versus vertical effective stress σ_v' in a linear scale.
- obtain the preconsolidation stress σ_c' directly by inspect $\mathrm{M} - \sigma_\mathrm{v}'$ curve, where σ_c' is determined by a change in the curve.
- determine the overconsolidated modulus M_{OC} for $\sigma_\mathrm{v}' < \sigma_\mathrm{c}'$ (in overconsolidated range) and determine the modulus number m in the normally consolidated range $\sigma_\mathrm{v}' > \sigma_\mathrm{c}'$. For clay $\mathrm{m} = \Delta M/\Delta\sigma_v'$

It is difficult to predict the strength–deformation characteristics of treated soils using the laboratory test results only (Topolnicki, 2004). Thus, appropriate in-situ stiffness and strength data must be obtained and utilized to evaluate the design parameters. By comparison with field observation, the predictive capacity of selected constitutive model can be assessed.

2.4.2 In-situ evaluations

In-situ soil tests are often of primary interests to geotechnical engineers. These tests can provide reliable information about soils on–site (Abu-Farsakh et al., 2003). Cone penetration test (CPT) is one of the most utilized in–situ tests for the determination of in–situ soil stratigraphy, identification of soil behaviour and evaluation of mechanical properties. The CPT consists of pushing into the ground a series of cylindrical rods with the cone at the base at a speed of 2 cm/second. During the push, the penetration resistance, sleeve friction, and pore pressure (Table 2.2) are generally measured at an interval between 25 mm and 50 mm (Potts and Zdravkovic´, 2001; Robertson and Cabal, 2009). The CPT measured quantities have been correlated with mechanical properties of conventional soils (Larsson and Åhnberg, 2005; Lunne et al., 1986; Robertson, 2009; Larsson and Mulabdic, 1991; Robertson, 1990; Robertson and Campanella, 1983; Kulhway and Mayne, 1990; Jefferies and Davies, 1993). These correlations are predictive of in–situ soils behaviour, and they can be used for soil classifications and evaluation of mechanical properties without the need for laboratory experiments (Robertson et al., 1986). Soil classification (Fig. 2.4) has been related to normalized cone resistance and friction ratio or pore pressure (Robertson 1990). Schneider et al. (2008) introduced new space for evaluation of soil behavior type of in–situ soil using normalized cone resistance and pore pressure (Fig. 2.5). Some well–known empirical correlations and their corresponding evaluated in–situ geotechnical parameters for the conventional cohesive soils are presented in Table 2.4. According to EuroSoilStab (2002), common CPT is very suitable for testing stabilized mass if the undrained shear strength is between 50 and 1000 kPa. Still, there are no empirical correlations developed for use in stabilized soils mass. Consequently, conventional CPT empirical relationships, which were developed for conventional soils are as well utilized in the stabilized mass. For instance, the undrained shear strength (s_u) from cone penetration test (CPT) data can be estimated from

$$s_u = \left(q_t - \sigma_{v0}\right) / N_{kt} \tag{3}$$

where:

q_t = total cone resistance, kPa,

σ_{v0} = total vertical stress, kPa,

N_{kt} = cone tip factor.

The N_{kt} value is usually obtained by calibrating the CPT data with known undrained shear strength from vane shear test (Kulhawy and Mayne, 1990). According to Robertson (2009), the value for N_{kt} ranges between 10 and 20 with an average value of 14 for insensitive soils.

The constrained modulus M from CPT data can be estimated from

$$M = \alpha_m(q_t - \sigma_{v0}) \quad (4)$$

where:

α_m = constrained modulus cone factor.

According to researchers (Sanglerat et al., 1972; Mayne, 2007; Robertson, 2009) values of α_m varies with soil type and net cone resistance with the values ranging from 1 to 20. Robertson (2009) suggested the following correlation for selection of constrained modulus cone factor α_m:

If $I_c \geq 2.2$, $\alpha_m = Q_{tn}$ when $Q_{tn} \leq 14$

$\alpha_m = 14$ when $Q_{tn} > 14$

If $I_c < 2.2$, $\alpha_m = 0.03[10^{0.55I_c+1.68}]$.

Table 2.2: Primary measured and corrected CPT quantities.

Primary quantity	Symbol	Corrected quantity	Source
Cone resistance	q_c	$q_t = q_c + (1-a) * u$	Lunne et al (1986)
Sleeve friction	f_s	$f_t = f_s - b * u$	Lunne et al (1986)
Pore pressure	u	-	

a = effective area ratio, which is defined as the ration between net area of the cone and area of the base cone; *u* = measured hydrostatic pore pressure just behind the cone; *b* = effective area ratio for the sleeve.

Table 2.3: Some useful CPT parameters for in-situ soil classifications.

Useful quantity	Symbol	Empirical Expression	Source
Normalized cone resistance	Q_{tn}	$[(q_t - \sigma_{v0})/p_a](p_a/\sigma'_{v0})^n$	Robertson (2009)
Normalized friction ratio	F_r	$100f_t/(q_t - \sigma_{v0})$	Robertson (2009;1990)
Pore pressure ratio	B_q	$\Delta u/(q_t - \sigma_{v0})$	Robertson (2009;1990)
Normalized pore pressure	–	$\Delta u/\sigma'_{v0}$	Scheneider et al. (2008)
Soil behavior type index	I_c	$[(3.47 - \log Q_{tn})^2 + (\log F_r + 1.22)^2]^{0.5}$	Robertson (2009)
Stress exponent	n	$0.381I_c + 0.05(\sigma'_{v0}/p_a) - 0.15$	Robertson (2009)

σ_{v0} and σ'_{v0} = total and effective vertical stress, respectively. p_a = atmospheric pressure.

Table 2.4: Some engineering parameters and corresponding CPT empirical correlations.

Pameters	Symbol	Empirical correlation	Source
In-situ constrained modulus	M	$\alpha_m(q_t - \sigma_{v0})$	Lunne et al. (1986)
Undrained shear Strength	s_u	$(q_t - \sigma_{v0})/N_{kt}$	Lunne et al. (1986)
Overconsolidation ratio	OCR	$k(q_t - \sigma_{v0})/\sigma'_{v0}$	Kulhway and Mayne (1990)
Preconsolidation stress	σ'_c	$k(q_t - \sigma_{v0})$	Kulhway and Mayne (1990)
Soil sensitivity	S_t	$7.1/F_r$	Robertson (2009)

where α_m = constrained modulus cone factor, N_{kt} = tip cone factor, and k = constant.

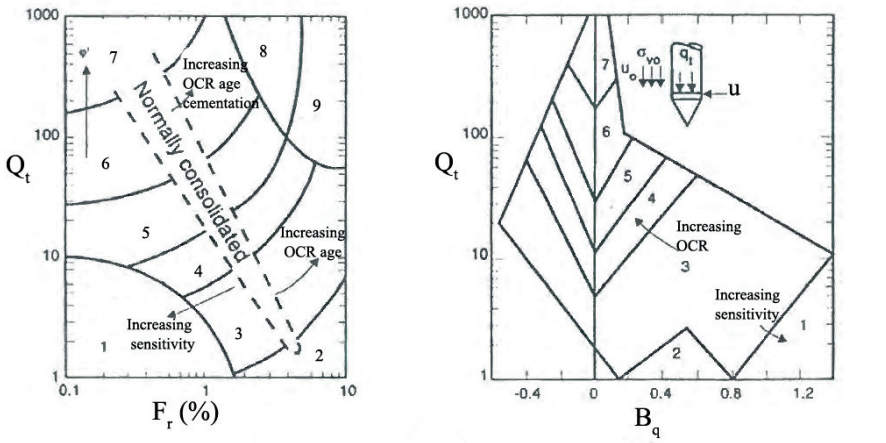

Zone	Soil Behaviour type	Zone	Soil Behaviour type	Zone	Soil Behaviour type
1	Sensitive, fine grained	4	Silt mixture: clayey silt to silty clay	7	Gravelly sand to sand
2	Organic soils-peats	5	Sand mixtures: silty sand to sand silty	8	Very stiff sand to clayey sand
3	Clays-clay to silty clay	6	Sands: clean sands to silty sands	9	Very stiff fine grained

Fig. 2.4: Proposed soil behavior type classification system from CPTU data (Robertson et al., 1990).

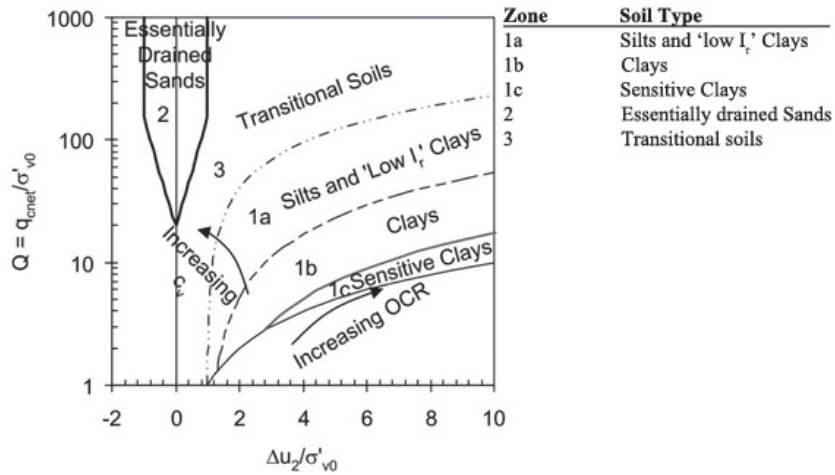

Fig. 2.5: Proposed soil behavior type classification system from CPTU data (Schneider et al., 2008).

3. Strength, compressibility and durability evaluations

To exemplify treatability of high water content dredged sediments (DS) for geotechnical applications, laboratory and field tests studies were carried out. Initial laboratory tests studies on the possibility to improve the mechanical properties of high water content dredged sediments (DS) were carried out by Fossenstrand (2009) and Lagerlund (2010a, 2010b). The goal of these laboratory test study were to prescribe the design recipe and the amount of binder to be utilized at the large-scale field test. Laboratory test study presented in this work was carried out as a follow up test study of the field work and to fulfill the objectives of the present research work. In this study, high water content dredged sediments were defined as follows: *for a given unit weight of dredged sediment the weight of water is greater than the weight of solids*. Consequently, the methodologies that were utilized during this research work may not necessarily apply to other *DS in which the weight of water is less than the weight of solids*.

3.1 Laboratory test and evaluations

During the laboratory test study the following materials and methods were utilized. Strength development, compressibility behaviour, and durability of high water content stabilized dredged materials (SDM) were evaluated.

3.1.1 Materials

3.1.1.1 Dredged sediments

High water content dredged sediments (DS) were obtained from Port of Oskarshamn, which is located in south-eastern coast of Sweden. The studied DS had received water content between 200% and 400%. Based on the received water content, the DS were categorized into two, namely; DS-A and DS-B. The average water content for DS-A and DS-B were 283% and 356%, respectively. Results from X-rays diffraction (XRD) analysis (Fig. 3.1) on representative samples of the studied DS show that quartz and feldspars mineral groups of Albite (plagioclase feldspars), microcline (alkali feldspars) and Biotite were the dominating minerals. Qualitative analyses of mineral phases associated with the two studied DS are presented in Table 3.1**.** The two DS were not analyzed for presence of contaminants. Physical properties of the studied DS are shown in Table 3.2. Wet sieving was carried out on the received DS to obtain the particle size distributions and cumulative organic matters. The DS particles, which were retained on all sieve sizes less than 4 mm were dried and pulverized. The pulverized powders were then burnt in a furnace at 800 °C for a period of one hour to determine the weight of organic matters, which was utilized to compute losses

of ignition (LOI). Generally, the studied DS were mainly of organic nature. The percentage passing soil particles were estimated by subtracting the corresponding percentage LOI from retained dry mass on the respective sieve size. The LOI was conservatively utilized to obtain the actual soil particle size distribution as shown in Fig. 3.2.The cumulative percentage LOI of the studied DS with particles diameter less than 4 mm were 235% and 413% for DS-A and DS-B, respectively. These values were proportional to the water content of the studied DS as shown in Table 3.2. The plasticity indexes of the studied DS were 32 and 37 for DS-A and DS-B, respectively. On average, the studied DS comprised of about 4% clay, 76% silt and 20% fine sand particles. Consequently, the DS could be placed below A-line and classified as organic silt in accordance with unified soil classification system (USCS) as shown in Fig. 3.3.

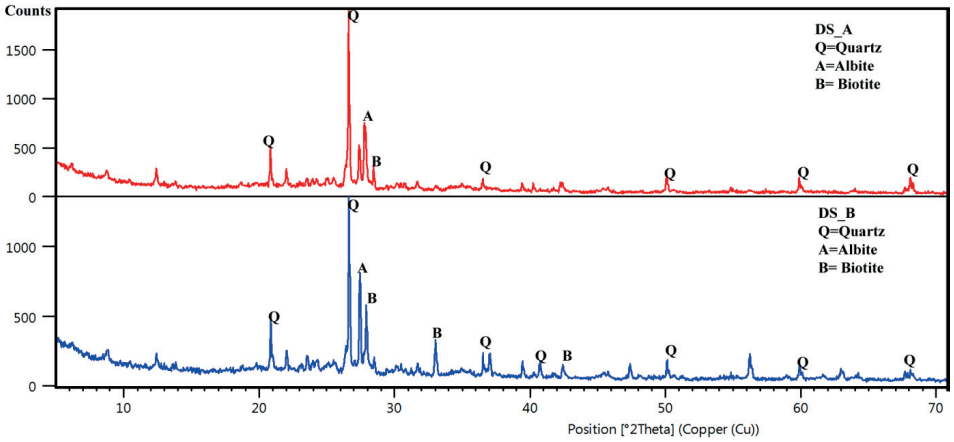

Fig. 3.1. X-ray diffractions patterns on representative samples of the studied DS.

Table 3.1. Minerals phases associated with the studied dredged sediments based on High score plus analysis.

Mineral name	Chemical formula	Score_DS-A	Score_DS-B
Quartz	SiO_2	48	53
Albite	$NaAlSi_3O_8$	21	32
Annite	KFe_3^{2+} $NaAlSi_3O_{10}(OH,F)_2$	6	-
Dolomite	$CaMg(CO_3)_2$	10	-
Biotite	$K(Mg,Fe)_3AlSi_3O_{10}(F,OH)_2$	8	13
Pyrite	FeS_2	-	57

Table 3.2. Physical properties of the studied dredged sediments: LOI = cumulative loss of ignition on DS with particles size <= 2 mm, Gs = specific gravity, w = average initial water content. LL = liquid limit. PL = plastic limit, and ρ = average bulk density, e_0 = void ratio.

	w (%)	LL (%)	PL (%)	ρ g/cm^3	LOI (%)	Gs	e_0
DS-A	283	120	88	1.19	235	2.5	8.1
DS-B	356	122	85	1.17	413	2.4	8.3

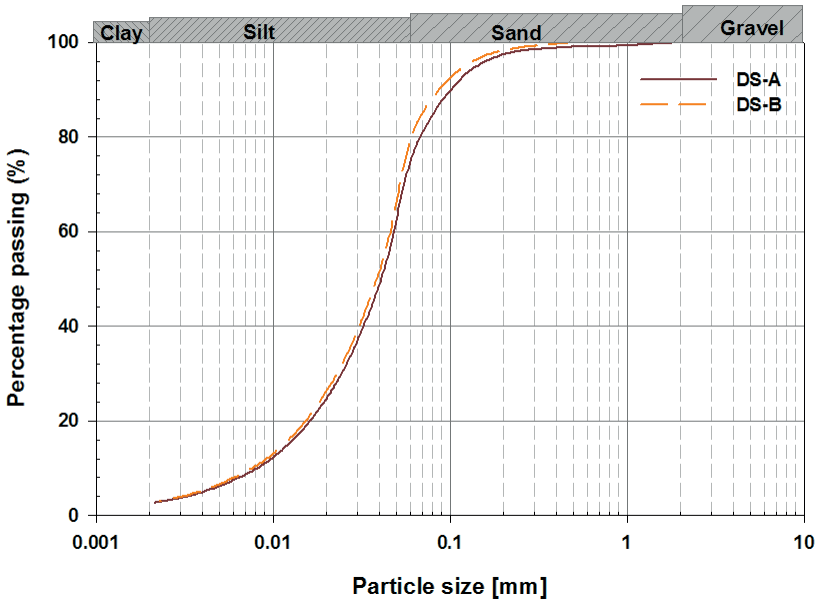

Fig. 3.2. Particle size distribution curve for the studied DS after being corrected for organic content.

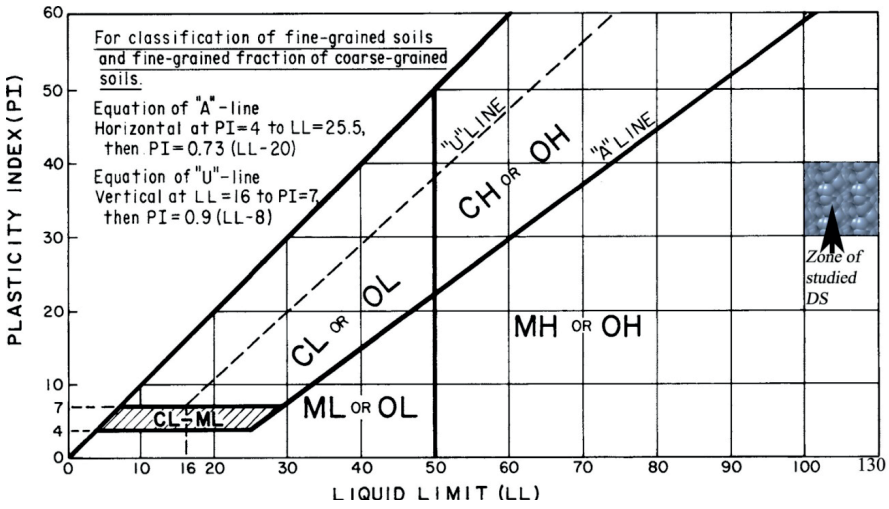

Fig. 3.3. Unified soil classification system plasticity chart for classification of fine grained soils (ASTM D 2486).

3.1.1.2 Binder

The use of composite binders for stabilization–solidification of the dredged sediments (DS) is increasing due to increased artificial pozzolanas that can be utilized as supplementary cementitious materials (SCM). Thus, during this study, both composite and single binders were utilized.

Composite binder (CB) comprised a combination of Byggcement (BC), fly ash (FA) and ground granulated blast furnace slag (GGBS). Single binder utilized BC only to amend the DS. BC is produced by Cementa AB in Sweden. The FA and GGBS were obtained from Billerud Karlsborg paper mill (Billerud Korsnäs) and SSAB steel industry, respectively. The average mineral compositions for individual binder are presented in Table 3.3.

Table 3.3. Mineral composition for individual binder: FA = fly ash (Svensson and Andreas, 2012), GGBS = ground granulated blast furnace slag (Data: Courtesy of SSAB), and BC = Byggcement (Holm et al., 2015).

Chemical compound (%)	**FA**	**GGBS**	**BC**
CaO	21	31	63
SiO_2	43	34	18
Al_2O_3	10	13	5
MgO	4	17	
K_2O	5		

3.1.2 Methods

Samples were prepared by mixing dredged sediment with either composite binder (CB) or single binder by Byggcement (BC). The amounts of binder were estimated such that assumed immediate water content on stabilized dredged material (SDM) could be achieved.

3.1.2.1 Amount of binder

The amounts of binder were estimated such that the water content of 130%, 160%, 180%, 190%, 210% and 240% could be achieved immediately after mixing (i.e. during induction period). The following computations steps were utilized to obtain the amounts of binder.

- Bulk density ρ and initial water content w_0 of the dredged sediment (DS) were first determined.
- The volume of the DS was computed in accordance with:

$$V_{DS} = M_{DS} / \rho \quad (5)$$

where:

V_{DS} = one batch volume of the DS to be mixed with binder, cm^3,

M_{DS} = one batch weight of the DS to be mixed with binder, g.

For good workability and thorough blending, one batch of mixing consisted of 2000 g of the DS.

- Initial dry mass of solid particles m_s in 2000 g of the DS was then estimated in accordance with

$$m_s = M_{DS} / (1 + w_0). \quad (6)$$

- Mass of water m_w in 2000 g of DS was obtained by subtracting the amount of dry solids from the total weight of the DS in accordance with $m_w = M_{DS} - m_s$.

- Assuming that dissolution of binder results in reduced water content, the mass of binder m_b per 2000 g of the DS was computed using the assumed water content wc (in decimals) in the following expression:

$$wc = m_w/(m_b + m_s) \qquad m_w > m_s \tag{7}$$

- The prescribed binder quantity q_b in g/cm^3 was then computed from

$$q_b = m_b/V_{Ds}\,. \tag{8}$$

- Immediate bulk density of stabilized dredged material (SDM) ρ_{sdm} could be estimated using individual components in the blend in accordance with:

$$\rho_{sdm} = (M_{DS} + m_b)/(m_w + m_s/G_s + m_b/G_b) \qquad m_w > m_s \tag{9}$$

where:

G_s = specific gravity of solid particles, g/cm^3,

G_b = specific gravity of binder particles, g/cm^3.

The estimated amounts of binder were then thoroughly mixed with DS to obtain the SDM. Mixing was carried out using a spatula to produce representative samples of the SDM. The blended samples were further treated depending on the nature of sample preparations for testing. Thus, samples were molded in accordance with the unconfined compression, oedometer, and hydraulic conductivity tests.

Table 3.4. Utilized design recipes, assumed water content and estimated amounts of binder. q_b = binder quantity; q_c = cement quantity; w/b = water-binder ratio; w/c = water-cement ratio, wc = water content, and CP = maximum curing period.

DS	Binder	q_b (kg/m^3)	w/b	Ratio C/FA/GGBS	q_c (kg/m^3)	w/c	wc (decimal)	CP (days)
A	CB1	250	3.5	1:1:0.5	100	8.8	1.6	91
A	CB2	180	4.9	1:1:0.5	72	12.3	1.8	91
A	CB3	110	8.0	1:1:0.5	44	20.0	2.1	91
B	CB4	320	2.8	1:1:0.5	128	7.0	1.6	91
B	CB5	180	5.0	1:1:0.5	72	12.5	2.1	91
B	CB6	260	3.5	1:1:0.5	104	8.8	1.8	91
B	CB7	320	3.5	1:0.5:0.5	160	3.5	1.6	50
A	BC1	250	8.9	1:0:0	250	8.9	1.6	28
A	BC2	110	2.9	1:0:0	110	2.9	2.1	28
A	BC3	260	5.1	1:0:0	260	5.1	1.6	-
B	BC4	315	2.0	1:0:0	315	2.0	1.6	28
B	BC5	180	4.1	1:0:0	180	4.1	2.1	28
B	BC6	447	7.3	1:0:0	447	7.3	1.3	28
B	BC7	225	3.5	1:0:0	225	8.8	1.9	28
B	BC8	125	4.9	1:0:0	125	12.3	2.4	28

3.1.2.2 Samples for unconfined compression and oedometer testing

Samples for obtaining specimens for unconfined compression and oedometer tests were moulded in cylindrical polyvinyl chloride (PVC) tubes to obtain cylindrical samples of sizes 50 mm x 170 mm. The SDM were placed and allowed to fall freely to the bottom of the PVC tubes by vibrations of its bottom end without mechanical compaction. In order to obtain average test results, duplicate samples were prepared for each curing period.

In Sweden, it is customarily required to preload the stabilized volume immediately after mixing with a minimum preloading weight of 18 kPa. The initial preloading weight serves two purposes: firstly, squeeze out air trapped during mixing. Secondly, speed up consolidation process and bring the soil particles together for effective hydration reactions. The purpose for subsequent loading is to consolidate the stabilized mass for the load other than the service load (EuroSoilStab 2002). Accordingly, on the upper end of the PVC sample tubes, filter plugs were inserted. On top of each filter plug a preloading weight of 22 kPa was placed as shown in Fig. 3.4. The SDM samples in PVC tubes were cured underwater (Fig. 3.4) in a room with ambient temperature of 18°C ± 5°C. An open curing condition was adopted, where curing water could enter or leave the SDM samples through the filters. No pore water chemistry was considered in this study and therefore, tap water was utilized as curing water.

3.1.2.3 Samples for hydraulic conductivity testing

Samples for hydraulic conductivity tests were molded in Proctor molds of dimensions 102 mm x 112 mm without mechanical compaction. The inner surfaces of the Proctor molds were lined with a layer of bentonite clay to prevent any possible seepage along the interface (Fig. 3.5a). A preloading weight of 14 kPa was applied on top of the SDM for about 15 minutes (Fig. 3.5b) after filling the Proctor molds with the SDM. The aim for initial preloading was to compress the SDM sample for purpose of reducing shrinkage or decrease of the sample size under self-weight during permeation. The reduced volume (Fig. 3.5c) due to the immediate compression was refilled with the SDM sample (Fig. 3.5d). Thin layers of fresh DS were placed on both top and bottom end of the SDM surfaces to avoid filter clogging due to cementation (Fig. 3.5e). The top and bottom caps with double filters were finally covered on the Proctor molds (Fig. 3.5f), and samples were mounted for the hydraulic conductivity measurement.

Fig. 3.4. Open curing of the SDM samples for unconfined compression and oedometer tests.

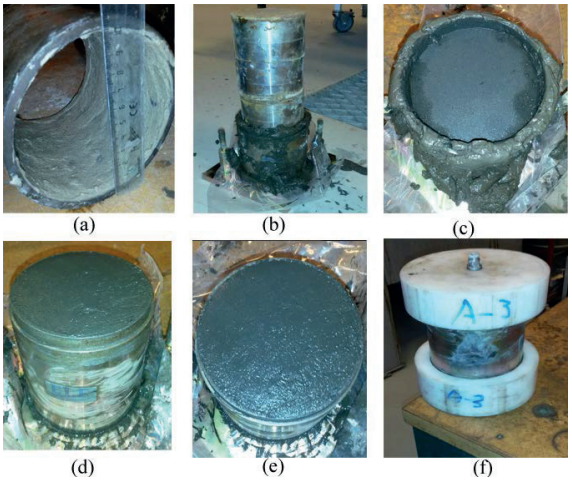

Fig. 3.5. Sample preparation for hydraulic conductivity tests. (a) lining of bentonite layer (b) application of surcharge to compress the SDM (c) consolidate part (d) filling the consolidated portion (e) application of layer of untreated DS (f) assemblage of the top and bottom cap for permeation.

3.1.2.4 Samples for durability testing

The changes in the unconfined compressive strength (UCS) or hydraulic conductivity (HC) values of stabilized soils subjected to freeze-thaw (f-t) cycles were utilized as performance indicator. Thus, parts of samples that were prepared for unconfined compressive strength (UCS) and samples for the hydraulic conductivity (HC) testing were also subjected to repetitive freeze-thaw cycles.

The change in the UCS and HC values were utilized as a measure of resistance of the SDM to repetitive freeze–thaw cycles. A complete freeze–thaw cycle (Fig. 3.6) was considered to gain a better understanding for healing potential during thaw consolidation after the impact of freeze–thaw processes under open and semi-closed freezing systems.

During open freeze-thaw (f-t) cycles, samples were kept in their preparation PVC tubes, which were then sandwiched between water saturated sand. Open f-t system was used in order to:

- Maintain the original curing conditions. Sand bath f-t method was used to minimize expansive forces of frozen water on the sides of the curing container.
- Allow continuous interchange between pore water in the specimens and the surrounding pore water during f-t cycles.
- Simulate field condition in which the SDM can be placed below groundwater level.

Considering a closed freezing system, loss or gain of water in the sample should be precluded (ASTM D 653). However, during this study, a fully closed freezing system was not achieved. Similar to open f-t system, samples were frozen and thawed in their original PVC tubes, but in the absence of curing water. The bottom sides of the PVC tubes were covered with tight vinyl caps to prevent loss of water. However, it was likely that during thaw, drainage of released water could occur through the top filter. Consequently, under this f-t condition, the system was considered as semi–closed freezing system. This system was utilized to compare the influence of bottom liners on the strength of contained contaminated stabilized dredged materials, which are subjected to f-t systems.

3.1.2.5 Freeze–thaw process

A freezer with capability of freezing to –30°C was utilized as a freezing cabinet during freeze–thaw (f-t) test study. Copper wire thermocouple instrumentation was utilized to determine a period for a complete f-t cycle on samples for unconfined compressive strength (UCS) and hydraulic conductivity (HC) evaluation (Fig. 3.7). Evolution of temperature on the SDM samples under UCS assessment only is shown in Fig. 3.8. Thermocouple instrumentation shows that it would take about 24 hours (Fig. 3.8a) and 12 hours (Fig. 3.8b) to complete one f-t cycle under open and semi–closed f-t systems, respectively. Nonetheless, 24 hour period was utilized to define a complete f-t cycle on the UCS samples under both open and semi–closed systems. Samples for hydraulic conductivity (HC) measurement required 48 hours to complete one traditional f-t cycle. The thermocouple data were not presented due to problems in data recording.

Thermocouple data instrumentation show that under both open and semi-closed freezing systems, drop and rise of temperature toward 0 °C occurred rapidly. Based on the thermocouple instrumentation data (Fig. 3.9a), we can deduce that when the temperature of freezing air (F-TT) approaches and decreases below 0 °C, the rate of freezing slows down. Likewise, when the temperature of thawing air (F-TT) approaches and rises above 0 °C, the rate of thawing turn out to be low. This observation suggests that the actual freeze and thaw conditions occur when the temperature of freezing and thawing air is below and above 0 °C, respectively.

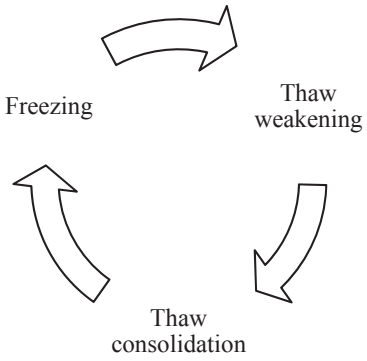

Fig. 3.6. A Schematic view of a complete freeze–thaw process.

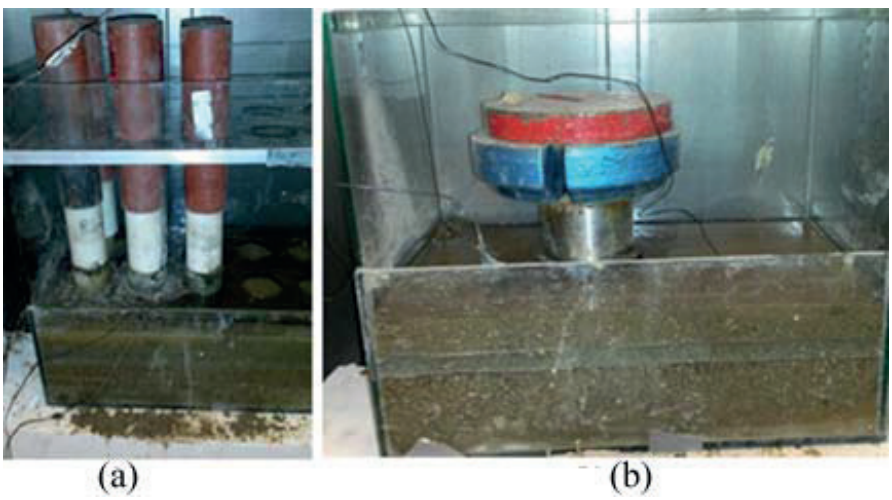

Fig. 3.7. Thermocouples instrumentation during freeze–thaw cycles under open freezing system (a) samples for UCS evaluation (b) Example of sample for hydraulic conductivity test and the UCS assessment.

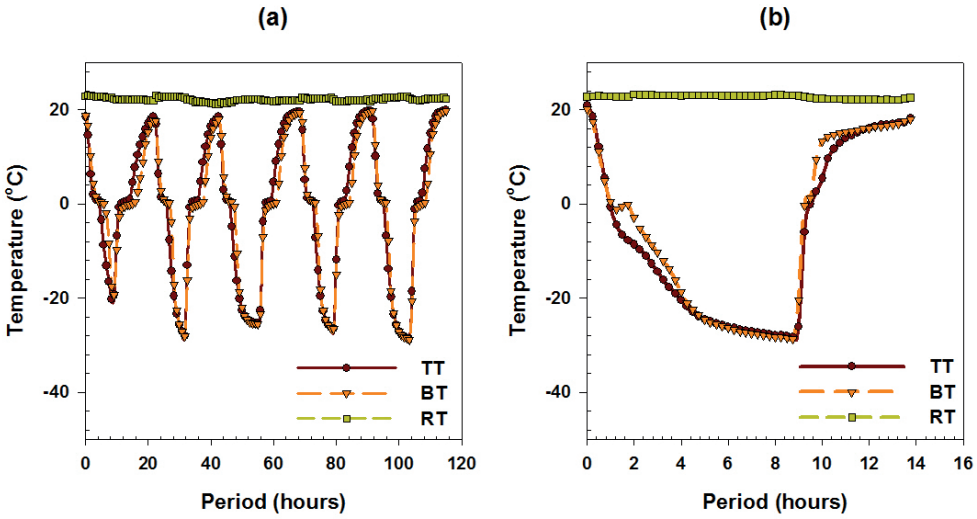

Fig. 3.8. Evolution of temperature in the SDM samples during (a) five open freeze-thaw cycles (b) one semi-closed freeze-thaw cycle.

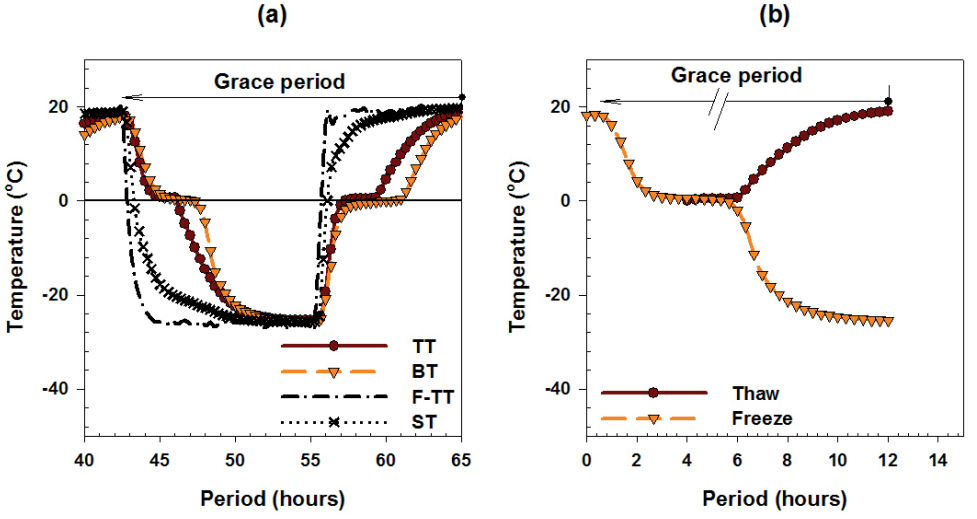

Fig. 3.9. Traditional freeze-thaw (f-t) cycle (a) required grace period before subsequent freezing.(b) depicted incomplete traditional freeze-thaw cycle.

Generally, in the northern parts of the world, the four seasons of the year (i.e. winter, spring, summer, and autumn) are fixed with small variations. Thus, traditional assessments of the impact of freeze-thaw cycles do consider winter and spring seasons only. In other words, winter and spring seasons are the only parts of the year that make the depicted semi f-t cycle in Fig. 3.9(b).

Thus, it was hypothesized that the durability of the stabilized materials cannot be assessed based on two seasons only. Accordingly, for a complete f-t cycle, Fig. 3.9(a) suggests that to assess the impact of f-t cycles on the SDM, it might be beneficial to consider a grace period (GP) for thaw consolidation. This period could be associated with summer and autumn weather conditions. It was postulated that during the GP for thaw consolidation, the SDM will strive to regain its original strength values after the impact of freeze-thaw, hence healing potential for SDM with damaged properties.

3.1.3 Test setup and evaluations

3.1.3.1 Immediate water content

The amounts of binders were estimated based on expected water content during induction period. Thus, immediately after mixing, a representative sample from each stabilized dredged material (SDM) was utilized to determine the immediate water content of the SDM. The representative samples of the SDM were oven dried for 24 hours at a constant temperature of 105 °C. The computed water content was utilized to verify the anticipated water content values that were utilized for estimation of the amounts of binders.

3.1.3.2 Unconfined compression test

After a prescribed curing period, PVC sample tubes were taken out of the curing container and mounted on a mechanical jack, which was used to extrude specimens for testing. Specimens for unconfined compression tests were obtained by extruding and trimming 100 mm height sample. Unless otherwise stated, the unconfined compression tests on all specimens were carried out using strain–controlled method at a deformation rate of 1.0 mm/min. The tests were conducted on unfrozen samples after prescribed curing period shown in Table 3.4. The control strength (CS) values for samples A-BC3, B-CB7, and A-CB2 which were subjected to f-t cycles were obtained on unfrozen samples tested after curing period of 28, 50 and 91 days, respectively. Subsequent tests on these samples were carried out after prescribed f-t cycles to assess the UCS values (i) immediately after thaw period (i.e. thaw weakening, TW) and (ii) after grace period (GP) of thaw consolidation (TC) as shown in Fig. 3.10. The GP for TC was determined based on thaw period (TP) and number of number of thaw (i.e. traditional f-t cycles (X) as shown in Fig. 3.10). For instance, 1 f-t cycle that requires 12 hour of thaw will have 24 hours of GP for TC (i.e. 12 x 1 + 12=24) as shown in Table 3.5. The UCS values, which were measured during TW and TC, were compared with the CS values to assess the impact of traditional f-t and healing potential of the SDM with damaged strength, respectively.

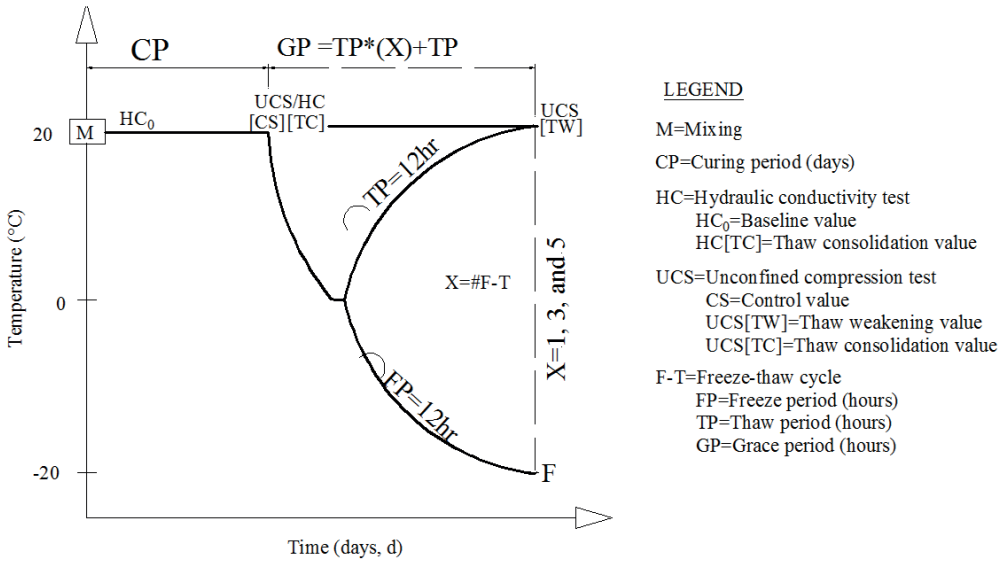

Fig. 3.10. Schematic diagram for HC/UCS testing and evaluation in relation to time and temperature conditions.

Table 3.5: Duration for grace period (GP) of thaw consolidation relative to number of freeze–thaw cycles and thaw period (TP).

Freeze–thaw cycle	**Thaw Period (TP) (hours)**	**Grace Period (GP) (hours)**
1	12	24
3	12	48
5	12	72

3.1.3.3 Oedometer tests

Immediately after mixing, representative specimens from each SDM samples were moulded in oedometer rings of dimensions 40 mm x 20 mm. These specimens were subjected to oedometer tests to assess immediate compression behaviour. Subsequent oedometer tests were carried out on the SDM samples after prescribed curing period. Specimens were obtained by trimming 20 mm height SDM samples from the PVC tubes, which remained after obtaining the specimens for UCS assessments. An oedometer ring with sharp edge at one end was used to trim a required diameter of 40 mm to obtain specimens for the oedometer tests. One–dimensional consolidation tests on the specimens were carried out in standard oedometer tests using sustained increment load (IL) ratio of 1.0. The effective vertical stress of 10 kPa was applied on the specimens during the initial seating. The subsequent effective vertical stresses were obtained by doubling the sustained load to obtain values of 20, 40, 80, 160, 320 and 640 kPa. Each load lasted for 24 hours before subsequent load increment. Thus, the oedometer tests under IL lasted for 7 days. No unloading–reloading tests were performed on specimens.

3.1.3.4 Hydraulic conductivity test

The hydraulic conductivity (HC) tests were carried out on A-BC3 and B-CB7 samples only. This was done to evaluate the influence of single and composite binder (CB) on HC of treated DS. The HC tests were carried out using rigid wall permeater under a constant head method at a hydraulic gradient of about 7 in accordance with ASTM D 5856. Prior to freeze-thaw (f-t) cycles, the baselines HC were established. Thus, curing of these samples took place concurrent with permeation to establish the baseline HC values prior to f-t cycles. Samples were then subjected to 1, 3, 4 and 5 open f-t cycles with intermittent permeation. A preloading weight of 24 kPa was applied during f-t cycles as shown in Fig. 3.7b. This load was utilized to mimic field surcharge of at least 18 kPa, which is normally utilized in Sweden as cover on contained stabilized wastes. At the end of 5 f-t cycles, cylindrical specimens with dimensions 50 mm x 90 mm were extruded, trimmed and subjected to the unconfined compression test at a deformation rate of 0.9 mm/min to determine the UCS values.

3.1.4 Results and discussion

3.1.4.1 Water content

The amounts of binders were estimated based on anticipated water content of the stabilized dredged material (SDM) immediately after mixing (i.e. during induction period). It was hypothesized that dissolution of binder will reduce the water content by the same amount of its own weight. The water content of stabilized mass immediately after mixing would be in accordance with Eq. (7). The estimated amounts of binders are shown in Fig. 3.11(a) as a function of expected water content. Results show that for the same assumed immediate water content, the amounts of binder increased with increasing initial water content of the dredged sediments (DS). This suggests that the use of constant amount of binder at varying initial water content of the DS would result in variations of water content of the SDM. The measured water content values immediately after mixing relative to expected values were presented in Fig. 3.11(b). The discrepancy between the anticipated and measured water content varied with the amount and type of binder. The differences between the anticipated and measured water content values for BC-treated DS during the induction period (0d) ranged between 4.0% and 10.8%, with an average value of 5%. The difference between anticipated and measured water content values during the induction period increased with decreasing amount of Byggcement. This observation was due to increased amount of unbound water, which evaporated during mixing. On the other hand, the deviations of measured water content from assumed values increased with curing period and increasing amount of Byggcement.

This suggests that hydration of cement contributed to reduction of free water. Regardless of the amount of binder, the deviation of measured water content from expected values on CB-treated DS ranged between 2.0 % and 4.0%. The average deviation on DS-A and DS-B were 3.1% and 2.7%, respectively. The measured water content remained almost the same with curing period as shown in Fig. 3.12. This phenomenon indicated that (i) there was a dormant period for hydration reaction of composite binder (ii) water for hydration reactions was drawn from the curing container by capillary action due to under water curing, and the lodged water remained the same. Nevertheless, the immediate water content of the SDM was predicted with reasonable confidence (Fig. 3.11b).

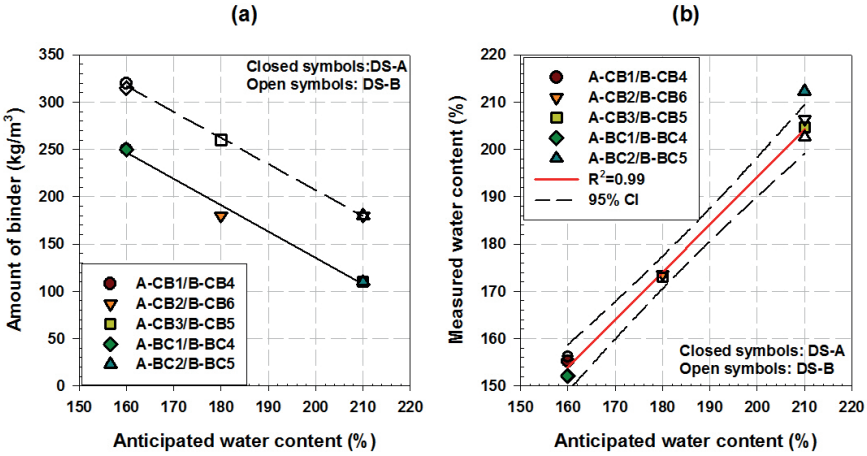

Fig. 3.11: Relations between anticipate water content and (a) estimated amount of binder (b) measured water content during induction period.

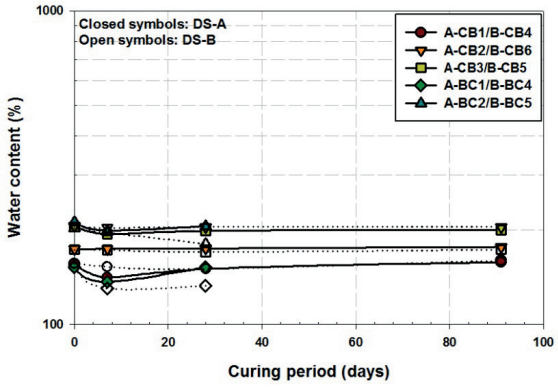

Fig. 3.12. Variations of measured water content during curing period.

3.1.4.2 Unconfined compressive strength

The unconfined compressive strength (UCS) values of studied stabilized dredged materials (SDM) varied with curing period, the type and amounts of binder as shown in Table 3.6 and Fig. 3.13. Except for BC-treated DS, the influence of curing period on strength increase on CB-treated DS was minor. The improved strength for all CB-treated DS occurred during the first 28 days, except for A-CB3 (Fig. 3.13). The amounts of binders were estimated based on the anticipated immediate water content. Results show that for the same immediate water content of the SDM, the UCS values for BC–treated DS were higher than the UCS values for CB–treated DS. The UCS values and water content of BC-treated DS increased and decreased with curing time, respectively. Figure 3.13 shows that at same amount of binder (constant initial water content of DS), the measured UCS value of A-BC1 samples were about 6 times the UCS values of A-CB1 samples (Fig. 3.13a). Likewise, the UCS values of B-BC4 samples were 10 times the UCS value of B-CB4 (Fig. 3.13b). Furthermore, no clear correlations between the amount of CB or water/binder ratio and the achieved UCS values were observed as shown in Fig. 3.14(a) and Fig. 3.15(a), respectively. Figure 3.14(b) and Fig. 3.15(b) show that regardless of initial water content of the DS, the type and amounts of binder, the UCS values increased with increasing cement quantity in the blend (i.e. decreasing water/cement ratio). These results suggest that for prescribed curing period the improved strength of the SDM were due to cement hydration only. Richardson and Groves (1997) observed that regardless of composition of blast furnace slag or fly ash, the main hydration products and principal binding phases in all calcium silicate–based pastes are the calcium silicate hydrate (CSH) gels. Consequently, for minimum UCS of 100 kPa, Fig. 3.15(b) suggests the maximum water/cement (w/c) ratio of 4.5. Accordingly, Fig. 3.15b shows that the UCS could be reasonably predicted by

$$UCS = 50 p_a (w/c)^{-2.6} \quad (10)$$

where:

p_a = atmospheric pressure, kPa,

w/c = water/cement ratio.

Gallavres (1992) presented similar correlation in the form of $UCS = q_0(w/c)^{-n}$, where n = 3 and q_0 = 4000 kPa and 6000 kPa for 7 and 28 days strength, respectively. Lee et al. (2005) observed that water–cement ratio alone is insufficient to account for all salient factors affecting the strength of clay–cement mix. Instead, the relative proportions of all three constituents cement, clay particles and water, is likely to affect the interaction between clay and cement, and thereby the resulting strength. Consequently, Lee et al. proposed that the UCS could be predicted by $UCS = q_0 e^{m(s/c)}(w/c)^{-n}$, where m is a constant, which is equal to 0.6 and s/c is the solid-cement ratio.

Table 3.6. Measured water content and achieved unconfined compressive strength (UCS) values on BC and CB-treated DS during curing period (days, d).

SDM	Water content (%)				Measured UCS (kPa)		
	0	7d	28d	91d	7d	28d	91d
A-CB1	155	141	150	157	45	47	49
A-CB2	174	174	175	177	24	23	28
A-CB3	205	194	199	200	9	14	20
B-CB4	156	152	150	160	26	32	29
B-CB5	206	203	204	204	21	20	24
B-CB6	173	173	170	173	27	28	32
A-BC1	152	137	152	-	288	298	-
A-BC2	212	199	206	-	29	35	-
B-BC4	152	130	133	-	234	282	-
B-BC5	203	196	181	-	34	57	-
B-BC6	125	110	105	-	531	866	-
B-BC7	177	162	147	-	94	107	-
B-BC8	214	224	219	-	20	25	-

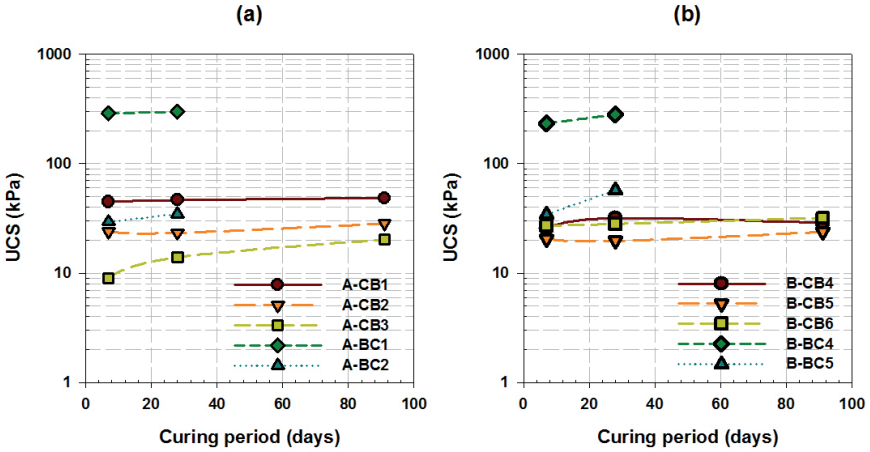

Fig. 3.13. Influence of curing period, type and amounts of binder on unconfined compressive strength of stabilized (a) DS-A (b) DS-B.

Figure 3.16(a) and Fig. 3.16(b) shows that the UCS values increased with decreasing water content and increasing bulk density, respectively. Figure 3.17 show that the UCS values could reasonably be correlated with bulk density/water content (ρ/wc) ratio (Fig. 3.17a) in form:

$$UCS = 2.3e^{A\rho/wc} \quad (11)$$

where:

2.3 = dimensionless constant,

A = a dimensional constant, m^2/s^2. Thus, A is gravitational field strength on untreated dredged sediment at depth z (in Nm/kg) from earth surface (i.e. $A = gz$).

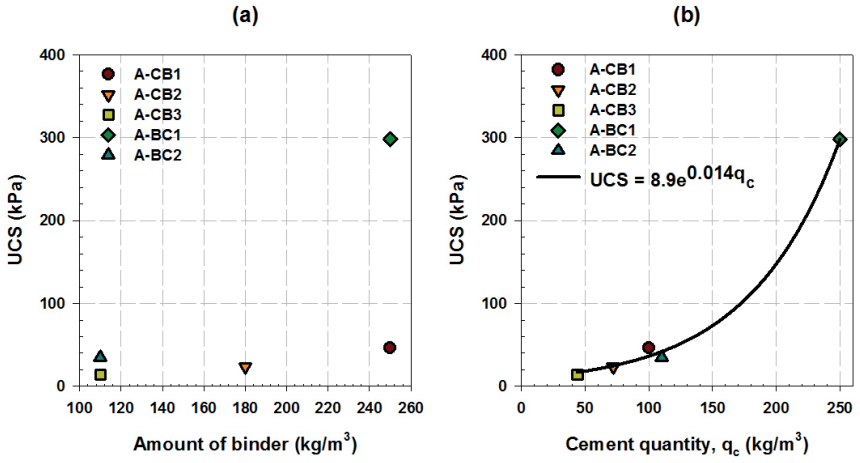

Fig. 3.14. Influence of (a) amount of binder (b) cement quantity on the unconfined compressive strength (UCS).

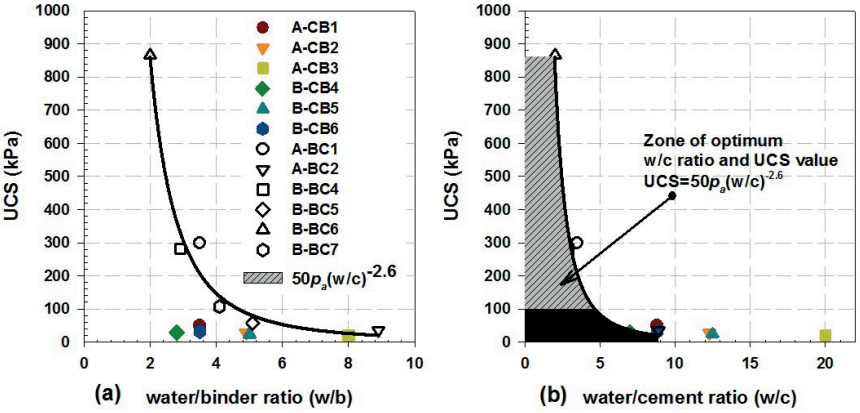

Fig. 3.15. Influence of (a) water/binder ratio (b) water/cement ratio on the unconfined compressive strength (UCS).

The improved strength of the studied DS was due to the hydration of cement. Consequently, Fig. 3.17(b) indicates that the UCS could be estimated based on the cement quantity in the blend by

$$UCS = 14.3e^{Bq_C} \quad (12)$$

where:

14.3 = dimensionless constant,

B = gravitational field strength on blended mix, Nm/kg.

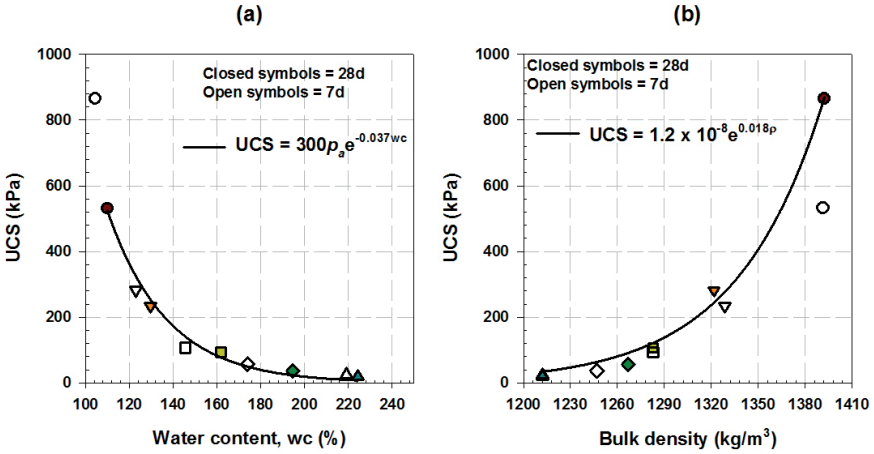

Fig. 3.16. Variations of unconfined compressive strength with (a) water content (b) bulk density on BC-treated DS-B.

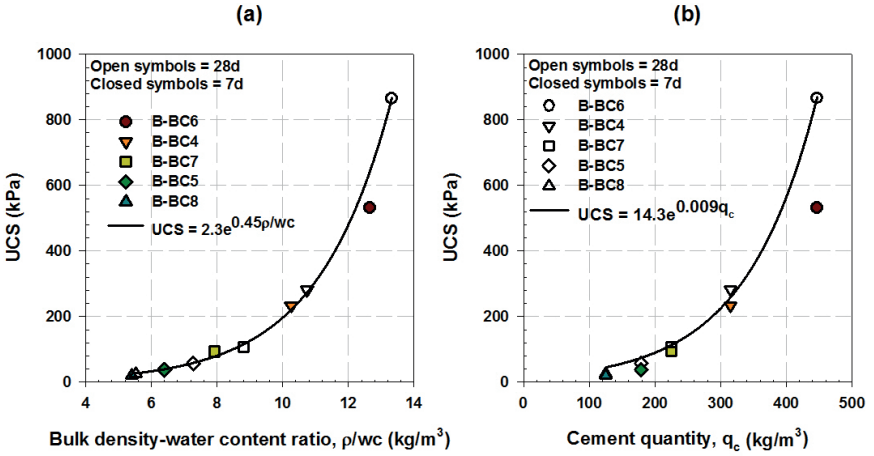

Fig. 3.17. Relationship between the unconfined compressive strength and (a) bulk density-water content ratio (b) cement quantity.

By Eq. (11) and (12), the UCS value of stabilized dredged sediments comprised of two strength components in form:

$$UCS = 1.15e^{A\rho/w} + 7.15e^{Bq_C} \quad (13)$$

The first term to the right hand of Eq. (13) refers to the strength of soft soils deposit to support its own weight and other limited loads. This strength was referred to as the gravitational field strength. The second term refers to the improved strength as result of additions of cement/binder.

This component of strength was referred to as improved strength, which depends on the type and amounts of binders. Regardless of the amount of composite binder (CB), results of this study show that most of achieved improved strength on CB-treated DS was due to cement hydration. Furthermore, the measured UCS on both CB and BC-treated DS decreased with increasing w/c ratio (Fig. 3.15). The minimum UCS of 100 kPa could be achieved at w/c ratio of 4.5. Consequently, improved strength of high water content dredged sediment depends on the amount of cement in the blend.

Within the scope of this study, the following are the two main factors that contributed to low amount of cement or increased water/cement ratio:

- Partial substitution of cement for fly ash or blast furnace slag decreased the amount of cement in the mix. As a result, water/cement ratio increased.
- underwater discharge of the SDM immediately after mixing contributed to increased water/cement ratio and minor reduction of lodged water during curing (Table 3.6). The anticipated water content DS remained almost the same during curing, especially for CB-treated DS. This suggests absence of hydration reaction, which is supported by dormant period for strength development (Fig. 3.13).

Other physicochemical factors that influenced strength development of composite binder-treated DS with physical properties shown in Table 3.2 were discussed in Paper I.

3.1.4.3 Compressibility behaviour

The compressibility of treated and untreated dredged sediments were evaluated in terms of stress-strain ($\varepsilon - log\sigma_v'$) and stress-modulus ($M - \sigma_v'$) relationships. The vertical strain for untreated DS increased linearly with applied effective vertical stress up to a value of 80 kPa. Surprisingly, no further vertical deformation were recorded with increasing effective vertical stress beyond 80 kPa (Fig. 3.18). At the end of consolidation test, the average water contents of untreated DS were found to be 81% and 77% for DS-A and DS-B, respectively. These values were below the plastic limit values of the untreated DS (Table 3.2). It follows that the DS were in solid or semi-solid state, which increased resistance to compression under subsequent load increment. Seemingly, the maximum effective vertical stress, which was required to reduce the initial water content of the untreated DS to a value below plastic limit, defined the apparent preconsolidation stress of treated DS.

The tangent modulus values were evaluated on both treated and untreated DS and for each load step. The evaluated maximum tangent modulus values on untreated DS were about 6000 kPa at change in effective vertical stress from 40 kPa to 80 kPa (Fig. 3.18).

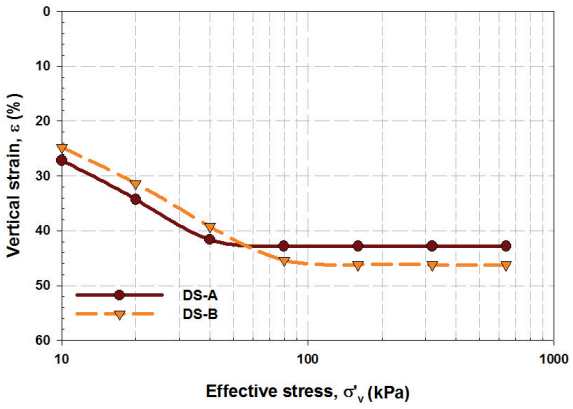

Fig. 3.18. Stress-strain curves for untreated DS.

Unlike the shape of $\varepsilon - log\sigma_v'$ curves of untreated DS, the shape of $\varepsilon - log\sigma_v'$ curves for treated DS varied with curing period, type and amounts of binder. For the same curing period, the shape of the stress–strain curves were influenced by the type and amounts of binders. Based on the deformation properties of treated DS, three phases of hydration mechanism that influenced the compressibility of the studied SDM were identified. These are induction phase (IP), nucleation and crystallization phase (NCP), and hardening phase (HP). Table 3.7 presents distinguishing characteristic associated with IP, NCP and HP, which affect compressibility of the SDM as described in Paper II and hereafter:

Induction phase

Specimens were considered in induction phase (IP) when subjected to oedometer tests immediately after mixing. In relation to the stress-strain curve of untreated DS, Fig. 3.19 presents the stress-strain curves of treated DS subjected to the oedometer tests immediately after mixing. Generally, irrespective of the type and amounts of binders, the shape of stress–strain curves for treated DS showed a well–defined break in the $\varepsilon - log\sigma_v^{'}$ curves (Fig. 3.19). Relative to the vertical deformation of untreated DS, the vertical deformations of treated DS were all reduced. The magnitude of reduced vertical deformations of treated DS varied with the amounts of binder. The reduction in immediate vertical deformations could be a result of slow hydration of binder.

Researchers (Ogawa et al., 1980; Yousuf et al., 1995) have shown that immediately after mixing (i.e. induction period) a thin protective layer of calcium silicate hydrate (CSH) is formed around cement particle's surface. During this period, calcium silicate minerals dissociates into charged silicates and calcium ions. The charged silicate ions concentrate as a thin layer on the surface of cement grains to prevent the interaction of the cement surface with water. This mechanism of hydration process caused delay in fully hydration of binder. According to Sherwood (1993) hydration is a slow process proceeding from the surface of the cement grains while the centre of the grains may remain unhydrated. Consequently, the unhydrated portion of the binder behaved like a solid particle, which increased resistance to compression. Thus, the immediate vertical deformations were significantly reduced depending on the amount of unhydrated binder particles.

Table 3.7 Distinguishing characteristics associate with IP, NCP, and HP that affect the compressibility of the SDM.

Phase	***Characteristics***
IP	i. Occurs immediately after mixing. ii. A protective layer is formed on the particle surface of binder, which prevent penetration of water. iii. The unhydrated portion of the binder behaves like solid particles, which increase resistance to compression. iv. Tangent modulus increases due to increasing resistance to vertical deformation. v. The maximum effective vertical stress, which is required to reduce the initial water content of untreated dredged sediments (DS) to a value below plastic limit, defines the apparent preconsolidation stress of the SDM. vi. Sensitive clay behaviour describes the compressibility of the SDM.
NCP	i. Occurs when the protective layer become more permeable, which allows penetration of water molecules. ii. Plasticity of the treated DS decreases due to increasing plastic limit. iii. Loss of the apparent preconsolidation stress and tangent modulus occurs. iv. The tangent modulus increases about linearly with applied effective vertical stress. v. Normally consolidated clay settlement behaviour dictates the compressibility behaviour of the SDM.
HP	i. Occurs as a result of solidification, hardening, and loss of plasticity on protective layer. ii. Protective layer become impermeable and water may become lodged in. iii. The apparent preconsolidation stress has increased to the value equal to the UCS. iv. The tangent modulus increases exponentially with applied effective vertical stress. v. The ultimate vertical deformation is controlled by the tangent modulus of untreated DS, at applied effective vertical stress in excess of increased preconsolidation pressure. vi. Silt-sand soil compression behaviour describes the deformation behaviour of the SDM.

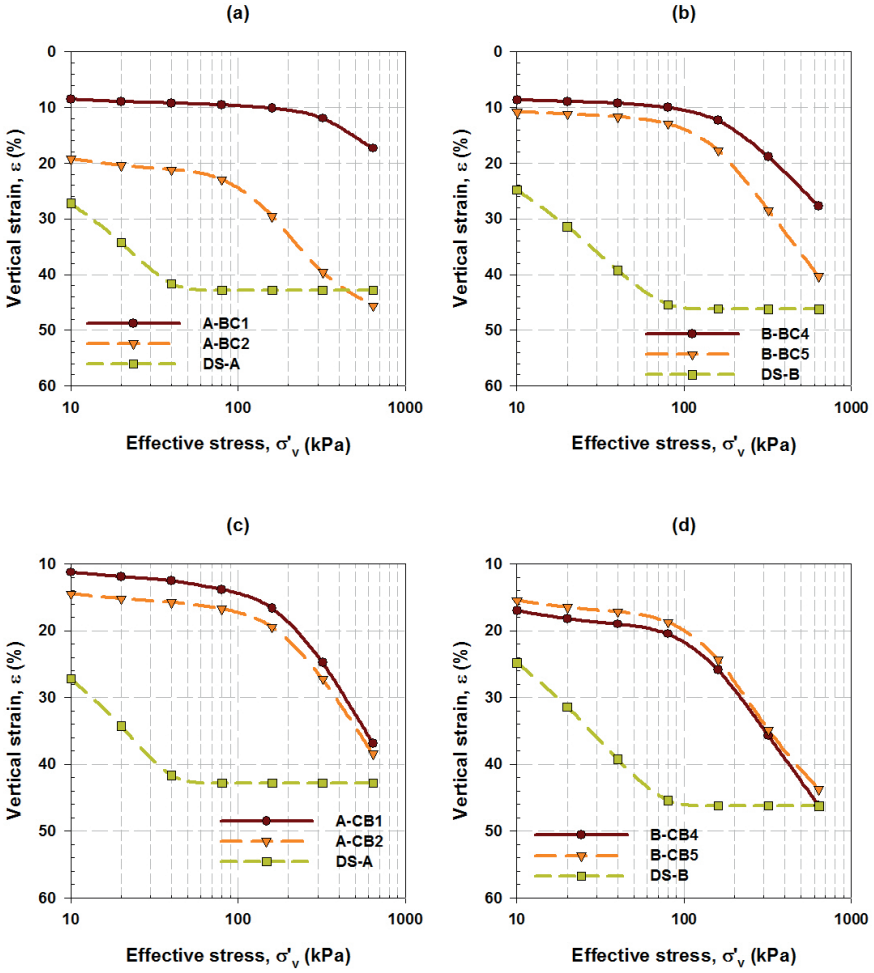

Fig. 3.19. Example of Stress–strain curves for SDM subjected to oedometer tests during induction phase (IP).

Significant reductions in vertical deformations for all samples were observed during initial seating under applied effective vertical stress of 10 kPa as shown in Fig. 3.19. However, regardless of type and amount of binder, increased vertical deformations were observed for applied effective vertical stress above 80 kPa (Fig. 3.19). Thus, during IP, the SDM showed rigidity behaviour at applied effective vertical stress between 20 kPa and 80 kPa. Compressibility behaviour occurred under applied effective vertical stress above 80 kPa. Åhnberg (2007) reported that stabilized soils behaved in overconsolidated manner when the consolidation stress was less than the preconsolidation pressure. And, in normally consolidated manner when the utilized consolidation stress was higher than the preconsolidation stress.

It can be assumed that during the IP the preconsolidation stress of the SDM was equal to 80 kPa. This value was equal to the maximum effective vertical stress value that was required to reduce the water content of the untreated DS to a value below the plastic limit. Accordingly, the increased vertical deformations could be associated with increased plastic limit of the DS due to addition of binders. Regardless of the type and amount of binder, the measured water content values for all treated DS were above plastic limit as shown in (Table 3.6). Sherwood (1993) observed that addition of lime will increase plastic limit of treated soils. Although lime was not directly utilized in this study, cement hydration produces lime as calcium hydroxide (CH). Chrysochoou et al. (2010) showed that low cement dosage contains inadequate free lime. Sherwood (1993) reported that at lime content below 4%, the plastic limit of lime-treated soil increases significantly and remained almost constant with increasing percentage of lime above 4%. Thus, samples with low amount of cement contained low amount of lime. Consequently, the plastic limit on these samples increased considerably. As a result, increased vertical vertical deformations of the stabilized mass at applied effective vertical stress above the preconsolidation stress σ_c' occurred.

Regardless of the amount of binder, significant compression on all treated DS occurred at applied effective vertical stress above 80 kPa. In Sweden, a preloading weight of 18 kPa is normally applied immediately after mixing. However, the amount of weight for subsequent preloading is not defined. Based on these test results, effective vertical stress below apparent preconsolidation stress during subsequent application of preloading weight can be considered insufficient to compress the stabilized mass in IP. Furthermore, test results show that for sufficient compression, selected preloading weight must be applied all at once immediately after mixing. The practical implication for this observation is that under insufficient compression of the SDM, hardening of binder paste (CSH membrane) will take place at insufficient packing of blended DS particles. The ultimate effect becomes an increased void ratio and formation of metastable fabrics in the SDM. Mitchell and Soga (2005) observed that soil metastable structure occurs when particles and particle groups flocculate and pack inefficiently, which is a typical characteristics of sensitive clay soils. Sensitive clay soils are characterized by high voids ratio, low hydraulic conductivity or undrained condition. The compressibility of sensitive clays is relatively low until the consolidation pressure exceeds the preconsolidation stress (Mitchell and Soga 2005). Thus, it can be concluded that sensitive clay behaviour describes the compressibility of the SDM during the IP. According to Janbu (1998), the stress exponent in Eq. (2) for sensitive clay is between -0.5 and -0.3.

Irrespective of the type and amounts of binders, the $\sigma_v' - M$ curves for all specimens subjected to oedometer test immediately after mixing were characterized by an increase in tangent modulus to the maximum value M_m followed by abrupt drop to lower modulus M_L value (Fig. 3.20).

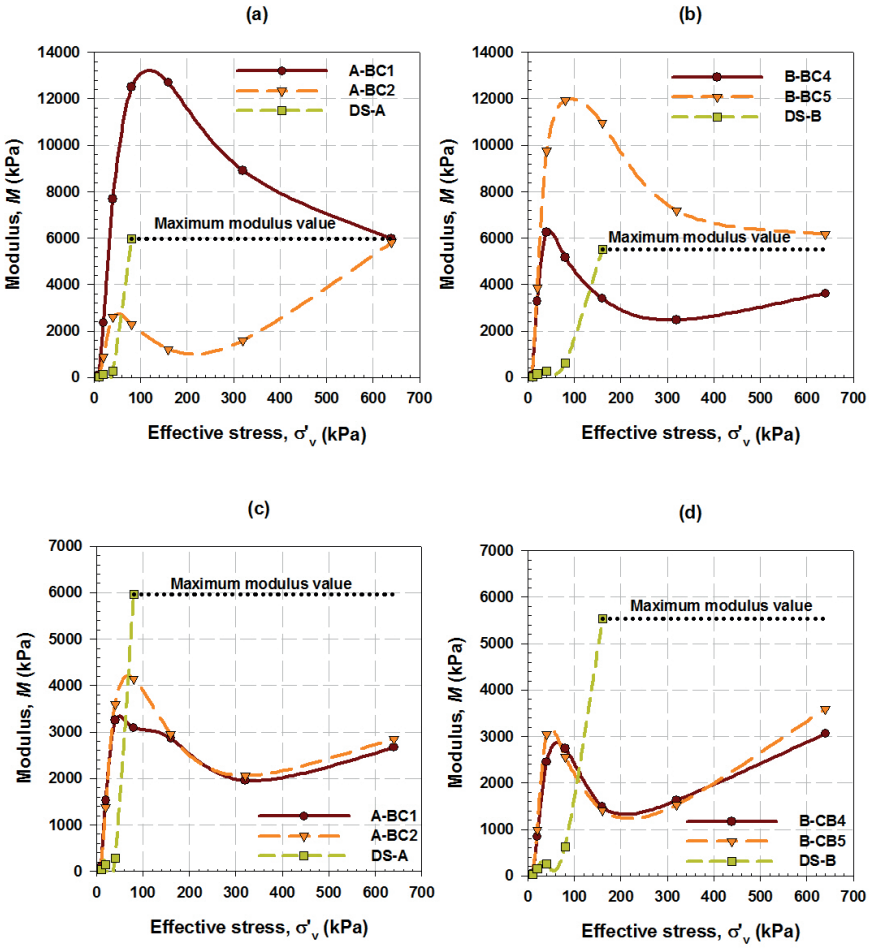

Fig. 3.20. Example of stress–Modulus behaviour for SDM subjected to oedometer tests during induction phase (IP).

Specimens, which exhibited increased in tangent modulus with maximum value above 6000 kPa followed by a sudden drop, the tangent modulus further decreased with increasing effective vertical stress above 80 kPa. The trend indicated decreasing tangent modulus toward a constant value of about 6000 kPa as shown in Fig. 3.20(a and b). On the other hand, for specimens that exhibited increased tangent modulus *M* with maximum value below 6000 kPa prior to a sudden drop, the modulus increased again with increasing applied effective vertical stress above 80 kPa. The trend indicated increasing modulus to a common value of about 6000 kPa as shown in Fig. 3.20. The evaluated tangent modulus values varied significantly without clear correlation between the computed tangent modulus and type or the amount of binders.

Nonetheless, the maximum initial tangent modulus values (prior to a sudden drop) for these specimens were obtained at effective vertical stress around 80 kPa. It can be assumed that the maximum effective vertical stress, which was required to reduce the initial water content of the untreated DS to a value below plastic limits, defined the apparent preconsolidation stress of treated DS. Furthermore, According to Janbu (1967), the constrained modulus for sensitive clay tends to drop abruptly when the applied surcharge approaches the preconsolidation stress σ_c' value. Consequently, it can be concluded that the apparent preconsolidation stress and tangent modulus of untreated DS determined the compressibility of the SDM during IP.

Nucleation and crystallization phase

The induction period (IP) ends when the protective layer changes to a more permeable membrane, which permits inward flow of water molecules, and outward migration of calcium ion and silicate ions. This results in accumulation of excess amount of calcium hydroxide (CH) on the fluid side of the membrane (nucleation) and precipitation (crystallization) of the CSH (Ogawa et al., 1980; Yousuf et al., 1995).

Regardless of the shape of $\varepsilon - log\sigma_v'$ curves (Fig. 3.21), specimens were considered in nucleation and crystallization phase (NCP) when the evaluated modulus values were below that of untreated DS (i.e. 6000 kPa), and indicated increasing trend in $\sigma_v' - M$ curves. Irrespective of the amount of binder, the evaluated modulus values for all CB–treated DS were below 6000 kPa during the curing period of up to 91 days. The compression modulus increased about linearly with effective vertical stress above apparent preconsolidation stress as shown in Fig. 3.21(c and d). The $\sigma_v' - M$ relationships for these specimens during NCP could be idealized as linear with effective vertical stress as shown in Fig. 3.22 (c and d). This behaviour is a typical characteristic of normally consolidated clay. According to Janbu (1998), for normally consolidated clay the modulus increases linearly with effective vertical stress change when the effective vertical stress is greater than the preconsolidation stress, and the stress exponent in Eq.(2) is set to 1.0. Thus, it can be concluded that normally consolidated clay behaviour characterized the SDM in NCP.

Specimens in NCP showed little or no increase in initial tangent modulus. In other words, these samples were characterized by loss of apparent preconsolidation stress σ_c' and tangent modulus M. However, the vertical deformations during initial seating under 10 kPa were significantly reduced. The reductions in initial compression were mainly due to initial consolidation under preloading weight of 22 kPa. This phenomenon suggests that after application of the initial preloading weight, subsequent application of consolidation stress of magnitude, which is less or equal to the initially applied preloading weight will has no influence on increased compression.

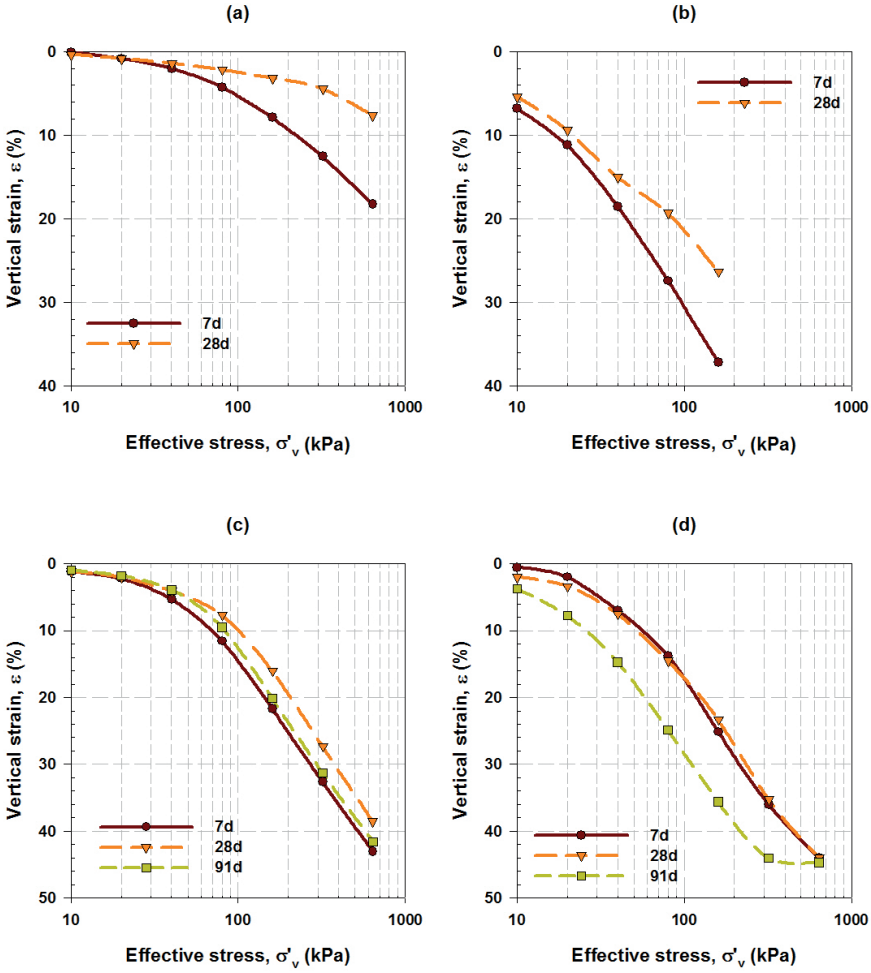

Fig. 3.21. Example of stress–strain curves for SDM subjected to oedometer test during NCP (a) A-BC2 (b) B-BC2 (c) A-CB1 (d) B-CB2.

Results from consolidation test study show that for sufficient compression, selected preloading weight must be applied all at once immediately after mixing. The loss in preconsolidation stresses and overconsolidated modulus could be related to the weakening effect of water on CSH membrane due to increased amount of lodged water and slow dissipation of pore water because of decreased hydraulic conductivity. Åhnberg (2006) observed that specimens with low strength due to either a very short period of curing time or stabilized with ineffective binder, were regarded as normally consolidated when consolidated for effective stress high than the apparent preconsolidation stess.

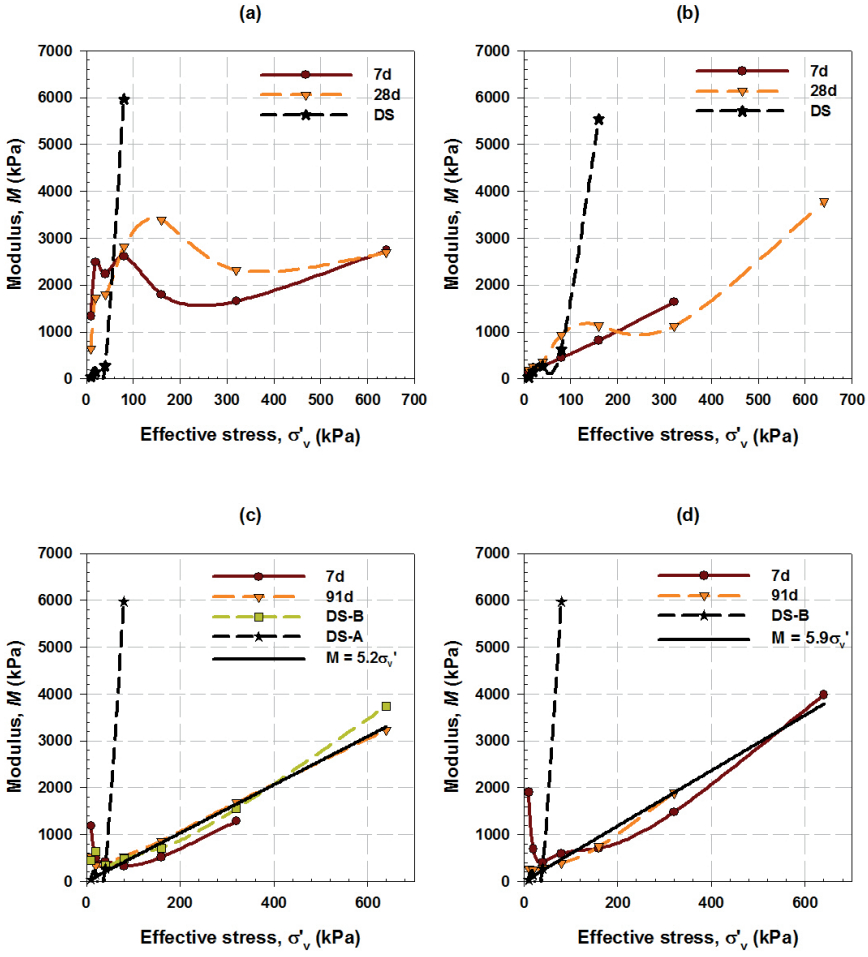

Fig. 3.22. Example of stress–Modulus behaviour for SDM subjected to oedometer test during NCP. (a) A-BC2 (b) B-BC2 (c) A-CB1 (d) B-CB2.

Wang et al (2011) observed that the increased amount of free water caused weakening effect on the CSH. Hwang and Shen (1991) reported that at high water content, increased moisture surrounding the grains requires greater time for the formation of rigorous structural network of hydrates which will eventually fill voids. As a result of decreased hydraulic conductivity, dissipation of pore pressure under increment load was impaired. Consequently, the water content of the SDM remained well above plastic limit and the vertical deformation increased with increasing applied effective vertical stress.

Hardening phase

Hardening phase (HP) is associated with significant increase in thickness and stiffness or solidifying of the protective layer. As a result, resistance to vertical deformations will increase. This phenomenon results in increased compression modulus regardless of the shaper of stress-strain curves. Thus, all specimens with evaluated modulus in excess of 6000 kPa were considered in hardening phase (HP).

All specimens with evaluated maximum modulus in excess of 6000 kPa were considered in hardening phase (HP). The $\sigma_v' - M$ relationship for these specimens were characterized by exponential increase in modulus followed by decrease when the modulus exceeded the magnitude of 6000 kPa as shown in Fig. 3.24. According to Janbu (1998), the modulus for silt sand varies with the effective vertical stress raised to power of 0.5. Thus, it can be concluded that the compression behaviour of silt sand defines the compressibility of the SDM in the hardening phase (HP).

The decrease in modulus that can be realized in Fig. 3.24 could be due to breakage or collapse of protective layer (CSH bonds) at applied effective vertical stress higher than the apparent preconsolidation stress. This observation suggests that the preloading weight of 22 kPa was not sufficient for particle groups of blended DS to flocculate and pack efficiently. As a result, the HP occurred under insufficient packing, which caused formation of metastable structure in the SDM as discussed under IP. Although during the HP phase, the preconsolidation stress had increased by a set amount to a value of 320 kPa. However, when effective vertical stress in excess of increased preconsolidation stress was applied, the metastable fabric collapsed causing sudden drop of the tangent modulus. Consequently, the tangent modulus of the untreated DS determined the maximum deformation of the SDM. Consequently, it might be beneficial to utilize the tangent modulus of untreated DS to estimate the maximum deformations of treated DS especially, when the preconsolidation stress of the SDM becomes uncertain. Topolnick (2004) observed that any safe design will require that the stresses inside the stabilized soil body do not exceed the capacity of soil–binder material. According to EuroSoilStab (2002), the hardening of cement will glue soil particles together but it will not change the structure of the soil.

3.1.4.4 Hydraulic conductivity

Hydraulic conductivity (HC) of the stabilized mass varied with type of binder. The HC of Byggcement (BC)–treated DS was slightly higher than that of composite binder (CB)–treated DS.

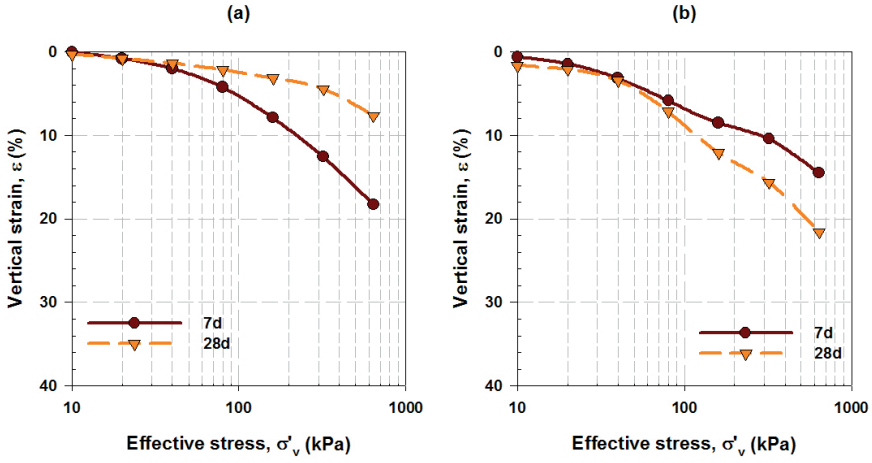

Fig. 3.23. Example of stress–strain curves for SDM with increased amount of BC subjected to oedometer test during curing. (a) A-BC1 (b) B-BC1.

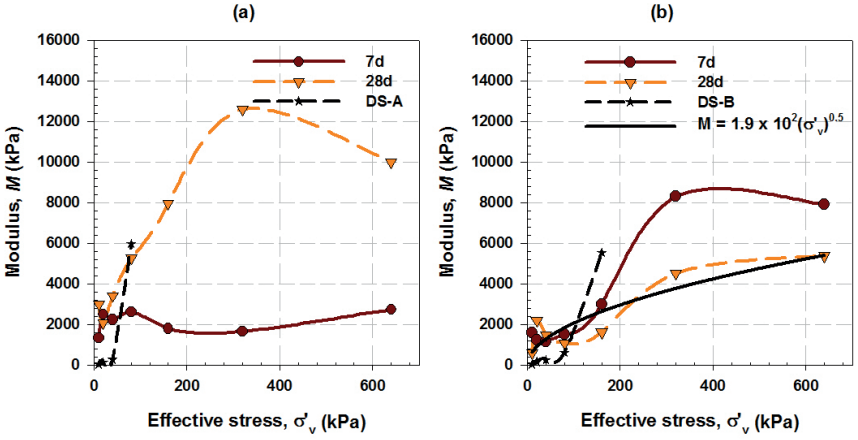

Fig. 3.24. Example of stress–Modulus behaviour for SDM with increased amount of BC subjected to oedometer test during HP. (a) A-BC1 (b) B-BC1.

As shown in Fig. 3.25, the baseline hydraulic conductivity value of 4.8 x 10^{-8} m/s for A-BC3 sample could be established after the first 7 days of curing. The baseline hydraulic conductivity value of around 2.6 x 10^{-8} m/s for B-CB7 could be established after at least 25 days of curing. These periods coincide with the curing time for which most of improved strength on CB and BC-treated DS occurred (Fig. 3.13). Thus, the steady state condition of HC could be utilized to indicate dormant period or end of hydration reaction for strength development.

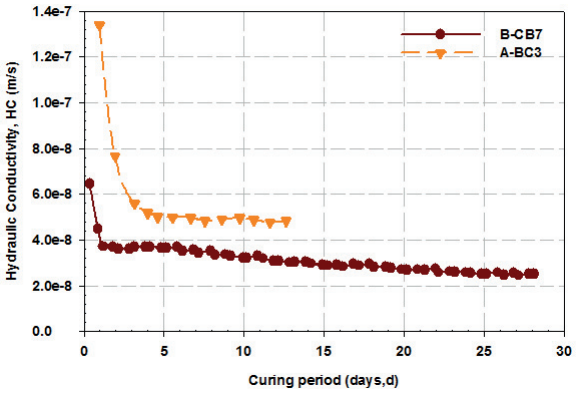

Fig. 3.25. Hydraulic conductivity of single and composite binder–treated DS.

The lowest HC value was measured on sample B-CB7 (Fig. 3.25) probably due to the presence of fly ash and GGBS. Marsh et al. (1985) observed that fly ash in general can cause substantial reduction in HC of unfrozen stabilized soils. The high HC value on A-BC3 sample may have been contributed by cement hydration, which causes aggregation of particles and increased pore sizes. According to Quang and Chai (2015), the HC of a porous medium is a function of the microstructure of the pores (sizes and distributions) and pore water properties. Hydration of cement agglomerates several small aggregates into a large one. Larger pore size and uniform pore distribution are associated with high HC values (Paper III and Paper IV). Likewise, cement-treated dredged sediments with high water content may have a higher concentration of Ca^{2+} and, a thinner diffusive double layer, which tend to exhibit a higher hydraulic conductivity compared to thicker diffusive double layer (Quang and Chai, 2015).

According to researchers (Vapali et al. 1999; Nagaraj and Miura, 2001), fine-grained soils have two levels of structure, microstructure and macrostructure level, both of which are present in natural and compacted clay soils. Regardless of identical mineralogy, texture and method of preparation, the resulting macrostructure of the specimens prepared at different initial water content is different. The structure and aggregation of fine-grained soil is highly influenced by the initial or molding water content. Clay soils with high initial water content are more homogeneous with the large pore spaces not interconnected or in a closed state. These specimens offer more resistance to water flow. Consequently, the microstructure of specimens compacted wet of optimum water content controls the water flow (Paper IV).

Specimens with low initial water content (i.e. dry of optimum water content) contain relatively large pore spaces, which are located between the clods of the soil. Thus, the macrostructure controls the initial discharge. Benson and Daniel (1990) studied the influence of clods on hydraulic conductivity of unfrozen highly plastic clay. Their results show that the outcome of clods and inter-clods pores occurring during soil processing and compaction controlled the hydraulic conductivity of the compacted soil. The clod size had a large influence on the hydraulic conductivity of the compacted soils.

3.1.4.5 Durability

The change in baseline hydraulic conductivity (HC_0) and the unconfined compressive strength (UCS) values of stabilized dredged materials (SDM) were used as indirect measure for resistance to repetitive freeze–thaw (f-t) cycles. The HC_0 values were 4.6×10^{-8} m/s and 2.6×10^{-8} m/s for A-BC3 and B-CB7 samples, respectively (Fig. 3.25). These samples were subjected to 1, 3, 4, and 5 f-t cycles with intermittent permeation. Results show that the HC values for A-BC3 sample remained almost same during intermittent permeations following 1, 3, 4, and 5 f-t cycles as shown in Fig. 3.26. On the other, the HC values for B-CB7 sample decreased by a factor of 0.3 of the baseline value after 1 f-t cycle. During subsequent f-t cycles, the HC values for this sample increased by a factor of 1.7, 2.3 and 3.5 times the baseline value after 3, 4 and 5 f-t cycles, respectively (Fig. 3.26).

The control strength (CS) values for specimens from A-CB2 and B-CB5 samples were 28 kPa and 24 kPa, respectively (Table 3.6). Due to low UCS values on A-CB2 and B-CB5, only specimens from A-CB2 sample were subjected to three consecutive open f-t cycles for assessing preliminary results. Regardless of number of f-t cycles, specimens from A-CB2 sample were subjected to the grace period for thaw consolidation (TC) of 24 hours only. These specimens showed healing potential on damaged A-CB2 samples during 24 hours of grace period. However, it was found that the grace period for TC should be defined based on the number of f-t cycles and thaw period (TP) (Fig. 3.10). For this reason, the UCS results from A-CB2 sample were not included. The average control UCS values for specimens from A-BC3 and B-CB7 samples were 299 kPa and 87 kPa, respectively. Accordingly, B-CB7 samples were subjected to 1, 3 and 5 f-t cycles. Specimens from A-BC samples were subjected to 3 consecutive open f-t cycles to evaluate healing potential on the SDM with increased UCS value.

The unconfined compressive strength (UCS) indicated decreased values for all specimens tested immediately after thaw (i.e. during thaw weakening, TW) under both open and semi-closed freezing conditions as shown in Fig. 3.27. Results show that the measured UCS values for specimens from B-CB7 sample under open f-t conditions decreased by 41%, 65% and 33% after 1, 3 and 5 f-t cycles, respectively (Fig. 3.27a). The measured UCS values under semi-closed f-t system decreased by 54%, 80% and 73% of the CS value after 1, 3 and 5 f-t cycles, respectively (Fig. 3.27b). As anticipated, the measured UCS values on samples tested after a grace period for thaw consolidation (TC) indicated improved strength.

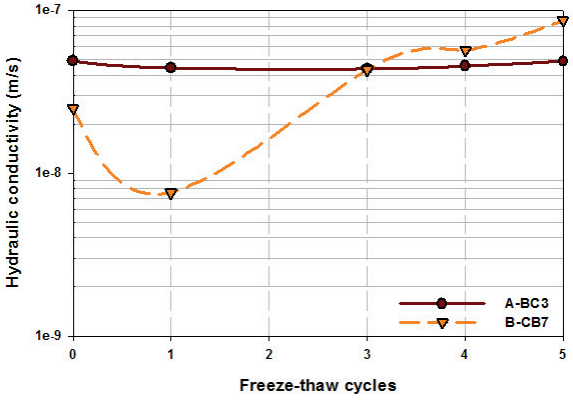

Fig. 3.26. Variations in hydraulic conductivity of treated DS due to freeze-thaw cycling.

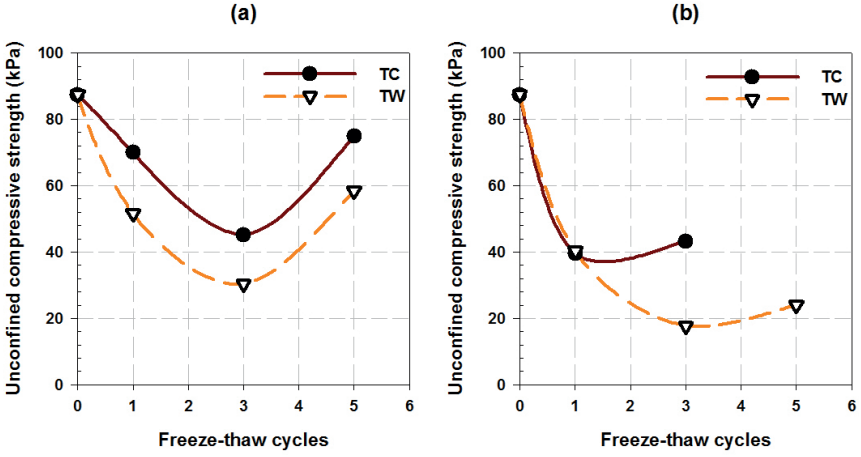

Fig. 3.27. Impact of freeze–thaw weakening (TW) and thaw consolidation (TC) on the average unconfined compressive strength of B-CB7 sample under (a) open freeze–thaw systems (b) semi-closed freezing systems.

The measured UCS values for specimens from B-CB7 sample during TC showed decreased values by 20%, 48% and 14% after 1, 3 and 5 open f-t cycles, respectively. For B-CB7 sample under semi-closed f-t system, no significant gain in the UCS value was observed after 24 hours of TC. However, after 3 f-t cycles and 48 hours of TC, specimens from B-CB7 sample under semi-closed f-t conditions indicated significant gain in the UCS value. The measured UCS value on this sample after grace period for TC was 46 kPa compared to 18 kPa, which was measured during TW as shown in Fig. 3.27b. Specimens for the UCS assessment after 5 f-t cycles under semi–closed f-t system failed during freezing action due to rupture of PVC tube. Nonetheless, these results suggest that thaw consolidation (TC) may act as healing phase after detrimental effects of freezing action have taken place. Furthermore, under semi-closed f-t systems, TC can be limited.

The stress–strain curves for specimens from sample B-CB7 and A-BC3 are shown in Fig. 3.28 and Fig. 3.29, respectively. In Fig. 3.28(b) and Fig. 3.29(b), the stress–strain curve for samples B-CB7 and A-BC3, which were subjected to 5 f-t cycles concurrent with HC measurement, are also presented. The stress-strain curves for specimens tested during TC indicated brittle behaviour compared to those tested during TW. Furthermore, the stresses at failure on these specimens were comparable to the stresses at failure on specimens, which were packed in PVC tubes for assessing the UCS only. These results indicate consistency behaviour of the SDM samples under open f-t conditions. Thus, the grace period (GP) for TC can be implemented either intermittently (i.e. between f-t cycles) or at the end of prescribed f-t cycles.

Failure modes

The failure modes for all specimens tested during thaw weakening (FTW) were dominated by bending and buckling of specimens, without definite failure plane (Fig. 3.30 and Fig. 3.31). Under both open and semi-closed freeze–thaw systems, buckling of specimens was more dominant after 3 f-t cycles (FTW3) as shown in Fig. 3.30 and Fig. 3.31. The lowest UCS values were also measured after the same number of freeze–thaw cycles under both freeze-thaw conditions (Fig. 3.27). This phenomenon could be associated with increased amount of released water, which caused undrained conditions. Physical observation indicated surface moist on the SDM samples during unconfined compression tests as shown in Fig. 3.30 (e.g. FTW3). Thus, specimens experienced an increased excess pore pressure due to undrained condition. All specimens tested after grace period for thaw consolidation (FTC) developed fully and well–defined transverse failure plane with little or no surface moist as shown in Fig. 3.30 and Fig. 3.31.

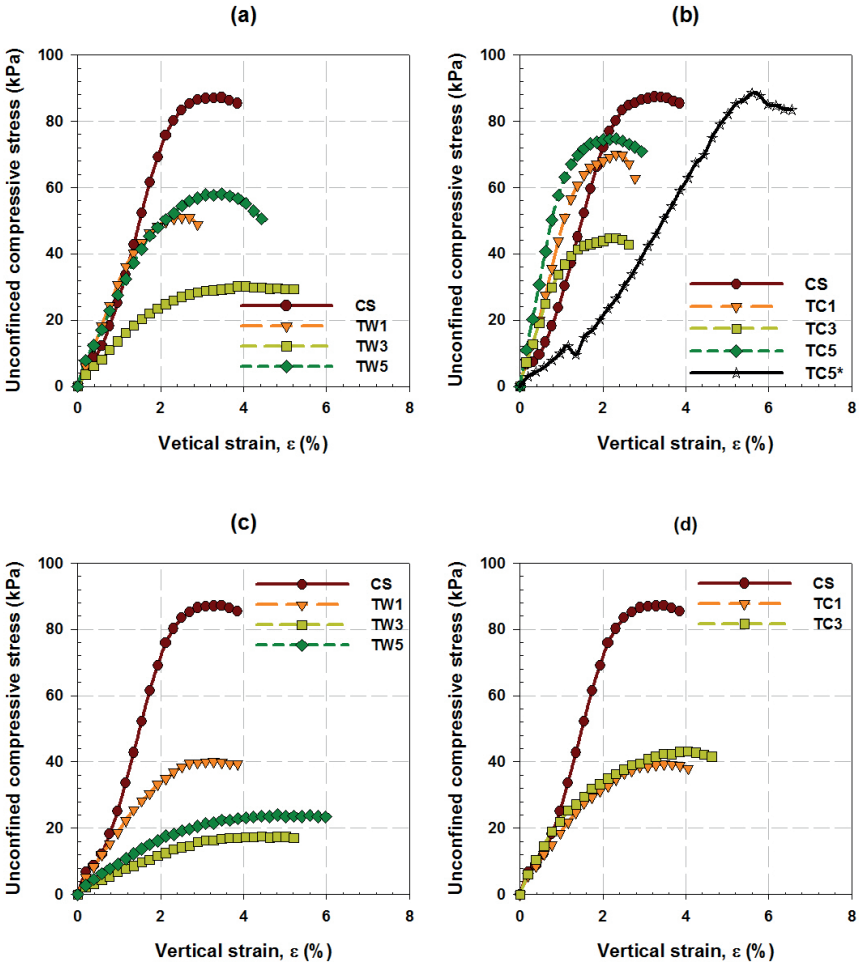

Fig. 3.28. Stress-strain curves for B-CB7 samples during (a and c) thaw weakening (TW) and (b and d) thaw consolidation (TC) after 1. 3, and 5 open freeze-thaw cycles.

Repetitive freeze-thaw cycling was found to have detrimental effect on stabilized dredged materials (SDM). Results show that the effect of freeze–thaw cycles on the UCS of the SDM depends on the type of binder, freezing system, time of testing (Paper III), and water content in relation to the hydraulic conductivity (HC) as described hereafter with the help of a conceptual model.

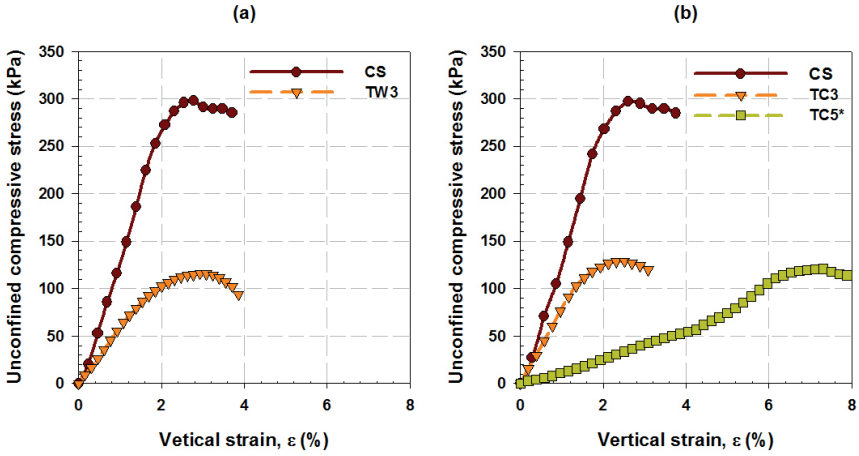

Fig. 3.29. Stress-strain curves for A-BC3 samples during (a) thaw weakening (TW) and (b) thaw consolidation (TC) after 3 open freeze-thaw cycles.

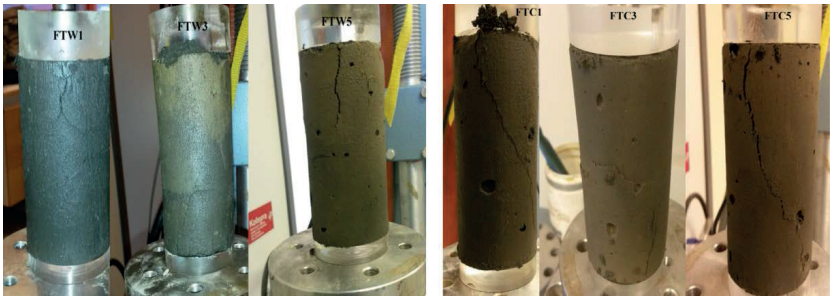

Fig. 3.30: Typical failure features during unconfined compression test during thaw weakening (TW) and consolidation (TC) after 1, 3 and 5 open freeze-thaw cycles on B-CB7.

Fig. 3.31. Typical failure features during unconfined compression test for specimens tested during thaw weakening (TW) and consolidation (TC) after 1, 3 and 5 semi-closed freeze-thaw cycles on B-CB7.

Effect of hydraulic conductivity on strength

Freeze-thaw (f-t) process induces phase changes of water without dehydration (Paper V). The SDM with low hydraulic conductivity (HC) and increased amount of freezing water will experience significant loss in strength with prolonged thaw weakening regardless of achieved UCS values. Jamshidi and lake (2015) reported decreased HC values (i.e. improved performance) hand in hand with reduction of 30% in UCS value (i.e. performance degradation). If the hydraulic conductivity is significantly low, the water released during thaw will generate excess pore pressure during loading (Simonsen et al. 1999). As a result, failure will occur under undrained condition and the measured strength will show decreased values. According to Knutsson (1983), the water accumulated as ice during freezing is released during thaw. Depending on the hydraulic conductivity, the released water can be trapped within the soil. Increased water content leads to a potential risk of water saturation and high pore pressure, which in turn reduces the shear strength of soil. On the other hand, increased initial water content or pore water will favor decreased HC (Makusa et al. 2012; Vappali et al. 1999). The SDM will be filled with water, which is released during thaw. As a result, during permeation the rate of inflow will be higher than the outflow. Prolonged thaw (thaw consolidation, TC) allows released water to dissipate and reduce the amount of free water, which in turn reduces the excess pore pressure and increases effective stress. It follows that, during loading, the rate of dissipation of excess pore water pressure turns out to be proportional to the rate of loading. Consequently, the effect of undrained condition becomes insignificant. Knutsson and Rydén (1984) reported that if the HC value is high, the water will drain at the same rate as new water is released, and the decrease in strength of the soil will be limited. This argument is supported by the HC test results presented in Fig. 3.26 in relation to UCS values in Fig. 3.28 and Fig. 3.29. It is obvious that the measured UCS values were related to the HC values. As a result of increased HC value on B–CB7 sample, the measured UCS value approached the control strength (CS) value (Fig. 3.28a). The HC for A-BC remained almost the same; consequently, the UCS value was reduced by 60% of the CS (Fig. 3.29b). Jamshidi and Lake (2015) reported increased HC value of up to 50 times baseline value hand in hand with a strength gain of about 14% on compacted stabilized sand. Guthrie et al. (2012) observed that for cement–treated soils, there can be a correlation between the UCS and HC values.

Conceptual model

The loss in strength is attributed to the amount of released water during thaw weakening in relation to the HC of the SDM. If the hydraulic conductivity of the SDM is low, the rate of dissipation of excess pore pressure (EPP) will be low compared to rate of loading.

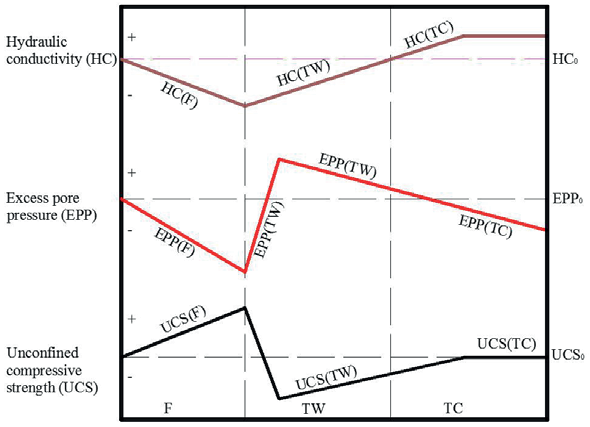

Fig. 3.32. Conceptual model for describing the relationship between unconfined compressive strength and hydraulic conductivity and excess pore pressure on the SDM due to freeze-thaw cycles.

This phenomenon will cause undrained conditions on the SDM. As a result, failure will occur under undrained condition, which is normally associated with low strength. Increased hydraulic conductivity as a result of freezing action on one hand may cause discharge of contained contaminants to the surrounding (detrimental outcome). Considering healing potential on the damaged SDM with reduced strength, increased hydraulic conductivity may cause increased rate of dissipation of excess pore pressure, reduced undrained conditions, and improved strength (enhanced outcome). Fig. 3.32 presents a conceptual model for describing the relationship between hydraulic conductivity (HC), excess pore pressure (EPP), and unconfined compressive strength (UCS) on the SDM due to the effect of freeze-thaw cycles (Paper III).

While the proposed model may be applied to all stabilized soils and sediments, it should be noted that even one continuous local crack may cause dramatic increase in HC values. This is especially, true for compacted stabilized soils with low water content. Development of local cracks and resulting increased HC may not contribute to overall dissipation of excess pore water under load. Thus, the proposed model is valid for high water content self-weight or preloaded consolidating stabilized soft soils and sediments. These materials tend to have good stress distribution without formation of local cracks.

Suggested protective measures

In order to maintain the integrity of the SDM, it can be beneficial to protect them from severe effect of repetitive freeze–thaw cycles. Protection of the SDM can be dealt with by either placing the stabilized material at depths below frost line or by using capping system. The choice of cap lining system will depend on the primarily function of the liner material and geotechnical applications of the SDM. The core objective of capping should be to prevent or minimize infiltration of water in stabilized mass. Freeze-thaw (f-t) process induces phase changes of water without dehydration (Paper V). Thus, increased amount of free water will cause increased (i) expansive force during freezing (ii) amount of free water during thaw. The former will result in increased formation of micro-cracks (either interconnected or disconnected depending on the achieved UCS). If the formed micro-cracks were not interconnected (in case of high UCS value in relation to the expansive forces), the later will cause increased excess pore pressure under load. If the formed micro-cracks were interconnected (in case of low UCS value in relation to the expansive forces), increased hydraulic conductivity may occur, which may cause discharge of leachate to the surrounding. Consequently, the capping system should have low hydraulic conductivity and durable under harsh repetitive freeze-thaw cycles and different physicochemical interactions.

The effect of repetitive freeze-thaw cycles on the hydraulic conductivity of well-known capping material such as silty till and geosynthetic clay liner (GCL) was investigated. Details on materials and methods of preparations and testing of silty till and GCL are presented in paper (IV) and (V), respectively. Results show that the baseline hydraulic conductivity (HC) of silty till falls within the same range of the HC values that are normally prescribed on the stabilized dredged mass (i.e. around 10^{-9} m/s). However, expansive forces exerted by frozen water on compacted silty till result in formation of clods or flocs, which ultimately, increase the hydraulic conductivity of silty till by up to 24 times the baseline value as shown in Fig. 3.33 (Paper IV). On the other hand, the hydraulic conductivity of the GCL was not affected by cation exchange complex (Fig. 3.34) or repetitive freeze–thaw cycles (Fig. 3.35) with detailed discussion presented in Paper V. In addition, geosynthetic clay liners under certain conditions can provide better capping than conventional compacted clay liners. As a result of thin layer, the GCLs partially seem to replace thick compacted clay layers and protective cover. Figure 3.36 shows that more wastes can be accommodated while using a thin frost protection layer of the GCL than using compacted clay liner. Thus, if the primary aim is to minimize leachate, the SDM can be protected by using the GCL. However, if the end use of the SDM will involve geotechnical loading conditions, the SDM should be placed below frost depth and protected against water penetration.

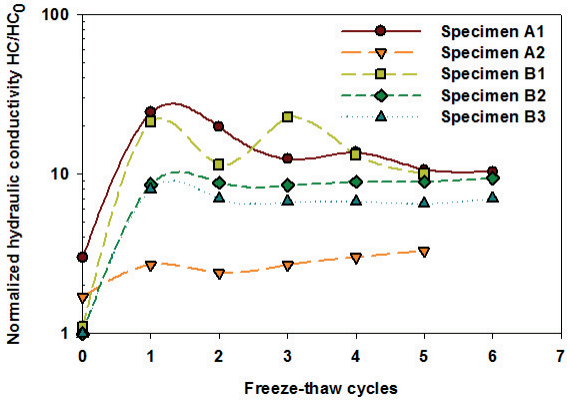

Fig. 3.33. Variations in normalized hydraulic conductivity of silty till with number of freeze-thaw cycles.

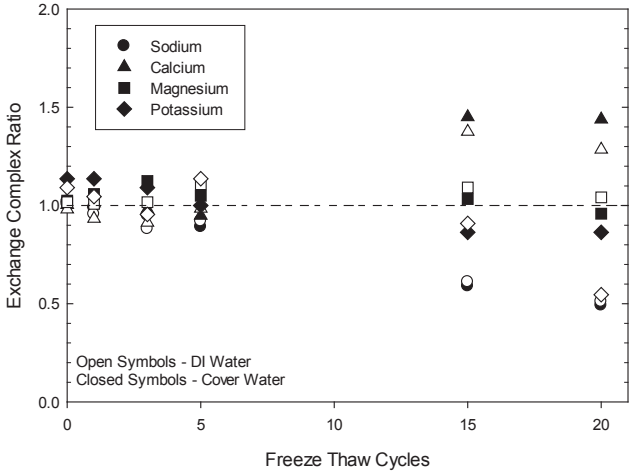

Fig. 3.34. Exchange ratio (final bound cation concentration normalized over original bound cation concentration) as a function of number of freeze-thaw cycles for GCL specimens undergoing single permeation.

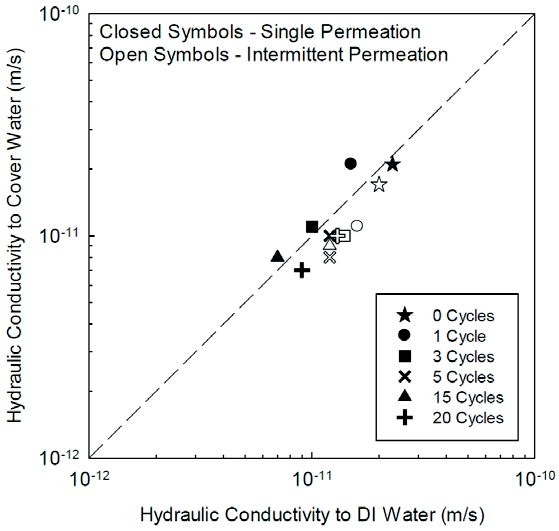

Fig. 3.35. Hydraulic conductivity of GCLs permeated with cover water (CW) compared to GCLs permeated with dionized (DI) water for the same number of freeze-thaw cycles.

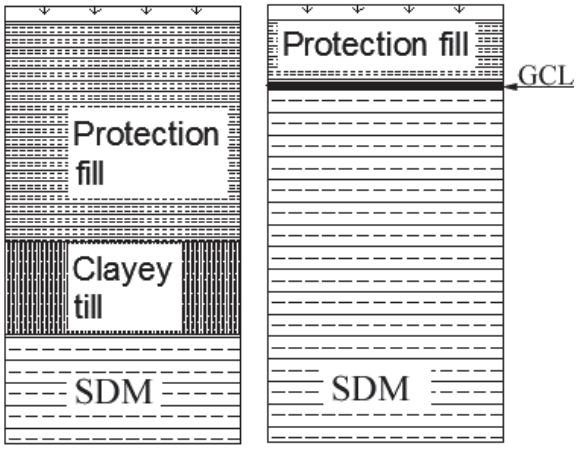

Fig. 3.36: Utilization of GCL as capping on stabilized dredged may increase storage space and reduce thickness of required protection fill for geoenvironmental applications.

3.2 Case study

In order to exemplify the geotechnical properties of in-situ treated high water content dredged sediments, a large-scale field test was carried out at Granudden terminal of Port of Gävle in Sweden (Fig. 3.37a). Mixing and backfilling operations at the large–scale field test started at the end of October 2010 and continued through the end of November 2010.

The sequence of operations at the large–scale field test is shown in Fig. 3.37(b). Reclaimed area and mechanical dredges are shown in Fig. 3.37(b)-A. The mechanical dredges were used to remove underwater volumes of contaminated sediments (from the upper part of the sediments down to 0.5 m). The dredged sediments were transported in barges to on–site treating facility (i.e. ProSol2010), which is shown in Fig. 3.37(b)-B. About 8,000 m^3 of the stabilized contaminated dredged material (SCDM) was utilized in a reclaimed area as a structural backfill material (Holm et al., 2012). The SCDM was preloaded with fill of selected gravel as shown in Fig. 3.37(b)-C. The application of preloading weight is usually carried out immediately after completion of mixing and placing of the stabilized mass for curing. However, the first phase of the application of the surcharge started on February 6, 2011 (i.e. about 65 days after completion of mixing and placement). According to Holm et al. (2012), the delay in the application of the preloading weight was due to too little strength of the SDM to support the selected preloading weight. During the first phase of preloading, a selected gravel of about 1.0 m high (equivalent to an average value of 18 kPa) was applied over a 4 days period. The second phase of preloading was carried out from March 7–16, 2011 using the same gravel fill of about 1.5 m high (equivalent to an average value of 27 kPa, placed over a 9 days period). For quality assurance, determination of geotechnical properties and classification of soil behaviour, several cone penetration tests (CPT) were carried out at different curing period as shown in Fig. 3.38. In this study, the curing period was counted from the first day of the application of the first phase of preloading weight. Field settlements were recorded at monitoring points F1, F2, F3 and F4 (Fig. 3.38). A typical cross-section view at the large-scale field test is shown in Fig. 3.39. Figure 3.40 presents examples of the measured CPT data obtained in April (67d), June (135d), and October, 2011 (250d). The measured settlement values at F1, F2, F3, and F4 are shown in Fig. 3.41. The measured field settlement ranged from 0.25 m (F4) to about 1.2 m at (F2). A detailed analysis of the contaminants has been published by Holm et al. (2012).

Meaningful quantitative predictions of field behavior are possible if undisturbed soil samples or in-situ tests are used for determination of engineering properties (Potts and Zdravković, 2001). Thus, numerical simulation supported with field observations can validate suitability of selected constitutive model and the evaluated material properties.

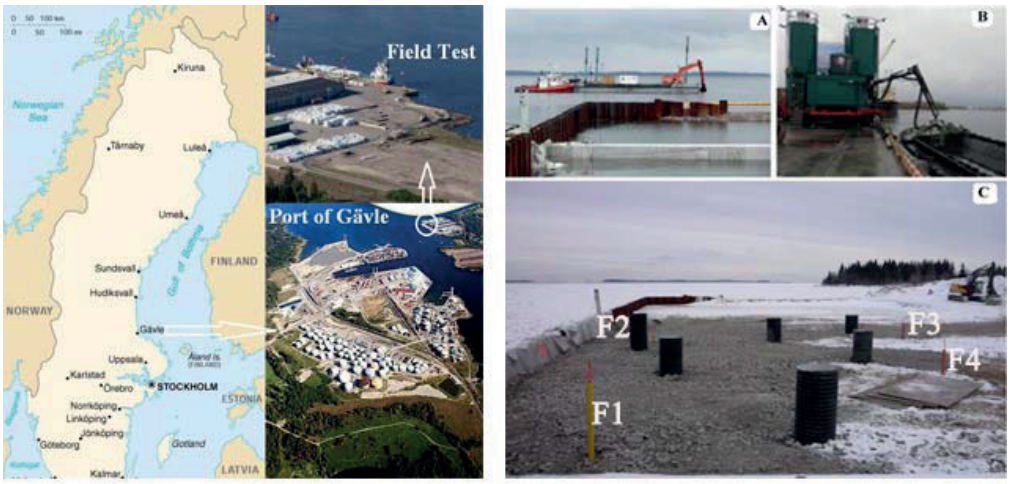

Fig. 3.37. (a) location of large–scale field test at Port of Gävle, Sweden. (b) Sequence of operations during the large-scale field test. A = dredging and reclamation, B = Process stabilization-solidification, C = preloading and settlement monitoring at reclaimed area (Photo: Courtesy of WSP, PEAB, and Port of Gävle).

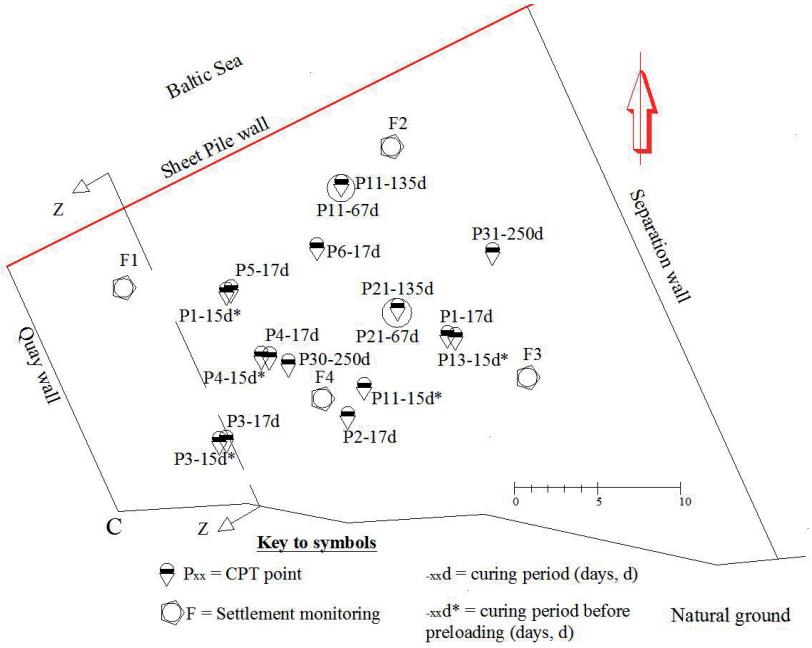

Fig. 3.38. Schematic plan view of location of some of CPT points relative to settlement monitoring points at the large–scale field test.

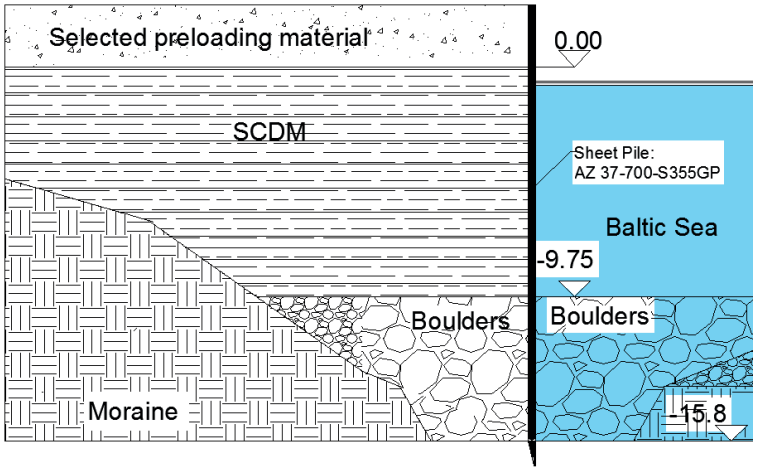

Fig. 3.39. Actual cross section view along Z-Z (Fig. 3.38) at the large-scale field test.

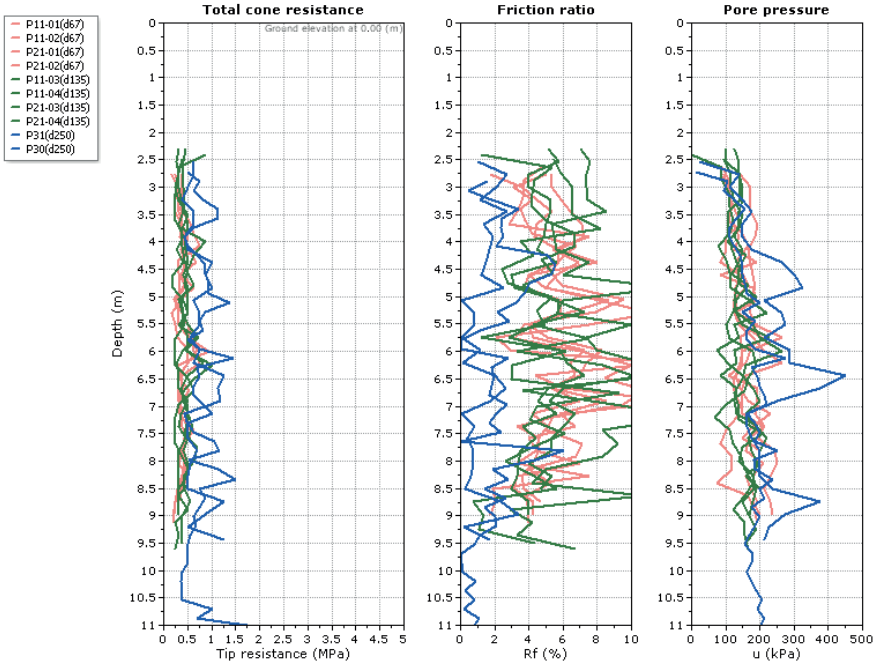

Fig. 3.40. Reproduced CPT measured quantities during curing period (plot: Courtsey of Dr. Peter Robertson at Greggdrilling).

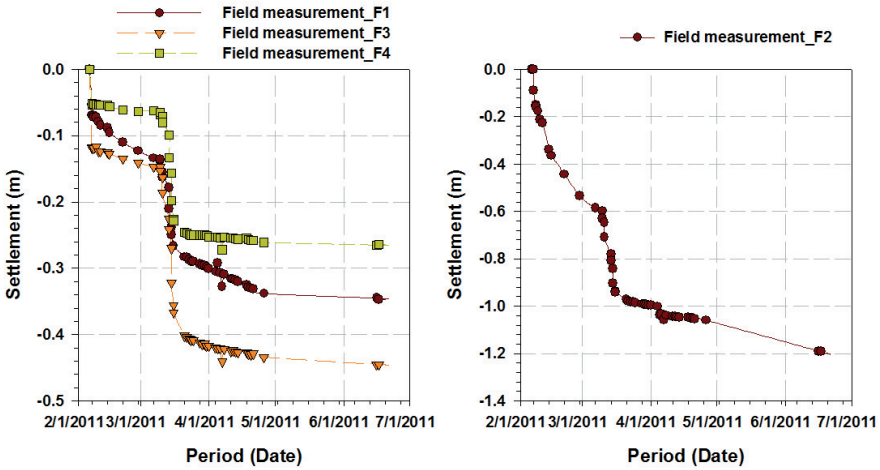

Fig. 3.41. Progressive settlement measurement at F1, F2, F3, and F4 (Data: Courtesy of WSP).

3.2.1 Simulation of field settlement

Simulation of settlement was carried out in PLAXIS 2D geotechnical software (Brinkgreve et al., 2011). The primary objectives were to demonstrate the applicability of conventional CPT empirical correlations in evaluation of stiffness and strength parameters of stabilized contaminated dredged material (SCDM).

Shear strength and constrained modulus values were evaluated using established CPT empirical correlations presented by Eq. (3) and Eq. (4), respectively. The SCDM fill at the large–scale field test was subdivided into horizontal layers of thickness between 0.23 and 0.30 m. The selected layer thicknesses were considered sufficient to capture the variations in stiffness and strength properties along the entire depth, and close to CPT sampling interval of 0.25. The evaluated properties were utilized in finite element method (FEM) to simulate the field settlements.

Simulation of field settlement was carried out using Mohr Coulomb (MC) material model and undrained loading condition. This loading condition was chosen because the SCDM in slurry condition would experience undrained behaviour. Fine mesh was chosen after sensitive analysis by varying mesh sizes from coarse mesh to very fine mesh. PLAXIS input parameters in MC model under undrained loading conditions involved the use of oedometer modulus (as in-situ constrained modulus) and an assumed undrained Poisson's ratio of 0.4. The undrained shear strength was utilized as the only strength parameter. Plastic analysis was used during layer placement and preloading. After completion of backfill operations, preloading weight was placed and initial displacements were reset to zero. This was done in order to mimic field operation, where recording

of the field settlements stated after application of preloading weight on the SCDM fill. PLAXIS consolidation analyses were carried out after each stage of preloading. In the first step, the SCDM fill was preloaded with 18 kPa. Consolidation analyses followed for the period of 30 days. The second period of preloading started after 30 days of consolidation with an application of an average additional effective load of 27 kPa. This stage was again followed by consolidation analysis to minimum excess pore pressure (EPP). An example of computation is presented for CPT data from point P3. The constrained modulus, E_{oed} and undrained shear strength, S_u, which were evaluated at CPT point P3 are presented in Table 3.8. Figure 3.42 presents simplified 2D numerical model showing typical boundary conditions. The anchor rod shown is for illustration purpose only. The length of the anchor rod was equal to the width of the model in the actual simulations. Figure 3.43 displays one–dimensional deformed fine mesh at the end of consolidation analysis across CPT point P3. The maximum vertical deformation of 0.21 m on the SCDM fill across P3 is shown in Fig. 3.44. Similar computations were carried out for the other CPT data points.

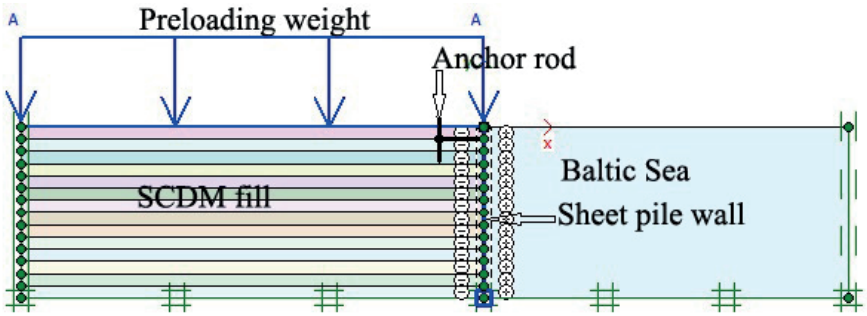

Fig. 3.42. Simplified PLAXIS 2D model through CPT P3 showing boundary conditions.

Table 3.8: Input parameters for PLAXIS simulation of the SCDM fill across CPT point P3.

Layer ID	**1**	**2**	**3**	**4**	**5**	**6**	**7**
E_{oed} (kN/m^2)	849	2387	1083	1189	2924	1493	4376
S_u (kN/m^2)	16	27	18	19	29	21	35
Depth (m)	4.06-3.77	3.77-3.48	3.48-3.19	3.19-2.90	2.90-2.61	2.61-2.32	2.32-2.02
Layer ID	**8**	**9**	**10**	**11**	**12**	**13**	**14**
E_{oed} (kN/m^2)	6603	2728	1545	1250	383	589	407
S_u (kN/m^2)	43	27	20	18	10	12	10
Depth (m)	2.02-1.74	1.74-1.45	1.45-1.16	1.16-0.87	0.87-0.58	0.58-0.29	0.29-0.0

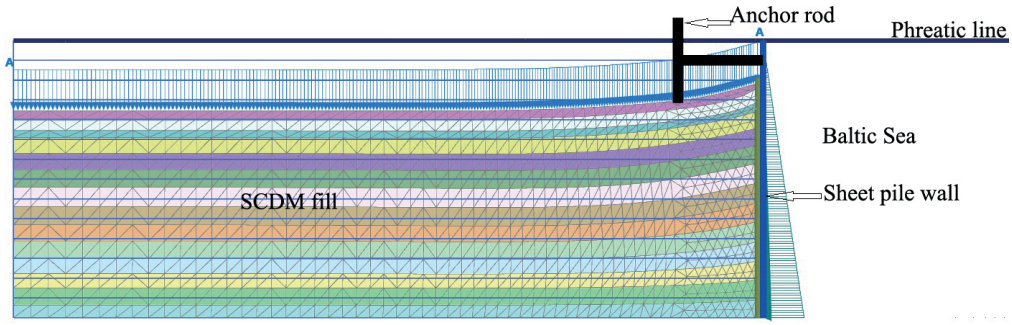

Fig. 3.43. Simplified PLAXIS 2D model through CPT P3 showing exaggerared (scaled up to five times) deformed mesh at the end of consolidation analysis.

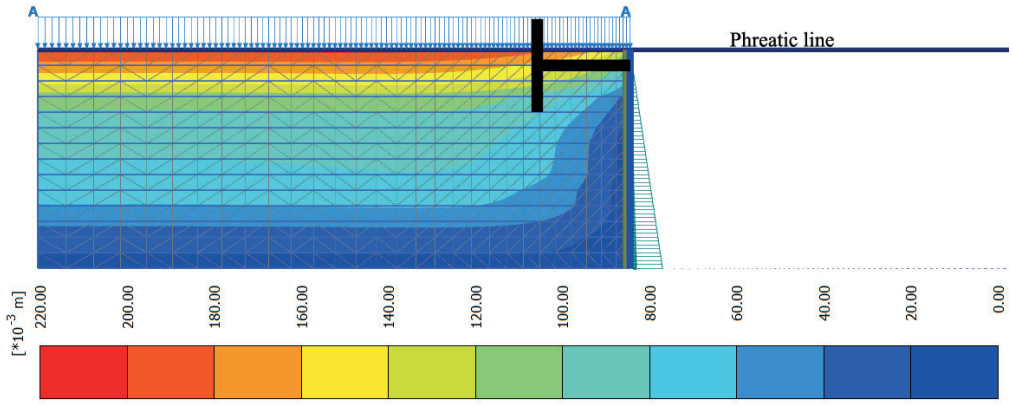

Fig. 3.44. Simplified PLAXIS 2D model showing maximum vertical deformation of 0.21 m across CPT P3.

3.2.2 Simulation results and discussion

The computed settlement values were compared with measured settlement values using cumulative settlement curves. The measured field settlement values varied significantly across the large-scale field test. Based on recorded settlement values (Fig. 3.41), the compressibility behaviour (Paper II) and simulation result (Paper V), it was found that the SDM were either in induction phase (IP) or nucleation and crystallization phase (NCP) at the time of application of preloading weight.

- ✓ During the first phase of preloading, the SCDM at settlement monitoring points F3 and F4 were in IP. The SCDM at measuring points F2 and F4 were in nucleation and crystallization phase (NCP).
- ✓ During the second phase of preloading the SCDM at all measuring points were in NCP.

Consequently, comparisons between simulated and measured settlement values were not restricted to the evaluated stiffness of the SCDM in the vicinity of settlement monitoring points.

The comparisons aimed at finding out the stiffness properties, which characterized the observed settlement values during the two phases of preloading. For instance, Fig. 3.45 shows that the stiffness properties of the SCDM at the settlement monitoring point F4 were similar to those attained at CPT point P5 during the first phase of consolidation. During the second phase of preloading, the stiffness properties of the SCDM at F4 were similar to those occurring at CPT points P2.

During the two phases of preloading, Fig. 3.46 shows that the stiffness properties at F2 were similar to those existing at CPT point P21. Nevertheless, it was concluded that the CPT empirical correlations which were developed for use in conventional cohesive soils are applicable in the SDM as well (Paper VI). However, repeatability of the CPT data in the SDM is unlikely. For that reason, the CPT data and evaluated design parameters can be considered as valid only at the time of testing. The differences between simulated and measured settlement values could be related to the:

i. Different loading conditions in the field and PLAXIS simulations.

Results from consolidation test study show that for sufficient compression, selected preloading weight must be applied all at once. This is because, after the first day of application of preloading weight, subsequent application of consolidation stress with magnitude less than or equal to the initial preloading weight have no influence on increased settlement of the SDM. This is the case especially, during induction phase (IP). However, if the same consolidation stress is applied during NCP, it may contribute to the increased settlement value.

At the large-scale field test, the initial and subsequent preloading stress of 18 kPa and 27 kP, respectively were applied over couple of days. In other words, during the first and final stage of preloading, the applied daily consolidation stresses were 4.5 kPa and 3.0 kPa, respectively. During simulations of field settlement, the consolidation stress of 18 kPa and 27 kPa were applied all at once. Laboratory consolidation test results have shown that during induction phase, application of subsequent consolidation stress with magnitude below preconsolidation stress have no influence on increased settlement. This different may have contributed to the discrepancies between simulated and measured values.

ii. Evaluated input parameters (constrained modulus and shear strength).

There can be some limitations in the utilized empirical correlations for evaluations of constrained modulus cone factor in Eq. (3) and the assumed value of N_{kt} in Eq. (4) as discussed below.

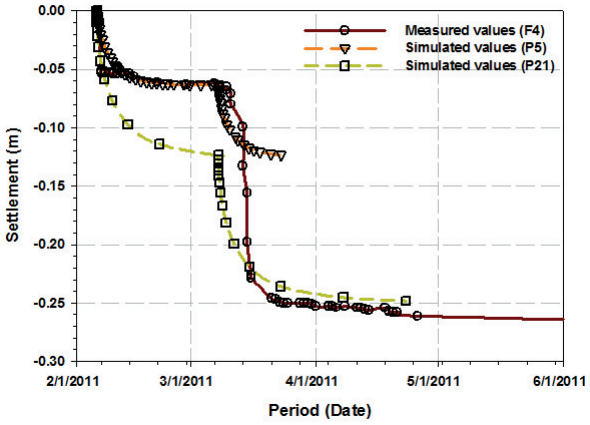

Fig. 3.45. Example of simulated field settlement values at CPT points 5 and 21 relative to the measured settlement values at F4.

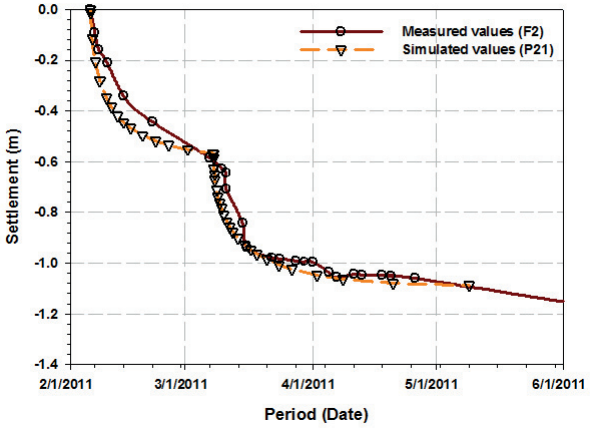

Fig. 3.46. Example of simulated field settlement value at CPT_P21 relative to the measured values at F2.

3.2.3 Limitations

3.2.3.1 Evaluations of constrained modulus cone factor

The constrained modulus cone factor α_m depends on soil type. Evaluations of soil behaviour type using conventional CPT classification charts requires the use of normalized net cone resistance Q_{tn}.

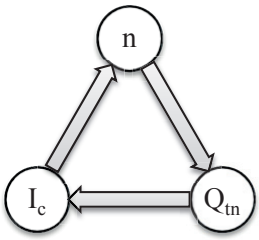

Fig. 3.47. Mutual reliance of input parameters for evaluation of constrained modulus cone factor.

However, the normalized net cone resistance Q_{tn}, depends on stress exponent n, which is influenced by soil behaviour type index I_c. Thus, Q_{tn}, n, and I_c are mutually dependent as shown in Fig. 3.47. In other words, as shown in Table 2.3, the value for n, which depends on I_c is an input parameter for evaluation of Q_{tn}. However, I_c depends on Q_{tn} as an input parameter. For stabilized dredged material (SDM), the value for stress exponent n will change with curing period as discussed in Paper II. The variations in the stress exponent n will affect the evaluated α_m and ultimately, the in-situ constrained modulus M. As a result, proper evaluation of α_m will depend on true value of stress exponent n.

Identifying soil behaviour type and the stress exponent n during curing period is essential for proper evaluation of constrained modulus cone factor α_m. During verification of field settlement, the value for n was assumed to be equal to 1.0 throughout the curing period. This assumption was too conservative. As a result of this assumption, the evaluated I_c values were above 2.2 and the values for α_m were either equal to 14 or normalized cone resistance Q_{tn} value in accordance with Eq.(4).

3.2.3.2 Evaluation of in-situ strength

Evaluation of the undrained shear strength from CPT data requires the use of tip cone factor N_{kt}, which is a constant value. The N_{kt} value is usually obtained by calibrating the CPT data with known undrained shear strength from vane shear test (Kulhawy and Mayne, 1990). The undrained shear strength of the SDM increases with curing period. In addition, repeatability of CPT data in the SDM can be unlikely (Paper VI). Thus, evaluation of shear strength during curing period may require repeated calibration of CPT data to obtain new values for the cone factor, N_{kt}. During evaluation of undrained strength values, the N_{kt} value of 14 was utilized. According to Holm et al. (2012), the N_{kt} value of 17 was utilized to evaluate the undrained shear strength at the large–scale

field test. Thus, the N_{kt} value of 14 may have over predicted the actual in-situ strength of the SCDM.

To avoid repeated calibration of the CPT data, it could be beneficial to utilized real time CPT data for evaluation of undrained shear strength. The induced CPT effective stress could be utilized to estimate the undrained shear strength of the SDM. The proposed CPT induced effective stress could be estimated from

$$\sigma'_{CPT} = r_\sigma \left(q_t - u_0\right)/\left(2.3 - r_\sigma\right) \tag{14}$$

where:

σ'_{CPT} = CPT induced effective vertical stress, kPa.

r_σ = total stress reduction factor, given by $r_\sigma = 2.3\rho_d/\rho$, where ρ_d and ρ are dry and bulk density of the SDM, respectively.

u_0 = hydrostatic pore pressure, kPa.

Detailed derivation of Eq. Eq. (14) was presented in Paper VII. To avoid confusion with coefficient of earth pressure at rest, the effective vertical stress-characteristic ratio k_0 in paper VII, was redefined here as total stress reduction factor and denoted by r_σ. The CPT induced effective stress Eq. (14) was correlated to the undrained shear strength of the SCDM in the form:

$$s_u = 0.1\sigma'_{CPT} \tag{15}$$

where 0.1 is a proportionality constant. Notice that the value of the constant is equal to the penetration length. According to Sandven (2010) for sampling interval of 20 mm and 50 mm, the penetration length is equal to 0.1 m and 0.2 m, respectively. The sampling interval of 20 mm was utilized during the cone penetration tests at the large–scale field test. The undrained shear strength evaluated using proposed correlation presented by Eq. (15) agreed well with established conventional correlation presented in Eq. (3) for N_{kt} value of 17 as shown in Fig. 3.48.

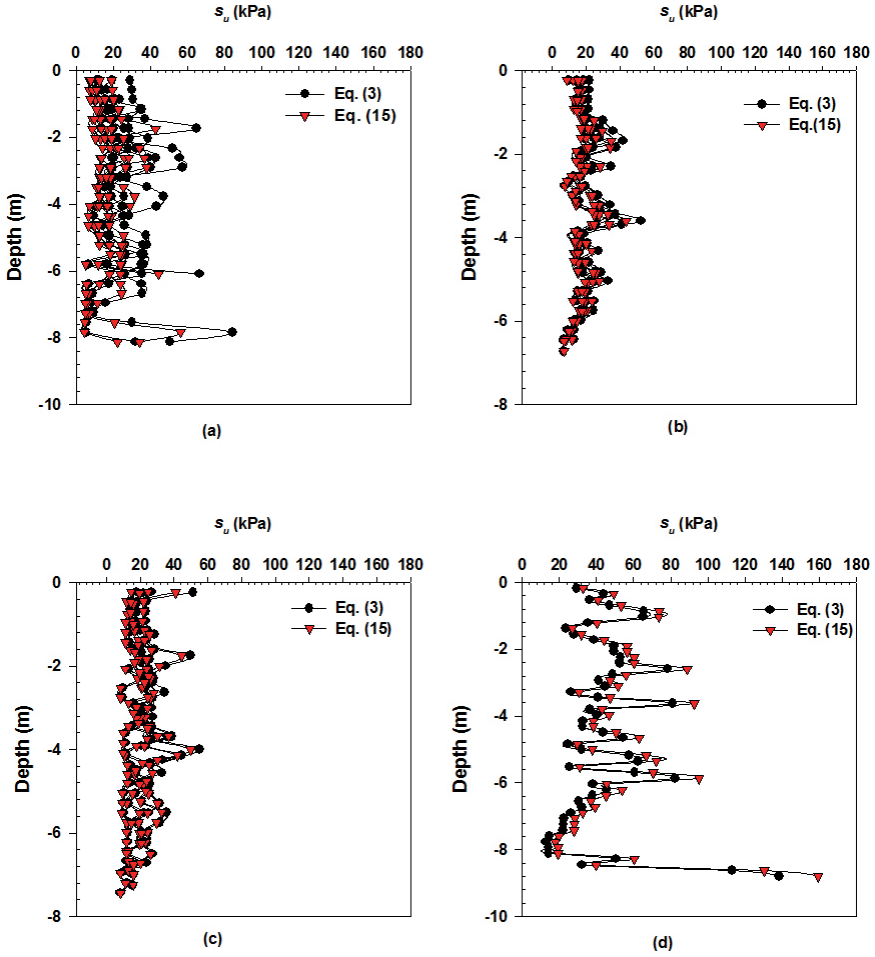

Fig. 3.48. Evaluations of undrained shear strength using proposed relative to conventional empirical correlations after (a)17d, (b) 67d (b) 135d (c) 250 days(d) of curing.

4. Conclusions

The main objectives of the research work were presented. To fulfill these objectives, simulation of field settlement and laboratory tests studies were carried out. Results were presented and discussed. The purposes of the research work were fulfilled with the following concluding remarks:

4.1 Strength

Laboratory test study indicated that the improved strength of composite binder-treated dredged sediment was influenced by the amount of cement in the blend. Thus, within the scope of this study, the following factors contributed to increased water/cement ratio and delayed strength development at the large-scale field test:

- ✓ The use of constant amount of composite binder at increasing initial water content of dredged sediment.
- ✓ Underwater discharge of stabilized mass immediately after mixing.

4.2 Compressibility behaviour

Based on laboratory test study, three phases of hydration process influencing the compressibility of the stabilized dredged material (SDM) were identified. These are induction phase (IP), nucleation and crystallization phase (NCP), and Hardening phase (HP) as described below:

- IP was associated with formation of impermeable protective layer on surface of binder particles, which resist penetration of water molecules. The unhydrated portion of binder increased resistance to deformation.
- NCP was connected to the change from impermeable to permeable protective layer. The plastic limit increased accompanied by loss of apparent preconsolidation stress and tangent modulus.
- HP was connected to increased thickness, stiffness and solidification of protective layer. HP was accompanied with increased apparent preconsolidation stress and tangent modulus.

Within the scope of this study, the variations in measured field settlements at the large-scale field test were caused by different hydration phases of the SDM fill at the time of preloading. The following remarks are drawn:

- ✓ The SDM fill was either in IP or NCP at the time of first phase of preloading.
- ✓ The SDM in IP exhibited sudden compression on the first day of application of preloading weight only. Subsequent daily applications of the same amount of preloading weight had no influence on increased compression.

- ✓ The SDM in the NCP experienced excessive settlement on the first day and under daily application of the preloading weight.

4.3 Durability

Like conventional cohesive soils, stabilized dredged materials (SDM) are susceptible to repetitive freeze-thaw cycles. Result from laboratory test study show that degree of damage caused by freeze-thaw action depends on the type of binder and freeze-thaw method. The healing of damage SDM with reduced strength depends on the grace period of thaw consolidation.

- ✓ Inclusion of supplementary cementing material such as fly ash and granulated blast furnace slag enhanced resistance of the SDM to freeze-thaw cycles.
- ✓ Open freeze-thaw method showed less detrimental effect compare to closed freeze-thaw method.
- ✓ The reduced strength of the SDM due to freeze-thaw process was recovered during thaw-consolidation process.

Contained contaminant requires capping system to protect the SDM from animal burrowing and ingression of water. This can be achieved by using soil covers such as compacted silt till or geosynthetic clay liners. Geosynthetic clay liners provide effective capping material for environmental protection compare to the compacted silt till.

4.4 Use of CPT

The conventional CPT empirical correlations can as well be utilized in the stabilized dredged material, if appropriate input parameters are utilized. The following are the main limitations associated with the use of conventional CPT empirical correlation for evaluations of in-situ strength and stiffness of the SDM:

- ✓ Repeatability of CPT data in the SDM is unlikely. The evaluated stiffness and strength values therefore, should be considered as valid at particular test point and curing period.
- ✓ Stress exponent varies with curing period. Thus, appropriate stress exponent should be utilized during curing to obtain the corresponding constrained modulus cone factor.
- ✓ During curing, the tip cone factor will vary. Accordingly, calibration of CPT data will be necessary to obtain the corresponding strength value.

To avoid repetitive calibration of CPT data for obtaining the tip cone factor, total stress reduction factor was proposed. A new empirical correlation for estimation of undrained shear strength was then suggested which makes use of CPT induced effective stress and penetration length.

5. Suggestions for future work

The improved strength, reduced compressibility and durability of stabilized dredged sediments depend on methods of stabilization, physicochemical interactions between the dredged sediments and binder.

5.1 Method of stabilization-solidification

Process stabilization-solidification technology makes use of constant amount of binder at varying water content of incoming dredged sediments. As a result, the geotechnical properties of the stabilized material may vary significantly. Further research is required for installation of sensors that can detect variations of water content in the incoming DS and regulate the amount of binder accordingly.

Underwater curing (submergence) of high water content stabilized materials prior to initial setting, may significantly affect the water/cement ratio, which may cause delay in setting and increased weakening effect of calcium silicate bond. It can be beneficial to consider dewatering of the reclaimed area prior to the discharge of the stabilized mass.

5.2 Properties of dredged sediments

The nature of dredged sediments determines the reactivity of selected binder and achieved strength. Further research should focus on the achieved strength, reduced compressibility and durability of treated sediments in relation to physical properties of sediments (particle sizes, organic matter, and rock forming minerals, bulk density or water content).

5.3 Binder

Traditionally, the amount of binder is estimated by trial and error. The minimum amount of binder that will meet the desired geotechnical properties is usually selected. The amount of binder could be estimated based on physical properties of the dredged sediments such as bulk density and initial water content. An initial study showed promising results. Further studies should be carried out to establish correlations between achieved strength and estimated amount of binder based on initial bulk density of dredged sediment.

Based on the laboratory and field test study, improved strength due to reactivity of fly ash (FA) and ground granulated blast furnace slag (GGBS) remained questionable. Further studies are suggested to investigate the reactivity of FA from paper mill industry and GGBS at high water/binder ratio.

6. References

Abu-Farsakhi, M., Tumay, M. and Voyiadjis, G. (2003). Numerical parametric study of piezocone penetration test in clays. *International Journal of Geomechanics, Vol. 3*(2), 170-181.

Al-Tabbaa, A. and Evans, W. (1998). Pilot in-situ auger mixing treatment of a contaminated site - Part I: treatability study. *Proceedings of the Institution of Civil Engineers-Geotechnical Engineering*, *Vol. 131*, pp. 52-59.

Andersson, R., Carlsson, T. and Leppänen, M. (2000). Hydraulic cement based binders for mass stabilization of organic soils. *Soft Ground Technology*. Noordwijkerhout, The Netherland.

ASTM D 2435/D2435M. (2011). Standard test methods for on-dimensional consolidation properties of soils using increment loading. In *Annual Book of ASTM Standards*. West Conshohocken, PA: ASTM International.

ASTM D 560. (1996). *Standard test methods for freezing and thawing compacted soil-cement mixtures.* West Conshohocken, PA: ASTM International.

ASTM D 5856. (2007). Standard test method for measurement of hydraulic conductivity of porous material using a rigid-wall, compaction-mold permeameter. In *ASTM standards.* West Conshohocken, PA: ASTM International.

ASTM D 653. (2011). Standard terminologies relating to soil, rock and contained fluid. In *Annual Book of ASTM Standards.* West Conshohocken: ASTM International.

ASTM D 7099. (2010). *Standard terminology relating to frozen soils and rock.* West Conshohocken, PA: ASTM International.

Atkinson, J. (2007). *The mechanics of soils and foundations* (2 uppl.). London/NY: Taylor and Francis.

Beeghly, J. and Schrock, M. (2010). Dredged material stabilization using the pozzolanic or sulfo-pozzolanic reaction of lime byproduct to make an engineered structural fill. *International Journal of Soil, Sediment and Water, Vol. 3*(1), Article 6.

Bemben, S. (1986). Brittle behavior of a varved clay during laboratory consolidation tests, consolidation of soils: testing and evaluation. (R. N. Yong, & F. C. Townsend, Eds.) *ASTM STP 892*, 610-626.

Benson, C., Wang, X., Gassner, F., and Foo, D. (2008). Hydraulic conductivity of two geosynthetic clay liner permeated with an aluminum residue leachate. *Proceedings of GeoAmericas 2008 – The First Pan American Geosynthetics Conference and Exhibition* (pp. 94-101). Cancun, Mexico: Industrial Fabrics Association International (IFAI), Roseville, Minn.

Benson, C.H. and Othman, M.A. (1993). Hydraulic conductivity of compacted clay frozen and thawed in-situ. *Journal of Geotechnical Engineering*, 276-294.

Benson, C.H., and Daniel, D.E. (1990). Influence of clods on hydraulic conductivity of compacted clay. *J. Geotechnical engineering, 116*, 1231-1248.

Bijen, J. (1996). Benefit of slag and fly ash. *Construction and Building Material, 10*(5), 309-314.

Boone, S.J. and Lutenegger, A.J. (1997). Carbonates and cementation of glacially derived cohesive soils in New York state and Southern Ontario. *Canadian Geotechnical Journal, 34*, 534-550.

Brinkgreve, R.B.J., Engin, E. and Swolfs, W.M. (2011). *Plaxis 2D 2011: material models manual.* Delft: PLAXIS BV.

Cammack, R., Attwood, T. K., Campbell, P.N., Parish, J.H., Smith, A. D., Stirling, J. L. and Vella, F. (2006). *Oxford Dictionary of Biochemistry and Molecular Biology (2nd Edition).* Retrieved from http://www.knovel.com/web/portal/browse/display?_EXT_KNOVEL_DISPLAY_bookid=3987&VerticalID=0.

Campanella, R.G., Gillespie, D. and Robertson, P.K. (1982). Pore pressures during cone penetration testing. *2nd European Symposium on Penetration Testing* (pp. 507-512). Amsterdam, The Netherlands: AA. Balkema.

Carlsson, E. and Elander, P. (2001). Investigation of repeated cycles of freezing and thawing effects on a clayey till used as sealing layer over sulphide-rich tailings at the Kristinerberg mine, Northen Sweden. *Proceedings in Securing the Future*, *Vol. 1*, ss. 58-71. Skellefteå.

Cássia de Brito Glvão, T., Elsharief, A., and Gustavo, F. S. (2004). Effect of lime on permeability and compressibility of two tropical residual soils. *Journal of environmental engineering*, 881-885.

Chamberlain, E. and Gow, A. (1979). Effect of freezing and thawing on the permeability and structure of soils. *Engineering Geology, Vol. 13*(1-4), 73-92.

Chew, S.H., Kamruzzaman, H.M. and Lee, F.H. (2004). Physicochemical and engineering behavior of cement treated clay. *Geotechnical and Geoenvironmental Journal, 130*(7), 696-706.

Chrysochoou, M. and Dermatas, D. (2006). Evaluation of ettringite and hydrocaluminate formation for heavy metal immobilization: Literature review and experimental study. *Journal of hazardous materials, 136*, 20-33.

Cortellazo, G. and Cola, S. (1999). Geotechnical characteristics of two Italian peats stabilized with binders. *Proceeding of dry mix methods for deep soil stabilization* (ss. 93-100). Stockholm: Balkerma.

Crawford, B. (1986). State of the art: evaluation and interpretation of soil consolidation tests. *ASTM Special Technical Publication, 892*, 71-103.

EuroSoilStab. (2002). *Development of design and construction methods to stabilize soft organic soils: design guide for soft soil stabilization.* CT97-0351, European Commission, Industrial and Materials Technologies Programme (Rite-EuRam III) Bryssel.

Forsman, J., Maijala, A. and Järvinen, K. (2008). Case Stories, harbours-mass stabilization of contaminated dredged mud in Sörnäinen, Helsinki. *International Mass Stabilization Conference 2008.* Lahti, Finland.

Fossenstrand, I. (2009). *Stabilization and solidification of dredged Sediments at Port of Gävle.* Luleå: Luleå University of Technology.

Gallavresi, F. (1992). Grouting improvement of foundation soils. *Proc., Grouting, soil improvement and geosythetic* (ss. 1-38). New York: ASCE.

Garbin, J.E., Mann, J., McIntosh, A.K. and Desai, R. K. (2011). Mass stabilization for settlement control of shallow foundation on soft organic clayey soils. *Geo-frontiers 2011: advances in geotechnical engineering, 13-16 March 2011.* Dallas, Texas, USA: ASCE 2011.

Grozic, J.L.H, Lunne, T., and Pande, S. (2003). An oedometer test study on the preconsolidation stress of glaciomarine clays. *Canadian Geotechnical Journal*, 857-872.

Hebib, S. and Farrell, E.R. (1999). Some experiences of stabilizing Irish organic soils. *Proc. of dry mix methods for deep soil stabilization* (ss. 81-84). Stockholm: Balkema.

Hewitt, R. and Daniel, D. (1997). Hydraulic conductivity of geosynthetic clay liners after freeze-thaw. *Journal of Geotechnical and Geoenvironmental Engineering, Vol. 123*(4), 305-313.

Holm, G., Bengtsson, P., and Larsson, L. (2012). *Field test at Port of Gävle, Sweden.* Linköping: Swedish Geotechnical Institute.

Holm, G., Larsson, L., Pettersson, M., Mácsik, J., Knutsson, S., and Makusa, G. (2015). *Durability-An expert study with focus on geo-constructions containing stabilized contaminated soils or sediments.* Linköping: Swedish Geotechnical Institute.

Holm, G., Rogbeck, Y. and Berglund, C. (2005). Stabilization and solidification of contaminated ground: a preliminary study. *Proceedings of the International Conference on Deep Mixing.* Stockholm.

Hwang, C. and Shen, D. (1991). The effect of blast-furnace slag and fly ash on the hydration of Portland cement. *Cement and Concrete Research, 21*, 410-425.

Ingles, O.G. and Metacalf, J.B. (1972). *Soil stabilization: principles and practice.* London: Butterworth and Company.

Jamshidi, R. J., and Lake, C. B. (2015). Hydraulic conductivity and strength properties of unexposed and freeze-thaw exposed cement-stabilized soils. *Canadian Geotechnical Journal, 52*, 283-294.

Jamshidi, R. J., Lake, C. B., and Barnes, C. L. (2014). Examining Freeze/Thaw cycling and its impact on the hydraulic performance of cement-treated silty sand. *Journal of Cold Regions Engineering*.

Janbu, N. (1967). *Settlement calculation based on the tangent modulus concept. Three lectures* (Bulletin 2 ed.). Trondheim: Norwegian University of science and technology.

Janbu, N. (1998). *Sediment deformations. A classical approach to stress-strain-time behaviour of granular media as developed at NTH over a 50 year period.* (Bulletin 35 ed.). Trondheim: Norwegian University of science and technology.

Jefferies, M.G. amd Davies, M.P. (1993). Use of CPT to estimate equivalent SPT N60. *Geotechnical testing journal*, 458-468.

Jelisic, N. and Leppänen, M. (1999). Mass stabilization of peat in road and railway construction. *Dry Mix Method for Deep Soil Stabilization* (pp. 59-64). Stockholm: Balkema, Rotterdam.

Kamon, M. and Nontananandh, S. (1991). Combining industrial wastes with lime for soil stabilization. *Geotechnical Engineering, 117*(1), Paper No. 25411.

Karlsrud, K. and Hernandez-Martinez, F.G. (2013). Strength and deformation properties of Norwegian clays from laboratory tests on high-quality block samples. *Canadian Geotechnical Journal*, 1273-1293.

Knutsson, S. (1983). *A theoretical model for calculation of pore water pressure and settlements in thawing soil (in Swedish).* Luleå, Sweden: Luleå University of Technology.

Knutsson, S., and Rydén, C.G. (1984). *Pore water pressure in thawing soil, a theoretical model (in Swedish).* Luleå, Sweden: Luleå University of Technology.

Kraus, J., Benson, C., Erickson, A. and Chamberlain, E. (1997). Freeze-thaw and hydraulic conductivity of bentonitic barriers. *Journal of Geotechnical and Geoenvironmental Engineering, Vol. 123*(3), 229-238.

Kulhway, F.H. and Mayne, P.W. (1990). *Manual on estimating soil properties for foundation design.* Palo Alto: Electrical Power Research Inst.

Lagerlund, J. (2010a). *Stabilization-solidification of dredged sediments from Port of Gävle, Step 1 (in Swedish).* Vattenfall Research and Development AB, Report. U09:109.

Lagerlund, J. (2010b). *Stabilization-solidification of dredged sediments from Port of Gävle, Step 2 (in Swedish).* Vattenfall Research and Development AB. Report. U10:162.

Larsson, R. and Mulabdic, M. (1991). *Piezocone tests in clays.* Linköping: Swedish Geotechnical Institute.

Larsson, R. and Åhnberg, H. (2005). On evaluation of undrained shear strength and preconsolidation pressure from common field tests in clay. *Canadian Geotechnical journal*, 1221-1231.

Lee, F.H, Lee, Y., Chew S.H., and Yong, K.Y. (2005). Strength and modulus of marine clay-cement mixes. *Journal of geotechnical and geoenvironmental engineering*, 178-186.

Liu, S.Y., Zhang, D.W., Liu, Z.B., and Deng, Y.F. (2008). Assessment of unconfined compressive strength of cement stabilized marine clay. *Marine Georesources and Geotechnology*, 19-35.

Locat, J., Bérubé, M-A. and Choquette, M. (1990). Laboratory investigations on the lime stabilization of sensitive clays: shear strength development. *Canadian Geotechnical Journal, Vol. 27*(3), 294-304.

Lunne, T., Andersen, H.K., Low, E.H., Randolph, F.M. and Sjursen, M. (2011). Guidelines for offshore in-situ testing and interpretation in deep water soft clays. *Canadian Geotechnical Journal, Vol. 48*(4), 543-556.

Lunne, T., Eidsmoen, T., Gillespie, D. and Howland, J.D. (1986). Laboratory and field evaluation on cone penetrometer. *Proceedings of ASCE Specialty Conference In Situ'86:Use of In Situ Tests in Geotechnical Engineering* (pp. 714-729). Blacksburg,: GSP 6, ASCE.

Lunne, T., Robertson, P.K., and Powell, J.J.M. (1997). *Cone penetration testing in geotechnical practice.* New York: Blackie Academic, EF Spon/Routledge.

Maher, A., Bennert, T., Jafari, F., Douglas, W.S. and Gucunski, N. (2004). Geotechnical properties of stabilized dredged material from New York-New Jersey Harbor. *Journal of the Transportation Research Board*, 86-96.

Maher, A., Douglas, W.S and Jafari, F. (2006). Field placement and evaluation of stabilized dredged material from the New York-New Jersey Harbor. *Marine Georesources and Geotechnology, Vol. 24*, 251-263.

Makusa, G. (2013a). *Soil stabilization methods and materials in engineering practice.* State of the art review, Luleå University of Technology, Department of Civil, Environmental and Natural Resources Engineering, Luleå, Sweden.

Makusa, G. (2013b). *A review of geotechnical behavior of stabilized soils: design and analysis considerations.* State of the art review, Luleå University of Technology, Department of Civil, Environmental and Natural Resources Engineering, Luleå, Sweden.

Makusa, G.P., Mattsson, H., and Knutsson, S. (2012). Verification of field settlement of in-situ stabilized dredged sediments using cone penetration test data. *Electronic journal of Geotechnical Engineering, 17/Y*, 3365-3680.

Marsh, B.K., Day. R.L., and Bonner, D.G. (1985). Pore structure characteristics affecting the permeability of cement paste containing fly ash. *Cement and Concrete Research, 15*, 1027-1038.

Massarch, K. R. and Topolnicki, M. (2005). Regional report: European practise of soil mixing technology. *Proceeding of the international conference on deep mixing-best practice and recent advances.* Stockholm.

Mayne, P. (2007). *Cone penetration testing state-of-practice.* Washington, DC: Transportation Research Board Synthesis Study.

Mitchell, J. K. and Soga, K. (2005). *Fundamentals of soil behavior* (3rd ed.). New York: John Wiley and Sons.

Muir Wood, D. (1990). *Soil behaviour and critical state soil mechanics.* New York: Cambridge University Press.

Nagaraj, T.S. and Miura, N. (2001). *Soft clay behavior: analysis and assessment.* Rotterdam, The Netherland: A.A. Balkema.

PIANC. (2009). *Dredged material as a resource: options and constraints.* Report No. 104-2009.

Potts, D.M. and Zdravkovic´, L. (2001). *Finite element method in geotechnical engineering application.* Thomson Telford.

Pousette, K., Mácsik, J., and Jacobsson, A. (1999). Peat soil sample stabilized in laboratory-experiences from manufacturing and testing. *Proc. of dry mix methods for deep stabilization* (pp. 85-92). Stockholm: Balkema.

Quang, N.D., and Chai, C.J. (2015). Permeability of lime-and cement-treated clayey soils. *Canadian Geotechnical Journal, 52*, 1221-1227.

Rajasekaran, G. and Rao, S.N. (2002). Permeability characteristics of lime treated marine clay. *Journal of Ocean Engineering, 29*, 113-127.

Rekik, B. and Boutouil, M. (2009). Geotechnical properties of dredged marine sediments treated at high water/cement ratio. *Geo-marine Letters*(29), 171-179.

Richardson, G.R., Groves, G.W. (1997). The structure of the calcium silicate hydrate phases present in hardened pastes of white Portland cement/blast-furnance slag blend. *Journal of Materials Science*(32), 4793-4802.

Robertson, P. (1990). Soil classification using the cone penetration test. *Canadian Geotechnical Journal, Vol. 27*(1), 151-158.

Robertson, P. (2009). Interpretation of cone penetration tests - a unified approach. *Canadian Geotechnical Journal, Vol. 46*(11), 1337-1355.

Robertson, P.K. and Campanella, R.G. (1983). Interpretation of cone penetration tests-Part II (Clay). *Canadian Geotechnical Journal, Vol. 20*(4), 734-745.

Roger, C.D.F and Glendinning, S. (1993). Modification of clay soils using lime. *Proc. of the seminar held at Loughborough University on lime stabilization* (pp. 99-114). London: Thomas Telford.

Sanglerat, G. (1972). *The penetrometer and soil exploration.* Amsterdam, the Netherlands: Elsevier Science Ltd.

Schneider, A.J., Randolph, M.F., Mayne, P.W. and Ramsey, N.R. (2008). Analysis of factors influencing soil classification using normalized piezocone tip resistance and pore pressure parameters. *Journal of Geotechnical and Geoenvironmental Engineering, Vol. 134*(11), 1569-1586.

Sherwood, P. (1993). *Soil stabilization with cement and lime. State of the art review.* London: Transport Research Laboratory, HMSO.

Sing, W.L., Hashim, R. Ali, H.F. (2008). Engineering behavior of stabilized peat soil. *European Journal of Scientific Research, 21*(4), 581-591.

Sparrevik, M., Hernandez-Martinez, F., Eggen, A. and Eek, E. (2008). *Stabilization and solidification of contaminated sediments.* Norwegian Geotechnical Institute (NGI).

Sridharan, A. and Rao, G.V. (1973). Mechanism controlling volume change of saturated clays and the role of effective stress concept. *Géotechnique, 23*(3), 359-382.

Sridharan, A. Prakash, K. (1999). Influence of clay mineralogy and pore-medium chemistry on clay sediment formation. *Canadian Geotechnical Journal, 36*, 961-966.

Svensson, M., and Andreas, L. (2012). *Characterization report-byproduct from Billerud Karlsborg AB (In Swedish).* Luleå, Sweden: Luleå University of Technology.

Sällfors, G. (1975). *Preconsolidation pressure of soft, high-plastic clays.* Göteborg, Sweden: Chalmers University of Technology.

Taylor, H. (1990). *Cement Chemistry.* New York: Acadamic Press Limited.

Taylor, H. (1997). *Cement chemistry.* London: Thomas Telford Publishing.

Terzaghi, K., Peck, R.B. and Mesri, G. (1996). *Soil mechanics in engineering practice* (3rd ed.). New York: John Wiley and Sons.

Topolnicki, M. (2004). *In-situ soil mixing: ground improvement.* (M. Kirsch, Ed.) London: Spon Press.

USEPA. (1993). *Solidification/stabilization and its application to wastes material.* Technical resource document: EPA/530/R-93/012.

Wang, X. and Lee, H. (2009). Simulation of a temperature rise in concrete incorporating fly ash and slag. *Materials and Structures, 43*, 737-745.

Vapalli, S.K., Fredlund, D.G., and Pufhal, D.E. (1999). The influence of soil structure and stress history on the soil-water characteristics of a compacted till. *Geotechnique, 49*, 143-159.

Viklander, P. (1998). Permeability and volume changes in till due to cyclic freeze-thaw. *Canadiana Geotechnical Journal, Vol. 35*, 471-477.

Yousuf, M., Mollah, A., Vempati, R.K., Lin, T.-C, and Cocke, D.L. (1995). The interfacial chemistry of solidification-stabilization of metals in cement and pozzolanic material systems. *Waste Management*, 137-148.

Yu, Y., Ugai, K., and Pu, J. (1997). Study of mechanical properties of soil-cement mixture for a cutoff wall. *Journal of soil and foundations, 37*(4), 93-103.

Zienkiewicz, O. (2000). *Finite element method: The Basis* (5 uppl., Vol. 1). Butterwooths.

Åhnberg, H. (2006). Consolidation stress effects on the strength of stabilized Swedish soils. *Ground Improvement, Vol.10*(1), 1-13.

Åhnberg, H. (2007). On yield stresses and the influence of curing stresses on stress paths and strength measured in triaxial testing of stabilized soil. *Canadian Geotechnical Journal, Vol. 44*(1), 54-66.

Åhnberg, H., Bengtsson, P.-E. and Holm, G. (2001). Effect of initial loading on the strength of stabilized peat. *Proceedings of the ICE - Ground Improvement, Vol. 5*(1), 35-40.

PART II

Appended papers

Paper I

Makusa, G.P., Mácsik, J., Holm, G., and Knusson, S. (Submitted). Process Stabilization–solidification and physicochemical factors influencing strength development of treated dredged sediments (Submitted: *Geo-Chicago 2016: Sustainability, Energy and Geoenviroment conference*)

Process Stabilization–solidification and Physicochemical Factors Influencing Strength Development of Treated Dredged Sediments

Gregory P. Makusa[1], S.M.ASCE, Josef Mácsik[2], Göran Holm[3], Sven Knutsson[4].

[1]PhD student, Department of Civil, Environmental and Natural resources engineering, Luleå University of Technology, Sweden. gregory.makusa@ltu.se
[2]Ecoloop, Stockholm, Sweden. josef.macsik@ecoloop.se
[3]Director, Swedish Geotechnical Institute, Linköping, Sweden. goran.holm@swedgeo.se
[4]Professor, Department of Civil, Environmental and Natural resources engineering, Luleå University of Technology, Sweden. sven.knutsson@ltu.se

ABSTRACT: Process stabilization–solidification (PSS) is a convenient technology for amending high water content dredged sediments (DS) with binders. The PSS equipment comprises of a chassis that carries a pugmill and silos of up to four binders. Primary binders such as cement can be supplemented with pozzolanas materials. In this study, physicochemical interactions of single and composite (ternary) binders on strength development of treated DS are examined based on laboratory and a large–scale field tests. The findings of this study show that fixed amount of cement content at increasing initial water content of the DS contribute to decreased level of calcium ions in the blend. Organic matter in the DS retains calcium ions liberated during cement hydration. This causes delay in formation of calcium hydroxide (CH), nucleation and crystallization of calcium silicate hydrates (CSH). Delay in the formation of CH hinders pozzolanic reaction of mineral admixture. Furthermore, increased amount of free water surrounding the stabilized mass causes weakening effect on CSH bond and pH neutralization. It is concluded that strength development of dredged sediments will depend on the amount of cement in the blend in relation to mineral admixture, initial water content of the DS, and the amount of organic matters.

INTRODUCTION

Stabilized dredged material can have improved strength and reduced compressibility. These properties can make the stabilized dredged material (SDM) suitable for use in a structural or non-structural backfill. It is important to conduct both laboratory and field investigations to assess the treatability of the dredged sediments for engineering applications. The aim of laboratory tests on representative samples of the DS is to prescribe the design mixture, amount of binders or composite binders, and to predict in-situ performance of the stabilized mass.

Process stabilization–solidification (PSS) is an emerging technology for blending high water content dredged sediments (DS) with binders. The PSS equipment comprises of a chassis that carries pugmills and silos of up to four binders. The mixing process is controlled from a control room. The proportions of binder and the DS are regulated and checked on real time while maneuvering the position of the

pumps that transport the DS from the barge to the pugmill. ProSol2010 (Fig. 1) is an example of the PSS equipment that was developed by PEAB, a Swedish construction company. It is environmentally friendly, quiet and dustless equipment. It can mix more than 300 m^3 of sediments per hour (Holm et al. 2012).

The use of composite (ternary) binders for stabilization–solidification of the DS is increasing. Primary binders such as cement can be blended with pozzolanic materials such as fly ash (FA) and granulated blast furnace slag (GGBS). Cement hydration is a complex process with a series of not very well known chemical reactions (Taylor, 1997). The hydration of cement incorporating supplementary cementitious materials (SCM) such as FA and GGBS is even more complicated due to the co-existence of cement hydration and the pozzolanic reactions of the mineral admixtures (Wang and Lee, 2009). ASTM C595 defines pozzolanas as siliceous and aluminous materials, which in itself possesses little or no cementitious values. However, in finely divided form and in the presence of moisture it reacts with calcium hydroxide (CH) at ordinary temperature to form compounds possessing cementitious properties. Clay minerals such as kaolinite, smectite, illite and mica are pozzolanic in nature whereas, fly ashes are artificial pozzolanas materials. Blast furnace slag has chemical composition similar to that of cement. It is, however, not cementitious by itself, but it possesses latent hydraulic properties which can develop in cementitious product when dissolved in an activator such as CH (ASTM 595).

The presence of natural pozzolanas in the DS may influence the hydration reactions of artificial pozzolana materials utilized as SCM. The present study examines the physicochemical factors that affect the hydration of the SCM and strength development of treated dredged sediment.

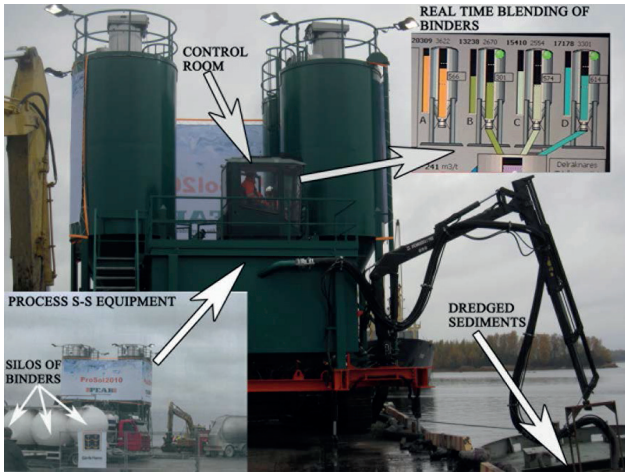

FIG. 1. Process stabilization–solidification (ProSol2010) equipment at work.

CASE STUDY

To study the possibility to improve the mechanical properties of the dredged sediment (DS), initial laboratory tests were carried out by Fossenstrand (2009) and Lagerlund (2010a, 2010b). Lagerlund (2010b) utilized typical dredged sediments from the Port of Gävle with average water content of 450 %. Byggcement (BC), Bio fly ash (BFA) and ground granulated blast furnace slag (GGBS) were utilized. Cementa AB is producer of BC in Sweden. The BFA and GGBS were obtained from Vattenfall power plant and Merox AB, respectively. BFA and GGBS were utilized as supplementary cementitious material (Holm et al., 2012). A design recipe with a mix combination of BC/BFA/GGBS by 40%/40%/20%, respectively by total weight of binder was selected. It was concluded that a binder dosage of 150 kg/m3 by total weight of the DS would meet the desired unconfined compressive strength of 140 kPa (equivalent to undrained shear strength of 70 kPa) after 91 days of curing. This amount of composite binder was chosen based on cost analysis and the fact that minimum shear strength of 50 kPa is sufficient for structural backfill (Holm et al., 2012; EuroSoilStab, 2002).

In order to exemplify geotechnical properties of in–situ treated DS, a large–scale field test was carried out at Granudden terminal at Port of Gävle in Sweden. Mixing and backfilling operations at the large–scale field test started at the end of October 2010 and continued through the end of November 2010. The sequence of operations at the large–scale field test is shown in Fig. 2. Mechanical dredges (Fig. 2A) were utilized to remove underwater volumes of fine sediments from Sea bottom down to a depth of 0.5 m. The dredged sediments were transported in barges to on–site treating facility (i.e. ProSol2010) which is partly shown in Fig. 2B. About 8,000 m^3 of the stabilized dredged material (SDM) was utilized in a reclaimed area as a structural backfill material (Holm et al., 2012; Makusa et al., 2012). The SDM at the large–scale field test was preloaded with a fill of selected gravel as shown in Fig. 2C. Application of preloading weight is usually carried out immediately after completion of backfilling. However, the placing of the surcharge at the test site was delayed due to low strength of the SDM to support the selected preloading weight (Holm et al., 2012). Consequently, the first phase of the application of the surcharge started on February 6, 2011 (i.e. about 65 days after completion of mixing and placement). A selected gravel of about 1.0 m high (equivalent to an average value of 18 kPa) was applied over a 4 days period. The second phase of preloading was carried out from March 7–16, 2011 using the same gravel fill of about 1.5 m high (equivalent to an average value of 27 kPa). For quality assurance, determination of undrained shear strength and classification of soil behaviour, several cone penetration tests (CPT) were carried out after different length of curing. Figure 2D presents an example of CPT profile obtained in October 4, 2011. The measured average total cone resistance was in the range of 0.5 MPa–0.7 MPa. Holm et al. (2012) reported average undrained shear strength of 50 kPa after curing period of about 365 days. These values were significantly lower than anticipated values based on initial laboratory tests study. Consequently, a laboratory test study was initiated to qualitatively find out factors that contributed to the observed field strength.

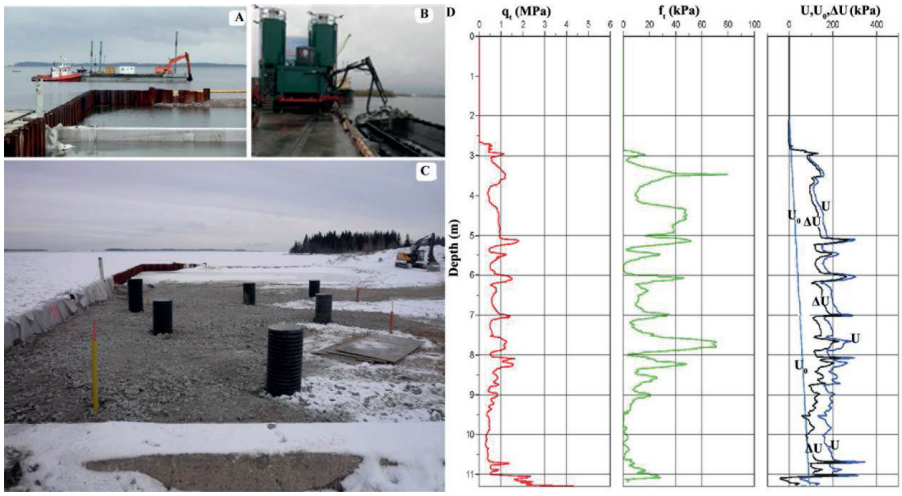

FIG. 2. Sequence of operations during the large-scale field test. A= dredging and reclaimed area, B=PSS equipment, C=preloading and monitoring instrumentation, and D=CPT profile after 250 days of curing. q_t is the total cone resistance, f_t is the sleeve friction. U, U_0 and ΔU are the CPT pore pressure, hydrostatic pore pressure and excess pore pressure, respectively (Data: Courtesy of WSP).

STUDY ON FACTORS INFLUENCING FIELD STRENGTH

Materials and Methods

Due to lack of necessary volumes of material from Port of Gävle, this study utilized dredged sediments (DS) from Port of Oskarshamn (about 380 km south of Gävle), where dredging activities were taking place. The DS used were of two types, namely DS-A and DS-B. The average initial water content of DS-A and DS-B were 283% and 356%, respectively. Results from X-rays diffraction (XRD) analysis on representative samples of the studied DS showed that quartz and feldspars mineral groups of Albite (plagioclase feldspars), microcline (alkali feldspars) and Biotite were the dominating minerals. Qualitative analyses of mineral phases associated with DS are presented in **Table 1.** Physical properties of the studied DS are shown in **Table 2**. Generally, the studied DS were mainly of organic nature. According to Pousette et al. (1999), organic soils and peat are rich in water content of up to 2000% with high porosity and organic content. Accordingly, organic matters on the studied DS were obtained by wet sieving process to obtain particles size distributions. The DS particles retained on sieve size less than 4 mm were dried and pulverized. The pulverized powders were then burnt in a furnace at 800°C to determine the organic matter, which was utilized to compute losses of ignition (LOI). The cumulative percentages LOI for the DS particles with diameter less than 4 mm were 235% and

413% for DS-A and DS-B, respectively (**Table 2**). These values were proportional to the water content of the DS. Most of DS particles that were retained on sieve size 4 mm and above were debris and barks of trees.

Binders used were either a combination of Byggcement (BC), unclassified fly ash (FA) and ground granulated blast furnace slag (GGBS) or single binder by BC only. The FA and GGBS were obtained near Luleå city in Sweden, from Billerud Karlsborg paper mill (Billerud Korsnäs) and SSAB steel industry, respectively. The average mineral compositions for individual binder are presented in **Table 3**.

Table 1. Phases of minerals associated with studied dredged sediments.

Mineral name	Chemical formula	Score_DS-A	Score_DS-B
Quartz	SiO_2	48	53
Albite	$NaAlSi_3O_8$	21	32
Annite	KFe_3^{2+} $NaAlSi_3O_{10}(OH,F)_2$	6	-
Dolomite	$CaMg(CO_3)_2$	10	-
Biotite	$K(Mg,Fe)_3AlSi_3O_{10}(F,OH)_2$	8	13
Pyrite	FeS_2	-	57

Table 2. Physical properties of studied dredged sediments: LOI is the loss of ignition on DS with particles size <= 2mm, Gs is the specific gravity, w is the average initial water content. LL is liquid limit. PL is the plastic limit, and ρ is the average bulk density.

	w (%)	LL (%)	PL (%)	ρ g/cm^3	LOI (%)	Gs
DS-A	284	120	88	1.19	235	2.53
DS-B	357	122	85	1.17	413	2.37

Table 3. Mineral composition for individual binder: FA-Fly ash (Svensson and Andreas, 2012), GGBS-ground granulated blast furnace slag (Data: Courtesy of SSAB), and BC-Byggcement (Holm et al. 2015).

Chemical compound	FA (%)	GGBS (%)	BC (%)
CaO	21	31	63
SiO_2	43	34	18
Al_2O_3	10	13	5
MgO	4	17	
K_2O	5		

Sample Preparations and Testing

Samples were prepared by amending dredged sediment at received water content with either composite binder (CB) or single binder by BC only as shown in **Table 4**. The amounts of binders were estimated such that at different initial water content of

the DS, the same immediate water content could be achieved on treated DS-A and DS-B during induction period. A detailed approach on how to estimate the amount of binders based on anticipated immediate water content was presented by Makusa et al. (submitted to International Journal). The immediate water content of 160%, 180%, and 210% was selected and the amount of binder between 100 kg/m^3 and 320 kg/m^3 was utilized. These are typical amounts of binders for stabilization of high water content dredged sediments in Sweden (EuroSoilStab, 2002). The variations in achieved water content were used to assess the effect of varying water content on the strength of stabilized mass.

Mixing was carried out using a spatula to produce a representative sample of the SDM. The duration for mixing was kept short (about 5 minutes), yet, the mixing speed ensured that the stabilized material became homogenous as per EuroSoilStab (2002) directives. Immediately after mixing, a representative sample from each SDM was utilized to determine the immediate water content. The remaining samples were molded in cylindrical polyvinyl chloride (PVC) tubes to obtain cylindrical samples with dimensions 50 mm x 170 mm. The SDM samples were placed in the PVC tubes and allowed to fall freely to the bottom of the tubes by vibrations of its bottom end without mechanical compaction. In order to obtain average test results, duplicate samples were prepared for each design recipe. An open curing condition was adopted, where curing water could enter or leave the SDM samples through bottom or top filters. On the other end of PVC sample tubes, filter plug was inserted and a preloading weight of 22 kPa was placed as shown in Fig. 3. The SDM samples were cured under water in a room with ambient temperature of 18 °C ± 5.

After prescribed curing period, sample tubes were removed out of the curing container and mounted to a mechanical jack, which was used to extrude the SDM specimens for unconfined compression test. Specimens were obtained by extruding and trimming 100 mm height of the SDM samples. The unconfined compression test was carried out using strain–controlled method at a deformation rate of 1 mm/min.

Table 4. Design recipes utilized to prepare samples of stabilized dredged materials (SDM).

DS	SDM	Binder Dosage kg/m^3	Recipe C/FA/GGBS	Cement quantity kg/m^3	Assumed water content (%)	Curing period (days)
A	A-CB1	250	1:1:0.5	100	160	7,28,91
A	A-CB2	180	1:1:0.5	72	180	7,28,91
A	A-CB3	110	1:1:0.5	44	210	7,28,91
A	A-BC1	250	1:0:0	250	160	7,28
A	A-BC2	110	1:0:0	110	210	7,28
B	B-CB1	320	1:1:0.5	128	160	7,28,91
B	B-CB2	180	1:1:0.5	72	210	7,28,91
B	B-CB3	260	1:1:0.5	104	180	7,28,91
B	B-BC1	315	1:0:0	315	160	7,28
B	B-BC2	180	1:0:0	180	210	7,28

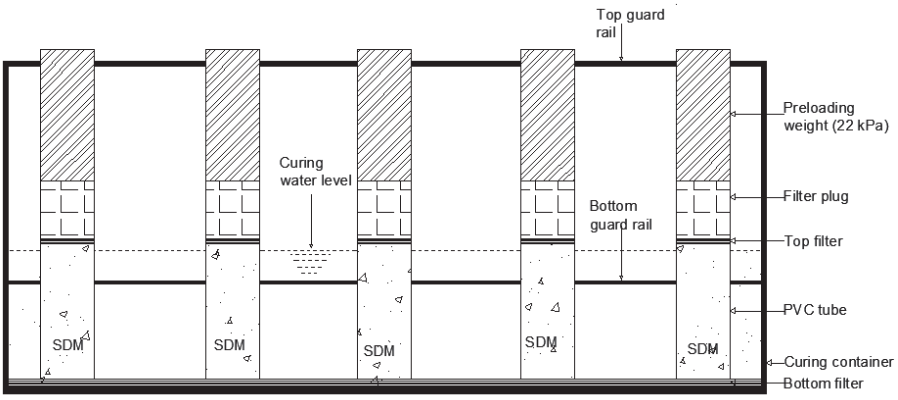

FIG. 3. A cross section view through a curing container showing PVC tube with SDM, bottom and top filters, and applied preloading weight.

RESULTS

Influence of binder on initial water content

The amounts of binders were estimated based on the anticipated water content of treated dredged sediments (DS). As expected, addition of dry binders reduced the initial water content of the DS. The anticipated water content agrees reasonably well with the measured water content during induction period as shown in Fig. 4(a). The amount of water content of the DS decreased with increasing amounts of binder as shown in Fig. 4(b). Results show that at varying initial water content of the DS, uniform water content of the SDM could be achieved by varying the amounts of binder (Fig. 4b).

Influence of binder on strength

The amounts and type of binders had an influence on the unconfined compressive strength (UCS) of treated DS. Figure 5 presents an example of the effect of binders on the UCS of treated DS-A. Results show that composite binder (CB)–treated DS-A (A1-A3) exhibited the lowest UCS values at the same amounts of binder as shown in Fig. 5(a). Furthermore, no correlation between the amount of binders and the achieved UCS values could be established. However, Fig. 5(b) indicates that the UCS values increased with increasing cement quantity in the blend. Furthermore, regardless of the type and amount of binder, DS treated with the same cement quantity attained approximately the same UCS values (e.g. A1 and A5). Irrespective of the type and amount of binder, the improved strength in all samples occurred during the first 7 days of curing as shown in Fig. 6.

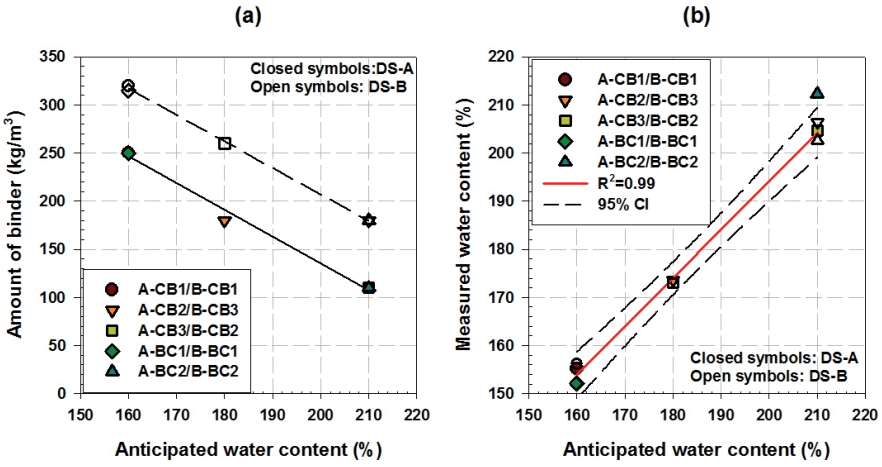

FIG. 4. Influence of the amount of binder on immediate water content of the SDM

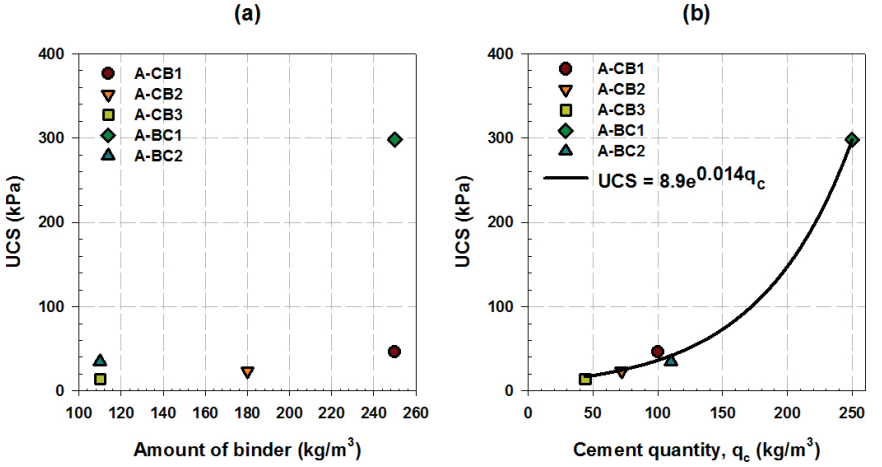

FIG. 5. Influence of (a) amount of binder (b) cement quantity on the UCS.

Influence of water content

The water content had influence on the achieved UCS values. Irrespective of the type and amount of binder, the UCS increased with decreasing water/cement (w/c) ratio (Fig. 7). Regardless of type of binder, the minimum UCS value of 100 kPa could be achieved at maximum w/c ratio of 4.5. The change in measured water content on the SDM during curing period was insignificant for CB–treated DS as

shown in Fig. 8. Results show that the measured water content in these samples remained almost the same as the predicted water content during the induction period (0 day). The only possible explanations for this are: (i) water for hydration reaction was drawn from curing container and the locked water within the SDM remained the same. (ii) there was continuous replacement of utilized lodged water by curing water through capillary action. Both of these phenomena may cause weakening effect on the CSH bond.

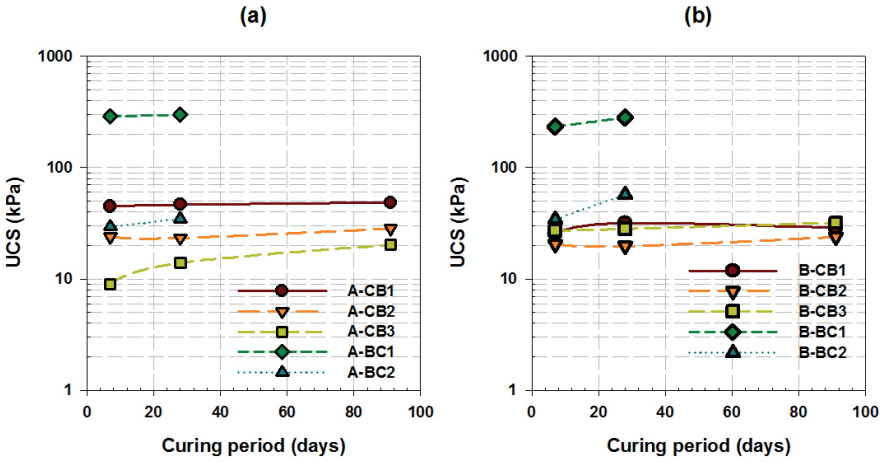

FIG. 6. Influence of curing period on the UCS (a) SDM-As (b) SDM-Bs.

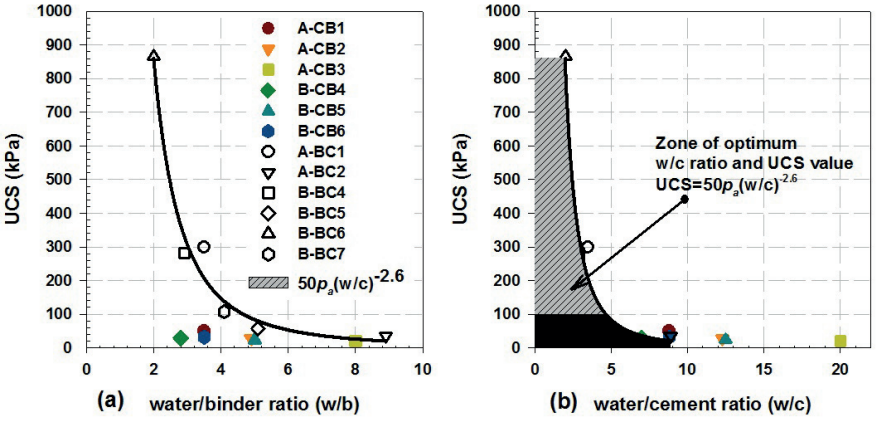

Figure 7. Influence of (a) water/binder ratio (b) water/cement ratio on the unconfined compressive strength (UCS)

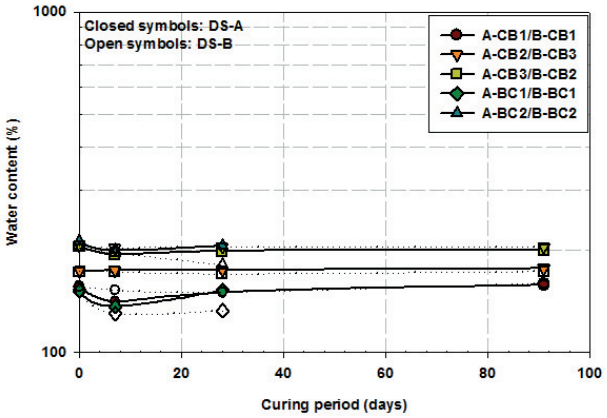

FIG. 8: Influence of underwater curing on water content of the SDM.

DISCUSSION

Successful stabilization–solidification of high water content dredged sediments depends on stabilization methods and materials. Process stabilization–solidification (PSS) utilizes constant amount of binders or composite binders to amend the dredged sediment (DS) at varying initial water content. The physicochemical interactions that influence the strength development of treated dredged sediments include cement quantity in the blend, mineral admixture, alkaline condition and water content as discussed hereafter.

Influence of cement quantity

Regardless of initial water content of the DS, the type and amounts of composite binder, the unconfined compressive strength (UCS) values increased with increasing cement quantity in the blend (i.e. decreasing water/cement ratio). These results suggest that for prescribed curing period the improved strength of the SDM were due to cement hydration only (Fig. 5b). Richardson and Groves (1997) observed that regardless of composition of blast furnace slag or fly ash, the main hydration products and principal binding phases in all calcium silicate–based pastes are the calcium silicate hydrate (CSH) gels. The measured UCS on both CB and BC-treated DS decreased with increasing w/c ratio (Figure 7). The minimum UCS of 100 kPa could be achieved at w/c ratio of 4.5. Consequently, improved strength of high water content dredged sediment depends on the amount of cement in the blend.

The following are the two main factors that contributed to low amount of cement and strength development:

- partial substitution of cement for fly ash or blast furnace slag decreased the

amount of cement in the mix. As a result, water/cement ratio increased.

- underwater discharge of the SDM immediately after mixing contributed to increased water/cement ratio.

Calcium hydroxide (CH) and calcium silicate hydrate (CSH) are the products of cement hydration. According to Sherwood (1993), reaction of CH brings up an increase in strength produced by cation exchange capacity rather than by cementing effect brought by pozzolanic reaction. However, organic soils have high exchange capacity. It can hinder the hydration process by retaining the calcium ions liberated during the hydration of calcium silicate and calcium aluminate in the cement to satisfy the exchange capacity (Hebib and Farrell, 1999; Åhnberg and Holm, 1999). **Table 2** shows that the studied DS contained excessive amount of organic matters. The cumulative percentage of organic matters was proportional to the water content of the DS. Thus, formation of CH was impaired, which caused dormant period on pozzolanic reaction of mineral admixtures. Wang and Lee (2009) reported some differences (i.e. dormant period) between cement hydration and the pozzolanic reaction of mineral admixtures.

Influence of mineral admixture

The pozzolanic reaction of mineral admixture will consume CH (Locat et al., 1990; Wang and Lee, 2009). The hydration rate of mineral admixture depends on the amount of the CH in the hydrating blend and the degree of hydration of the mineral admixture (Saeki and Monteiro, 2005). Upon cement hydration, calcium silicate minerals dissociate into charged silicate and calcium ions Ca^{2+} (Yousuf et al., 1995). The Ca^{2+} in a solution is removed by aluminum associated with mineral admixture and organic matter associated with dredged sediment (DS). This phenomenon depresses the Ca^{2+} concentration in the blend, which causes delay in the formation of CH, nucleation and crystallization of CSH gels (Hwang and Shen, 1991; Fajun et al., 1985). Generally, calcium hydroxide (CH) reacts with silica and alumina associated with the supplementary cementitious material (SCM) or DS to produce CSH and calcium aluminate hydrate (CAH). These are cementitious product similar to those of cement paste (Phair and Van Denventer, 2001; Taylor, 1997; Chrysochoou et al., 2010). However, the rate of reaction of the CH depends on the type of rock forming minerals and alkaline condition.

The studied dredged sediment (DS) contained significant amount of Albite ($NaAlSi_3O_8$). This rock forming mineral tends to delay formation of CSH and accelerates early formation of CAH due to increased amount of aluminum. Michiaki and Yoshikazu (1984) reported early formation of CAH and delayed formation of the CSH because of presence of the aluminium in albite minerals. According to Lee at el. (2013), CAH rapidly increases the compressive strength of treated soils. Accordingly, Figure 6 shows that rapid increase in strength occurred during the first 7 days of curing, irrespective of the type and amount of binder.

Influence of alkaline condition

In presence of calcium and alkaline condition, silica and alumina are the main elements required for formation of the CSH and CAH, respectively (Kamon and Nontanandh 1991; Chrysochoous et al., 2010). Literature study has shown that addition of lime will increase pH, which will favor solubility of siliceous and aluminous compounds associated with supplementary cementitious materials (SCM). Phair and Van Deventer (2001) reported strength increase with increasing pH. The UCS values obtained at pH 14 were 50 times larger than those obtained at pH 12.

Although lime was not directly utilized in this study, Chrysochoou et al. (2010) observed that low cement content contains inadequate free lime to buffer the pH. According to Kamon and Nontananandh (1991), the strength development associated with low amount of cement is attributed to an agglomeration caused by the exchange of calcium ions (Ca^{2+}), sodium ions (Na^{+}), and hydrogen ions (H^{+}). Thus, the long term increase in strength would depend on the cation exchange. It can be concluded that cation exchange will increase the amount of CH. This could cause elevated level of pH. However, underwater curing may lower the pH of the blend. As a result, the dormant period for reactivity of the SCM may last long.

Influence of water content

The studied DS contained significant amount of organic matters. The organic content was proportional to the initial water contents of the studied DS (**Table 2**). Haha et al. (2011) showed that high water–solid ratio may absorb some of heat of hydration, thereby prolonging the setting time. In addition to that, we postulate that increased amount of free water surrounding the SDM may supply surplus H^{+} by capillary action, especially prior to hardening of binder paste. This phenomenon may result in: (i) pH neutralization (ii) increased amount of free water surrounding the CSH and CAH. While low pH will impair further decomposition of the SCM, increased amount of free water will contribute to the formation of weak bonds. Wang et al (2011) observed that the compressive strength decreases because of weakening effect of water on CSH. According to Haha et al. (2011), at a high water–solid ratio, increased moisture surrounding the grains requires more time for the formation of rigorous structural network of hydrates to fill the voids. Consequently, weak CSH bonds contributed to low UCS values.

CONCLUSIONS

The physicochemical factors that influence the strength development of high water content treated DS were presented and discussed. The following are the two main factors that contributed to delayed strength development:

- partial substitution of cement for fly ash or blast furnace slag decreased the amount of cement in the mix by increasing water/cement ratio.
- underwater discharge of the SDM immediately after mixing contributed to

increased water/cement ratio and formation of weak CSH bonds.

The following the effects associated with low amounts of cement in the blend:

- reducing the amount of cement at increased water content and organic matter of the dredged sediments decreases the level of Ca^{2+} in the mix. Low Ca^{2+} in the blend delays formation of CH, nucleation and crystallization of CSH.
- the pozzolanic reaction of fly ash and blast furnace slag will depend on the amount of CH. Increased amount of CH will cause elevated pH, which will favor solubility and reactivity of pozzolanas material. CH will react with silicate and alumina associated with pozzolanas materials to produce CSH and CAH, which are cementitious product similar to those of cement for strength development.

Consequently:

- the amount of binder should be varied so that the amount of cement in the blend is proportional to water content.
- uniform water content on the SDM is achieved by varying the amount of binder at varying initial water content of dredged sediment during PSS.

ACKNOWLEDGEMENT

The authors would like to acknowledge Mr. Mats-Johan Rostmark at FriGeo AB for providing us with the dredged sediments for investigation. The Sustainable Management of Contaminated Sediments (SMOCS) project, Luleå University of Technology, Swedish Geotechnical Institute (SGI), and Ecoolop AB are hereby acknowledged for their technical and financial supports. Special thanks remain to laboratory technician Mr. Thomas Forsberg, Senior research engineer Kerstin Pousette for their help during laboratory experiments set up and testing.

REFERENCES

ASTM C 595. (1997). Standard specification for blended hydraulic cements. In *ASTM International.* ASTM International.

Chrysochoou, M., Grubb, G.N., Drengler, L.K and Malasavage, E.N. (2010). Stabilization dredged material. III: Mineralogical perspective. *Geotechnical and Geoenvironmental Engineering, 136*(8), 1037-1050.

EuroSoilStab. (2002). *Development of Design and Construction Methods to Stabilize Soft Organic Soils: Design Guide for soft soil stabilization.* Project No. BE-96-3177, CT97-0351: European Commission, Industrial and Materials Technologies Programme (Rite-EuRam III) Bryssel.

Fajun, W., Grutzeck, M.W. and Roy, D.M. (1985). The retarding effects of fly ash upon the hydration of cement pastes: the first 24 hours. *Cement and concrete research, 15*, 174-184.

Fossenstrand, I. (2009). *Stabilization and solidification of dredged Sediments at Port of Gävle.* Luleå: Luleå University of Technology.

Haha, M.B., Saout, G.L., Winnefeld, F., and Lothenbach, B. (2011). Influence of activator type on the hydration kinetics, hydrate assemblage and microstructural development of alkali-activated blast furnace slag. *Cem.*

Concr. Res., 41(3), 301-310.
Hebib, S. and Farrell, E.R. (1999). Some experiences of stabilizing Irish organic soils. *Proc. of dry mix methods for deep soil stabilization* (ss. 81-84). Stockholm: Balkema.
Holm, G., Bengtsson, P., and Larsson, L. (2012). *Field test at Port of Gävle, Sweden.* Linköping: Swedish Geotechnical Institute.
Holm, G., Larsson, L., Pettersson, M., Mácsik, J., Knutsson, S., and Makusa, G. (2015). *Durability-An expert study with focus on geo-constructions containing stabilized contaminated soils or sediments.* Linköping: Swedish Geotechnical Institute.
Hwang, C. and Shen, D. (1991). The effect of blast-furnace slag and fly ash on the hydration of Portland cement. *Cement and Concrete Research, 21*, 410-425.
Kamon, M. and Nontananandh, S. (1991). Combining industrial wastes with lime for soil stabilization. *Geotechnical Engineering, 117*(1), Paper No. 25411.
Lagerlund, J. (2010a). *Stabilization-solidification of dredged sediments from Port of Gävle, Step 1 (in Swedish).* Vattenfall Research and Development AB, Report. U09:109.
Lagerlund, J. (2010b). *Stabilization-solidification of dredged sediments from Port of Gävle, Step 2 (in Swedish).* Vattenfall Research and Development AB. Report. U10:162.
Lee, Y., Lim, D., Chun, B. and Ryou, J. (2013). Characterization of a sodium aluminate (NaAlO2)-based accelerator made via a tablet processing method. *Journal of Ceramic Processing Research, 14*(1), 87-91.
Locat, J., Bérubé, M-A., and Choquette, M. (1990). Laboratory investigations on the lime stabilization of sensitive clays: shear strength development. *Canadian Geotechnical Journal, Vol. 27*(3), 294-304.
Makusa, G. P., Montamen, N. T., Humad, A., and Knutsson, S. (Submitted). Unconfined compressive strength evaluation of cement-treated dredged sediments: unified approaches. *Geotechnical Testing Journal*.
Makusa, G.P., Mattsson, H., and Knutsson, S. (2012). Verification of field settlement of in-situ stabilized dredged sediments using cone penetration test data. *Electronic journal of Geotechnical Engineering, 17/Y*, 3365-3680.
Marchand, J., Bentz, D. P., Samson, E., and Maltais, Y. (2001). Influence of calcium hydroxide dissolution on the transport properties of hydrated cement systems. *Workshop on the role of calcium hydroxide in concrete* (pp. 119-129). Holmes beach, Anna Maria Island, Florida: National Institute of Standard.
Michiaki, H. and Yoshikazu, H. (1984). Experimental study on the reactivity of aggregate in concrete. *Bulletin of the International association of Engineering geology*, No. 30.
Phair, J.W. and Van Deventer, J.S.J. (2001). Effect of silicate activator pH on the leaching and material characteristics of waste-based inorganic polymers. *Mineral Engineering, 14*(3), 289-304.
Pousette, K., Mácsik, J., and Jacobsson, A. (1999). Peat soil sample stabilized in laboratory-experiences from manufacturing and testing. *Proc. of dry mix methods for deep stabilization* (pp. 85-92). Stockholm: Balkema.
Richardson, G.R., Groves, G.W. (1997). The structure of the calcium silicate hydrate

phases present in hardened pastes of white Portland cement/blast-furnance slag blend. *Journal of Materials Science*(32), 4793-4802.

Saeki, T. and Monteriro, P.J.M. (2005). A model to predict the amount of calcium hydroxide in concrete containing mineral admixture. *Cement and Concrete Research, 35*, 1914-1921.

Sherwood, P. (1993). *Soil stabilization with cement and lime. State of the art review.* London: Transport Research Laboratory, HMSO.

Svensson, M., and Andreas, L. (2012). *Characterization report-byproduct from Billerud Karlsborg AB (In Swedish).* Luleå, Sweden: Luleå University of Technology.

Taylor, H. (1997). *Cement chemistry.* London: Thomas Telford Publishing.

Wang, X. and Lee, H. (2009). Simulation of a temperature rise in concrete incorporating fly ash and slag. *Materials and Structures, 43*, 737-745.

Yousuf, M., Mollah, A., Vempati, R.K., Lin, T.-C, and Cocke, D.L. (1995). The interfacial chemistry of solidification-stabilization of metals in cement and pozzolanic material systems. *Waste Management*, 137-148.

Åhnberg, H. and Holm , G. (1999). Stabilization of some Swedish organic soils with different types of binders. *Proc. of dry mix methods for deep soil stabilization* (ss. 101-108). Stockholm: Balkema.

Paper II

Makusa, G.P. and Knusson, S. Influence of hydration phases on compressibility behaviour of high water content stabilized stabilized dredged sediments: an oedometer test study (Submitted: *Canadian Geotechnical Journal*)

Influence of hydration phases on compressibility behaviour of high water content stabilized dredged sediments: an oedometer test study

Gregory P. Makusa[1*] and Sven Knutsson[2]

[1]PhD Student, Department of Civil, Environmental and Natural resources engineering, Luleå University of Technology, SE-97187, Luleå, Sweden. Tel: +46 920 491688. Email: gregory.makusa@ltu.se

[2]Professor, Department of Civil, Environmental and Natural resources engineering, Luleå University of Technology, SE-97187, Luleå, Sweden. Tel: +46 920 491332. Email: sven.knutsson@ltu.se

*Corresponding author: alternative email: gmakusa@yahoo.com

Abstract: It is customarily required to apply preloading weight on stabilized dredged material (SDM) within 3 hours after mixing. The preloading weight serves two purposes: (i) as working platform for subsequent mixing work and (ii) to compress stabilized volume and bring soil particles close together for effective hydration. The purpose for subsequent preloading weight is to consolidate the stabilized mass for load other than service load. A laboratory test study was carried out on high water content SDM to evaluate compressibility behaviour within 3 hours after mixing and after 7, 28 and 91 days of curing. Based on the deformation behaviour of the studied SDM, three phases of hydration process influencing the compressibility of the SDM are identified. These are induction phase (IP), nucleation and crystallization phase (NCP), and hardening phase (HP). During IP, a protective layer is formed on the surface of binder particles. The SDM exhibit increased tangent compression modulus due to increased resistance to compression under daily application of preloading weight below apparent preconsolidation stress. NCP occurs when the protective layer become more permeable, which allows penetration of water molecules. Plasticity of binders increases which cause loss of apparent preconsolidation pressure and tangent compression modulus. HP is significant increase in thickness and stiffness of the protective layer. The tangent compression modulus and apparent preconsolidation stress increases by a set amount. This hinders further compression of the SDM and crashing of hardening cementatious bonds may occur. It is concluded that the maximum tangent compression modulus of untreated DS controls the maximum deformation of the SDM in all phases when the apparent preconsolidation become uncertain.

Keywords: preconsolidation stress, tangent modulus, stabilization-solidification, dredged sediments, induction, nucleation, crystallization, hardening.

Introduction

Dredged fine sediments are normally associated with high water content, low shear strength and high compressibility under load. Stabilization-solidification technology provides a cost effective method for amending high water content dredged sediments (DS) with binders to obtain stabilized dredged materials (SDM). The SDM can have improved strength and reduced compressibility. These properties can make the SDM suitable for geotechnical applications such as structural or non-structural backfill in either road embankments or reclaimed areas. However, stabilization-solidification technology is a site-specific project and there are no general rules for mix design to achieve a certain strength and stiffness. Thus, it is common practice that initial tests are conducted in the laboratory to obtain adequate data concerning the unconfined compressive strength (UCS) of the SDM before a full scale project can take over (EuroSoilStab 2002). The UCS is usually used as criteria for evaluation of strength and deformation behavior of the stabilized mass. According to Åhnberg (2007), the apparent preconsolidation pressure for stabilized soils is brought by cementation action. The cementation process and consolidation stress applied during curing greatly affect the apparent preconsolidation stress. This pressure is strongly linked to the strength of the stabilized mass and has considerable influence on its deformation behaviour. Bemben (1986) suggested that for cemented soils, the relevant preconsolidation stress is the only stress existing at the time of cementation.

For improved strength and reduced compressibility, it is common practice to preload the stabilized volume within 3 hours after mixing. According to Åhnberg et al. (2001), the ultimate increase in strengths of stabilized mass is not governed by applied preloading weight, but the amount of compression resulting from applied load. An increased initial compression will reduce the distances between binder grains and particles and facilitate the build-up of

bonds by the outer hydration products formed by the binders. In Sweden, gravel fill of about 1.0 m (equivalent to 18 kPa) is usually applied within 3 hours after mixing (EuroSoilStab 2002). Other researchers (Garbin et al. 2011; Anderson et al. 2000) have reported the applications of fill material of thickness in the range between 0.6 and 1.0 m. The initial preloading weight serves two purposes: (i) as a working platform during subsequent mixing and (ii) to compress the stabilized volumes and bring soil particles close together for effective hydration and remove air entrapped during mixing. Prior to hardening, additional consolidation stress is applied. According to EuroSoilStab (2002), the purpose for subsequent applications of preloading weight is to consolidate the stabilized mass for higher loads than self-weight. Forsman et al. (2008) and Holm et al. (2012) reported total thickness of about 2.5 m (equivalent to 45 kPa). However, the magnitude or thickness and the time for applications of additional consolidation stress are not defined.

Consolidation of stabilized dredged material (SDM) is the measure of its compressibility under sustained effective vertical stress due to dissipation of pore water. It can be assessed based on the extent to which the stabilized mass structure impedes the movement of pore fluid. The obstruction of pore water in the SDM can occur because of two reasons. Firstly, the existing pore water can be lodged in due to cementation action (Bemben 1986). Secondly, the initial pore water in the specimens is utilized during on–going hydration reactions. While the first possibility may prevent a change in void ratio, the latter may cause decreased initial water content and hydraulic conductivity. As a result, the compressibility of the SDM may be impaired.

To verify that hydration stage of binders may influence the compressibility of stabilized dredged material, a number of oedometer tests were carried out. This test was chosen because is the most utilized laboratory test for evaluation of deformation characteristics of

soils. The test has remained popular because of its simplicity in obtaining data for evaluation of stiffness parameters for use in design analysis. According to Crawford (1986), a primary objective of the consolidation test is to estimate the maximum pressure (i.e. preconsolidation stress) that may be applied to the soil without causing large deformation. Contrary, in stabilized dredged material (SDM), preconsolidation pressure defines the minimum consolidation stress, which can cause sufficient compression and bring the soil particles close together for effective hydration and improved strength. Thus, this laboratory test study was carried out to evaluate the compressibility behaviour of the high water content stabilized dredged sediments within 3 hours after mixing and during curing.

Materials

Dredged sediments

High water content dredged sediments (DS) were obtained from Port of Oskarshamn, which is located on the south-eastern coast of Sweden. The studied DS had received water content between 200% and 400%. Based on the received water content, the DS were categorized into two, namely; DS-A and DS-B. The average water content for DS-A and DS-B were 283% and 356%, respectively. Grain size distribution analysis was carried out using wet sieving method. For each sieve size less than 4 mm, the loss of ignition (LOI) on retained sediment was determined as shown in Table 1. The actual soil particles size in the DS were estimated by subtracting the percentage of organic content from their corresponding retained mass. The two studied DS were found to have the same particle size as shown in Fig. 1, but different amount of cumulative organic matter. The cumulative LOI were found to be proportional to the received water content as shown in Table 2.

The plasticity index of the studied DS-A and DS-B were 32% and 37%, respectively. Thus, the studied DS were classified as organic silt in accordance with ASTM D 2486.

Table 1: Percentage organic content retained on each sieve size.

	LOI (%)	
Sieve size	**DS-A**	**DS-B**
5.6	-	-
4	-	-
2	75.0	120.7
1	40.7	97.1
0.5	40.4	44.3
0.25	27.0	40.9
0.125	21.0	43.2
0.063	12.8	28.4
<0.063	18.7	38.1

Table 2. Physical properties of studied dredged sediments: LOI = loss of ignition on DS with particles size <= 2mm, Gs = specific gravity, w = average initial water content. LL = liquid limit. PL = the plastic limit, and ρ = average bulk density.

	w	**LL**	**PL**	**ρ**	**LOI**	**Gs**
	(%)	**(%)**	**(%)**	**g/cm^3**	**(%)**	
DS-A	283	120	88	1.19	235	2.53
DS-B	356	122	85	1.17	413	2.37

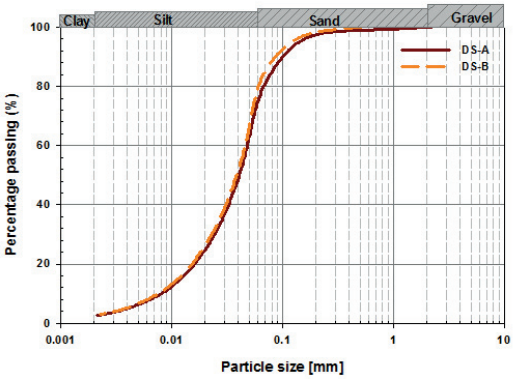

Fig. 1. Particle size distribution for dredged sediments corrected for organic matter.

Binder

The use of composite binders (CB) for stabilization–solidification of the dredged sediments (DS) is increasing due to increased artificial pozzolanas that can be utilized for partial substitution of cement. Thus, both blended binders comprising of Byggcement (BC), fly ash (FA) and ground granulated blast furnace slag (GGBS) or single binder by BC only were utilized to amend the DS. The CB was prepared by mixing BC:FA:GGBS at a ratio of 1:1:1/2, respectively by the total weight of binder. This ratio was chosen to mimic the stabilized dredged material (SDM), which was utilized at a large–scale field test at Port of Gävle (Holm et al. 2012). BC is produced by Cementa AB in Sweden. The off classified FA and GGBS were obtained from Billerud Karlsborg paper mill (Billerud Korsnäs) and SSAB steel industry, respectively. Table 3 shows the mineral composition of BC, FA and GGBS.

Table 3.Chemical compound for utilized fly ash, FA (Svensson and Andreas, 2012) and ground granulated blast slag, GGBS (Data: Courtesy of SSAB).

Chemical compound (%)	**FA**	**GGBS**	**Cement**
CaO	21.0	31	63
SiO_2	42.8	34	18
Al_2O_3	9.5	13	5
MgO	3.5	17	
K_2O	5.0		

Methods

Sample preparations and testing

Samples were prepared by blending dredged sediment at received water content with either composite binder (CB) or single binder as shown in Table 4. Mixing was carried out using a spatula to produce representative samples of the SDM. The duration for mixing was kept short (less than 5 minutes), yet, the mixing speed ensured that the stabilized material became homogenous as per EuroSoilStab (2002) directives.

Within 3 hours after mixing, parts of the stabilized samples were utilized to prepare specimen for the oedometer test. The remaining samples were moulded in cylindrical polyvinyl chloride (PVC) tubes to obtain cylindrical samples with dimensions 50 mm x 170 mm. The SDM was placed in the PVC tubes and allowed to fall freely to the bottom of the tubes by vibrations of its bottom end without mechanical compaction. In order to obtain average test results, duplicate samples were prepared. The sample tubes were placed in a curing container filled with water as shown in Fig. 2. An open curing condition was adopted, where curing water could enter or leave the SDM through the bottom filter by capillary action. This was done to reflect field condition, where the SDM was placed in reclaimed area filled with sea water. On the upper end of PVC sample tubes, filter plugs were inserted and preloading weight of 22 kPa were applied. The SDM samples were cured in laboratory room with ambient temperature of 18°C ± 5 for period shown in Table 4 before testing.

Table 4: Design recipes utilized to prepared the stabilized dredged material (SDM)

DS	Binder	Binder Dosage kg/m^3	Ratio C/FA/GGBS	Water/binder ratio	Cement quantity kg/m^3	Water/cement ratio	Curing period (days)
A	CB1	250	1:1:0.5	3.5	100	8.8	7,28,91
A	CB2	180	1:1:0.5	4.9	72	12.3	7,28,91
B	CB1	320	1:1:0.5	2.8	128	7.0	7,28,91
B	CB2	180	1:1:0.5	5.0	72	12.5	7,28,91
A	BC1	250	1:0:0	3.5	250	3.5	7,28
A	BC2	110	1:0:0	8.9	110	8.9	7,28
B	BC1	315	1:0:0	2.9	315	2.9	7,28
B	BC2	180	1:0:0	5.1	180	5.1	7,28

After a prescribed curing period, the sample tubes were taken out of the curing container and mounted to a mechanical jack, which was used to extrude the SDM sample from the PVC tubes. Specimens for oedometer test were obtained by trimming 20 mm height of the SDM sample. An oedometer ring with sharp edge at one end was used to trim a required diameter of 40 mm. A one-dimensional consolidation test was carried out using standard oedometer test

equipment. The oedometer tests were performed using sustained increment load (IL) ratio of 1.0. During initial seating, an effective vertical stress of 10 kPa was applied on specimens. The sustained load lasted for 24 hours before subsequent load increment. The sustained effective vertical stress on the specimens was doubled after every 24 hours to obtain consolidation stress values of 20, 40, 80, 160, 320 and 640 kPa. Thus, the oedometer test under IL lasted for 7 days. No unloading–reloading tests were performed on specimens.

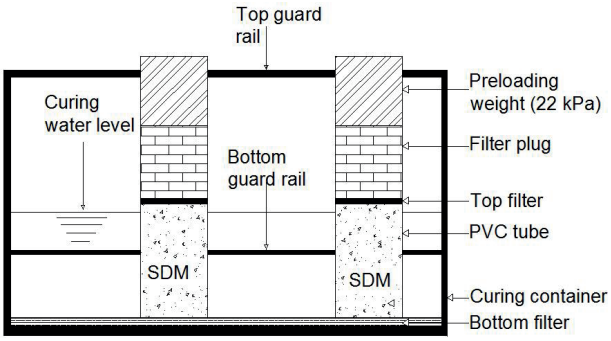

Fig. 2.Curing of the SDM sample under preloading weight in open water system.

Evaluations of test results

By interpreting the stress-strain curves from oedometer test results, compressibility parameters such as preconsolidation stress and tangent compression modulus can be obtained. According to Grozic et al. (2003), the preconsolidation stress (σ_c') interpreted from oedometer tests provides important information on the stress history of the soil, which in turn can be correlated to many behavioural properties. Researchers (e.g. Janbu 1963; Janbu 1998; Karlsrud and Hernandez-Martinez 2013; Crawford 1986; Sällfors 1975) have shown that soil specimen during oedometer test will have a relatively stiff response at stresses below preconsolidation stress and a soft response at stresses above σ_c'. The constrained modulus is

expected to drop to minimum value at applied effective stress near σ_c' and then increase with increasing applied effective stress values above preconsolidation stress σ_c'.

The accuracy in evaluating the preconsolidation stress $\sigma_c^{'}$ depends on the shape of compression curves in the $e - log\sigma_v^{'}$ or $\varepsilon - log\sigma_v^{'}$ curve, where e is the void ratio, ε is the vertical strain and $\sigma_v^{'}$ is the applied effective vertical stress. Well-known is Casagrande method (ASTM D 2435) or method proposed by Sällfors (1975). These techniques provide fast approach for obtaining the $\sigma_c^{'}$ provided there is a well-defined break in the $e - log\sigma_v^{'}$ or $\varepsilon - log\sigma_v^{'}$ curve.

The tangent compression modulus M, which was proposed by Janbu (1963) is preferred as a standard measure for the deformation characteristics for all types of soils. The modulus M varies with effective vertical stress σ_v' and all variation could be accounted for by:

$$[1] \qquad M = mp_a\left[\frac{\sigma_v'}{p_a}\right]^{(1-n)}$$

where m is the constrained modulus number, p_a is the atmospheric pressure, and n is the stress exponent. Janbu (1998) suggested the following steps for obtaining preconsolidation stress σ_c' and modulus number, m:

- obtain the tangent compression modulus from $M = \Delta\sigma_v'/\Delta\varepsilon$ for each load step.
- plot M versus effective vertical stress σ_v' in linear scale.
- obtain the preconsolidation stress σ_c' directly by inspecting $M - \sigma_v'$ curve, where σ_c' is determined by a change in the curve.
- determine the overconsolidated modulus M_{OC} for $\sigma_v' < \sigma_c'$ (in overconsolidated range) and determine the modulus number m in the normally consolidated range $\sigma_v' > \sigma_c'$.

Test results and discussion

The compressibility of untreated and treated high water content dredged sediment (DS) were evaluated in terms of stress-modulus ($M - \sigma_v'$) and stress-strain ($\varepsilon - log\sigma_v'$) relationships. The vertical strain of untreated DS increased linearly with applied effective vertical stress to a value of 80 kPa as shown in Fig. 3. At the end of consolidation test, the average water contents of untreated DS were found to be 81% and 77% for DS-A and DS-B, respectively. These values were below the plastic limit values of untreated DS as shown in Table 2. It can be concluded that at applied effective vertical stress of 80 kPa, the water contents of the DS were already reduced to a value below plastic limit. It follows that the DS were either in semi-solid or solid state, which increased resistance to compression during subsequent load increment.

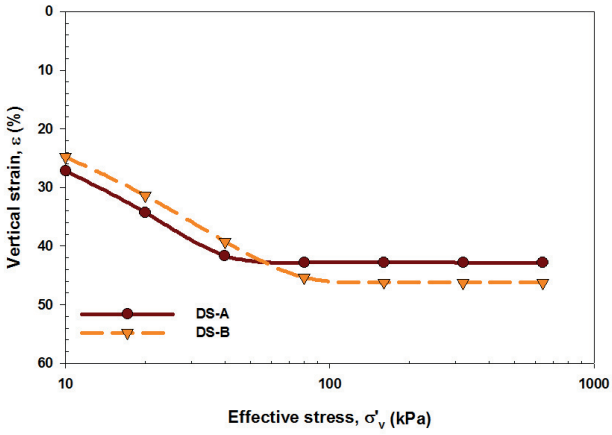

Fig. 3. Stress-strain curves for untreated DS.

Unlike the shape of $\varepsilon - log\sigma_v'$ curves of untreated DS, the shape of $\varepsilon - log\sigma_v'$ curves for treated DS varied with curing period, type and amounts of binders. For the same curing

period, the shape of the stress–strain curves were influenced by the type and amounts of binders. In relation to the stress-strain curve of untreated DS, Fig. 4 presents the stress-strain curves of treated DS subjected to the oedometer test within 3 hours after mixing. Generally, regardless of the type and amounts of binders, the shape of stress–strain curves for treated DS showed a well–defined break in the $\varepsilon - log\sigma_v^{'}$ curve (Fig. 4).

The tangent compression modulus values were evaluated on both treated and untreated DS and for each load step. The $\sigma_v' - M$ curves of untreated and treated DS are shown in Fig. 5 for samples subjected to oedometer test within 3 hours after mixing. The evaluated maximum tangent compression modulus values on untreated DS were about 6000 kPa, at the change in effective vertical stress from 40 kPa to 80 kPa. Beyond this value, the tangent compression modulus was undefined because no further vertical strains were recorded with the change in effective vertical stress (Fig. 3). Irrespective of the type and amounts of binders, the $\sigma_v' - M$ curves for all specimens subjected to oedometer test within 3 hours after mixing were characterized by an increase in tangent compression modulus to the maximum value M_m followed by abrupt drop to lower modulus M_L value as shown in Fig. 5. For specimens that exhibited increased tangent compression modulus values above 6000 kPa followed by a sudden drop, the tangent compression modulus further decreased with increasing effective vertical stress above 80 kPa. The trend indicated decreasing tangent compression modulus toward a constant value of about 6000 kPa as shown in Fig. 5(a and b). On the other hand, for specimens that exhibited increased tangent compression modulus M with maximum value below 6000 kPa prior to a sudden drop, the modulus increased again with increasing applied effective vertical stress above 80 kPa. The trend indicated increasing compression modulus as shown in Fig. 5.

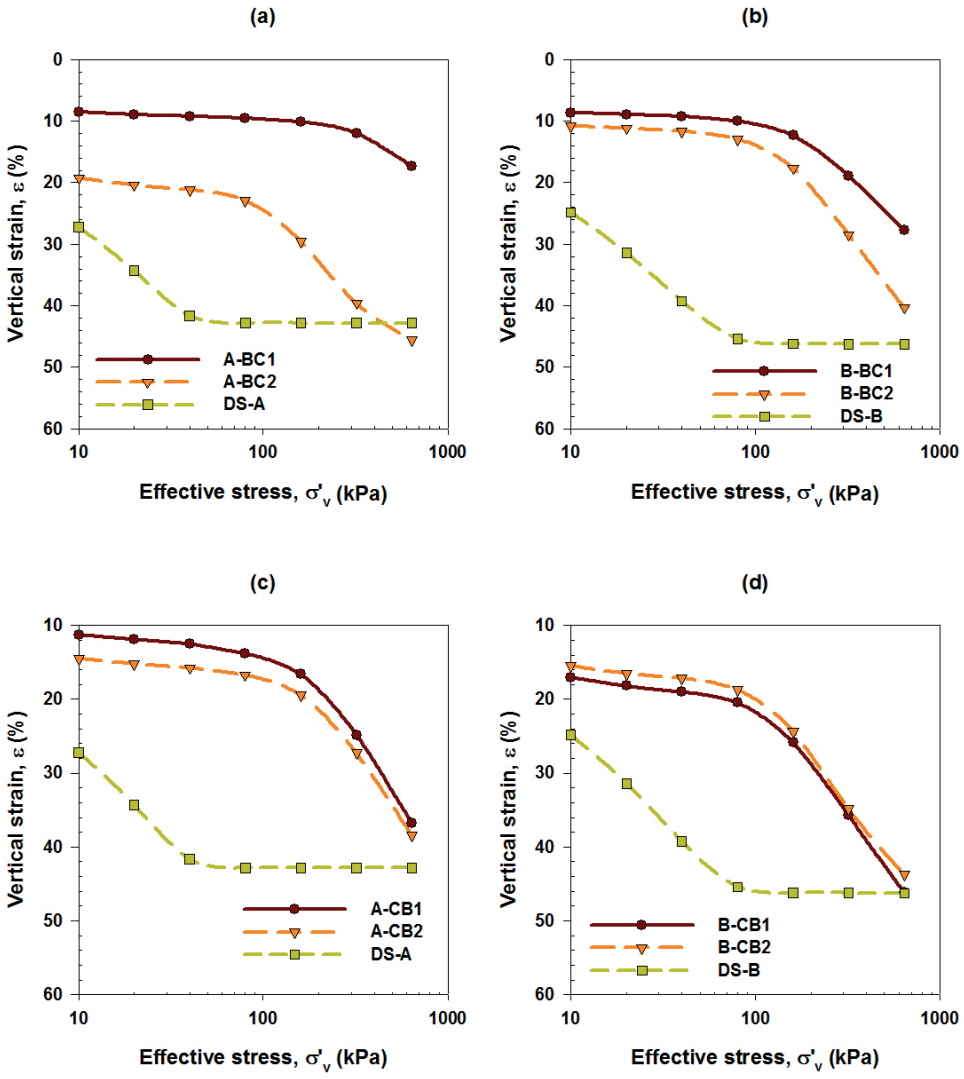

Fig. 4. Example of shape of stress–strain curves for untreated DS in relation to the stress–strain curves of the SDM subjected to oedometer test within 3 hours after mixing.

The evaluated tangent compression modulus values varied significantly without clear correlation between the calculated increased tangent compression modulus and type or the amount of binders. Nonetheless, the maximum tangent compression modulus values prior to a

sudden drop for these specimens were obtained at effective vertical stress around 80 kPa. Seemingly, the maximum effective vertical stress, which was required to reduce the initial water content of the untreated DS to a value below plastic limit, defined the apparent preconsolidation stress of treated DS.

Compared to the stress-strain curves for specimens tested within 3 hours after mixing, the stress-strain curves for specimens tested during curing period were less rounded in $\varepsilon - log\sigma_v'$ curves as shown in Fig. 6 and Fig. 8. The shape varied with the type and amount of binders. Generally, the shape of BC-treated DS varied with the amount of binder. At reduced amounts of BC, the shape of the stress–strain curves of BC-treated DS exhibited excessive deformation as shown in Fig. 6(for B-BC2 sample) similar to the untreated DS (Fig. 3). At increased amount of BC, the shape of the stress–strain curves for BC-treated DS was more or less rounded with or without a well–defined break in the $\varepsilon - log\sigma_v'$ curve as shown in Fig. 6 (A-BC2 sample) and Fig. 8(for A-BC1 and B-BC1 samples). Regardless of the amounts of binder, the shape of stress-strain curves for CB-treated DS were less rounded without a well–defined break in the $\varepsilon - log\sigma_v'$ curve as shown in Fig. 6 (for A-CB1 and B-CB2 samples).

The evaluated modulus values of treated DS during curing period varied with curing period, type and amount of binder. However, regardless of the type and amount of binder, specimens tested during curing showed little or no increase in overconsolidation modulus M_{OC}. For specimens that showed little increase in M_{OC}, the drop of it occurred at applied effective stress between 20 kPa and 40 kPa. Thus, these samples were characterized by loss of σ_c' and M_{OC}. Irrespective of the amounts of binder, the evaluated modulus values for all CB-treated DS were below 6000 kPa. The $\sigma_v' - M$ relationship on these samples could be idealized as linear as shown in Fig. 7 (for A-CB1 and B-CB2).

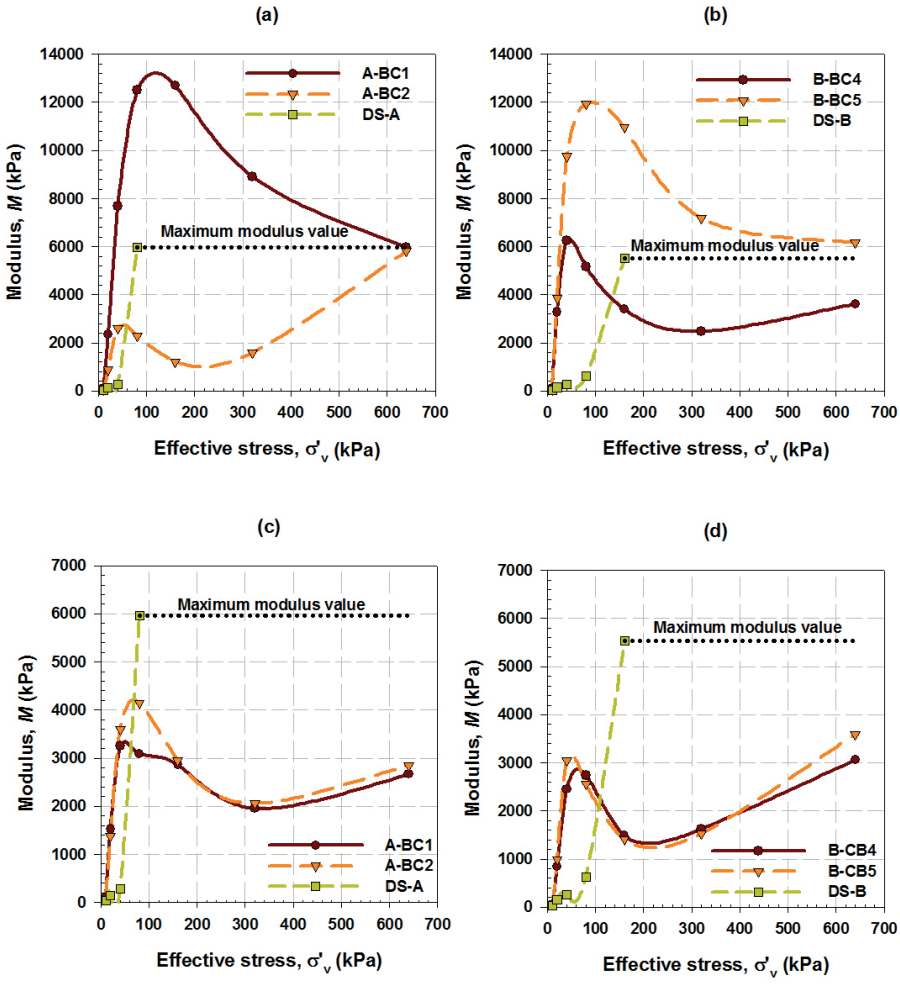

Fig. 5. Example of evaluated stress–Modulus relationship for untreated DS in relation to the SDM subjected to oedometer test within 3 hours after mixing.

The $\sigma_v' - M$ curves for these samples indicated increasing trend toward 6000 kPa. Generally, depending on the amount of BC or curing period, the modulus for BC–treated DS increased exponentially with increasing effective vertical stress as shown in Fig. 7 (for A-BC2) and Fig. 9. Likewise, increased modulus values in excess of 6000 kPa were followed by decrease in modulus values during subsequent load increment as shown in Fig. 9.

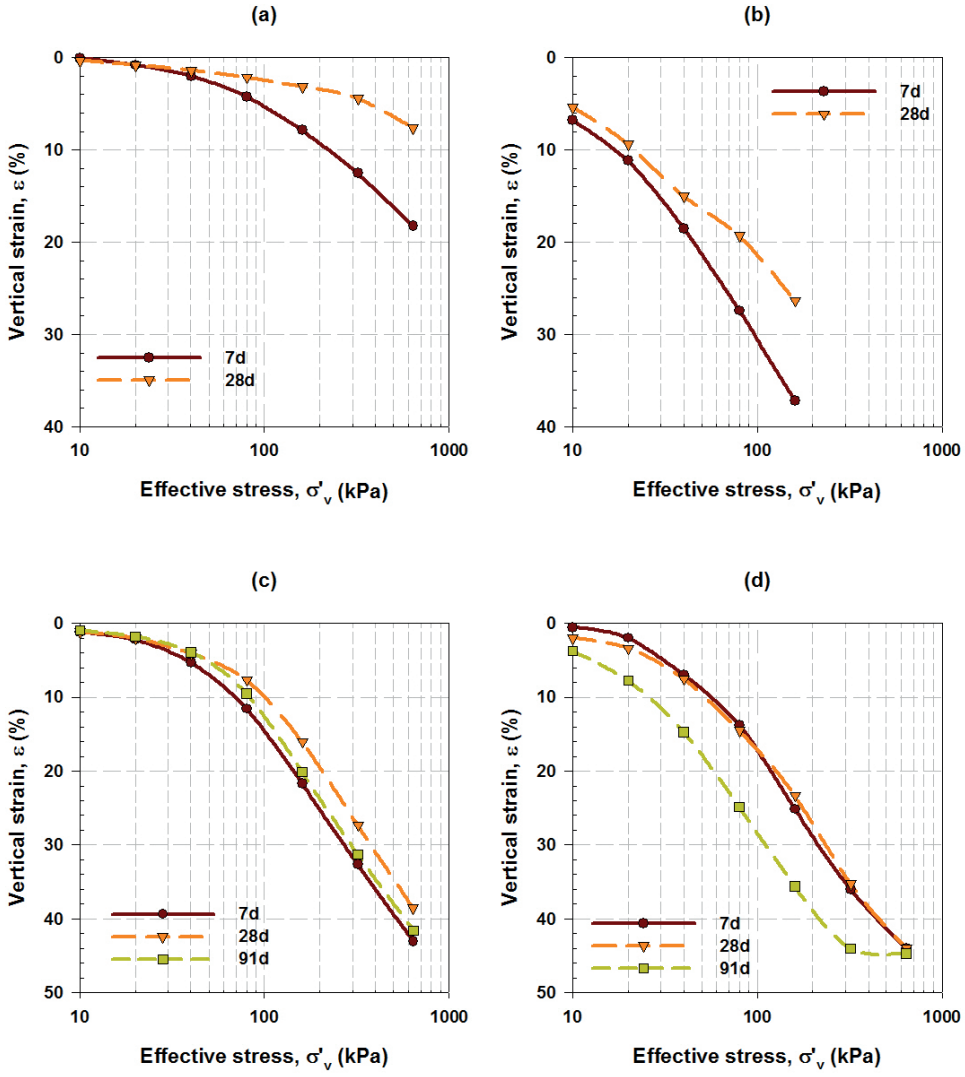

Fig. 6. Example of stress–strain curves for SDM subjected to oedometer test subjected to oedometer test during curing. (a) A-BC2 (b) B-BC2 (c) A-CB1 (d) B-CB2

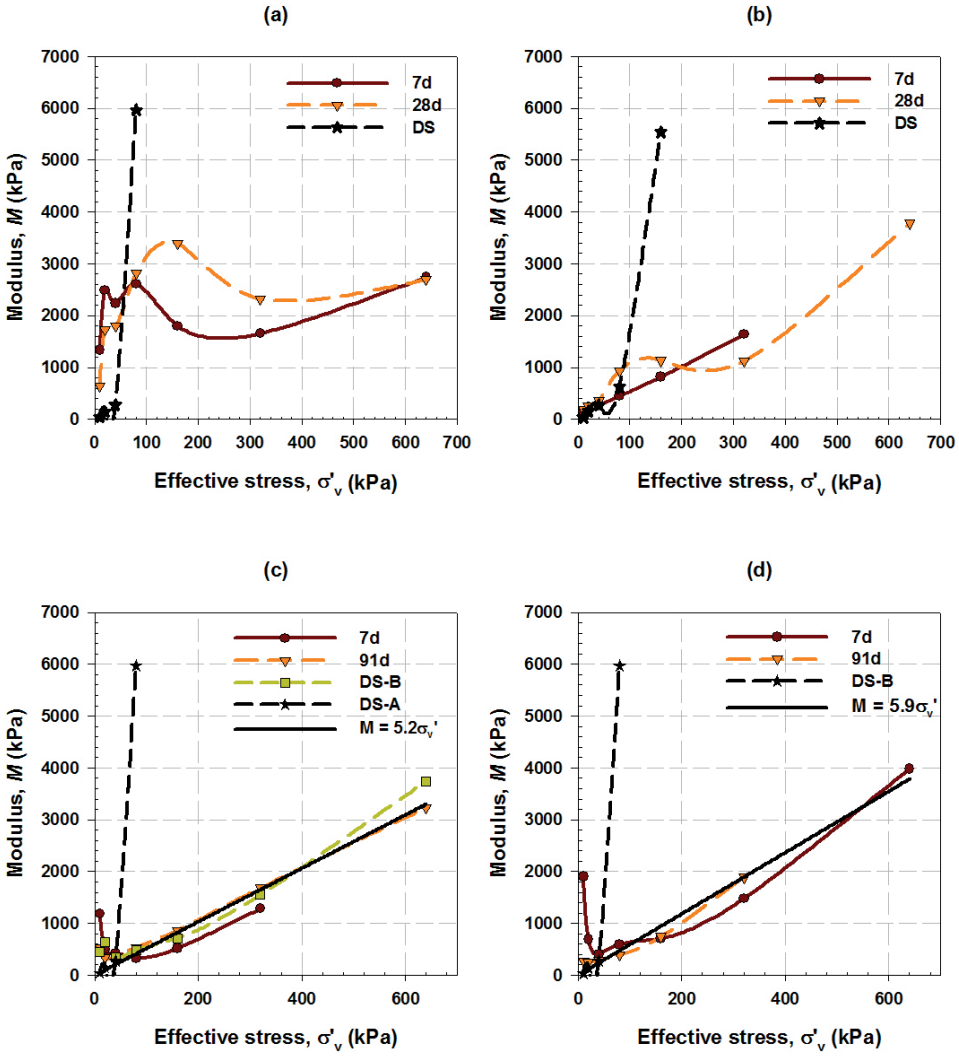

Fig. 7. Example of evaluated stress–Modulus relationship for SDM subjected to oedometer test during curing. (a) A-BC2 (b) B-BC2 (c) A-CB1 (d) B-CB2

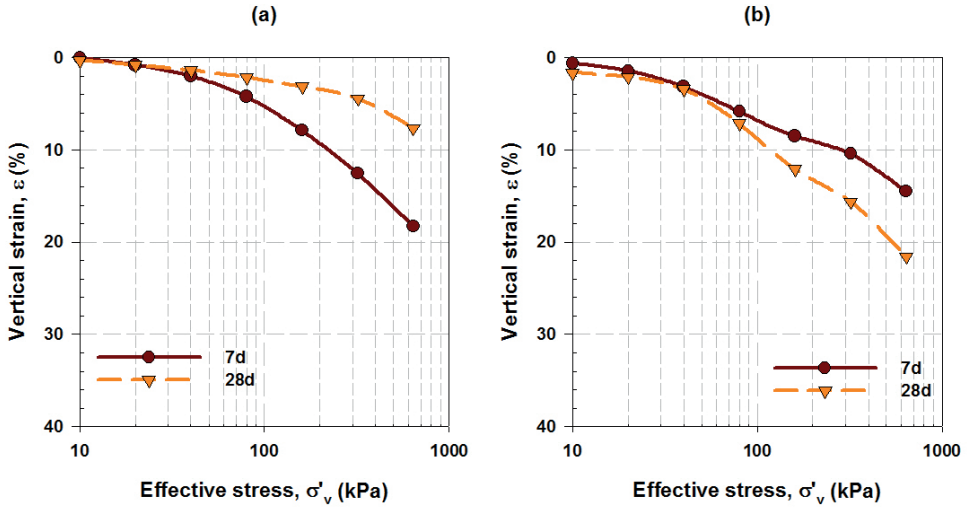

Fig. 8. Example of stress–strain curves for SDM subjected to oedometer test during curing. (a) A-BC1 (b) B-BC1

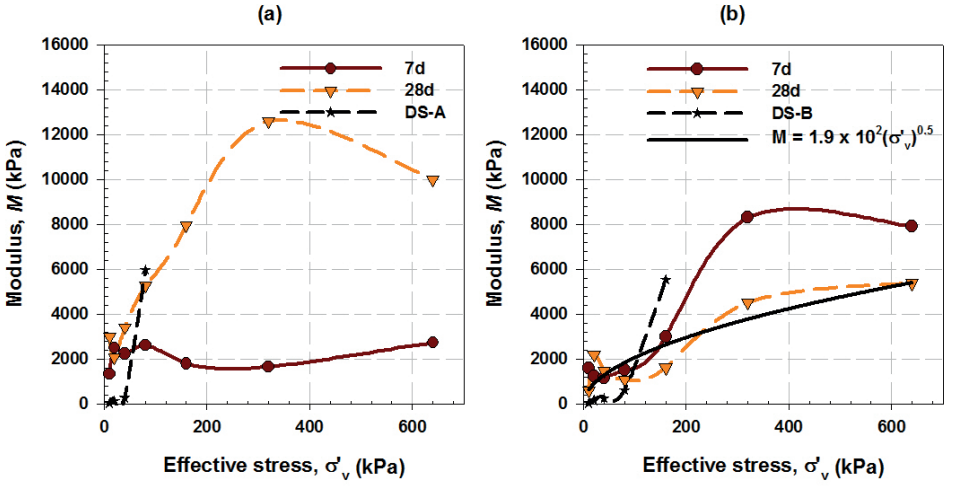

Fig. 9. Example of stress–Modulus behaviour for SDM during curing. (a) A-BC1 (b) B-BC1

Based on the deformation properties of treated DS, three phases of hydration mechanism that influenced the compressibility of the studied SDM were identified. These are induction

phase (IP), nucleation and crystallization phase (NCP), and hardening phase (HP) as described hereafter:

Induction phase

Specimens were considered in induction phase (IP) when subjected to oedometer test within 3 hours after mixing. In general, relative to the vertical deformation of untreated DS (Fig. 3), the vertical deformations of treated DS were all reduced, and the magnitude of reduction varied with the amounts of binder. The reduction in immediate vertical deformations could be a result of slow hydration of binder. Researchers (Ogawa et al. 1980; Yousuf et al. 1995) have shown that within 3 hours after mixing (i.e. induction period) a thin protective layer of calcium silicate hydrate (CSH) is formed around cement particle's surface. During this period, calcium silicate minerals dissociates into charged silicates and calcium ions. The charged silicate ions concentrate as a thin layer on the surface of cement grains to prevent the interaction of the cement surface with water. Thus, we consider that this mechanism of hydration process caused delay in immediate hydration and dissolution of binder. According to Sherwood (1993) hydration is a slow process proceeding from the surface of the cement grains while the centre of the grains may remain unhydrated. Consequently, the unhydrated portion of the binder behaved like a solid particles, which increased resistance to compression depending on the amount of unhydrated binder particles.

Irrespective of type and amounts of binder, increased vertical deformations were observed during initial seating under 10 kPa and at applied effective vertical stress above 80 kPa (Fig. 4). Thus, during IP, the SDM showed rigidity behaviour at applied effective vertical stress between 20 kPa and 80 kPa. Compressibility behaviour occurred under applied effective vertical stress above 80 kPa. Åhnberg et al. (2007) reported that stabilized soils behaved in overconsolidated manner when the consolidation stress was less than the preconsolidation

pressure. It behaved in normally consolidated manner when utilized consolidation stress was higher than the preconsolidation stress. It could be assumed that during the IP the preconsolidation stress of the SDM was equal to 80 kPa. This value was equal to the maximum effective vertical stress value that was required to reduce the water content of the untreated DS to a value below the plastic limit. Accordingly, the observed increase in vertical deformation could be associated with increased plastic limit of the DS as a result of addition of binder. Regardless of the type and amount of binder, the measured water content values for all treated DS (Table 4) were above plastic limit (Table 2). Sherwood (1993) observed that addition of lime will increase plastic limit of treated soils. Although lime was not directly utilized in this study, cement hydration produces lime as calcium hydroxide (CH). Chrysochoou et al. (2010) showed that low cement dosage contains inadequate free lime. Sherwood (1993) reported that the plastic limit of soil treated with lime content below 4% increases and remains almost constant with increasing percentage of lime above 4%. Thus, samples with low amount of cement contained low amount of lime. Consequently, the plastic limit on these samples increased considerably, which caused increased vertical deformations of the stabilized mass at applied effective vertical stress above 80 kPa as shown in Fig. 4. Regardless of the amount of binder, significant compression on all treated DS occurred during initial seating under 10 kPa and at applied effective vertical stress above 80 kPa. Thus, for sufficient compression, selected preloading weight must be applied all at once within 3 hours after mixing. The practical implication for this observation is that due to insufficient compression of the SDM, hardening of binder paste will take place at insufficient packing of blended DS particles. The ultimate effect is an increased void ratio and formation of metastable fabrics in the SDM. Mitchell and Soga (2005) observed that soil metastable structure occurs when particles and particle groups flocculate and pack inefficiently, which is

a typical characteristic of sensitive clay soils. These soils are characterized by high voids ratio, low hydraulic conductivity or undrained condition. The compressibility of sensitive clays is relatively low until the consolidation pressure exceeds the preconsolidation stress (Mitchell and Soga 2005). These arguments are in accordance with the finding of this study. It can be concluded that sensitive clay behaviour controlled the compressibility of the SDM during the IP.

Regardless of the type and amount of binder, the $\sigma_v' - M$ curves for all specimens subjected to oedometer test during IP were characterized by an increase in overconsolidation modulus M_{OC} followed by abrupt drop to lower modulus M_L value as shown in Fig. 5. According to Janbu (1967), the constrained modulus for sensitive clay tends to drop abruptly when the applied surcharge approaches the preconsolidation stress σ_c' value. For specimens that exhibited increased M_{OC} values with maximum value above 6000 kPa followed by a sudden drop, the modulus further decreased with increasing effective vertical stress above 80 kPa. The trend indicated decreasing modulus toward a constant value of about 6000 kPa as shown in Fig. 5 (a and b). On the other hand, for specimens that exhibited increased M_{OC} values with maximum value below 6000 kPa prior to a sudden drop, the modulus increased again with increasing applied effective vertical stress above 80 kPa. The trend indicated increasing modulus toward a constant value of about 6000 kPa as shown in Fig. 5. The measured M_{OC} values varied significantly without clear correlation between the evaluated M_{OC} and type or the amount of binders. Nonetheless, the maximum M_{OC} values for these specimens were obtained at effective vertical stress around 80 kPa. Consequently, the preconsolidation stress and tangent compression modulus of untreated DS determined the compressibility of the SDM during IP.

Nucleation and crystallization phase

The induction period (IP) ends when the protective layer changes to a more permeable membrane, which permits inward flow of water molecules, and outward migration of calcium ions and silicate ions. This results in accumulation of excess amount of calcium hydroxide (CH) on the fluid side of the membrane (nucleation) and precipitate (crystallization) of CSH (Ogawa et al. 1980; Yousuf et al. 1995).

Regardless of the shape of $\varepsilon - log\sigma_v'$ curve, specimens were considered in nucleation and crystallization phase (NCP) when the maximum evaluated modulus values were below that of untreated DS (i.e. 6000 kPa), and this is indicated by the increasing trend in $\sigma_v' - M$ curves. Regardless of the amounts of binder, the evaluated modulus values for all CB–treated DS were below 6000 kPa during the curing period of up 91 days (Fig. 7). The $\sigma_v' - M$ relationship for these specimens could be idealized as linear as shown in Fig. 7(c and d). This behaviour is a typical characteristic of normally consolidated clay. According to Janbu (1998), for normally consolidated clay the modulus increases linearly with effective vertical stress change, when the effective vertical stress is greater than the preconsolidation stress. Thus, it can be concluded that normally consolidated clay behaviour characterized the SDM in NCP.

Specimens in the NCP showed little or no increase in overconsolidation modulus. For specimens that showed little increase in M_{OC}, a sudden drop occurred at applied effective stress between 20 kPa and 40 kPa. Thus, samples in NCP were characterized by loss of apparent preconsolidation stress σ_c' and lower tangent compression modulus.

However, the immediate vertical deformations during initial seating under 10 kPa were significantly reduced. Except for sample B-CB2 (91d) and B-BC2 (Fig. 6), no significant compressions were observed under applied effective vertical stress between 10 kPa and 20 kPa. All measured vertical strains were below 5%. The reduction in immediate compression during initial seating was partly related to consolidation under effective stress of 22 kPa and due to hydration reactions. This phenomenon suggests that applications of additional consolidation stress, which is less or equal to the initial preloading weight will have no influence on further compression of the SDM. The loss of apparent preconsolidation stresses could be related to the increased plastic limit as a result of increased plasticity of binder. Thus, for increased compression and improve strength; it can be beneficial to apply subsequent preloading weight during NCP.

Hardening phase

Hardening phase (HP) is associated with significant increase in thickness and stiffness or solidifying of the protective layer. As a result, resistance to vertical deformations will increase. This phenomenon results in increased compression modulus regardless of the shaper of stress-strain curves. Thus, all specimens with evaluated modulus in excess of 6000 kPa were considered in hardening phase (HP). The $\sigma_v' - M$ curves were characterized by exponential increase in modulus followed by decrease when the modulus exceeded the magnitude of 6000 kPa as shown in Fig. 9. According to Janbu (1998), the modulus for silt sand varies with the effective vertical stress raised to power of 0.5. Thus, the compression behaviour of silt sand described the compression behaviour of the SDM in the hardening phase (HP). This type of behaviour was observed on BC–treated DS with increased amount of BC (A-BC1, and B-BC1).

The decrease in modulus that can be observed in Fig. 9 could be due to breakage or collapse of hardened CSH bonds at applied effective vertical stress higher than the preconsolidation stress. Thus, during the HP phase, the preconsolidation stress was increased by a set amount to a value of 320 kPa. Despite increased preconsolidation stress, the tangent compression modulus of the untreated DS determined the maximum deformation of the SDM at applied effective vertical stress in excess of increased preconsolidation stress. Thus, it might be beneficial to utilize the tangent compression modulus of untreated DS to estimate the maximum deformation when the preconsolidation stress of the SDM becomes uncertain. Topolnick (2004) observed that any safe design will require that the stresses inside the stabilized soil body do not exceed the capacity of soil–binder material.

Conclusions

The compressibility behaviour of stabilized dredged material (SDM) depends on hydration stages of binder during curing period. Results from this study show that, three phases of the hydration process determine the compressibility of high water content SDM during curing. These are induction phase (IP), nucleation and crystallization phase (NCP), and hardening phase (HP). The following are the distinguishing characteristics associated with each phase in relation to compressibility of the SDM:

- Induction phase (IP) occurred immediately after mixing. A protective layer was formed around the surface of binder particles and the inner portion remained unhydrated. The unhydrated portion of binder increased resistance to vertical compression. The SDM compression behaviour resembled that of sensitive clay.
- Nucleation and crystallization phase (NCP) occurred when the protective layer become more permeable, which allowed penetration of water molecules. The plasticity of binder attained its maximum values, which caused loss of the apparent preconsolidation stress and

lower tangent compression modulus. This phenomenon caused increased compressibility of the SDM during subsequent daily application of loading weight. The normally consolidated clay compression behaviour described the SDM deformation behaviour.

- Hardening phase (HP) was associated with significant increase in thickness and stiffness of the protective layer. Except for crushing, normal compression of the SDM was hindered. The apparent preconsolidation stress and tangent compression modulus indicated increased value. Silt sand deformation behaviour described the compressibility of the SDM.

In all phases of hydration process the tangent compression modulus of untreated DS determined the maximum vertical deformation of the SDM.

Acknowledgments

The authors would like to acknowledge Mr. Mats-Johan Rostmark at FriGeo Company for providing us with the dredged sediments for investigation. The Sustainable Management of Contaminated Sediments (SMOCS) project and Luleå University of Technology are hereby acknowledged for their technical and financial supports. Special thanks remain to laboratory technician Mr. Thomas Forsberg and senior research engineer Kerstin Pousette for their help during laboratory experiments.

References

Andersson, R., Carlsson, T. and Leppänen, M. (2000). Hydraulic Cement Based Binders for Mass Stabilization of Organic Soils. *Soft Ground Technology*. Noordwijkerhout, The Netherland.

ASTM D 2435/D2435M. (2011). Standard test methods for on-dimensional consolidation properties of soils using increment loading. In *Annual Book of ASTM Standards*. West Conshohocken, PA: ASTM International.

ASTM D 653. (2011). Standard terminologies relating to soil, rock and contained fluid. In *Annual Book of ASTM Standards.* West Conshohocken, PA: ASTM International.

Bemben, S. (1986). Brittle Behavior of a Varved Clay During Laboratory Consolidation Tests. In R. Yong, & F. Townsend (Eds.), *Consolidation of Soils: Testing and Evaluation* (pp. 610-626). Philadelphia, PA: ASTM.

Crawford, B. (1986). State of the art: evaluation and interpretation of soil consolidation tests. *ASTM Special Technical Publication, 892*, 71-103.

EuroSoilStab. (2002). *Development of Design and Construction Methods to Stabilize Soft Organic Soils: Design Guide for soft soil stabilization.* CT97-0351, European Commission, Industrial and Materials Technologies Programme (Rite-EuRam III) Bryssel.

Forsman, J., Maijala, A. and Järvinen, K. (2008). Case Stories, Harbours-Mass Stabilization of Contaminated Dredged Mud in Sörnäinen, Helsinki. *International Mass Stabilization Conference 2008.* Lahti, Finland.

Garbin, J.E., Mann, J.,McIntosh, A.K. and Desai, R. K. (2011). Mass Stabilization for Settlement Control of Shallow Foundation on Soft Organic Clayey Soils. *Geo-frontiers 2011: advances in geotechnical engineering, 13-16 March 2011.* Dallas, Texas, USA: ASCE 2011.

Grozic, J.L.H, Lunne, T., and Pande, S. (2003). An oedometer test study on the preconsolidation stress of glaciomarine clays. *Canadian Geotechnical Journal*, 857-872.

Holm, G., Bengtsson, P., and Larsson, L. (2012). *Field test at Port of Gävle, Sweden.* Linköping: Swedish Geotechnical Institute.

Janbu, N. (1967). *Settlement calculation based on the tangent modulus concept. Three lectures* (Bulletin 2 ed.). Trondheim: Norwegian University of science and technology.

Janbu, N. (1998). *Sediment deformations. A classical approach to stress-strain-time behaviour of granular media as developed at NTH over a 50 year period.* (Bulletin 35 ed.). Trondheim: Norwegian University of science and technology.

Karlsrud, K. and Hernandez-Martinez, F.G. (2013). Strength and deformation properties of Norwegian clays from laboratory tests on high-quality block samples. *Canadian Geotechnical Journal*, 1273-1293.

Mitchell, J. K., and Soga, K. (2005). *Fundamental of Soil Behavior.* New York: John Wiley and Sons.

Svensson, M., and Andreas, L. (2012). *Characterization report-byproduct from Billerud Karlsborg AB (In Swedish).* Luleå, Sweden: Luleå University of Technology.

Sällfors, G. (1975). *Preconsolidation pressure of soft, high-plastic clays.* Göteborg, Sweden: Chalmers University of Technology.

Topolnicki, M. (2004). *In-situ soil mixing: ground improvement.* (M. Kirsch, Ed.) London: Spon Press.

Wang, X. and Lee, H. (2009). Simulation of a temperature rise in concrete incorporating fly ash and slag. *Materials and Structures, 43*, 737-745.

Åhnberg, H. (2007). On yield stresses and the influence of curing stresses on stress paths and strength measured in triaxial testing of stabilized soil. *Canadian Geotechnical Journal, Vol. 44*(1), 54-66.

Åhnberg, H., Bengtsson, P.-E., and Holm, G. (2001). Effect of initial loading on the strength of stabilized peat. *Proceedings of the ICE - Ground Improvement, Vol. 5*(1), 35-40.

Paper III

Makusa, G.P., Mácsik, J., Holm, G., and Knusson, S. A laboratory test study on effect of freeze–thaw cycles on strength and hydraulic conductivity of stabilized dredged sediments (Submitted: *Canadian Geotechnical Journal*)

A laboratory test study on effect of freeze–thaw cycles on strength and hydraulic conductivity of high water content stabilized dredged sediments

Gregory Makusa[1]*, Josef Mácsik[2], Göran Holm[3], Sven Knutsson[4]

[1] PhD Student, Department of Civil, Environmental and Natural resources engineering, Luleå University of Technology, SE-97187, Luleå, Sweden. Email: gregory.makusa@ltu.se

[2] Ecoloop, Stockholm, Sweden, josef.macsik@ecoloop.se

[3] Swedish Geotechnical Institute, Linköping, Sweden, goran.holm@swedgeo.se

[4] Professor, Department of Civil, Environmental and Natural resources engineering, Luleå University of Technology, SE-97187, Luleå, Sweden. Email: sven.knutsson@ltu.se

*Corresponding author: alternative email: gmakusa@yahoo.com

Abstract: A laboratory test study was carried out to investigate the impact of freeze–thaw cycles on hydraulic conductivity (HC) and unconfined compressive strength (UCS) of high water content stabilized dredged material (SDM). Dredged sediments with initial water content in the range of 200–400% were blended with single and composite binders. In this study, a complete freeze–thaw cycle is considered to gain a better understanding of the impact of freeze–thaw processes on UCS and HC of the SDM. A grace period for thaw (i.e. thaw consolidation) is included to assess healing potential of the SDM on damaged UCS. Results from this study show that the type of binder and achieved UCS determine HC value and the connectivity of micro cracks formed due to freezing action. Significant impact of freeze-thaw on the HC of the SDM occurs when partial substitutions of cement for fly ash and slag is utilized. The decrease in the UCS values depends mainly on the HC, freezing system, and whether the specimens were tested during thaw weakening or thaw consolidation. The findings of this study show that: (i) minor reduction in the UCS value occurs on samples with high HC value. (ii) detrimental effects of freezing action on the UCS are greater under semi-closed than open freezing conditions (iii) a significant decrease in the UCS values is exhibited when specimens are tested during thaw weakening under both freezing systems. (iii) the reduction in UCS values is less when specimens are tested during thaw consolidation. (iv) the healing potential on the sample with reduced UCS values occurs during thaw consolidation when cement is supplemented with fly ash and slag.

Keywords: Freeze–thaw, dredging, hydraulic conductivity, stabilization-solidification, unconfined compressive strength, thaw weakening, thaw consolidation, durability.

Introduction

In cold regional climates, repetitive freeze–thaw (f-t) cycles can have detrimental effect on stabilized soft soils and sediments. Researchers have shown that f-t cycling has significant effects on strength and hydraulic conductivity of stabilized soils (Al-Tabbaa and Evans 1998a; Topolnicki 2004; Maher et al. 2006; Jamshidi et al. 2014; Holm et al. 2015; Jamshidi and Lake 2015). Freezing water in stabilized materials produces expansive forces, which cause an increase in volume and bonds breakage. Maher et al. (2006) concluded that the increase in volume and bond fracture on stabilized dredged sediments resulted in permanent loss of strength. However, Jamshidi and Lake (2015) reported both increase and decrease in unconfined compressive strength (UCS) of cement–stabilized silty sand. Al-Tabbaa and Evans (1998a, 1998b) carried out a treatability study on made ground comprising of soils ranging from clayey silty to fine and coarse sand with water content between 9.4% and 9.9%. Using percentage dry mass loss as criteria for assessing the impact of f-t cycles on stabilized soils, Al-Tabbaa and Evans (1998a) reported failure of all laboratory treated soils at freezing temperature of -20°C. However, for same design recipes treated in-situ, all samples survived the f-t criteria at freezing temperature of 0°C and -10°C and failed at -20°C (Al-Tabbaa and Evans 1998b). When the hydraulic conductivity (HC) becomes of major concern, especially on stabilized contaminated dredged sediments, both increase and decrease in HC with number of f-t cycles have been reported (Al-Tabbaa and Evans 1998b; Jamshidi and Lake 2015; Jamshidi et al. 2014). These contradictory results are partly due to: (i) absence of common testing methods and interpretation of the test results. (ii) different mix designs used in these studies, initial water contents of soils, and achieved strength (iii) incomplete f-t cycle during the laboratory test studies.

The current practice for assessing the resistance of compacted cement-treated soils to f-t cycles utilizes percentage dry mass loss as performance indicator (ASTM D560). However, mass loss does not correspond to internal structure that controls the hydraulic conductivity and strength of cement–treated soil (Jamshidi et al. 2014; Jamshidi and Lake 2015). In addition, the percentage dry mass loss criteria may be suitable on compacted cement–treated soils with initial water content of less than 100%. At present, studies on the impact of f-t cycles on high water content (greater than 100%) treated fine dredged sediments are limited. Jamshidi and Lake (2015) indicated that at increased water content, stabilized mass are vulnerable to f-t cycles. Modification in mix design by increasing cement content, reducing water content or incorporating pozzolanic materials may increase resistance of cement–treated soils to f-t process (Al-Tabbaa and Evans 1998a; Jamshidi and Lake 2015).

During the four seasons of a year, the actual field weather condition involves freezing phase–thaw weakening phase–thaw consolidation phase–freezing phase. A pictorial view of a typical complete freeze–thaw cycle is presented in Fig. 1. Physical effects for each phase are defined in ASTM D7099 as follows: Freezing phase is associated with changing of phase from water to ice in soil or rock. Frozen water (ice) produces expansive forces, which causes an increase in soil volume, and may cause some breakage of bonds in stabilized soils. Thaw weakening phase refers to a reduction in shear strength due to the decrease in effective stress as a result of slow dissipation of excess pore pressures when frozen cohesive soils containing ice are thawing under load. Thaw consolidation phase refers to the process by which the density and effective stress increases due to the escape of pore water under the weight of soil itself or an applied load.

Based on the literature, traditional f-t cycling does not define or consider the period for thaw consolidation. Though freezing action involves weakening to the stabilized material, we

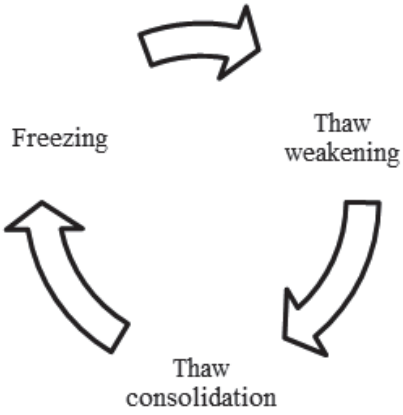

Figure 1. Schematic view of a complete freeze–thaw cycle.

postulate that thaw consolidation may act as a healing phase. Jamshidi and Lake (2015) reported a wide range of potential healing for damaged hydraulic conductivity values of stabilized mass after a post-exposure curing period of over 120 days.

Soil stabilization is a site–specific project and there are no general rules for mix design to achieve a certain strength, stiffness, permeability, and durability (Al-Tabbaa and Evans 1998a). The durability of stabilized dredged material (SDM) is of main concern due to its increasing use as structural backfill during land reclamation in harbours and ports, and as base or subbase materials in road embankments. Durability evaluation of geo-materials based on weather condition is a challenging aspect in the field of geo-construction. In cold regions, harsh weather condition causing f-t cycles is of major concern on the mechanical properties of the SDM. Durability is required to evaluate the resistance of stabilized mass to repeated f-t cycles. However, laboratory tests cannot completely simulate field conditions. In the absence of laboratory test methods or standards that can simulate universal field environments, durability assessment becomes a site-specific problem.

The aim of the present study is to investigate the impact of f-t cycling on the UCS and HC of the high water content stabilized dredged materials utilized as structural backfill material in northern parts of the world. In these applications the stabilized dredged materials (SDM) is placed below groundwater level. Thus, a test program was developed to assess the effect of open and semi closed f-t cycling. Extended thaw period is allowed prior to testing to assess the impact of thaw consolidation on unconfined compressive strength (UCS) and hydraulic conductivity (HC) of the SDM.

Laboratory tests

Material

The use of composite binders for stabilization–solidification of the dredged sediments (DS) is increasing due to increased artificial pozzolanas that can be utilized as supplementary cementitious materials (SCM). Primary binders such as cement can be blended with pozzolanic materials such as fly ash (FA) and ground granulated blast furnace slag (GGBS). However, (Wang and Lee, 2009), the hydration of cement incorporating SCM such as FA and GGBS is complicated due to the co-existence of cement hydration and the pozzolanic reactions of the mineral admixtures. In this study, dredged sediments were treated with both composite (ternary) binder and single binder.

Dredged sediments

Dredged sediments (DS) were obtained from Port of Oskarshamn, which is located in the south-eastern coast of Baltic Sea in Sweden. The salinity of water in the Baltic Sea is between 0 and 10 parts per thousand along the Swedish coast (Al-Hamady and Reker 2007). The studied DS had received water content between 200% and 400%. Based on the received water content, the DS were categorized into two, namely; DS-A and DS-B. The average initial water

content was 283% and 356%, for DS-A and DS-B, respectively. X-ray diffraction (XRD) patterns on representative samples of the studied DS are presented in Fig. 2. The results of XRD show that quartz and feldspars mineral groups of Albite (plagioclase feldspars), microcline (alkali feldspars) and Biotite were the dominating minerals. Quantitative analyses for mineral composition in the studied DS were not carried out because the study was not focused on the influence of individual minerals on strength of treated DS. The DS were not analyzed for presence of contaminants. Physical properties of the studied DS are shown in Table 1. Generally, the studied DS were mainly of organic nature. Accordingly, wet sieving was carried out on the DS to obtain the particle size distributions and cumulative organic matters. The DS particles retained on all sieve sizes less than 4 mm were dried and pulverized. The pulverized powders were then burnt in a furnace at 800 °C to determine the organic matter, which was utilized to compute losses of ignition (LOI). The LOI was conservatively utilized to obtain the actual soil particle size distribution as shown in Fig. 3 by subtracting percentage LOI from each retained dry mass. Thus, on average the studied DS comprised about 4%, 76% and 20% clay, silt and fine sand particles, respectively.

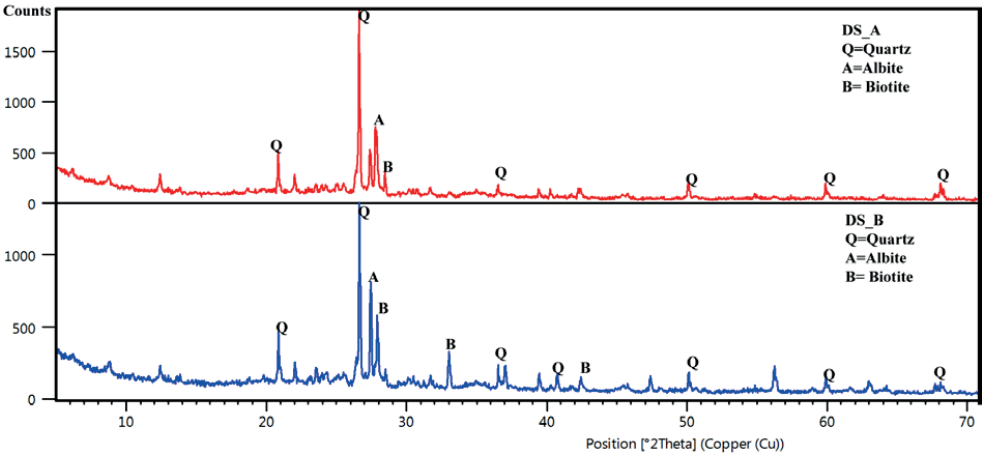

Figure 2. X-ray diffraction patterns on representative samples of the studied dredged sediments (DS).

Consequently, the studied DS could be classified as highly organic clayey silt sand. The cumulative percentage LOI for the DS with particles diameters less than 4 mm were 235% and 413% for DS-A and DS-B, respectively (Table 1). These values were proportional to the water content of the studied DS.

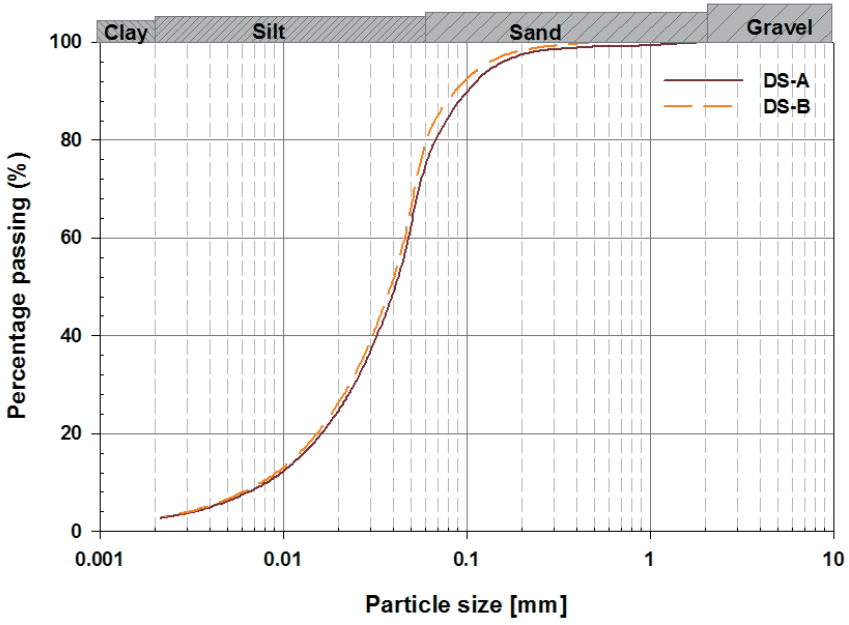

Figure 3. Particle size distribution for the studied DS after has been corrected for organic matter content and debris.

Table 1. Physical properties of studied dredged sediments: LOI = loss of ignition on DS with particles size <= 2mm, Gs = specific gravity, w = average initial water content. LL = liquid limit. PL = the plastic limit, and ρ = average bulk density**.**

	w (%)	LL (%)	PL (%)	ρ g/cm^3	LOI (%)	Gs
DS-A	283	120	88	1.19	235	2.53
DS-B	356	122	85	1.17	413	2.37

Binders

Binders used were either a combination of Byggcement (BC), off-specified fly ash (FA) and ground granulated blast furnace slag (GGBS) or single binder by BC only. BC is produced in Sweden by Cementa AB. The FA and GGBS were obtained from Billerud Karlsborg paper mill (Billerud Korsnäs) and SSAB steel industry, respectively. Billerud Korsnäs and SSAB are all located near Luleå City in northern part of Sweden. FA and GGBS were utilized as supplementary cementitious materials (SCM). Table 2 presents the average mineral compositions for individual binder components.

Table 2. Mineral composition for individual binder: FA = off-specified fly ash (Svensson and Andreas, 2012), GGBS = ground granulated blast furnace slag (Courtesy of SSAB), and BC = Byggcement (Holm et al. 2015).

Chemical compound (%)	FA	GGBS	BC
CaO	21.0	31	63
SiO_2	42.8	34	18
Al_2O_3	9.5	13	5
MgO	3.5	17	
K_2O	5.0		

Two composite binder (CB) recipes, namely CB1 and CB2 were utilized to amend the DS at received water content. CB1 was prepared by mixing BC:FA:GGBS at a ratio of 1:1:0.5, respectively by weight of total binder. CB1 was utilized to amend both DS-A and DS-B. CB2 was prepared at reduced amount of FA by blending BC:FA:GGBS at a ratio of 1:0.5:0.5, respectively. Single binder by BC only was utilized to amend DS-A to determine the effect of incorporating SCM such as FA and GGBS on strength development and resistance to f-t processes.

Regardless of different initial water content, DS-A and DS-B were both treated with 180 kg/m^3 of the DS to produce A-CB1 and B-CB1, respectively. The stabilized mass had different immediate water content. The measured water contents were 180% and 210% for A-CB1 and B-CB1, respectively. The amount of CB2 and BC were estimated such that an

assumed immediate water content of 160% could be achieved immediately after mixing, and the UCS of at least 280 kPa could be attained after 28 days of curing on BC treated DS. The selected immediate water content and achieved strength was based on previous study by *G.P. Makusa, N.T. Montamen, A. Humad and S. Knutsson* (submitted to International Journal). As a result of different initial water contents of the studied DS, DS-A was treated with BC at a dosage of 260 kg/m^3 to produce A-BC with immediate water content of 160%. DS-B was blended with CB2 at a dosage 320 kg/m^3 to produce B-CB2 with the same immediate water content. A summary of design recipes that were utilized in this laboratory test study is presented in Fig. 4 and Table 3.

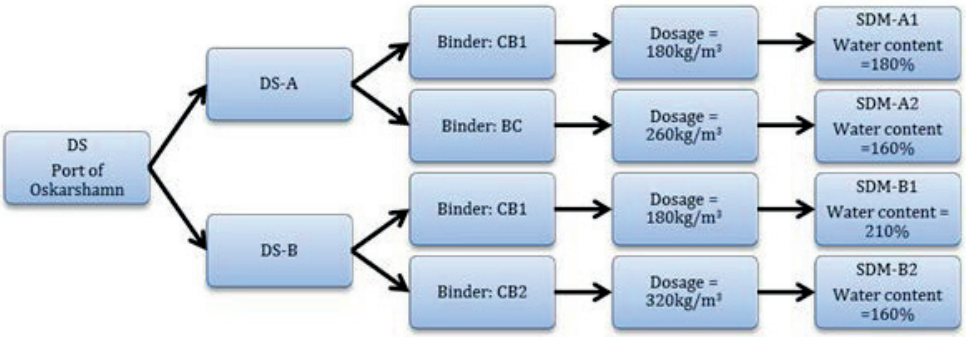

Figure 4. Schematic view of design recipes utilized during this laboratory test study.

Methods

Samples for unconfined compression testing

Samples for the UCS assessment were prepared by packing the SDM in polyvinyl chloride (PVC) tubes of size 50 mm by 170 mm without mechanical compaction. The SDM samples were placed in the PVC tubes and allowed to fall freely to the bottom of the tubes by vibrations of its bottom end. The SDM samples were cured under water in a curing container as shown in Fig. 5. No pore water chemistry was considered in this study and therefore, tap

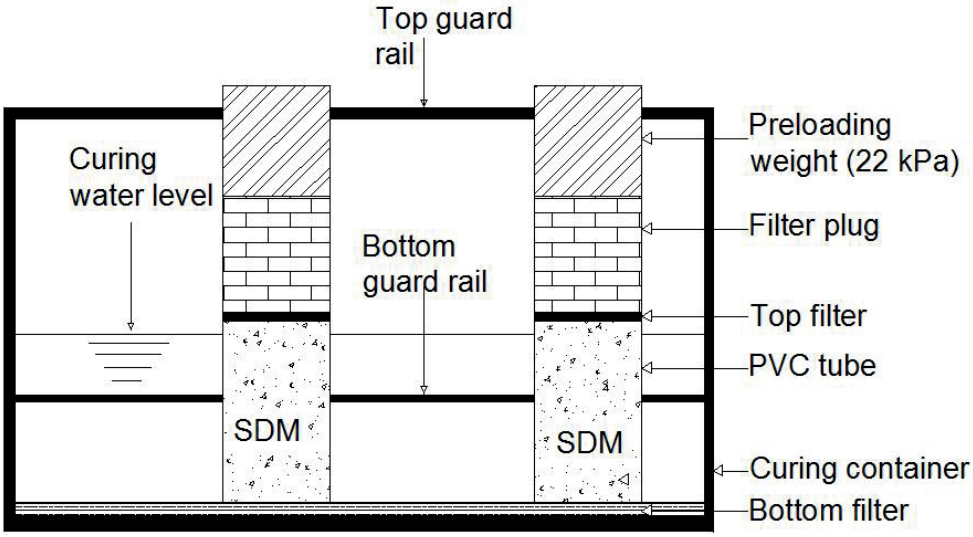

Figure 5. A cross section view through a curing container showing the PVC tube, SDM, bottom and top filters, preloading weight, curing water level, PVC tubes, and guard rails.

water was utilized as curing water. At the bottom of the curing container, a filter was placed to facilitate continuous exchange of pore water during curing period. This curing system was adopted to simulate field conditions, where the stabilized dredged sediments may be deposited below ground water level. In Sweden, it is customarily required to preload the stabilized volume immediately after mixing with a minimum preloading weight of 18 kPa. The initial preloading weight serves two purposes: firstly, squeeze out air and water trapped during mixing. Secondly, speed up consolidation of the stabilized mass and bring the particles together for effective hydration reactions (EuroSoilStab 2002). Accordingly, at the top of the SDM samples, a filter plug was inserted and a preloading weight of 22 kPa was applied. Literature (Taylor 1997) has shown that at least 28 days of curing is needed to attain 90% hydration reactions for cement treated DS. However, partial substitution of cement for pozzolanic materials may require curing period in excess of 28 days for pozzolanic reaction to take place and contribute to strength development. Thus, samples A-CB1 and B-CB1 were

subjected to a curing period of 91 days, whereas, A-BC was cured for 28 days. As a result of increased amount of cement in CB2, stabilized mass B-CB2 was cured for 50 days. After prescribed curing periods samples were subjected to open and semi-closed f-t systems.

During open f-t cycles, samples were kept in their preparation PVC tubes, which were then sandwiched between water saturated sand. Open f-t system was used in order to (i) maintain the original curing conditions. Sand bath f-t method was used to minimize expansive forces of frozen water on the sides of the curing container. (ii) allow continuous interchange between pore water in the specimens and the surrounding pore water during f-t cycles. (iii) simulate field condition in which the SDM can be placed below groundwater level.

When a closed–freezing system is considered, loss or gain of water in the sample should be precluded (ASTM D 653). However, during this study, a fully closed freezing system was not achieved. Similar to open f-t system, samples were frozen and thawed in their original PVC tubes in the absence of curing water. The bottom side of the PVC tubes was covered with tight vinyl cap to prevent loss of water. However, it was likely that during thaw, drainage of released water could occur through the top filter. Consequently, this f-t system was considered as semi–closed freezing system. These systems were utilized to compare the influence of open and closed freezing systems on the strength of stabilized dredged materials subjected to either open or closed f-t cycles.

Samples for hydraulic conductivity testing

To assess the effect of freeze–thaw (f-t) cycles on hydraulic conductivity (HC) of single and composite binders treated DS, only samples from A-BC and B-CB2 were utilized. Samples were molded in Proctor molds of dimensions 102 mm x 112 mm without mechanical compaction. The inner surfaces of the Proctor molds were lined with a layer of bentonite clay to prevent any possible seepage along the interface. A preloading weight of 14 kPa was

applied for about 15 minutes immediately after filling the Proctor molds with the SDM. The aim for the initial preloading was to squeeze out air and free water in the samples, and also to speed up consolidation as discussed earlier. This was considered important for reducing late shrinkage or decrease of the sample size during permeation. The reduced volume due to compression under initial preloading was refilled and leveled. Thin layers of fresh DS were placed on top and bottom end of the SDM surfaces to avoid filter clogging due to cementation. The top and bottom cap with double filters were finally covered on the Proctor molds, and samples were mounted for the HC measurement. Thus, curing of these samples took place concurrent with permeation to establish baseline HC values prior to f-t cycles.

Freeze–thaw process

A freezer with capability of freezing to –30°C was utilized as a freezing cabinet during freeze–thaw (f-t) test study. Copper wire thermocouple instrumentation was utilized to determine the period for a complete f-t cycle on samples for unconfined compressive strength (UCS) and hydraulic conductivity (HC) evaluation. Evolution of temperature on the SDM samples under UCS assessment only is shown in Fig. 6. Thermocouple instrumentation shows that it would take about 24 hours (Fig. 6a) and 12 hours (Fig. 6b) to complete one f-t cycle under open and semi–closed f-t systems, respectively. Nonetheless, 24 hour period was utilized to define a complete f-t cycle on UCS samples under both open and semi–closed systems. Samples for hydraulic conductivity (HC) measurement required 48 hours to complete one traditional f-t cycle. The thermocouple data were not presented due to a problem in data recording.

Based on the thermocouple instrumentation data (Fig. 7a), we can deduce that when the temperature of freezing air (F-TT) approaches and decreases below 0°C, the rate of freezing slows down. Likewise, when the temperature of thawing air (F-TT) approaches and rises

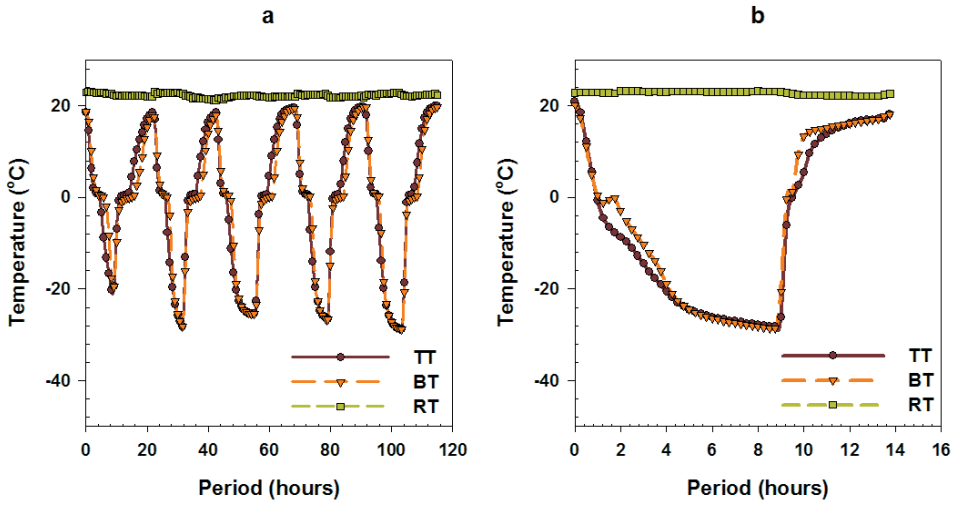

Figure 6. Evolution of temperature in the SDM during (a) open five freeze–thaw cycles (b) one semi-closed freeze–thaw cycles for samples under UCS assessment. RT = Room temperature; TT = Temperature at the top of the sample; BT = Temperature at the bottom of the sample.

above 0°C, the rate of thawing turn out to be low. This observation suggests that the actual freeze and thaw conditions occur when the temperature of freezing and thawing air is below and above 0°C, respectively. Under both freezing systems, drop and rise of temperature toward 0°C occurred rapidly. An enlarged pictorial view of incomplete traditional f-t cycle can be depicted in Fig. 7(b), which suggests that the traditional f-t cycle is an incomplete cycle.

Generally, in the northern parts of the world, the periods of four seasons of the year (i.e. winter, spring, summer, and autumn) are fixed with small variations. This is to say, winter and spring seasons are only part of a year that make the depicted semi f-t cycle in Fig. 7b. Thus, in cold regions climate the durability of the stabilized materials cannot be assessed based on two seasons only. Accordingly, for a complete f-t cycle, Fig. 7a suggests that it might be beneficial to consider a grace period (GP) for thaw consolidation, which could be associated

with summer and autumn weather conditions. It can be postulated that during the GP, the SDM will strive to regain its original strength values after the impact of freeze-thaw.

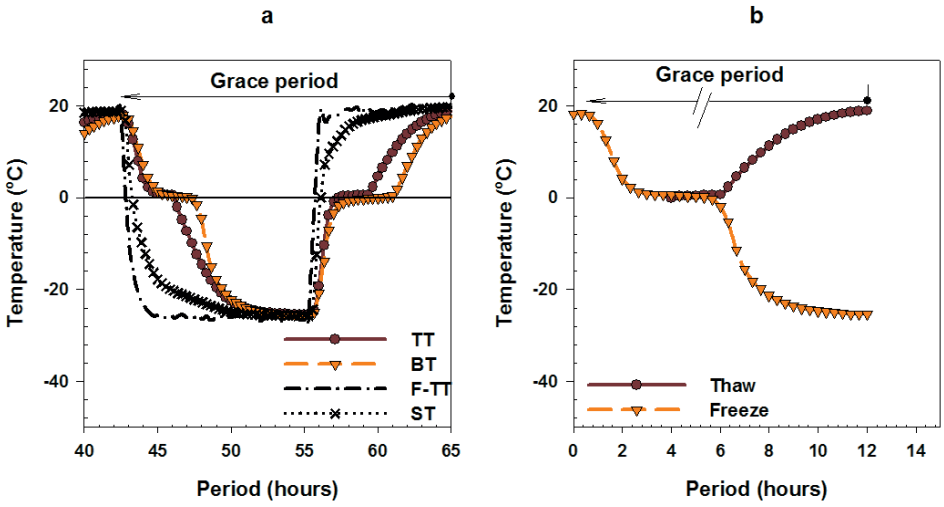

Figure 7. Freeze–thaw process (a) Example of freeze–thaw cycle and required grace period for thaw consolidation. (b) visualized traditional freeze–thaw cycle and grace period for a complete freeze–thaw cycle. TT = Temperature at the top of the sample; BT = Temperature at the bottom of the sample, F-TT =Temperature of freezing/thawing air, and ST = Temperature of water saturated sand.

Test setup and evaluations

The unconfined compression test was carried out using strain–controlled method at a deformation rate of 1mm/min. Figure 8 presents a schematic diagram for testing time and conditions. The unconfined compression tests were conducted on unfrozen specimens after prescribed curing period (CP) to establish control strength (CS). Subsequent tests were carried out after prescribed f-t cycles (X) to assess the UCS values (i) immediately after thaw period (i.e. thaw weakening, TW) and (ii) after grace period (GP) for thaw consolidation (TC). The GP for thaw consolidation was determined based on thaw period (TP) and number of traditional f-t cycles (X) as shown in Fig. 8. For instance, 1 f-t cycle that requires 12 hours of

thaw would have 24 hours of GP for TC (i.e. 12 x 1 + 12 =24) as shown Table 4. The UCS values, which were measured during TW and TC were compared with the CS values to assess the impact of freezing action on the strength and healing potential on SDM sample with damaged UCS.

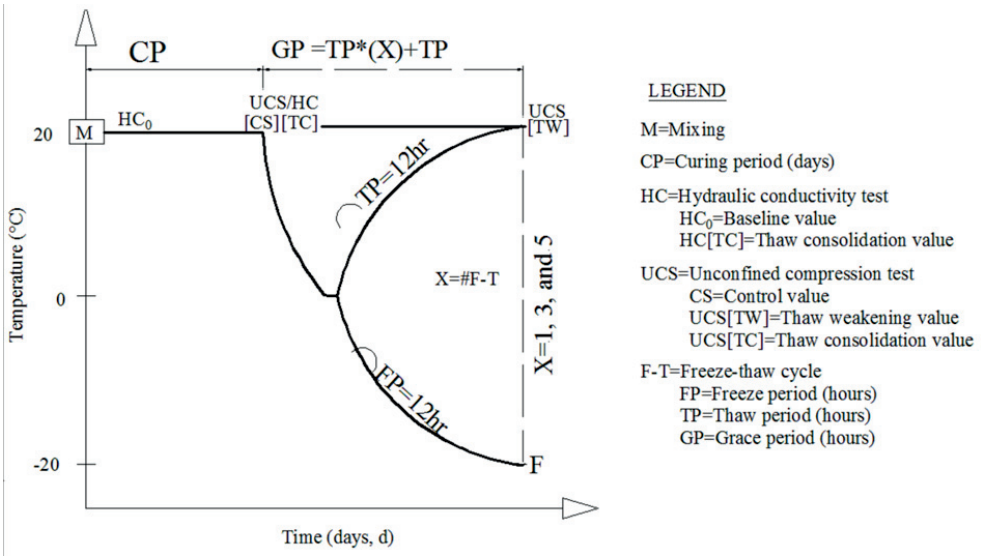

Figure 8. Schematic diagram for HC/UCS testing time and conditions.

The hydraulic conductivity (HC) test was carried out using a constant head method at a hydraulic gradient of about 7 in accordance with ASTM D 5856. Prior to f-t cycles, the baselines HC_0 were established. Samples were then subjected to 1, 3, 4 and 5 open f-t cycles with intermittent permeation. A preloading weight of 24 kPa was applied during f-t cycles as shown in Fig. 9. This load was utilized to mimic field surcharge of at least 18 kPa, which is typically utilized as cover on contained stabilized wastes. At the end of 5 f-t cycles, cylindrical specimens with dimensions 50 mm x 90 mm were extruded, trimmed and subjected to unconfined compression test at a deformation rate of 0.9 mm/min to determine the UCS values.

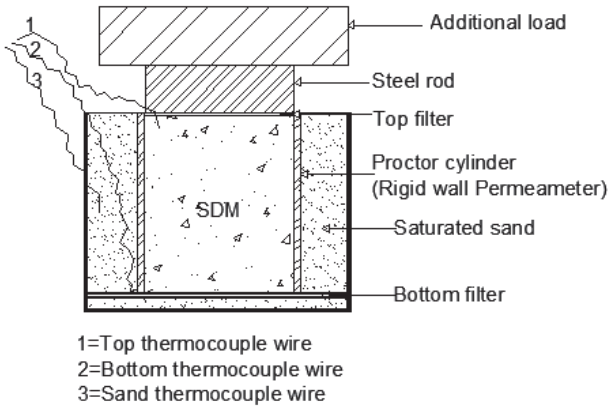

Figure 9. A cross section view through a Proctor mold during freeze–thaw cycles for samples under hydraulic conductivity measurement.

Test results and discussion

Hydraulic conductivity

The baseline hydraulic conductivity (HC_0) values were established prior to freeze–thaw (f-t) cycles. The values for HC_0 were 4.6 x 10^{-8} m/s and 2.6 x 10^{-8} m/s for A-BC and B-CB2, respectively. These values were established after 15 and 28 days of curing for A-BC and B-CB2 samples, respectively. The lowest HC_0 value was measured on B-CB2 sample (Fig. 10) probably due to the presence of fly ash and GGBS. Marsh et al. (1985) observed that fly ash in general can cause substantial reduction in HC of unfrozen stabilized soils. The high HC_0 value on A-BC sample may have been contributed by cement hydration, which causes aggregation of particles and increased pore sizes. According to Quang and Chai (2015), the HC of a porous medium is a function of the microstructure of the pores (sizes and distribution) and pore water properties. Hydration of cement agglomerates several small aggregates into a large one. Larger pore size and uniform pore distribution are associated with high HC values.

Literature (Yousuf et al. 1995; Hwang and Shen 1991; Fajun et al. 1985) have shown that upon cement hydration, the calcium silicate minerals dissociate into charged silicate and calcium ions Ca^{2+}, which is removed by aluminum associated with supplementary cementitious material (SCM). This phenomenon depresses the Ca^{2+} concentration in the blend, and results in a thicker diffusive double layer, which is associated with low HC. In absence of SCM, cement-treated high water content sediments may have a higher concentration of calcium ion (Ca^{2+}), which causes a thinner diffusive double layer. According to Quang and Chai (2015), high concentrations of Ca^{2+} tend to exhibit a higher hydraulic conductivity due to thinner diffusive double layer compared to thicker diffusive double layer. Thus, due to consumption of Ca^{2+} by aluminum associated with FA and GGBS, B-CB2 sample experienced thicker diffusive double layer, little formation of agglomerated clumps of aggregates, and non-uniform pores distribution. Consequently, B-CB2 sample exhibited the lowest baseline HC compared to A-BC sample (Fig. 10).

Freezing action results in formation of a network of cracks and micro cracks (Jamshidi and Lake 2015; Jamshidi et al. 2014; Benson and Othman 1993; Chamberlain et al. 1990; Chamberlain and Gow 1979; Kraus et al. 1997). This results in agglomerations of clods and formation of macro-and micro-structure (Makusa et al. 2013; Benson and Daniel 1990). If these cracks are well connected, they may result in increased hydraulic paths, which will cause increased hydraulic conductivity (HC). The HC values for A-BC sample remained almost the same during intermittent permeation following 1, 3, 4, and 5 f-t cycles as shown in Fig. 10. On the other hand, the HC value for B–CB2 sample decreased by a factor of 0.3 of the baseline value after 1 f-t cycle. The HC values increased by a factor of 1.7, 2.3 and 3.5 times the baseline value after 3, 4 and 5 f-t cycles, respectively. It can be postulated that the

connectivity of formed cracks and increased HC value depend on the achieved unconfined compressive strength (UCS).

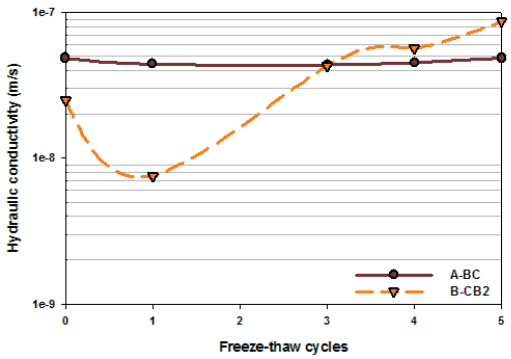

Figure 10. Observed variations in hydraulic conductivity during open freeze–thaw cycles for samples A–BC and B–CB2.

Unconfined compressive strength

The measured control strength (CS) values for A-CB1 and B-CB1 were 28 kPa and 24 kPa, respectively. The CS values for A-BC and B-CB2 were 299 kPa and 87 kPa, respectively. The UCS value for A-BC sample was about 3.4 times the UCS value for B-CB2 sample. The only possible explanation for this difference in the CS values is that the measured UCS values on treated DS were mainly brought by cement hydration. It can be assumed that the pozzolanic reactions of SCM had no influence on improved strength for the curing period of up to 91 days. Thus, the differences in CS values were because of different water/cement (w/c) ratio and presence of mineral admixture in B-CB2 sample as shown in Table 3. Researchers (Yousuf et al. 1995; Hwang and Shen 1991; Fajun et al. 1985) have shown that presence of mineral admixture and organic matter depresses the Ca^{2+} concentration in the blend, which causes delay in the formation of calcium hydroxide (CH), nucleation and crystallization of calcium silicate hydrates (CSH) gels, and strength development.

Frozen water produces expansive forces, which cause the increase in volume and some bond breakage in stabilized mass. A-CB1 samples were subjected to 3 f-t cycles to assess the preliminary results. Regardless of number of f-t cycles, a grace period (GP) for thaw consolidation (TC) of 24 hours only was utilized. Although the healing potential on A-CB1 sample with damaged UCS was promising, it was found that the GP for TC should be defined based on the number of f-t cycles (X) and thaw period (TP) as defined in Fig. 8. Thus, results from A-CB1 were not included in this paper. The GP for TC on sample B-BC2 and A-BC were defined based on TP and f-t cycles as shown in Table 4. Thus, B-CB2 samples were subjected to 1, 3, and 5 open and closed f-t cycles. A-BC samples were subjected to 3 consecutive open f-t cycles only to assess the healing potential on the SDM with high UCS value.

The measured UCS indicated decreased values for all specimens tested immediately after thaw (i.e. during thaw weakening, TW) under both open and semi-closed f-t systems. Results (Fig. 11) show that the measured UCS values on B-CB2 sample under open f-t system decreased by 41%, 65% and 33% after 1, 3 and 5 f-t cycles, respectively (Fig. 11a). The measured UCS values under semi-closed f-t system indicated decreased values by 54%, 80% and 73% of the CS value after 1, 3 and 5 f-t cycles, respectively (Fig. 11b). The reduced UCS value immediately after thaw could be associated with increased amount of water content. Wang et al (2011) observed that the compressive strength decreases due to the weakening effect of water on calcium silicate hydrate (CSH). Thus, the effect of thaw weakening (TW) on the UCS could be regarded as temporary phenomenon waiting for dissipation of pore water surrounding the CSH bond.

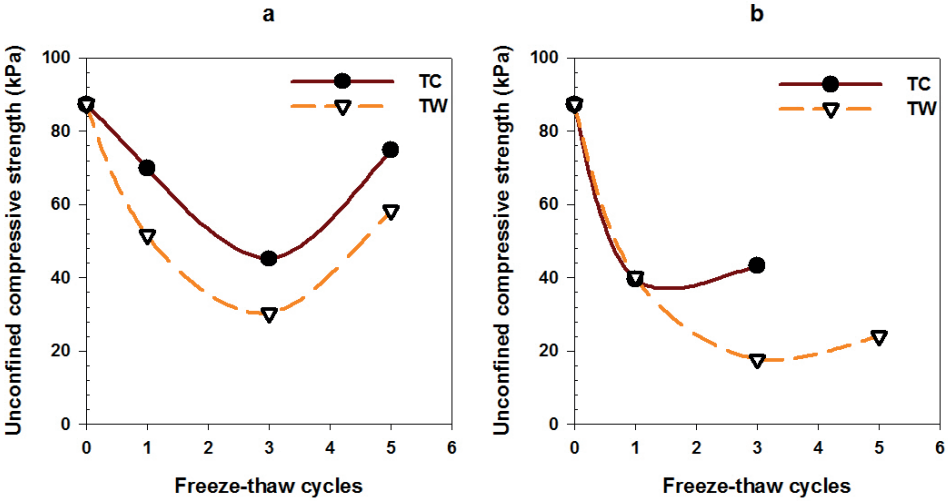

Figure 11. Impact of freeze–thaw weakening (TW) and thaw consolidation (TC) on the average unconfined compressive strength for B-CB2 samples under (a) open freeze–thaw system (b) semi-closed freeze–thaw system

Specimens tested after the grace period (GP) of thaw (i.e. thaw consolidation, TC) showed improved damaged UCS values under both open and semi–closed f-t systems. The measured UCS values on B-CB2 samples under thaw consolidation (TC) indicated less decrease in the UCS values. The UCS values decreased by 20%, 48% and 14% after 1, 3 and 5 open f-t cycles, respectively. For B-CB2 sample under semi-closed f-t system, no significant gain in UCS was observed after 24 hours of TC. However, after 3 f-t cycles and 48 hours of GP for TC, B-CB2 sample under semi-closed f-t system indicated significant gain in the UCS values. The measured UCS value on these samples after TC was 46 kPa compared to 18 kPa, which was measured during TW as shown in Fig. 11b. Specimen for the UCS assessment after 5 f-t cycles under semi–closed f-t system failed during freezing due to rupture of PVC tube. These results suggest that TC may act as healing phase after detrimental effects of freezing action have taken place. Furthermore, under semi-closed f-t systems, TC can be limited.

The stress–strain curves for the tested specimens from sample B-CB2 and A-BC are shown in Fig. 12 and Fig. 13, respectively. The stress–strain curves from specimens that were subjected to 5 f-t cycles concurrent with HC measurement are also presented in Fig. 12b and Fig. 13b for B-CB2 and A-BC samples, respectively. The stress at failure on these specimens was comparable to stress at failure on the samples, which were packed in PVC tubes for assessing the UCS only. As shown in Fig. 12b and Fig. 13b, the measured UCS values for sample B-CB2 and A-BC after 5 f-t cycles concurrent with HC measurements were 1.3% and 59.5% above and below the CS values, respectively. These values indicate consistency behaviour of the SDM samples under open f-t systems. Thus, TC can be implemented either intermittently (i.e. between f-t cycles) or at the end of f-t cycles.

Effect of binder

Calcium hydroxide (CH) and calcium silicate hydrate (CSH) are the end products of cement hydration. Regardless of composition of blast furnace slag or fly ash, the main hydration products and principal binding phases in all calcium silicate-based pastes are CSH gels (Richardson and Groves 1997; Taylor 1997). According to Sherwood (1993), reaction of CH brings up an increased strength produced by cation exchange capacity rather than by cementing effect brought by pozzolanic reaction. However, researchers (Hebib and Farrell 1999; Åhnberg and Holm 1999) have shown that organic soils have high exchange capacity. It can hinder the hydration process by retaining the calcium ions liberated during the hydration of calcium silicate and calcium aluminate in the cement to satisfy the exchange capacity. Wang and Lee (2009) reported some differences (i.e. dormant period) between cement hydration and the pozzolanic reaction of mineral admixtures. As discussed earlier, decreased

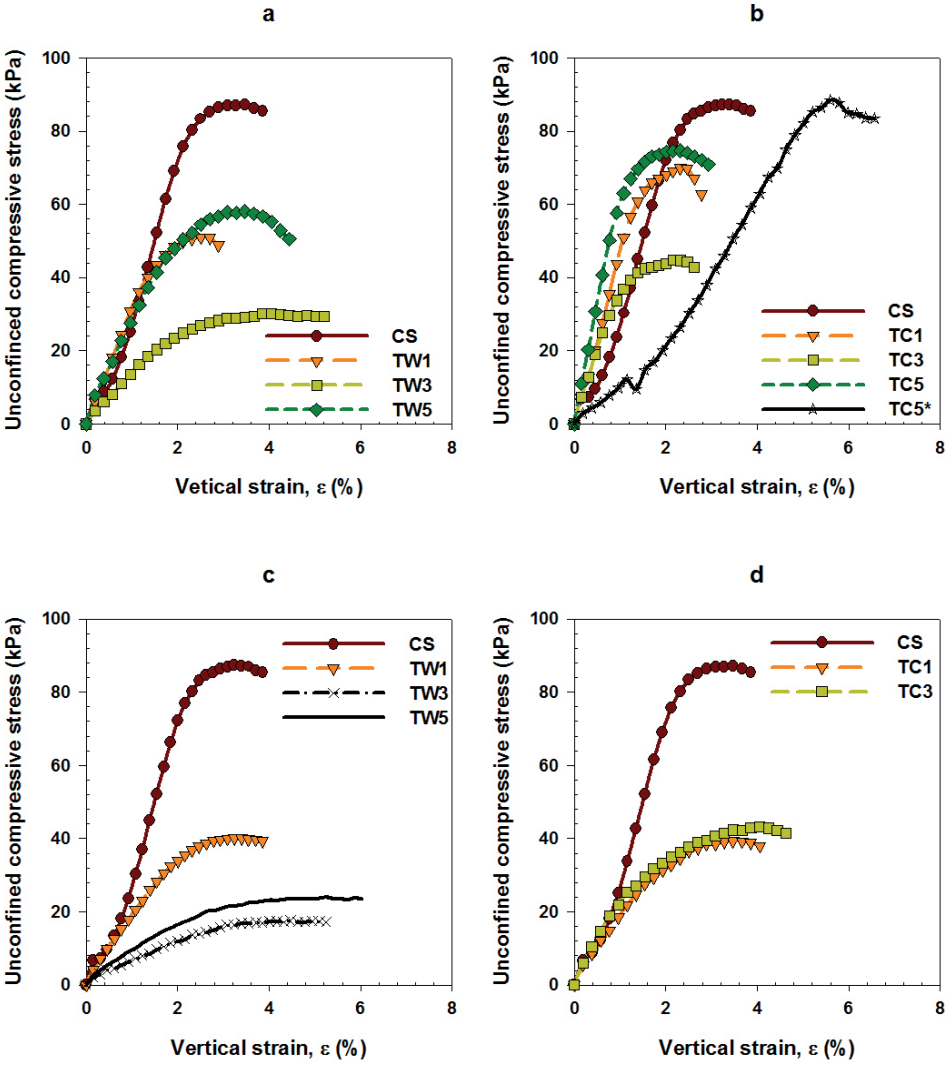

Figure 12. Stress–strain curves for B-CB2 samples during (a and c) thaw weakening (TW) and (b and d) thaw consolidation (TC). *Specimen from B-CB2 samples concurrent with hydraulic conductivity measurement.

amount of Ca^{2+} in the blend causes delay in the formation of CH, nucleation and crystallization of CSH gels, and strength development (Hwang and Shen 1991; Fajun et al. 1985). However, Necmi et al. (2007) concluded that FA as additive mixture enhances the freezing–thawing durability of granular soils. Results from this study show that presence of

FA and GGBS may help the SDM to regain some of the damaged strength during TC. Moreover, although FA may substantially contribute to reduced hydraulic conductivity; on other hand, inclusion of FA may cause increased hydraulic conductivity of the SDM subjected to f-t cycling. Nevertheless, the increase in HC values will depend on the achieved strength and baseline HC value.

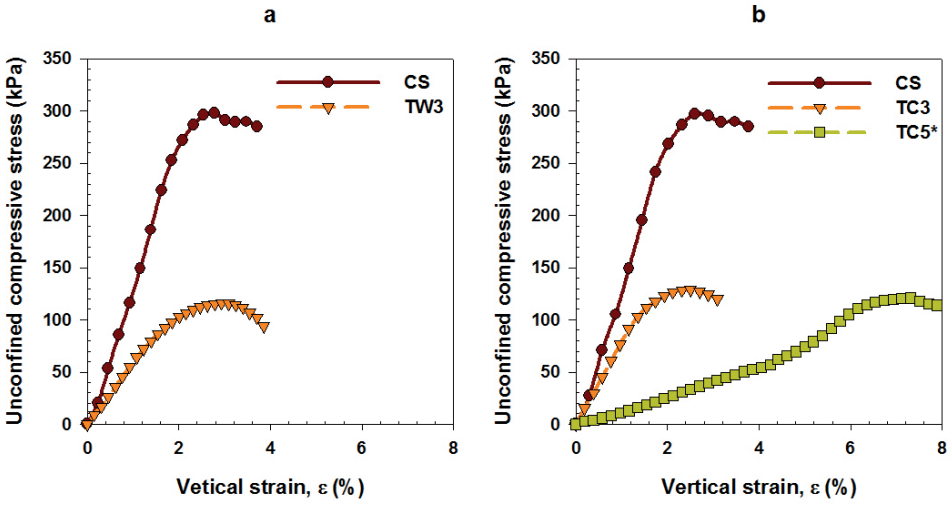

Figure 13. Stress–strain curves for A-BC sample during (a) thaw weakening (TW) and (b) thaw consolidation (TC). *Specimen from A-BC samples concurrent with hydraulic conductivity measurement.

Effect of strength on hydraulic conductivity

Depending on the achieved UCS values, the formed micro-cracks may become continuous interconnected or disconnected. For the SDM with low strength value, f-t cycles may result in formation of more interconnected micro cracks, and the HC will show increased values as shown in Fig. 10 for B-CB2 sample. On the other hand, for the same number of f-t cycles, the measured HC value on A-BC sample remained almost the same (Fig. 10). This suggests that, the CS value of 299 kPa was significantly high to cause increased brittleness and formation of

discontinuous micro-cracks on A-BC sample. As a result, the HC values for this sample remained almost the same.

Effect of hydraulic conductivity on strength

Freeze-thaw (f-t) process induces phase changes of water without dehydration (Makusa et al. 2014). Regardless of achieved UCS values, the SDM with low hydraulic conductivity (HC) value and increased amount of freezing water will experience significant loss in strength with prolonged thaw weakening. Jamshidi and lake (2015) reported decreased HC values (i.e. improved performance) hand in hand with reduction of 30% in UCS value (i.e. performance degradation). If the hydraulic conductivity is significantly low, the water released during thaw will generate excess pore pressure during loading (Simonsen et al. 1999). As a result, failure will occur under undrained condition and the measured strength will show decreased values. According to Knutsson (1983), the water accumulated as ice during freezing is released during thaw. Depending on the hydraulic conductivity, the released water can be trapped within the soil. Increased water content leads to a potential risk of water saturation and high pore pressure, which in turn reduces the shear strength of soil. On the other hand, increased initial water content or pore water will favor decreased HC (Makusa et al. 2012; Vappali et al. 1999). At increased freezing water, the SDM will be filled with water, which is released during thaw. As a result, during permeation the rate of inflow will be higher than the outflow. Prolonged thaw (thaw consolidation, TC) allows released water to dissipate and reduce the amount of free water, which in turn reduces the excess pore pressure and increases effective stress. It follows that, during loading, the rate of dissipation of excess pore water pressure turns out to be proportional to the rate of loading. Consequently, the effect of undrained condition becomes insignificant. Knutsson and Rydén (1984) reported that if the HC value is high, the water will drain at the same rate as new water is released, and the decrease in

strength of the soil will be limited. This argument is supported by the results of HC in Fig. 10 in relation to UCS values in Fig. 12b and Fig. 13b. It is obvious that the measured UCS values were related to the HC values. As a result of increased HC value on B–CB2 sample, the measured UCS value approached the control strength (CS) value (Fig. 12b). Jamshidi and Lake (2015) reported increased HC value of up to 50 times baseline value hand in hand with a strength gain of about 14% on compacted stabilized sand. The HC value for A-BC remained almost the same; consequently, the UCS value was reduced by 60% of the CS (Fig. 13b). Guthrie et al. (2012) observed that for cement–treated soils, there can be a correlation between the UCS and HC values.

Conceptual model

A conceptual model for describing the relationship between the hydraulic conductivity (HC), excess pore pressure (EPP), and the unconfined compressive strength (UCS) values due to the impact of freeze-thaw (f-t) cycles discussed earlier is presented in Fig. 14. The model suggests that during freezing, the hydraulic conductivity of freezing HC(F) sample will decrease continuously to a minimum value at the end of freezing (F) period. The excess pore pressure (EPP) will also decrease. The frozen pore water will contribute to additional strength. As a result, the expected measured UCS value will be higher than the control strength (CS) value. During thawing, as frozen pore water begins to melt, the hydraulic conductivity of thawing HC(TW) sample will start increasing toward the baseline value (HC_0). If a load is applied during this period, thawing water will generate high EPP, which will cause sudden decrease in the UCS values. If the value for HC_0 is significantly low and the amount of released water is substantially high, the period for thaw weakening can be prolonged and vice versa. On one hand, if discontinuous micro cracks were formed due to freezing action, the value for HC(TW) will approach HC_0 value, which will mark the end of thaw

weakening(TW). Thaw consolidation (TC) will take place under the baseline value HC_0. However, due to increased amount of released water, the EPP will not approach its baseline value at HC_0 and the measured UCS value will be less than the control strength (CS) value. On the other hand, if sufficient interconnected micro cracks were formed during freezing, the HC value will show increased values. As a result, thaw consolidation hydraulic conductivity HC(TC) may exceed the baseline value, and the period for thaw weakening may be shortened. Consequently, quick dissipation of EPP will occur, and reduction in strength will be insignificant.

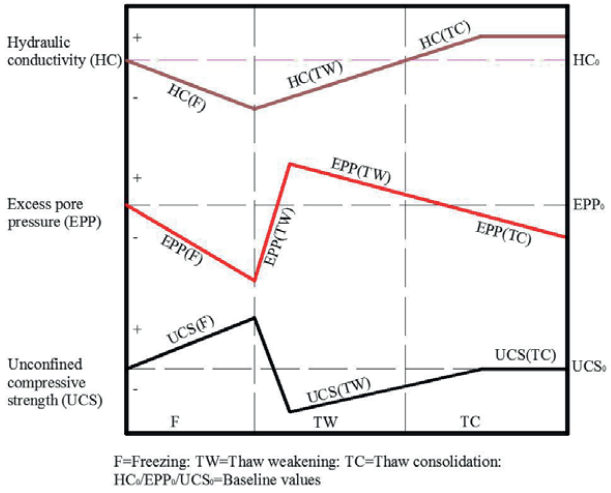

Figure 14. Conceptual model for describing the relationship between hydraulic conductivity, excess pore pressure and the unconfined compressive strength (UCS) due to the impact of a complete freeze-thaw cycle of high water content stabilized sediment. HC0, EPP0, UCS0 = baseline values, HC(), EPP(), UCS() = anticipated values during freezing (F), thaw weakening (TW), and thaw consolidation (TC).

While the proposed model may be applied to all stabilized soils and sediments, it should be noted that even one local continuous crack may cause dramatic increase in HC values. This is especially true for compacted stabilized soils with low water content. Development of local

cracks may not contribute to overall dissipation of excess pore water under load. Thus, the proposed model is valid for high water content stabilized soils and sediments. These materials tend to have good stress distribution without formation of local cracks.

Conclusions

Stabilized dredged materials (SDM) are susceptible to freeze-thaw (f-t) cycles similar to the conventional natural cohesive soils. Thaw consolidation may provide an opportunity for the SDM to rectify the damage caused by freezing action. The following concluding remarks can be obtained from this study:

- The hydraulic conductivity will decrease during thaw weakening and increase or attain the baseline value during thaw consolidation. The decrease in hydraulic conductivity during thaw weakening contributes to undrained conditions, which is due to increased pore water, especially if the baseline hydraulic conductivity was low. An increased hydraulic conductivity during thaw consolidation was mainly due to ample time the released water had when dissipating. During subsequent permeation the water will drain at the same rate as incoming water.
- The open freeze-thaw system allows quick dissipation of the pore water and shortens the effect of thaw weakening. Closed system of freezing impedes the movement of pore water and prolongs the period for thaw weakening, which results in strength reduction.
- The unconfined compressive strength (UCS) will decrease during thaw weakening and increase during thaw consolidation. The decrease in strength during thaw weakening is due to water released during thaw, which generates excess pore pressure and a corresponding decrease in effective stress. Thus, failure occurs under undrained condition. The water released during thaw weakening is drained out during thaw consolidation, resulting in increased effective stress and improved strength.

- The healing potential on the SDM samples with damaged UCS occur when cement is supplemented with fly ash and grounded granulated blast furnace slag.
- The knowledge of the effect of freeze–thaw cycles on the mechanical properties of the stabilized soils is very limited. This study proves that thaw consolidation has to be considered in the current testing methods in order to get a better understanding of the impact of freeze–thaw processes. This can be implemented either intermittently (i.e. between f-t cycles) or at the end of f-t cycles.

Acknowledgments

The authors would like to acknowledge Mr. Mats-Johan Rostmark at FriGeo Company for providing us with the dredged sediments for investigation. The Sustainable Management of Contaminated Sediments (SMOCS) project, Luleå University of Technology, Swedish Geotechnical Institution (SGI), Ecoolop Consultancy Company are hereby acknowledged for their technical and financial supports. Special thanks remain to laboratory technician Mr. Thomas Forsberg, Senior research engineer Kerstin Pousette for their help during laboratory experiments.

References

Al-Hamdani, Z. and Reker, J. (2007). *Towards marine landscapes in the Baltic Sea. Balance interim report #10.* Available at http://balance-eu.org: Online document: Retrieved: 2015-08-19. .

Al-Tabbaa, A. and Evans, W. (1998b). Pilot in-situ auger mixing treatment of a contaminated site - Part I: treatability study. *Proc. Instn Civ. Engrs Geotechn. Engng, 131*, pp. 52-59.

Al-Tabbaa, A., Evans, C.W., and Wallace, C.J. (1998a). Pilot in situ auger mixing treatment of a contaminated site: Part 2: site trial. *Proc. Instn Civ. Engrs Geotechn. Engng*, pp. 89-95.

ASTM D 560. (1996). *Standard Test Methods for Freezing and Thawing Compacted Soil-Cement Mixtures.* West Conshohocken, PA: ASTM International.

ASTM D 5856. (2007). Standard test method for measurement of hydraulic conductivity of porous material using a rigid-wall, compaction-mold permeameter. In *ASTM standards.* West Conshohocken, PA: ASTM International.

ASTM D 653. (2011). Standard terminologies relating to soil, rock and contained fluid. In *Annual Book of ASTM Standards*. West Conshohocken, PA: ASTM International.

ASTM D 7099. (2010). *Standard terminology relating to frozen soils and rock.* West Conshohocken, PA: ASTM International.

Benson, C.H. and Othman, M.A. (1993). Hydraulic conductivity of compacted clay frozen and thawed in-situ. *Journal of Geotechnical Engineering*, 276-294.

Chamberlain, E. and Gow, A. (1979). Effect of freezing and thawing on the permeability and structure of soils. *Engineering Geology, Vol. 13*(1-4), 73-92.

Chamberlain, E.J., Iskander, I., and Hunsiker, S.E. (1990). Effect of freeze-thaw on the permeability and macrostructure of soils. *Proc. Int. Symp. on frozen soil impacts on Agric., Range, and forest lands*, (pp. 145-155). Spokane, Washington.

Guthrie, W.S., Shea, M.S., and Eggett, D.L. (2012). Hydraulic conductivity of cement-treated soils and aggregates after freezing. *Cold Regional Engineering*.

Holm, G., Larsson, L., Pettersson, M., Mácsik, J., Knutsson, S., and Makusa, G. (2015). *Durability-An expert study with focus on geo-constructions containing stabilized contaminated soils or sediments.* Linköping: Swedish Geotechnical Institute.

Hwang, C. and Shen, D. (1991). The effect of blast-furnace slag and fly ash on the hydration of Portland cement. *Cement and Concrete Research, 21*, 410-425.

Jamshidi, R. J., and Lake, C. B. (2015). Hydraulic conductivity and strength properties of unexposed and freeze-thaw exposed cement-stabilized soils. *Canadian Geotechnical Journal, 52*, 283-294.

Jamshidi, R. J., Lake, C. B., and Barnes, C. L. (2014). Examining Freeze/Thaw cycling and its impact on the hydraulic performance of cement-treated silty sand. *Journal of Cold Regions Engineering*.

Knutsson, S. (1983). *A theoretical model for calculation of pore water pressure and settlements in thawing soil (in Swedish).* Luleå, Sweden: Luleå University of Technology.

Knutsson, S., and Rydén, C.G. (1984). *Pore water pressure in thawing soil, a theoretical model (in Swedish).* Luleå, Sweden: Luleå University of Technology.

Kraus, J., Benson, C., Erickson, A. and Chamberlain, E. (1997). Freeze-thaw and hydraulic conductivity of bentonitic barriers. *Journal of Geotechnical and Geoenvironmental Engineering, Vol. 123*(3), 229-238.

Maher, A., Douglas, W.S and Jafari, F. (2006). Field placement and evaluation of stabilized dredged material from the New York-New Jersey Harbor. *Marine Georesources and Geotechnology, Vol. 24*, 251-263.

Makusa, G. P., Mattsson, H., and Knutsson, S. (2013). Investigation of increased hydraulic conductivity of silty till subjected to freeze-thaw cycles (STP 1568). In H. Zubeck, & Z. Yang (Ed.), *Mechanical Properties of Frozen Soils. STP 1568*, pp. 33-48. Florida: ASTM International.

Makusa, G.P., Bradshaw, S.L., Berns, E., Benson, C.H and Knutsson, S. (2014). Freeze-thaw cycling concurrent with cation exchange and the hydraulic conductivity of geosynthetic clay liners. *Can. Geotech. Journal, 51*, 591-598.

Marsh, B.K., Day. R.L., and Bonner, D.G. (1985). Pore structure characteristics affecting the permeability of cement paste containing fly ash. *Cement and Concrete Research, 15*, 1027-1038.

Necmi., Y., Kalkan, E., and Akbulut, S. (2007). Modification of the geotechnical properties, as influenced by freeze-thaw, of granular soils with waste additives. *Cold Regions Science Technology, 48*, 44-54.

Quang, N.D., and Chai, C.J. (2015). Permeability of lime-and cement-treated clayey soils. *Canadian Geotechnical Journal, 52*, 1221-1227.

Richardson, G.R., Groves, G.W. (1997). The structure of the calcium silicate hydrate phases present in hardened pastes of white Portland cement/blast-furnance slag blend. *Journal of Materials Science*(32), 4793-4802.

Simonsen, E., and Isacsson, U. (1999). Thaw weakening of pavement structures in cold regions. *Cold Regions Science and Technology, 29*, 135-151.

Svensson, M., and Andreas, L. (2012). *Characterization report-byproduct from Billerud Karlsborg AB (In Swedish).* Luleå, Sweden: Luleå University of Technology.

Topolnicki, M. (2004). *In-situ soil mixing: ground improvement.* (M. Kirsch, Ed.) London: Spon Press.

Wang, X. and Lee, H. (2009). Simulation of a temperature rise in concrete incorporating fly ash and slag. *Materials and Structures, 43*, 737-745.

Vapalli, S.K., Fredlund, D.G., and Pufhal, D.E. (1999). The influence of soil structure and stress history on the soil-water characteristics of a compacted till. *Geotechnique, 49*, 143-159.

Paper IV

Makusa, G.P., Mattsson, H., and Knusson, S. (2013). Investigation of increased hydraulic conductivity of silty till subjected to freeze–thaw cycles. *ASTM International: STP 1568,* 33-46 on *Mechanical Properties of frozen soils*.

Mechanical Properties of Frozen Soils
STP 1568, 2013
Available online at www.astm.org
DOI:10.1520/STP156820120139

Gregory P. Makusa,[1] *Hans Mattsson,*[2] *and Sven Knutsson*[2]

Investigation of Increased Hydraulic Conductivity of Silty Till Subjected to Freeze–Thaw Cycles

REFERENCE: Makusa, Gregory P., Mattsson, Hans, and Knutsson, Sven, "Investigation of Increased Hydraulic Conductivity of Silty Till Subjected to Freeze–Thaw Cycles," *Mechanical Properties of Frozen Soils*, STP 1568, Hannele Zubeck and Zhaohui Yang, Eds., pp. 33–46, doi:10.1520/STP156820120139, ASTM International, West Conshohocken, PA 2013.[3]

ABSTRACT: The hydraulic conductivity of silty till increases when the till is subjected to freeze–thaw cycles. A dramatic increase normally occurs after the first freeze–thaw cycle, and the magnitude generally depends on the initial or molding water content. Freezing of silty till causes aggregations of clods and the formation of macrostructure. The initial or molding water content determines the number of freeze–thaw cycles required to complete the agglomeration of clods and the formation of stable macrostructures, which in turn controls the hydraulic conductivity of compacted specimens frozen and thawed in the laboratory. The findings of this study show that for specimens compacted wet of the optimum water content, a significant increase in the hydraulic conductivity was measured after the first freeze–thaw cycle. When specimens were compacted at the optimum water content, a number of freeze–thaw cycles were required in order to obtain the corresponding significant increase in the hydraulic conductivity.

KEYWORDS: hydraulic conductivity, freeze–thaw, silty till, microstructure, macrostructure, dry cover, clods

Manuscript received November 2, 2012; accepted for publication May 29, 2013; published online August 22, 2013.

[1]Dept. of Civil, Environmental and Natural Resources Engineering, Luleå Univ. of Technology, SE 97187, Luleå, Sweden (Corresponding author), e-mail: gregory.makusa@ltu.se

[2]Dept. of Civil, Environmental and Natural Resources Engineering, Luleå Univ. of Technology, SE 97187, Luleå, Sweden.

[3]ASTM Symposium on *Mechanical Properties of Frozen Soils* on January 31, 2013 in Jacksonville, FL.

Introduction

Till has been used in Sweden as a hydraulic barrier in landfills for many years. Investigations of the hydraulic conductivity of silty till have shown that it is sufficiently low to prevent the infiltration of water into the waste material. It has also been reported that the hydraulic conductivity of silty till, like that of cohesive soils, increases when the soil is subjected to a number of freeze–thaw cycles [1–3]. Various researchers have postulated a number of reasons for this. Among other causes, the formation of cracks due to ice lenses, changes in void ratios, the initial or molding water content, and overburden stress have been mentioned frequently. Studies have shown that the increased hydraulic conductivity of compacted cohesive soils is caused by the formation of cracks in frozen soils. However, Chamberlain and Gow [4] studied the hydraulic conductivity of four fine-grained soils subjected to freeze–thaw cycling, and their study reported increased hydraulic conductivity in clayey silt specimens that did not exhibit the formation of cracks. According to Viklander [1], the initial void ratio has a significant influence on the hydraulic conductivity change of fine-grained till subjected to freeze–thaw. His results showed that initially denser till soils exhibited increased hydraulic conductivity after the last cycle of freeze–thaw, whereas initially loose soils showed decreased hydraulic conductivity after the last cycle of freeze–thaw. These observations were similar to the findings of Chamberlain and Gow [4] on the hydraulic conductivity of compacted clay, but they are in contrast to those of Kim and Daniel [5], who observed the largest increase in hydraulic conductivity in specimens of compacted silty sand with a decrease in void ratio. These and other contentious results from earlier research [1–9] suggest that more mechanisms contributing to the increased hydraulic conductivity of frozen and thawed soils are involved. Most of the test results from the investigations referred to above show a high increase in hydraulic conductivity during permeation following the first freeze–thaw cycle. No significant (or only small) variations in increased hydraulic conductivity occur because of subsequent freeze–thaw cycles.

The present study sought to address the aggregation of clods due to freezing and the ultimate formation of macrostructures, which in turn control the hydraulic conductivity of thawed silty till. The study also investigated the effect of laboratory sample preparation, surcharge load, and compaction on the subsequent hydraulic conductivity of silty till subjected to freeze–thaw cycles.

Materials and Methods

The soil used in this study was a Swedish till frequently used as barrier material in landfills and earth dams [1–3]. The soil is to be utilized as dry cover for wastes originating from mining activities at Boliden Mineral AB in the

Gällivare area in northern Sweden. The soil was characterized with regard to grain size distribution by means of wet sieving. Sedimentation analysis via the pipet method showed that the clay content was less than 5 %. A modified Proctor test was carried out to establish the dry density–water content relationship. The soil samples for the Proctor test were prepared in accordance with Swedish laboratory test routines, in which representative soil samples are oven dried, rewetted with the desired water content, and compacted. Figure 1 presents the particle size gradation of a representative soil sample. The results of the characterization were similar to previous results from other researchers [1–3], and the studied soil was classified as silty till based on the Swedish soil classification system or SM (silty sand) in accordance with the Unified Soil Classification System.

Dry Density–Water Content Relationship

The investigated soil had a received water content between 10.43 % and 11.20 % with an average value of 10.80 % by mass, determined after oven drying portions of representative silty till for 24 h. Using the dried soil samples, a series of specimens was compacted in a modified Proctor apparatus at molding water contents of 2 %, 4 %, 6 %, 7 %, 8 %, 10 %, and 12 % by mass. The dry density–water content relationship curve was plotted. A maximum dry density (MDD) of 2.14 g/cm^3 was obtained at the optimum water content (OWC) of 6.70 %, as shown in Fig. 2. It follows from the Proctor curve (Fig. 2) that the

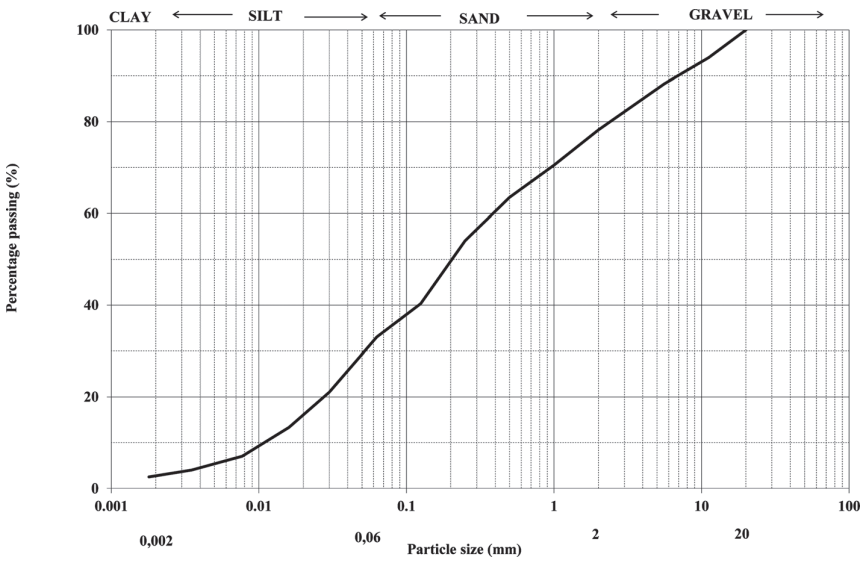

FIG. 1—*Particle size distribution for studied silty till.*

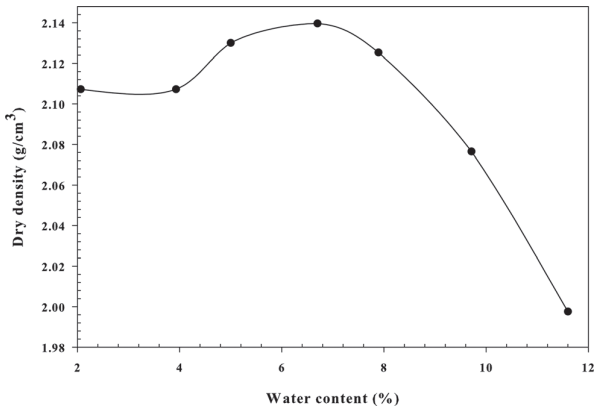

FIG. 2—*Dry density–water content relationship.*

average water content of 10.80 % corresponds to a dry density of 2.03 g/cm^3, which was equivalent to a 95 % degree of compaction.

Sample Preparation for Hydraulic Conductivity Test

A representative soil was processed to form two portions for the hydraulic conductivity test. Based on the methods of sample preparation, the laboratory experiment setup was divided into two categories, which involved the use of specimens from either soil sample A or soil sample B.

Sample A was prepared by oven drying a representative sample for 24 h. The oven-dried sample was then sieved to remove all particles larger than 20 mm prior to being mixed with the desired molding water contents. Two specimens, namely, specimens A1 and A2, were prepared from this soil sample. To mimic the received soil water condition, the soil sample for specimen A1 was molded with a water content of 10.80 % by mass and compacted into the permeameter. The soil sample for specimen A2 was molded at OWC and compacted into the permeameter, resulting in MDD in the Proctor curve.

To minimize the effect of processing the soil sample and preserve the natural soil suction capacity, another portion of representative silty till was sieved to remove soil particles larger than 20 mm without oven drying for sample B. Three specimens, namely, specimen B1, specimen B2, and specimen B3, were prepared at the received water condition for the hydraulic conductivity test.

Hydraulic Conductivity Test

In order to minimize double handling processes, five Proctor molds were manufactured. Each specimen was compacted in a rigid-wall Proctor mold 101.6 mm in diameter and 112.0 mm in height. Taking into account the initial

and molding water contents, all specimens were compacted to a 95 % degree of compaction except specimen A2, which was compacted to a 100 % degree of compaction. A filter was placed at the top and bottom of each specimen. The specimen molds were covered with top and bottom rigid plastic caps. All specimens were then set for the initial hydraulic conductivity prior to freeze–thaw cycling using a constant pressure head at a hydraulic gradient of 18 in accordance with ASTM D5856 [10]. The outflow was collected using upward flow, and the specimens were protected from upward movement by clamps. In order to simulate field conditions, in which the underlying material would not produce capillary action, no backpressure was applied to saturate the specimens. The outflow could be obtained within an hour; nevertheless, the test readings were taken every three hours during daytime, and a minimum of eight readings was considered sufficient. The average of the last four steady readings (within ±25 %) was reported as the hydraulic conductivity of a particular specimen. After the initial hydraulic conductivities of all specimens had been established, the top caps were removed and the molds were moved into a freezing cabinet. One-dimensional freezing in a closed system was desired. Therefore, the perimeters of the permeameter were covered with 35 mm of insulation foam. The bottom caps were placed in a Styrofoam insulator placed at the base of the freezing cabinet (Fig. 3). No backpressure was applied. Thermocouple instrumentation data showed that a duration time of 24 h was sufficient to freeze the specimens to −15°C and then thaw them to room temperature (Fig. 4). During freezing and thawing, specimen B2 and specimen B3 were loaded with 10 kPa and 25 kPa, respectively. Specimens B1, A1, and A2 were all frozen and

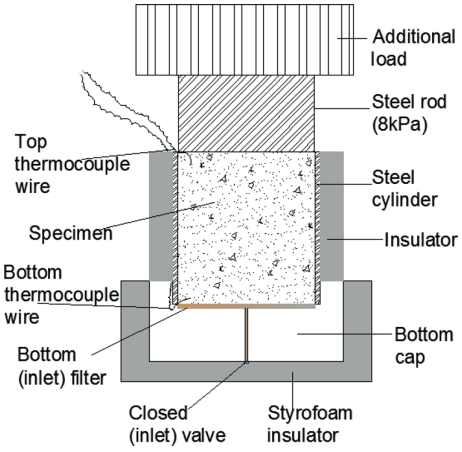

FIG. 3—*Schematic sketch of experimental device for one-dimensional freezing and thawing tests.*

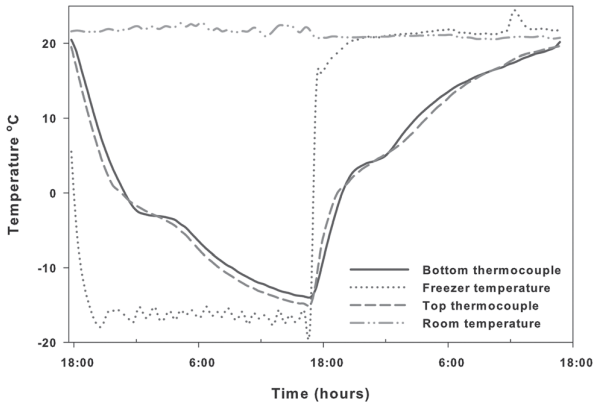

FIG. 4—*Progress of temperature within the silty till specimen from room temperature in a −15°C freezer.*

thawed without an overburden stress. The hydraulic conductivity results reported here are the average values of at least the last four steady readings.

Results

A summary of the test results is presented in Table 1. The results show that specimens from soil sample B compacted without oven drying the soil had low initial hydraulic conductivity relative to specimens from soil sample A compacted after the represented soil sample had been oven dried and rewetted to the desired water content. Thus, the average initial hydraulic conductivity value of 6.6×10^{-9} m/s of specimens from soil sample B was considered as the baseline hydraulic conductivity K_b of the studied silty till. It followed that all measured hydraulic conductivity values K were normalized over this baseline

TABLE 1—*Results of hydraulic conductivity tests.*

	Soil Sample A		Soil Sample B		
Freeze–Thaw Cycles	Specimen A1 (0 kPa), K, m/s	Specimen A2 (0 kPa), K, m/s	Specimen B1 (0 kPa), K, m/s	Specimen B2 (10 kPa), K, m/s	Specimen B3 (25 kPa), K, m/s
0	2.0×10^{-8}	1.1×10^{-8}	7.0×10^{-9}	6.5×10^{-9}	6.3×10^{-9}
1	1.6×10^{-7}	1.8×10^{-8}	1.4×10^{-7}	5.7×10^{-8}	5.3×10^{-8}
2	1.3×10^{-7}	1.6×10^{-8}	7.5×10^{-8}	5.8×10^{-8}	4.6×10^{-8}
3	8.2×10^{-8}	1.8×10^{-8}	1.5×10^{-7}	5.6×10^{-8}	4.4×10^{-8}
4	9.0×10^{-8}	2.0×10^{-8}	8.7×10^{-8}	5.9×10^{-8}	4.4×10^{-8}
5	7.0×10^{-8}	2.2×10^{-8}	6.6×10^{-8}	5.9×10^{-8}	4.3×10^{-8}
6	6.8×10^{-8}	—	—	6.2×10^{-8}	4.6×10^{-8}

TABLE 2—*Normalized hydraulic conductivity test results (K/K_b) for all specimens.*

	Soil Sample A		Soil Sample B		
Freeze–Thaw Cycles	Specimen A1 (0 kPa)	Specimen A2 (0 kPa)	Specimen B1 (0 kPa)	Specimen B2 (10 kPa)	Specimen B3 (25 kPa)
0	3.0	1.7	1.1	1.0	1.0
1	24.2	2.7	21.2	8.6	8.0
2	19.7	2.4	11.4	8.8	7.0
3	12.4	2.7	22.7	8.5	6.7
4	13.6	3.0	13.2	8.9	6.7
5	10.6	3.3	10.0	8.9	6.5
6	10.3	—	—	9.4	7.0

hydraulic conductivity. Table 2 presents the normalized hydraulic conductivity values. As can be seen, the hydraulic conductivity increased dramatically after the first freeze–thaw cycle. The increase was in the range of 2.7 to 24.0 times the baseline value. Specimen B1 and specimen A2 underwent five cycles only, which was considered sufficient. Svensson [11] carried out a parallel test for his Master's thesis using similar testing conditions with only oven-dried soil samples and obtained comparable results, except for the initial hydraulic conductivity.

Effect of Sample Preparation

Figure 5 presents the initial hydraulic conductivities of all tested specimens. Specimens from soil sample B showed low and consistent readings for three days of permeation, with an average initial hydraulic conductivity value of 6.6×10^{-9} m/s. Specimens from soil sample A showed higher initial hydraulic

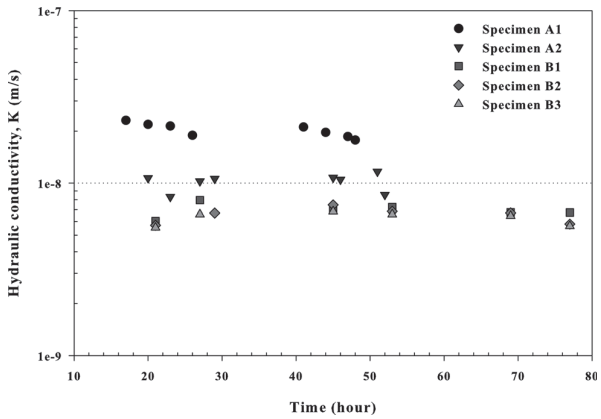

FIG. 5—*Initial hydraulic conductivity of specimens from soil samples A and B.*

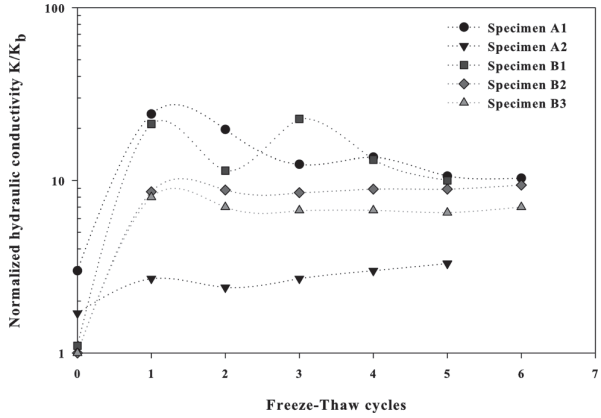

FIG. 6—*Normalized hydraulic conductivity of specimens versus number of freeze–thaw cycles.*

conductivity. Specimen A1 compacted wet of the OWC had an average initial hydraulic conductivity of 2.0×10^{-8} m/s, which was about three times the baseline hydraulic conductivity. Specimen A2 had an average initial hydraulic conductivity of 1.1×10^{-8} m/s. This value is about 1.7 times higher than the baseline hydraulic conductivity.

Effect of Freeze–Thaw and Surcharge Load

After being subjected to the first freeze–thaw cycles (Fig. 6), all specimens exhibited a significant increase in hydraulic conductivity. The hydraulic conductivity of specimen B2 loaded with 10 kPa initially increased by about nine times the baseline hydraulic conductivity and remained almost the same up to the sixth freeze–thaw cycle. Similarly, the hydraulic conductivity of specimen B3 loaded with 25 kPa initially increased by about eight times the baseline hydraulic conductivity. This initially increased hydraulic conductivity of specimen B3 decreased to about seven times the baseline hydraulic conductivity after the second freeze–thaw cycle, but it remained almost the same for the subsequent freeze–thaw cycles.

Effect of Freeze–Thaw and Compaction

After the first freeze–thaw cycle, the hydraulic conductivity of specimens of soil sample A compacted at desired water contents increased (Fig. 6). The initial increases in hydraulic conductivity for specimen A1 and specimen A2 were 24 and 3 times the baseline hydraulic conductivity, respectively. The hydraulic conductivity of specimen A1 decreased to about 11 times the

baseline hydraulic conductivity at the end of fifth freeze–thaw cycle. This increase and then decrease in hydraulic conductivity for specimen A1 was almost similar to that of specimen B1, which was compacted at the received water content and to the same degree of compaction as specimen A1. In contrast, the hydraulic conductivity of specimen A2 increased by about three times the baseline hydraulic conductivity at the end of the fifth freeze–thaw cycle.

Discussion

According to Vapalli et al. [12], fine-grained soils have two levels of structure, microstructure and macrostructure, both of which are present in natural and compacted clay soils. Regardless of the mineralogy, texture, and method of preparation, the resulting macrostructure of specimens prepared at different initial water contents will be different. The structure and aggregation of fine-grained soil is highly influenced by the initial or molding water content. Clay soils with a high initial water content are more homogeneous, with the large pore spaces not interconnected or in a closed state. These specimens offer more resistance to water flow. Consequently, the microstructure of specimens compacted wet of the OWC controls the water flow. In contrast, specimens with a low initial water content (i.e., dry of the OWC) contain relatively large pore spaces located between clods of soil. Thus, the macrostructure controls the initial discharge. Benson and Daniel [13] studied the influence of clods on hydraulic conductivity of unfrozen highly plastic clay. Their results show that the outcome of clod and inter-clod pores occurring during soil processing and compaction controlled the hydraulic conductivity of the compacted soil. The clod size had a large influence upon the hydraulic conductivity of the compacted soils. Samples of soil with initially small clods had lower hydraulic conductivity than samples compacted from material with initially large clods.

The term “microstructure” herein refers to soil specimens that are dominated by micro pores, whereas “macrostructure” refers to soil specimens in which the macro pore is dominant. “Clod” refers to the agglomeration of fine particles into small soil lumps within the specimen.

The differences in the initial hydraulic conductivity observed between specimens of the two soil samples A and B were due to different aggregations and soil-water affinities, which were caused by variations in initial water content and sample preparation. This resulted in the formation of clods with different physical characteristics. Specimens compacted from soil sample B had a higher initial water content. This allowed the saturation of natural clods during compaction, which flowed to fill the pore spaces. In additional to the flow of saturated clods, free water became available to fill the remaining pore spaces,

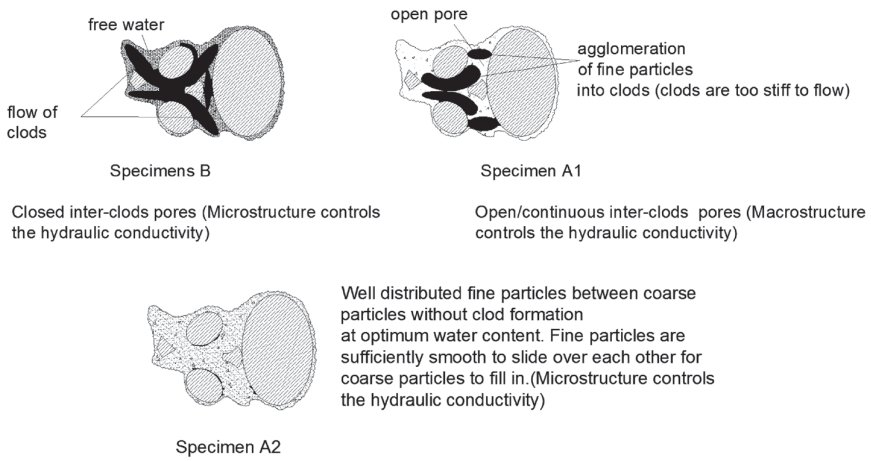

FIG. 7—*Enlarged schematic sketch of micro- or macrostructure levels of natural silty till compacted at different water contents.*

thus reducing the size of open inter-grained pores and inter-clod pores. Examples of the physical characteristics of specimen B are shown in Fig. 7 and Fig. 8(*b*); the resulting microstructure controls the hydraulic conductivity. Saturated specimens tend to have low soil suction. Specimen A1, which was molded and compacted at the received water content, indicated no degree of saturation during compaction, which means that the molding water content was not sufficient to mold and saturate the whole specimen. It can be postulated

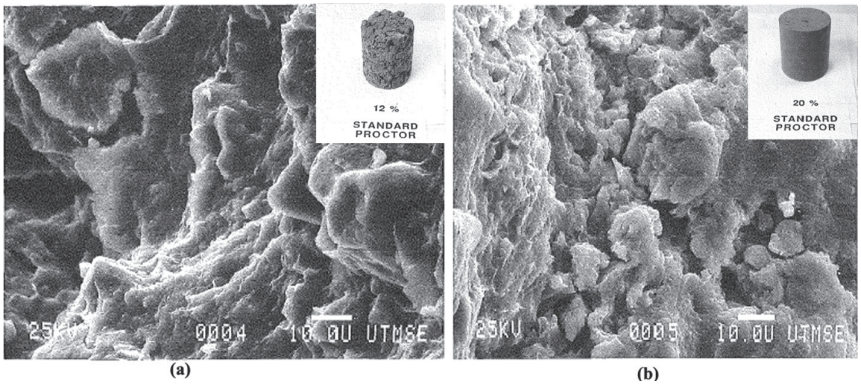

FIG. 8—*Scanning electron photomicrograph with corresponding photographs of soil compacted with water contents of (a) 12 % and (b) 20 % showing the physical characteristics of compacted clods (from Ref 13, with permission from ASCE).*

that the molding water was utilized in building up clods. According to Sharma [14], clods are formed via two mechanisms: coating deflocculated clay paste, and soil compaction. Consequently, during molding and compaction, stiff clods were formed with bridges between them, leaving interconnected large pores as shown in Fig. 7 (specimen A1) and Fig. 8(*a*), which provided a means for hydraulic paths. For that reason, macro pores became dominant and the macrostructure controlled the flow at high soil suction, which resulted in high initial hydraulic conductivity relative to those of specimen B. According to clod theory [13], soft, wet clods of soil are easier to remold than hard, dry clods. For specimens compacted at the optimum molding water content, the fine particles became sufficiently smooth (lubricated and friable), allowing them to slide past each other easily without sticking to each other. This allowed the coarse particles to penetrate, and the result was a uniform distribution of fine particles between coarse particles, as shown in Fig. 7 (specimen A2). Thus, the sizes of pore spaces were minimized and the hydraulic conductivity was controlled by the microstructure. According to Konrad [15], for well-graded Saint-Martyrs-Canadians till, the lowest fines (clay and silt) content of 12 % is sufficient to fill the voids between the sand and gravel particles.

Although silty till is classified as a non-cohesive soil [1,3], the water contents within the specimens gave it the ability to expand upon freezing. According to De Bruyn et al. [16], in order for the soil to expand when it freezes, it must be able to bind some amount of water that is not drained away by the force of gravity. Under the closed system, the only water that could freeze was the capillary and bound water and some remaining water in the hydraulic paths. During freezing, soil suction increased to the point of (or beyond) the air entry suction value (in the soil–water characteristic curve). At this point or beyond, it becomes difficult to remove water from soil particles because of high soil-water affinity [12]. Thus, the negative pore pressures generated between the bound water and soil particles created inter-particle bonds resulting in the formation of stable clods. The formed clods bridged one another, creating inter-clod pores (large pores), which became the ultimate hydraulic path at the time of permeation. Throughout the repeated process of desaturation (freezing), the aggregations of fines into strings and bulky clods continued, and during saturation (thawing and permeation) the inter-clod pores controlled the flow of water. According to Konrad [17], the relocation of particles occurs during freezing, and after thawing the clodded fine particles do not move back to their initial positions; this leads to permanent changes in the pore-size distribution characteristic.

Depending on the initial or molding water content and degree of saturation, the agglomeration of clods and ultimate formation of a stable macrostructure can occur either in the first freeze–thaw cycle or after subsequent freeze–thaw cycles. It follows that fine particles in specimens from soil sample B and specimen A1, which were compacted wet of optimum, aggregated into stable clods,

turning the whole specimen into macrostructure during the first freezing. During the first freezing, all possible clods were formed in specimens B1, B2, and B3, and after thawing and permeation the inter-clod pores became full of free water and the whole specimen became saturated again. Thus, during subsequent permeation, no extra-unsaturated pores were available to increase the hydraulic conductivity. The macrostructure controlled the flow at low soil suction, resulting in decreased or maintained increased hydraulic conductivity. Specimen A1, in contrast, had to undergo about five cycles before the inter-clod pores became saturated, after which the ultimate macrostructure controlled the hydraulic conductivity at a magnitude of about 10 times the baseline hydraulic conductivity. The continued increase in the hydraulic conductivity exhibited by specimen A2 suggested that the aggregation of fine particles into clods and the formation of macrostructures continued after five freeze–thaw cycles. This is because once the hydraulic paths have been defined during the initial permeation, it might take a long time to saturate soil particles located far away from these predefined hydraulic paths.

The surcharge loads reduced or maintained the size of inter-clod pores. Accordingly, specimens B2 and B3 had low increases in hydraulic conductivity relative to specimen B1. According to Benson and Daniel [13], in order to achieve low hydraulic conductivity in soils that form clods, large inter-clod pores must be eliminated during compaction. However, freezing action contributes to the formation of new clods, as discussed earlier, and sufficient overburden stress might be required in order to prevent the formation of these clods or completely break the clods and close the inter-clod pores.

Conclusion

The increase in the hydraulic conductivity of silty till due to freeze–thaw actions was investigated. We considered the effects of laboratory sample preparation, surcharge load, degree of compaction, and initial or molding water content on the hydraulic conductivity of silty till samples that were frozen and thawed in the laboratory. The following conclusions are drawn:

- Freezing action on silty till results in agglomerations of clods and the formation of macrostructures, which in turn increase the hydraulic conductivity of thawed silty till.
- For silty till compacted wet of the OWC, the hydraulic conductivity after the first freeze–thaw cycle was increased by 8 to 24 times the hydraulic conductivity of unprocessed silty till. All the significant increases in hydraulic conductivity were observed after the first freeze–thaw cycle.
- For silty till compacted at OWC and subjected to laboratory freeze–thaw action, several freeze–thaw cycles might be required in order to obtain the ultimate increase in the hydraulic conductivity.

Acknowledgments

The writers acknowledge Mr. Seth Mueller (Boliden Mineral AB) for providing materials for investigation of the effect of freeze–thaw on hydraulic conductivity of silty till. Special thanks are due to Mr. Thomas Forsberg, Ulf Stenamn (Soil Laboratory technician), and Jimmy Svensson (Master's student) for their daily support and skilled laboratory work.

References

[1] Viklander, P., "Permeability and Volume Changes in Till Due to Cyclic Freeze-Thaw," *Can. Geotech. J.*, Vol. 35, 1998, pp. 471–477.

[2] Viklander, P., 1997, "Compaction and Thaw Deformation of Frozen Soil: Permeability and Structural Effects Due to Freezing and Thawing," Ph.D. thesis, Luleå University of Technology, Luleå, Sweden.

[3] Carlsson, E., 2002, "Sulphide-rich Tailings Remediated by Soil Cover: Evaluation of Cover Efficiency and Tailings Geochemistry, Kristineberg, Northern Sweden," Ph.D. thesis, Luleå University of Technology, Luleå, Sweden.

[4] Chamberlain, E. and Gow, A., "Effect of Freezing and Thawing on the Permeability and Structure of Soils," *J. Eng. Geol.*, Vol. 13, Nos. 1–4, 1979, pp. 73–92.

[5] Kim, W. and Daniel, D., "Effects of Freezing on Hydraulic Conductivity of Compacted Clay," *J. Geotech. Engrg.*, Vol. 118, No. 7, 1992, pp. 1083–1090.

[6] Benson, C. and Othman, M., "Hydraulic Conductivity of Compacted Clay Frozen and Thawed in-situ," *J. Geotech. Engrg.*, Vol. 119, No. 2, 1993, pp. 276–294.

[7] Chamberlain, E. J., Erickson, E. A., and Benson, H. C., "Frost Resistance of Cover and Liner Materials for Landfills and Hazardous Waste Sites," *Special Report 97-29*, Corps of Engineers, Department of the Army, Cold Regions Research and Engineering Laboratory, Hanover, NH, 1997.

[8] Kraus, J., Benson, C., Erickson, A., and Chamberlain, E., "Freeze-Thaw and Hydraulic Conductivity of Bentonitic Barriers," *J. Geotech. Geoenviron. Eng.*, Vol. 123, No. 3, 1997, pp. 229–238.

[9] Benson, H. C., Abichou, H. T., Olson. A. M., and Bosscher, P. J., "Winter Effect on Hydraulic Conductivity of Compacted Clay," *J. Geotech. Engrg.*, Vol. 121, 1995, pp. 69–79.

[10] ASTM D5856-95: Standard Test Method for Measurement of Hydraulic Conductivity of Porous Material Using a Rigid-Wall, Compaction-Mold Permeater, *Annual Book of ASTM Standards*, ASTM International, West Conshohocken, PA, 2007.

[11] Svensson, J., 2012, "Hydraulisk konduktivitet i en morän: inverkan av frys- och tiningscykler vid olika överlaster och packningsgrader [Hydraulic Conductivity of Till: Influence of Freeze/Thaw Cycles at Different Overburden and Degree of Compaction]," M.S. thesis, Luleå University of Technology, Luleå, Sweden (in Swedish).

[12] Vapalli, S. K., Fredlund, D. G., and Pufhal, D. E., "The Influence of Soil Structure and Stress History on the Soil-Water Characteristics of a Compacted Till," *Geotechnique*, Vol. 49, 1999, pp. 143–159.

[13] Benson, C. H. and Daniel, D. E., "Influence of Clods on Hydraulic Conductivity of Compacted Clay," *J. Geotech. Engrg.*, Vol. 116, 1990, pp. 1231–1248.

[14] Sharma, K. P., "Clod Formation—A Serious Problem for Wheat Cultivation in Rice Wheat Cropping Sequence," *Journal of Agricultural Physics*, Vol. 1, 2001, pp. 76–79.

[15] Konrad, J. M., "Frost Susceptibility Related to Soil Index Properties," *Can. Geotech. J.*, Vol. 36, No. 3, 1999, pp. 403–417.

[16] De Bruyn, C. M. A., Collins, L. E., and Williams, A. A., "The Specific Surface, Water Affinity, and Potential Expansiveness of Clays," *J. Clay Miner.*, Vol. 3, No. 17, 1957, pp. 120–128.

[17] Konrad, J. M., "Physical Processes During Freeze-Thaw Cycles in Clayey Silts," *Cold Reg. Sci. Technol.*, Vol. 16, 1989, pp. 291–303.

Paper V

Makusa, G.P., Bradshaw, S., Bern, E., Benson, C.H., and Knusson, S. (2014). Freeze-thaw cycling concurrent with cation exchange and the hydraulic conductivity of geosynthetic clay liners. *Canadian Geotechnical Journal (51) 591-598.*

NRC Research Press

ARTICLE

Freeze–thaw cycling concurrent with cation exchange and the hydraulic conductivity of geosynthetic clay liners

Gregory P. Makusa, Sabrina L. Bradshaw, Erin Berns, Craig H. Benson, and Sven Knutsson

Abstract: A study was conducted to assess the effect of cation exchange concurrent with freeze–thaw cycling on the hydraulic conductivity of a geosynthetic clay liner (GCL). GCLs were prehydrated by contact with silica flour moistened with synthetic subgrade pore water and subsequently permeated with a solution representing the pore water in the cover soil over a tailings facility. Control tests were conducted using the same procedure, except deionized (DI) water was used as the permeant liquid to preclude cation exchange from the permeant liquid. The GCLs were subjected to 1, 3, 5, 15, and 20 freeze–thaw cycles, and the hydraulic conductivity and exchange complex were determined before and after freeze–thaw cycling to assess chemical changes that occurred during freezing, thawing, and permeation. GCLs undergoing freeze–thaw cycling experienced little to no cation exchange through 5 freeze–thaw cycles. After 20 freeze–thaw cycles, 50% of the sodium (Na^+) initially in the exchange complex was replaced by calcium (Ca^{2+}). Dissolution of calcite within the bentonite is a likely source of the Ca^{2+}. Hydraulic conductivity of the GCLs exposed to freeze–thaw cycling was lower than the hydraulic conductivity of a new GCL permeated with DI water ($<2.2 \times 10^{-11}$ m/s). A small increase in hydraulic conductivity (~2.3 times), which may have been caused by cation exchange, occurred between 15 and 20 freeze–thaw cycles, but the hydraulic conductivity remained below the hydraulic conductivity of a new GCL unexposed to freeze–thaw cycling and permeated with DI water.

Key words: geosynthetic clay liner, hydraulic conductivity, cation exchange, exchange complex, freeze, thaw, prehydration, bentonite, barrier.

Résumé : Une étude a été réalisée pour évaluer l'effet simultané de l'échange cationique et des cycles de gel–dégel sur la conductivité hydraulique d'un revêtement géocomposite bentonitique (GCB). Les GCB ont été pré-hydraté par contact avec de la farine de silice humidifiée avec de l'eau interstitielle synthétique, et par la suite ont été infiltré par une solution qui représente l'eau interstitielle dans un recouvrement de sol placé sur un site d'entreposage de rejets. Des essais témoins ont été réalisés avec la même procédure, sauf que de l'eau déionisée (DI) a été utilisée comme liquide d'infiltration pour éliminer les échanges cationiques provenant du liquide d'infiltration. Les GCB ont été soumis à un, trois, cinq, 15 et 20 cycles de gel–dégel, et la conductivité hydraulique et les complexes échangés ont été déterminés avant et après les cycles de gel–dégel pour évaluer les changements chimiques qui se sont produits durant le gel, le dégel et l'infiltration. Les GCB soumis aux cycles de gel–dégel démontrent peu à aucun échange cationique pendant 5 cycles de gel–dégel. Après 20 cycles de gel–dégel, 50 % du sodium (Na^+) initialement présent dans le complexe échangé a été remplacé par du calcium (Ca^{2+}). La dissolution de la calcite à l'intérieur de la bentonite est une source probable du Ca^{2+}. La conductivité hydraulique des GCB exposés aux cycles de gel–dégel était inférieure à la conductivité hydraulique d'un nouveau GCB infiltré avec de l'eau DI ($<2,2 \times 10^{-11}$ m/s). Une légère augmentation de la conductivité hydraulique (environ 2,3 fois), qui peut être causée par les échanges cationiques, s'est produite entre les cycles 15 et 20 de gel–dégel, mais la conductivité hydraulique est demeurée inférieure à celle d'un nouveau GCB non exposé aux cycles de gel–dégel et infiltré avec de l'eau DI. [Traduit par la Rédaction]

Mots-clés : géocomposite bentonitique, conductivité hydraulique, échange cationique, complexe échangé, gel, dégel, pré-hydratation, bentonite, barrière.

Introduction

Geosynthetic clay liners (GCLs) are widely used in waste containment facilities as hydraulic barriers. GCLs consist of a thin layer of granular or powdered bentonite clay encased between two geotextiles or glued to a geomembrane. Montmorillonite, the predominant clay mineral in bentonite, is largely responsible for the low hydraulic conductivity of GCLs. The hydraulic conductivity of bentonite is controlled by the relative amounts of unbound and bound pore water in the montmorillonite fraction. When a larger fraction of the pore water is bound, the flow paths are narrower and more tortuous, resulting in lower hydraulic conductivity (Chapuis 1990). Bound water is predominant in bentonites when the exchange complex of the montmorillonite is composed primarily of monovalent cations (e.g., Na^+), which are associated with osmotic swelling. For this reason, Na–bentonites are commonly used for GCLs and have low hydraulic conductivity for water (Jo et al. 2001, 2004; Kolstad et al. 2004).

The Na^+ cations in the exchange complex of Na–bentonite are susceptible to replacement ("cation exchange") by other cations present in the surrounding pore water, and from dissolution of calcite within the GCL (James et al. 1997; Egloffstein 2002; Guyonnet et al. 2005; Rauen 2007; Bradshaw et al. 2013; Hosney and Rowe 2013). Exchange can occur as the GCL hydrates on a

Received 2 April 2013. Accepted 20 January 2014.

G.P. Makusa and S. Knutsson. Department of Civil, Environmental, and Natural Resources Engineering, Luleå University of Technology, SE-971 87, Luleå, Sweden.
S.L. Bradshaw, E. Berns, and C.H. Benson. Geological Engineering, University of Wisconsin, 1415 Engineering Drive, Madison, WI 53706 USA.
Corresponding author: Craig H. Benson (e-mail: chbenson@wisc.edu).

subgrade, during permeation or as minerals within the bentonite dissolve. Replacement of Na^+ by Ca^{2+} or Mg^{2+} is common, as the exchange reactions are thermodynamically favorable (Sposito 1981) and Ca^{2+} and Mg^{2+} are ubiquitous in the geoenvironment (Meer and Benson 2007; Scalia and Benson 2011). When Ca^{2+} and Mg^{2+} are predominant in the exchange complex, a smaller fraction of pore water is bound and a greater fraction is mobile, resulting in higher hydraulic conductivity (Jo et al. 2001, 2004; Kolstad et al. 2004).

When cation exchange occurs concurrently with wet–dry cycling, increases in hydraulic conductivity of several orders of magnitude can occur depending on the number of cycles and degree of cation exchange (Lin and Benson 2000; Egloffstein 2002; Melchior 2002; Benson et al. 2007; Meer and Benson 2007; Scalia and Benson 2011). In contrast to wet–dry cycling, several studies have shown that the hydraulic conductivity of GCLs is unaffected by freeze–thaw cycling when the permeant liquid is deionized (DI) or tap water, even though ice lenses form in the frozen bentonite (Hewitt and Daniel 1997; Kraus et al. 1997; Rowe et al. 2004, 2006, 2008; Podgorney and Bennett 2006). This behavior contrasts that of compacted clays, which undergo similar increases in hydraulic conductivity of several orders of magnitude when exposed to freeze–thaw or wet–dry cycling (Chamberlain and Gow 1979; Zimmie and LaPlante 1990; Kim and Daniel 1992; Benson and Othman 1993; Othman et al. 1994; Albrecht and Benson 2001). Kraus et al (1997) show that GCLs undergoing freezing and thawing behave differently from compacted clay because the soft hydrated bentonite consolidates during thawing, closing cracks formed by ice lenses. Kraus et al (1997) also show that "thaw consolidation" can cause a small, but statistically significant reduction in hydraulic conductivity of GCLs.

Although several studies have shown that freeze–thaw cycling appears to have no significant effect on the hydraulic conductivity of GCLs, none of the past studies evaluated GCLs exposed to cation exchange during hydration, freezing and thawing, or permeation. Because cation exchange is a prerequisite for large increases in hydraulic conductivity for GCLs undergoing wet–dry cycling (Lin and Benson 2000; Benson and Meer 2009), the relevance of past studies on freezing and thawing of GCLs has been questioned. Moreover, Rowe et al. (2006) have shown that freeze–thaw cycling coincident with permeation by jet fuel, an aggressive liquid known to alter the fabric and hydraulic conductivity of bentonite, can result in modest increases in hydraulic conductivity of GCLs. By analog, a similar condition might occur when the bentonite in GCLs is exposed to cation exchange prior to or during freeze–thaw cycling, as cation exchange can also lead to an alteration of the fabric of bentonite.

The objective of this study was to evaluate the effect of freezing and thawing on the hydraulic conductivity of GCLs under conditions where cation exchange could occur during hydration, freezing and thawing, and permeation. Tests were conducted under conditions simulating a cover system for a tailing disposal facility located in the far northern regions of North America, where a composite barrier layer (geomembrane over GCL) was placed directly on tailings and overlay by 1 m of cover soil. The sulfidic tailings at this site were derived from a nickel and copper mine at the site. The GCLs were prehydrated by contact with synthetic subgrade pore water, subjected to freezing and thawing, and permeated with a synthetic cover pore water. Hydraulic conductivity and cation composition of the exchange complex were determined as a function of the number of freeze–thaw cycles.

Materials

Geosynthetic clay liner

The GCL used in this study was Bentomat ST manufactured by CETCO Lining Technologies (Hoffman Estates, Ill., USA). Bentomat ST consists of granular sodium bentonite with sand-size granules sandwiched between woven and nonwoven geotextiles bonded together with needlepunching with no supplemental thermal treatment. The GCL had an average mass/area of 5.5 kg/m^2 and an average initial (dry) thickness of 6.0 mm. The bentonite had an average initial water content of 19.3%. X-ray diffraction (Mineralogy Inc., Tulsa, Okla.) conducted using the method in Moore and Reynolds (1989) showed that the bentonite contained 84% montmorillonite, 9% quartz, 3% plagioclase feldspar, 2% clinoptilolite, 1% calcite, 1% illite, and traces of other minerals.

Bound cations, soluble cations, and cation exchange capacity (CEC) of the bentonite were determined using the method in ASTM (2010*a*) D7503. Soluble and bound cation concentrations were determined for the major cations (Na^+, Ca^{2+}, Mg^{2+}, and K^+) by inductively coupled plasma-optical emission spectrometry (ICP-OES) following US Environmental Protection Agency (USEPA) Method 6010B (USEPA 1996). CEC of the bentonite was 83 ± 5 cmol$^+$/kg. Mole fractions (X) of the major cations in the exchange complex were as follows: X_{Na} = 0.55, X_{Ca} = 0.29, X_{Mg} = 0.14, and X_K = 0.03.

Permeant liquids

Two permeant liquids were used to evaluate the hydraulic conductivity of the GCLs: type II DI water as defined in ASTM (2011) D1193 (control) and a synthetic cover pore water (CW). The synthetic cover pore water replicated the pore water in the surface layer overlying the composite barrier at the site. Concentrations of major cations (Ca^{2+}, Na^+, Mg^{2+}, K^+), pH, specific conductance, cationic strength (I_c), and the relative preponderance of monovalent cations and polyvalent cations in the permeant liquids are shown in Table 1. Cationic strength is analogous to ionic strength, but is computed with only the cation concentrations (Rauen and Benson 2008). The parameter RMD is used to describe the relative abundance of monovalent and polyvalent cations in the permeant and hydrating liquids (Kolstad et al. 2004):

$$\text{RMD} = \frac{M_M}{\sqrt{M_D}} \quad (1)$$

where M_M is the total molar concentration of monovalent cations and M_D is the total molar concentration of divalent and polyvalent cations. The CW solution was prepared by dissolving chloride salts in type II DI water with the pH adjusted with nitric acid (HNO_3) to match site conditions (Table 1). The I_c and RMD of the cover pore water are compared in Fig. 1 with I_c and RMD from pore waters in barrier soils from other sites in North America, as reported by Scalia and Benson (2010). The pore water from this cover soil is more dilute than typical, but also tends to be more divalent (lower RMD).

Hydrating subgrade

Acid-washed silica flour with silt-size particles was used to simulate the tailings subgrade layer on which the GCL was to be deployed. The silica flour was saturated with synthetic pore water similar to the pore water in the tailings at the mine site (Table 1) to simulate the nearly saturated tailings on which the cover was to be constructed. The synthetic pore water in the subgrade was prepared using the same methodology as the CW. The I_c and RMD of the tailings subgrade are shown in Fig. 1. The subgrade pore water tends to be more concentrated that than the subgrade and cover soils reported by Scalia and Benson (2010), and has lower RMD (is more divalent) than any of the other pore waters in the data set.

Methods

GCL specimen preparation

GCL specimens were prepared by cutting a circular disc (diameter = 102 mm) from a GCL roll using a razor blade and a steel ring

Table 1. Chemical characteristics of cover soil and subgrade pore waters.

Parameter	Cover soil pore water	Subgrade pore water
Ca (mmol/L)	0.07	5.96
Mg (mmol/L)	0.07	0.20
K (mmol/L)	0.05	0.001
Na (mmol/L)	0.21	0.41
pH	4.4	2.9
Cationic strength (mmol/L)	0.41	12.5
RMD ((mol/L)$^{0.5}$)	0.023	0.005

Note: Pore water Cl^- concentration = 0.55 mmol/L for cover soil, 12.7 mmol/L for subgrade.

Fig. 1. Cationic strength versus RMD for the synthetic pore water in the tailings subgrade and for cover soil in this study along with data from soils from North America as reported by Scalia and Benson (2010).

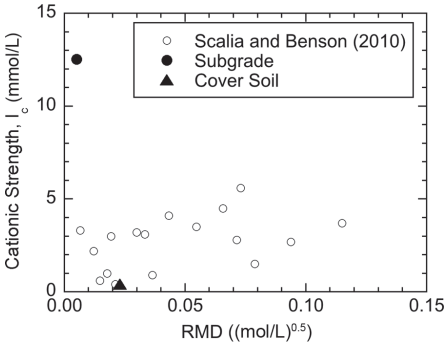

following the methods in Jo et al. (2001). Edges of the specimens were trimmed using scissors. Permeant liquid is often applied to the edge of GCL specimens during cutting to prevent loss of bentonite. However, for this study, the edge was not hydrated to ensure uniform prehydration. GCL specimens were handled with extreme care to prevent loss of bentonite. Bentonite loss was checked by comparing the weight of the trimmed specimen to the expected weight of single specimen without loss of bentonite (44.3 g). The trimmed specimens had a mass between 39.3 and 44.1 g, with an average of 41.5 g, indicating minimal loss of bentonite.

Prehydration

GCL specimens were prehydrated to a target water content of 70 ± 5% by contact with the saturated silica flour subgrade. The target hydration water content of 70% is based on GCL–subgrade hydration experiments reported in Bradshaw et al. (2013), and was intended to simulate the field subgrade hydration condition expected in a composite barrier. The silica flour was compacted into a 0.7 m × 1.3 m plastic bin in two lifts for a total thickness of 150 mm. The surface of each lift was tamped with a wooden tamper in a uniform pattern until compression was negligible. The silica flour was saturated with synthetic pore water by inundation. The synthetic pore water was slowly poured into the bin until the liquid level was just below the surface of the silica flour.

GCLs were placed on the moistened silica flour with the nonwoven side down and covered with a 0.1 mm thick plastic sheet to prevent moisture loss and to simulate a geomembrane. A 15 kPa stress was placed on the plastic sheet to ensure contact between the GCL and the silica flour, and to simulate the stress applied by overlying cover soil. The GCL specimens were removed periodically and weighed to ensure the target water content was met. Final subgrade hydration water contents ranged from 65.6% to 68.5% with an average water content of 68.0% after approximately 60 days. After hydration was complete, the weight and total thickness were measured within ±0.1 g and 0.01 mm, respectively.

The exchange complex after prehydration was determined and found to be nearly identical to the initial exchange complex (rows corresponding to zero cycles in Table 2), indicating that cation exchange during subgrade prehydration was negligible. Bradshaw et al. (2013) report similar findings for GCLs hydrated on subgrades for 30 days.

Freeze–thaw cycling

GCL specimens were subjected to 1, 3, 5, 15, and 20 freeze–thaw cycles in general accordance with the method in ASTM (2013) D6035. The intent was to simulate freeze–thaw cycling that would occur over a 20 year period with the GCL situated at a depth where one freeze–thaw cycle occurs annually. A 12 h period was used for both freezing and thawing so that one cycle could be completed in a 24 h period. A GCL instrumented with thermocouples was used to confirm that a 12 h freezing time was adequate to freeze the GCL. The phase change occurred in less than 2 h and an internal temperature of –18 °C was achieved at the center of the GCL within 3 h (Fig. 2).

After thawing (and permeation in some cases, see subsequent discussion), GCL specimens were removed from the permeameter, sealed in a plastic bag, and gently placed in a freezer set at –20 °C in the same orientation to be employed for hydraulic conductivity testing. After 12 h in the freezer, the specimens were removed, inserted between two geotextiles soaked with permeant liquid, and placed in a permeameter at room temperature (23 °C). GCL specimens were thawed in the permeameter with the stress applied (15 kPa) for 12 h with the influent and effluent lines closed. Specimens requiring additional freeze–thaw cycles before hydraulic conductivity testing were immediately transferred to the freezer after thawing. Specimens ready for hydraulic conductivity testing were permeated immediately after the thawing period (i.e., the influent and effluent lines were opened after 12 h) using the methods described subsequently.

All specimens were inspected visually after each freezing event and thawing event. No change in physical appearance of the GCL was observed.

Permeation

GCL specimens were permeated with DI water (control) or CW after hydration to define the hydraulic conductivity prior to freeze–thaw cycling. Additional permeation was conducted between freeze–thaw cycles for some specimens ("intermittent permeation" tests — permeation between some freeze–thaw cycles) or after freeze–thaw cycling was complete ("single permeation" tests — no permeation between freeze–thaw cycles). One GCL was permeated directly with DI water (no subgrade hydration or freeze–thaw cycling) to establish the baseline hydraulic conductivity for a new GCL.

All hydraulic conductivity tests were performed in general accordance with ASTM (2010*b*) D5084 using the falling-headwater constant-tailwater method. GCLs hydrated on the subgrade were immediately transferred into a flexible-wall permeameter after the target hydration water content was achieved. The GCL specimens were placed between two geotextiles (mass/area = 240 g/m^2) to promote uniform stress and evenly distribute the permeant liquid. An average effective stress of 15 kPa was applied to simulate the presence of cover soil above the GCL. Backpressure was not used to simulate the field condition and to prevent chemical alteration of the permeant liquid.

The average hydraulic gradient was 150, which is atypical of field conditions, but common when testing GCLs in the laboratory.

Table 2. Summary of bound cations (cmol$^+$/kg) in GCL specimens permeated with cover pore water or deionized (DI) water and subjected to prescribed freeze–thaw cycles. Initial bound cation concentration (cmol$^+$/kg): Na^+–48.0, Ca^{2+}–25.3, Mg^{2+}–12.0, K^+–2.2. Bond cation concentrations after subgrade prehydration (cmol$^+$/kg): Na^+–45.6, Ca^{2+}–24.9, Mg^{2+}–11.8, K^+–2.3.

		Bound cations (cmol$^+$/kg)							
		Cover water[a]				DI water[a]			
Prehydration condition	No. of freeze–thaw cycles	Na	Ca	Mg	K	Na	Ca	Mg	K
None	0	—	—	—	—	48.9	23.7	11.6	2.4
Subgrade prehydration	0	49.0	25.4	12.3	2.5	48.4	24.8	12.2	2.4
	1	47.5	25.6	12.7	2.5	45.9	23.6	12.1	2.3
	3	45.6	24.8	13.5	2.4	42.3	23.1	12.2	2.1
	5	42.8	24.0	12.6	2.2	44.2	24.9	13.3	2.5
	15	28.3	36.7	12.4	1.9	29.3	34.8	13.1	2.0
	20	23.6	36.4	11.5	1.9	24.5	32.5	12.5	1.2
	20[b]	23.2	38.5	13.5	2.0	24.3	38.8	12.6	1.9

[a]Permeant liquid.
[b]Specimens subjected to intermittent permeation; all others are single permeation.

Fig. 2. Evolution of temperature at the center of a GCL specimen cooled from room temperature in a –20 °C freezer.

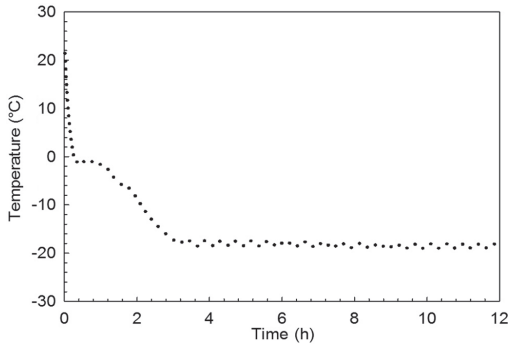

Shackelford et al. (2000) show that elevated hydraulic gradients have a much smaller impact on the effective stress and hydraulic conductivity of GCLs compared to specimens of compacted clay because GCLs are much thinner. Permeation continued until the hydraulic equilibrium criteria in ASTM (2010*b*) D5084 were met.

The total pore volumes of flow (PVF) during permeation after each freeze–thaw cycle was maintained approximately the same (≈1 to 2 PVF), except for the final hydraulic conductivity tests conducted after 20 freeze–thaw cycles (2.8 to 3.0 PVF). These permeation volumes are comparable with annual percolation rates reported by Benson et al. (2007) for a GCL used in a composite barrier in a final cover located in southwestern Wisconsin.

Results and discussion

Two sets of six GCL specimens were subjected to a prescribed number of freeze–thaw cycles (0, 1, 3, 5, 15, or 20 cycles) and then permeated after the prescribed number of freeze–thaw cycles was met (henceforth "single permeation" GCLs). Bentonite in these GCLs was analyzed for bound cations after the hydraulic conductivity test was terminated. Two additional GCL specimens were permeated after 0, 1, 3, 5, 15, and 20 freeze–thaw cycles, and are referred to henceforth as "intermittent permeation" GCLs. Bentonite from the intermittent permeation GCLs was analyzed for bound cations after all of the hydraulic conductivity tests were completed (i.e., after the 20th freeze–thaw cycle). The single permeation and intermittent permeation procedures were used to evaluate whether permeation between freeze–thaw cycles would induce additional cation exchange and potentially greater alterations in hydraulic conductivity.

Cation exchange during freeze–thaw cycling

Bound cation concentrations in the GCL before and after freeze–thaw cycling are summarized in Table 2. The change in major bound cation concentrations during freeze–thaw cycling is shown in Fig. 3 in terms of the "exchange ratio" defined as the ratio of the bound cation concentration after hydraulic conductivity testing to the bound cation concentration of a new GCL (Table 2). The solid lines in Fig. 3 represent an exchange ratio of 1.0 ± 0.1, which corresponds to the reproducibility of exchange complex measurements (Scalia and Benson 2011).

Little to no cation exchange occurred in GCLs permeated with DI water or CW during 1, 3, and 5 freeze–thaw cycles. At 15 freeze–thaw cycles, however, Ca^{2+} had replaced Na^+ in specimens permeated with both DI water and CW. Additional replacement of Ca^{2+} for Na^+ occurred between 15 and 20 cycles. In contrast, bound Mg^{2+} remained unchanged, even though Ca^{2+} and Mg^{2+} had similar concentrations in CW. The predominance of Ca^{2+} over Mg^{2+} can be attributed to the preference of Ca^{2+} over Mg^{2+} in the lyotropic series (Mitchell and Soga 2005) as well as calcite dissolution with the bentonite (described subsequently).

Replacement of Ca^{2+} for Na^+ was not anticipated for the specimens permeated with DI water, which was used specifically to preclude exchange. Moreover, cation exchange that occurred in specimens permeated with DI water was nearly identical to cation exchange in the specimens permeated with CW, suggesting that a source other than permeant water was supplying the exchangeable Ca^{2+}. One likely source of Ca^{2+} is dissolution of the calcite mineral from within the GCL. Bradshaw et al. (2013) observed similar Ca^{2+}-for-Na^{2+} replacement in GCLs hydrated on a subgrade and permeated with DI water, and determined that calcite within the bentonite was the source of Ca^{2+}. Similarly, laboratory studies by Guyonnet et al. (2005) and Rauen (2007) found 9%–57% replacement of Ca^{2+}-for-Na^+ in GCLs permeated directly with DI water or dilute (1.2 mmol/L) NaCl solutions.

The concentration of bound cations after 20 freeze–thaw cycles is shown in Fig. 4 for GCLs undergoing intermittent permeation and single permeation. The cumulative PVF during permeation at 20 cycles ranged between 2.8 and 3.0 regardless of the mode of permeation (intermittent or single permeation). Thus the bentonite in the GCLs was in contact with a similar volume of water and mass of solute. Except for Ca^{2+}, the data fall along the 1:1 line, indicating that cation exchange is nearly identical for intermittent permeation and single permeation. This was expected because the PVF was similar for all tests. However, GCLs permeated

Fig. 3. Exchange ratio (final bound cation concentration divided by original bound cation concentration) as a function of number of freeze–thaw cycles for GCL specimens undergoing single permeation.

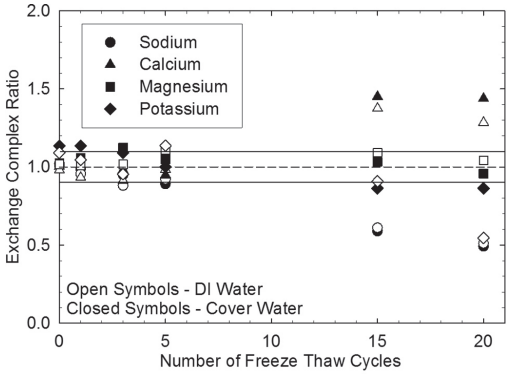

Fig. 4. Bound cation concentrations after 20 freeze–thaw cycles for GCLs that underwent intermittent or single permeation.

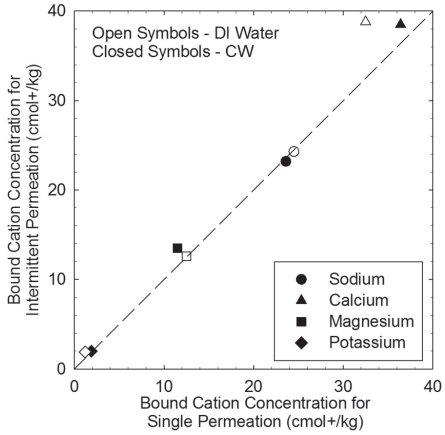

intermittently with CW and DI water had slightly more Ca^{2+} (1.1–1.2 times) in the exchange complex than GCLs undergoing single permeation. The additional Ca^{2+} in the exchange complex may be evidence that calcium exchange associated with calcite dissolution is exacerbated by permeation soon after thawing.

Hydraulic conductivity

Hydraulic conductivity for DI water and CW for GCLs is shown in Fig. 5 as a function of number of freeze–thaw cycles along with data from other studies where GCLs were exposed to freeze–thaw cycling and then permeated with DI or tap water under similar stress conditions (12–20 kPa). A summary of the hydraulic conductivities measured in this study is shown in Table 3. All of the hydraulic conductivity tests conducted after freezing and thawing came to equilibrium quickly, with no temporal trend in the hydraulic conductivity data for a given test.

Although Ca^{2+} replaced Na^{+} in the exchange complex of GCLs after 15 and 20 freeze–thaw cycles (Fig. 3), the hydraulic conductivity after exposure to freeze–thaw cycling was lower than the

Fig. 5. Hydraulic conductivity of GCLs as a function of freeze–thaw cycles for single or intermittent permeation with CW and DI water. GCLs from other studies had no prehydration and were permeated with DI water or tap water at a confining stress between 12.5 and 20 kPa.

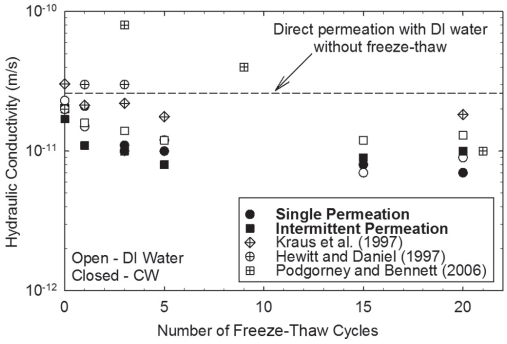

hydraulic conductivity of the GCL never exposed to freeze–thaw cycling. In fact, as also observed in past studies, the hydraulic conductivity gradually decreased over the first 5–10 freeze–thaw cycles. The hydraulic conductivity after 15 cycles was 0.4 to 0.7 times the hydraulic conductivity of a new GCL, which is similar to the decrease in hydraulic conductivity reported by Kraus et al. (1997) (0.55–0.66) for GCLs subjected to 20 freeze–thaw cycles with permeation by tap water between cycles. Kraus et al. (1997) attributed the reduction in hydraulic conductivity to "thaw consolidation," as described in Chamberlain and Gow (1979). However, in the current study, a systematic reduction in GCL thickness corresponding to thaw consolidation could not be identified from the data that were collected, precluding confirmation of thaw consolidation.

The hydraulic conductivity appears to increase slightly (~2.3×) between 15 and 20 cycles, which may be related to replacement of Na^{+} by Ca^{2+}. For example, Jo et al. (2004) show that GCLs permeated with dilute (20 mmol/L) $CaCl_2$ solutions exhibited very slow increases in hydraulic conductivity of similar magnitude concurrent with cation exchange. However, without additional data, a conclusion cannot be drawn regarding the mechanism causing the change in hydraulic conductivity or if additional changes would be realized after additional freeze–thaw cycles.

Longer-term testing is needed to determine if alterations in hydraulic conductivity would occur with a larger number of freeze–thaw cycles. However, if the replacement of Na^{+} by Ca^{2+} is associated primarily with Ca^{2+} from calcite dissolving within the bentonite, as the similarity in data for CW and DI water in Table 2 suggests, then appreciable changes in hydraulic conductivity are unlikely with greater freeze–thaw cycling. The hydraulic conductivity data from Podgorney and Bennett (2006) and Rowe et al. (2008), where GCLs were subjected to 100 freeze–thaw cycles, are consistent with this hypothesis. Calcite dissolution is common in GCLs during permeation (Bradshaw et al. 2013), and very likely occurred in the GCLs tested by Podgorney and Bennett (2006) and Rowe et al. (2008). Consequently, the GCLs tested by Podgorney and Bennett (2006) and Rowe et al. (2008) probably underwent as much exchange of Ca^{2+} for Na^{+} as observed in the current study, if not more, and yet increases in hydraulic conductivity did not occur over 100 freeze–thaw cycles.

Hydraulic conductivities of the GCLs permeated with CW are compared with hydraulic conductivities of GCLs permeated with DI water in Fig. 6. GCLs permeated with CW typically have slightly lower (1.3 times, on average) hydraulic conductivity than GCLs

Table 3. Hydraulic conductivities of GCL specimens hydrated on subgrades and cumulative pore volumes of flow (PVF) at end of testing of specimen.

		Hydraulic conductivity × 10^{-11} (m/s)		Cumulative pore volumes of flow[a]	
No. of freeze–thaw cycles	Intermittent or single permeation	DI water	Cover water	DI water	Cover water
0	Single	1.3–2.4[b]	1.7–2.4[b]	0.8	1.8
	Intermittent	2.0	1.7	—	—
1	Single	1.5	2.1	1.3	1.8
	Intermittent	1.6	1.1	—	—
3	Single	1.0	1.1	1.7	1.9
	Intermittent	1.4	1.0	—	—
5	Single	1.2	1.0	1.7	2.8
	Intermittent	1.2	0.8	—	—
15	Single	0.7	0.8	1.7	1.8
	Intermittent	1.2	0.9	—	—
20	Single	0.9	0.7	2.9	2.9
	Intermittent	1.3	1.0	3.0	2.8

Note: For GCL directly permeated with DI water and no freeze–thaw cycling, the hydraulic conductivity was 2.6 × 10^{-11} m/s and the PVF was 1.5. —, PVF not determined for test condition.

[a]PVF at end of test series.

[b]Range is from six replicate tests.

permeated with DI water. Hydraulic conductivities from the single permeation tests at 1, 3, and 15 cycles are exceptions. From a practical perspective, however, the difference in hydraulic conductivities obtained using DI water and CW is inconsequential. A paired t-test conducted at a significance level of 0.05 showed no statistical difference between the hydraulic conductivity to CW and DI water at each freeze–thaw increment.

Wet–dry versus freeze–thaw cycling

The findings in this study, and those in past studies by Kraus et al. (1997), Rowe et al. (2004, 2006, 2008), and Podgorney and Bennett (2006), indicate that freeze–thaw cycling of GCLs concurrent with cation exchange has a different impact on hydraulic conductivity than wet–dry cycling concurrent with cation exchange. Wet–dry cycling has been shown to induce large increases in hydraulic conductivity of GCLs in some cases (e.g., Meer and Benson 2007; Scalia and Benson 2011), whereas alterations in hydraulic conductivity attributed to freeze–thaw cycling tend to be small and inconsequential.

A key difference between the wet–dry and freeze–thaw processes is that wet–dry cycling induces cyclic dehydration and rehydration of the bentonite (Scalia and Benson 2011), whereas freeze–thaw induces phase change without dehydration. Scalia and Benson (2011) show that Na–bentonites transformed to Ca– or Mg–bentonite via cation exchange do not undergo osmotic swelling during rehydration. Consequently, the majority of the pore water is mobile and only a small fraction is bound and immobile, resulting in much higher hydraulic conductivity. In frozen bentonite, immobile water associated with the mineral surface undergoes phase change, but is retained within the bentonite. On thawing, this water most likely remains bound in the same manner that existed prior to freezing. This difference in the state of water within the bentonite likely is responsible for the very different impacts on hydraulic conductivity caused by wet–dry and freeze–thaw cycling.

The findings in this study are specific to the synthetic pore waters that were used for hydration and permeation. However, the synthetic pore waters had a greater preponderance of divalent cations than most pore waters encountered in the field (at least in North America), a condition that promotes replacement of Na by Ca or Mg. Thus, similar behavior should be expected for GCLs placed on subgrades or overlain by cover soil containing pore water with less abundance of divalent or polyvalent cations.

Fig. 6. Hydraulic conductivity of GCLs to CW compared with GCLs permeated with DI water for the same number of freeze–thaw cycles.

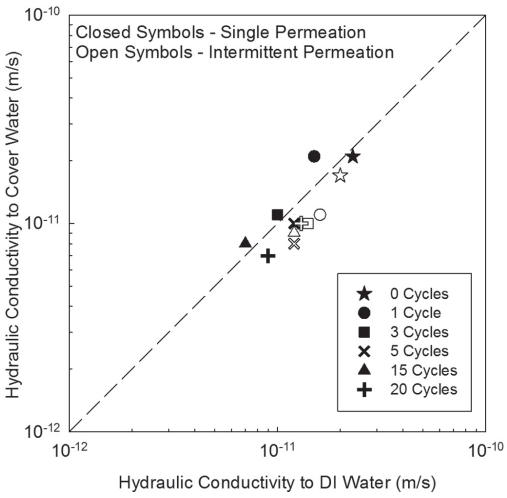

Summary and conclusions

Laboratory experiments were conducted to determine if freeze–thaw cycling affects the hydraulic conductivity of a GCL under conditions where cation exchange can occur during subgrade hydration, freezing and thawing, and permeation. The experiments were conducted to simulate conditions for a GCL buried in a cover deployed on a tailings disposal facility in the far northern area of North America at a depth that would impose one freeze–thaw cycle annually over a 20 year period. GCL specimens were prehydrated by contact with a moist subgrade containing synthetic subgrade pore water and then permeated with liquid representing the pore water in the overlying cover soil. Control tests were also conducted with DI water. GCL specimens were subjected to freeze–thaw cycles, with permeation conducted once (after 1, 3, 5,

15 or 20 cycles, "single permeation" tests) or after every freeze–thaw increment ("intermittent permeation" tests). Cation concentrations in the exchange complex were determined for freeze–thaw increments for single permeation and after 20 cycles for intermittent permeation.

Based on the findings of this study, the following observations and conclusions are made:

- Replacement of Na^+ by Ca^{2+} was not observed for up to 5 cycles, but was evident at 15 freeze–thaw cycles and was even greater at 20 cycles.
- GCLs exposed to as many as 20 freeze–thaw cycles have lower hydraulic conductivity than GCLs not exposed to freeze–thaw cycling, even when exposed to cation exchange during subgrade hydration and permeation. This change in hydraulic conductivity is similar to the changes reported by others from tests conducted without systematic means to induce cation exchange (e.g., during subgrade hydration or from the permeant solution).
- Small increases in hydraulic conductivity were observed between 15 and 20 freeze–thaw cycles, but insufficient data are available to determine the significance of the trend or the mechanism causing change. However, even at 20 cycles, hydraulic conductivity of the GCLs exposed to freezing and thawing and permeated with DI water or cover water was lower than the hydraulic conductivity of a GCL permeated directly with deionized water.
- GCLs permeated with DI water and cover pore water experienced similar replacement of Na^+ by Ca^{2+} at 15 and 20 freeze–thaw cycles. Dissolution of calcite within the bentonite, rather than permeation, is the likely source of Ca^{2+} causing exchange.

Acknowledgements

CETCO Inc. and the US Department of Energy (DOE) provided financial support for this study. Funding from DOE was provided under cooperative agreement DE-FC01-06EW07053 entitled "Consortium for risk evaluation with stakeholder participation III." Gregory Makusa was supported by Luleå University of Technology (Sweden) through an exchange program between Luleå University of Technology and the University of Wisconsin–Madison. The opinions, findings, conclusions or recommendations expressed herein are those of the authors and do not necessarily represent the views of CETCO, Luleå University of Technology or the DOE.

References

Albrecht, B.A., and Benson, C.H. 2001. Effect of desiccation on compacted natural clays. Journal of Geotechnical and Geoenvironmental Engineering, **127**(1): 67–75. doi:10.1061/(ASCE)1090-0241(2001)127:1(67).

ASTM. 2010*a*. Standard test method for measuring the exchangeable complex and cation exchange capacity of inorganic fine-grained soils. ASTM standard D7503. American Society for Testing and Materials, West Conshohocken, Pa.

ASTM. 2010*b*. Standard test methods for measurement of hydraulic conductivity of saturated porous materials using a flexible wall permeameter. ASTM standard D5084. ASTM International, West Conshohocken, Pa.

ASTM. 2011. Standard specification for reagent water. ASTM standard D1193. American Society for Testing and Materials, West Conshohocken, Pa.

ASTM. 2013. Standard test method for determining the effect of freeze-thaw on hydraulic conductivity of compacted or intact soil specimens using a flexible wall permeameter. ASTM standard D6035. American Society for Testing and Materials, West Conshohocken, Pa.

Benson, C., and Meer, S. 2009. Relative abundance of monovalent and divalent cations and the impact of desiccation on geosynthetic clay liners. Journal of Geotechnical and Geoenvironmental Engineering, **135**(3): 349–358. doi:10.1061/(ASCE)1090-0241(2009)135:3(349).

Benson, C.H., and Othman, M.A. 1993. Hydraulic conductivity of compacted clay frozen and thawed in situ. Journal of Geotechnical Engineering, **119**(2): 276–294. doi:10.1061/(ASCE)0733-9410(1993)119:2(276).

Benson, C.H., Thorstad, P.A., Jo, H., and Rock, S.A. 2007. Hydraulic performance of geosynthetic clay liners in a landfill final cover. Journal of Geotechnical and Geoenvironmental Engineering, **133**(7): 814–827. doi:10.1061/(ASCE)1090-0241(2007)133:7(814).

Bradshaw, S.L., Benson, C.H., and Scalia, J.S. 2013. Hydration and cation exchange during subgrade hydration and effect on hydraulic conductivity of geosynthetic clay liners. Journal of Geotechnical and Geoenvironmental Engineering, **139**(4): 526–538. doi:10.1061/(ASCE)GT.1943-5606.0000793.

Chamberlain, E.J., and Gow, A.J. 1979. Effect of freezing and thawing on the permeability and structure of soils. Engineering Geology, **13**(1–4): 73–92. doi:10.1016/0013-7952(79)90022-X.

Chapuis, R.P. 1990. Sand-bentonite liners: predicting permeability from laboratory tests. Canadian Geotechnical Journal, **27**(1): 47–57. doi:10.1139/t90-005.

Egloffstein, T. 2002. Bentonite as sealing material in geosynthetic clay liners – influence of electrolytic concentration, the ion exchange and ion exchange with simultaneous partial desiccation on permeability. *In* Clay geosynthetic barriers. Swets & Zeitlinger, Lisse. pp. 141–153.

Guyonnet, D., Gaucher, E., Gaboriau, H., Pons, C.-H., Clinard, C., Norotte, V., and Didier, G. 2005. Geosynthetic clay liner interaction with leachate: correlation between permeability, microstructure, and surface chemistry. Journal of Geotechnical and Geoenvironmental Engineering, **131**(6): 740–749. doi:10.1061/(ASCE)1090-0241(2005)131:6(740).

Hewitt, R.D., and Daniel, D.E. 1997. Hydraulic conductivity of geosynthetic clay liners after freeze-thaw. Journal of Geotechnical and Geoenvironmental Engineering, **123**(4): 305–313. doi:10.1061/(ASCE)1090-0241(1997)123:4(305).

Hosney, M.S., and Rowe, R.K. 2013. Changes in geosynthetic clay liner (GCL) properties after 2 years in a cover over arsenic-rich tailings. Canadian Geotechnical Journal, **50**(3): 326–342. doi:10.1139/cgj-2012-0367.

James, A.N., Fullerton, D., and Drake, R. 1997. Field performance of GCL under ion exchange conditions. Journal of Geotechnical and Geoenvironmental Engineering, **123**(10): 897–901. doi:10.1061/(ASCE)1090-0241(1997)123:10(897).

Jo, H.Y., Katsumi, T., Benson, C.H., and Edil, T.B. 2001. Hydraulic conductivity and swelling of nonprehydrated GCLs permeated with single species salt solutions. Journal of Geotechnical and Geoenvironmental Engineering, **127**(7): 557–567. doi:10.1061/(ASCE)1090-0241(2001)127:7(557).

Jo, H.Y., Benson, C.H., and Edil, T.B. 2004. Hydraulic conductivity and cation exchange in non-prehydrated and prehydrated bentonite permeated with weak inorganic salt solutions. Clays and Clay Minerals, **52**(6): 661–679. doi:10.1346/CCMN.2004.0520601.

Kim, W.-H., and Daniel, D.E. 1992. Effects of freezing on hydraulic conductivity of compacted clay. Journal of Geotechnical Engineering, **118**(7): 1083–1097. doi:10.1061/(ASCE)0733-9410(1992)118:7(1083).

Kolstad, D.C., Benson, C.H., and Edil, T.B. 2004. Hydraulic conductivity and swell of nonprehydrated geosynthetic clay liners permeated with multispecies inorganic solutions. Journal of Geotechnical and Geoenvironmental Engineering, **130**(12): 1236–1249. doi:10.1061/(ASCE)1090-0241(2004)130:12(1236).

Kraus, J.F., Benson, C.H., Erickson, A.E., and Chamberlain, E.J. 1997. Freeze-thaw cycling and hydraulic conductivity of bentonitic barriers. Journal of Geotechnical and Geoenvironmental Engineering, **123**(3): 229–238. doi:10.1061/(ASCE)1090-0241(1997)123:3(229).

Lin, L., and Benson, C.H. 2000. Effect of wet-dry cycling on swelling and hydraulic conductivity of GCLs. Journal of Geotechnical and Geoenvironmental Engineering, **126**(1): 40–49. doi:10.1061/(ASCE)1090-0241(2000)126:1(40).

Meer, S.R., and Benson, C.H. 2007. Hydraulic conductivity of geosynthetic clay liners exhumed from landfill final covers. Journal of Geotechnical and Geoenvironmental Engineering, **133**(5): 550–563. doi:10.1061/(ASCE)1090-0241(2007)133:5(550).

Melchior, S. 2002. Field studies and excavations of geosynthetic clay barriers in landfill covers. *In* Clay geosynthetic barriers. *Edited by* H. Zanzinger, R. Koerner, and E. Gartung. Swets and Zeitlinger, Lisse, the Netherlands. pp. 321–330.

Mitchell, J.K., and Soga, K. 2005. Fundamentals of soil behavior. 3rd ed. John Wiley and Sons, Inc., New York.

Moore, D.M., and Reynolds, R.C., Jr. 1989. X-ray diffraction and the identification of clay minerals. Oxford University Press, New York.

Othman, M., Benson, C., Chamberlain, E., and Zimmie, T. 1994. Laboratory testing to evaluate changes in hydraulic conductivity caused by freeze-thaw: state-of-the-art, hydraulic conductivity and waste containment transport in soils. *Edited by* S. Trautwein and D. Daniel. STP 1142. ASTM. pp. 227–254.

Podgorney, R.K., and Bennett, J.E. 2006. Evaluating the long-term performance of geosynthetic clay liners exposed to freeze-thaw. Journal of Geotechnical and Geoenvironmental Engineering, **132**(2): 265–268. doi:10.1061/(ASCE)1090-0241(2006)132:2(265).

Rauen, T.L. 2007. Effect of leachate from bioreactor and recirculation landfills on the hydraulic conductivity of geosynthetic clay liners. M.Sc. thesis, University of Wisconsin, Madison, Wisc.

Rauen, T.L., and Benson, C.H. 2008. Hydraulic conductivity of a geosynthetic clay liner permeated with leachate from a landfill with leachate recirculation. *In* Proceedings of GeoAmericas 2008, International Geosynthetics Society. [CD-ROM].

Rowe, R., Mukunoki, T., Li, M., and Bathurst, R. 2004. Effect of freeze-thaw on the permeation of arctic diesel through a GCL. Journal of ASTM International, **1**(2). doi:10.1520/JAI11741.

Rowe, R.K., Mukunoki, T., and Bathurst, R.J. 2006. Compatibility with Jet A-1 of a GCL subjected to freeze–thaw cycles. Journal of Geotechnical and Geoenvironmental Engineering, **132**(12): 1526–1536. doi:10.1061/(ASCE)1090-0241(2006)132:12(1526).

Rowe, R.K., Mukunoki, T., and Bathurst, R.J. 2008. Hydraulic conductivity to

Jet-A1 of GCLs after up to 100 freeze–thaw cycles. Géotechnique, **58**(6): 503–511. doi:10.1680/geot.2008.58.6.503.

Scalia, J., and Benson, C.H. 2010. Effect of permeant water on the hydraulic conductivity of exhumed GCLs. Geotechnical Testing Journal, **33**(3): 1–11. doi:10.1520/GTJ102609.

Scalia, J., and Benson, C.H. 2011. Hydraulic conductivity of geosynthetic clay liners exhumed from landfill final covers with composite barriers. Journal of Geotechnical and Geoenvironmental Engineering, **137**(1): 1–13. doi:10.1061/(ASCE)GT.1943-5606.0000407.

Shackelford, C.D., Benson, C.H., Katsumi, T., Edil, T.B., and Lin, L. 2000. Evaluating the hydraulic conductivity of GCLs permeated with non-standard liquids. Geotextiles and Geomembranes, **18**(2–4): 133–161. doi:10.1016/S0266-1144(99)00024-2.

Sposito, G. 1981. The thermodynamics of soil solutions. Oxford University Press, New York.

USEPA. 1996. Inductively coupled plasma-atomic emission spectrometry. USEPA test method 6010B. U.S. Environmental Protection Agency.

Zimmie, T., and LaPlante, C. 1990. The effect of freeze/thaw on the permeabiltiy of a fine-grained soil. *In* Proceedings of the 22nd Mid-Atlantic Industrial Waste Conference, Philadelphia, Pa.

Paper VI

Makusa, G.P., Mattsson, H., and Knusson, S. (2012). Verification of field settlement of in-situ stabilized dredged sediments using CPT data. *Electronic Journal of Geotechnical Engineering. Vol. 17/Y, 3665-3680*

EJGE

Verification of Field Settlement of In-situ Stabilized Dredged Sediments Using Cone Penetration Test Data

Gregory Paul Makusa

PhD Student
Department of Civil, Environmental and Natural resources engineering, Luleå University of Technology, Tel: +46 920 491688, SE – 971 87, Luleå, Sweden
e-mail: gregory.makusa@ltu.se

Hans Mattsson

Assistant Professor
Department of Civil, Environmental and Natural resources engineering, Luleå University of Technology, Tel: +46 920 492147, SE – 971 87, Luleå, Sweden
e-mail: hans.mattsson@ltu.se

Sven Knutsson

Professor
Department of Civil, Environmental and Natural resources engineering, Luleå University of Technology, Tel: +46 920 491332, SE – 971 87, Luleå, Sweden
e-mail: sven.knutsson@ltu.se

ABSTRACT

Utilization of in-situ mass stabilization for geotechnical applications is increasing. Laboratory tests may have drawbacks on valuations of engineering parameters for estimations of settlement of in-situ stabilized soil mass. Factors such as compression, mixing work, homogeneity and curing temperature may influence the differences in mechanical properties between laboratory test results and achieved field values. Therefore, utilization of appropriate in-situ mechanical parameters may be required during design analyses. Various in-situ tests are available for use in geotechnical context. Among others, cone penetration test (CPT) is one of most widely used in-situ tests. Numerous CPT empirical correlations are available for use in conventional soils. Utilization of such CPT empirical correlations for in-situ stabilized soils has to be examined. In this paper, the in-situ constrained modulus was evaluated using conventional CPT empirical correlation and utilized as oedometer modulus in finite element analysis for estimation of settlement of preloaded in-situ stabilized dredged sediments. The results show that, computed settlement values fall within the range of measured one. These findings suggest that, the cone penetration test and its empirical correlations, which were established for conventional soils, can also be utilized in stabilized soils.

KEYWORDS: field settlement, cone penetration test, in-situ constrained modulus, finite element method, PLAXIS, in-situ stabilization, contaminated dredged sediments, preloading

INTRODUCTION

Millions cubic meters of sediments will be dredged in Baltic Sea in the near future. About 4,000,000 cubic meters of sediments will be dredged at the Port of Gävle alone during Port expansion project. It is estimated that out of these 4,000,000, about 1,000,000 cubic meter is highly contaminated (Fossenstrand, 2009; SMOCS, 2010). Handling of these harmful sediments requires proper attention for sustainable development. In Sweden, Sea disposal of contaminated dredged sediments is banned. The Swedish environmental protection agency states, "Wastes are forbidden to be dumped at the Sea. Waiver is given where waste can be dumped without detrimental effects to human health and environment" (Swedish EPA, 2001). Therefore, sustainable management of contaminated dredged materials is motivated to beneficial reuse. The management of Port of Gävle identified stabilized contaminated dredged materials (SCDM) as alternative material to natural construction materials for structural backfill. Consequently, the Port of Gävle decided to consider the utilization of the SCDM as a base for new land, thus, reducing the use of natural resources and saving money compared to other handling alternatives of the contaminated dredged sediments (SMOCS, 2010). Nevertheless, the use of in-situ stabilized contaminated dredged sediments in geotechnical applications requires strong justification with regard to the achieved in-situ stiffness and strength parameters. Accordingly, it is common practice to carry out advance tests in the laboratory to obtain adequate information on stiffness and strength behavior of stabilized material before full-scale project can take over. Even so, in-situ stabilization of large volumes of soil mass may result into different stiffness and strength in contrary to presumed laboratory test results. According to Åhnberg *et al.* (2001), a number of factors such as compression, mixing work, homogeneity, curing temperature and stress situation may influence the differences in mechanical properties between laboratory test results and attained field values and that, the laboratory test results has to be utilized as a base for field operations. It follows that; appropriate in-situ soil mechanical parameters have to be utilized during geotechnical design. In-situ soil tests are of primary interest to geotechnical engineers compared to laboratory tests. The in-situ soil tests provide quick information on the behavior of soil at a particular site. Numerous in-situ soil tests are available, among others; the cone penetration test (CPT) is one of the most widely used in-situ soil tests. The CPT has many advantages over laboratory tests, some of those are:

- Insight soil stratigraphy is obtained.
- Conservative idealization of particular site into homogenous soil is avoided.
- The test is easier to conduct at minimum supervision and workmanship error.
- Instantaneously engineering parameters are obtained.

Several CPT empirical correlations, which were established for conventional soils are available for use. However, not much research has been done to verify if the CPT correlation developed for conventional soils are also applicable to the stabilized soil mass. The aim of this paper is to verify the measured field settlement by finite element analysis (FEA). The FEA utilizes the oedometer modulus, which is evaluated as in-situ constrained modulus using CPT empirical correlations. The CPTs data and measured field settlement values were taken from the large-scale field test at the Port of Gävle in Sweden.

PORT OF GÄVLE

The Port of Gävle, owned by the Municipality of Gävle is one of the ten biggest import and export harbors in Sweden. The Port lies in the inlet of the Gulf of Bothnia, about 200 km north of Stockholm (Figure 1). According to the Swedish meteorological and hydrological institute

(http://www.smhi.se/en), Gävle has a similar climate as the rest of central part of Sweden with an average air temperature of -5°C in January and +17°C in July. Thousands of ships call at this Port every year exporting and importing various products to and from northern and central parts of Sweden. Examples of products are coffee, steel, timber and oil. The Port is currently in a phase of expansion to increase its cargo handling capacity by 40%. The increase will boost the Port handling capacity from the current 5 million tons to over 7 million tons per year (Fossenstrand, 2009, SMOCS, 2010). The project phases include dredging of sediments in order to deepen and widen the entrance channel, construction of new environmental quays and expansion of existing container terminals. Ports and harbors are identified as 'hot spots' for contaminated sediments. Because of environmental restrictions, the contaminated dredged sediments at the Port of Gävle will be amended by a stabilization solidification technology. The amended materials will be utilized as structural backfill in acquiring new land from the Baltic Sea. Investigations on strength-deformation characteristics of the stabilized dredged sediments were carried out in laboratory to found out the desired design recipe for structural backfill. A large-scale field test was carried out at Granudden terminal (Figure 1) to verify laboratory test results for in-situ stabilized dredged sediments.

LARGE SCALE FIELD TEST

The stiffness and strength parameters measured in laboratory may differ from the one achieved in the field, not only because of compression due to preloading but also due to curing temperature and stress distribution. Therefore, laboratory tests can only be used as a base for assessments of appropriate type of binder and the mixing ratio (Åhnberg et al, 2001). Thus, in order to find out the in-situ strength-deformation characteristics of the SCDM fill, a large-scale field test was carried out. A basin of 30 m x 30 m was obtained from the Baltic Sea at Granudden terminal. The basin comprised of natural ground to the south, a quay wall to the west side, sheet pile wall to the north side (Baltic Sea side) and to the east is a separation wall of plastic curtail (Figure 5). Freshly contaminated dredged sediments at average water content of 450% were mixed with binders using the on-site pugmill. The mix proportional of 180 kg of binders (cement: 35%, fly ash: 35% and Merit®5000: 30% by weight) per cubic meter of freshly dredged sediments were applied. The mix was then discharged under water in the reclaimed area (Figure 2). From the laboratory test results, it was predetermined that, a minimum unconfined compressive strength (UCS) of 140 kPa and a permeability of less than 10^{-9} m/s would be achieved within 91 days (d) of curing (Fossenstrand, 2009).

Backfilling of the reclaimed area began on October 29, 2010 and continued through January 23, 2011, when the final layer of the SCDM was placed in the reclaimed area. The total SCDM of about 9,000 cubic meters were utilized in the large-scale field test. The curing period was counted from the last day of backfill (i.e. January 23, 2011); the slurry form of SCDM fill prevented an immediate application of preloading weight. Thus, the application of first phase of preloading weight was done on February 6, 2011. The settlement monitoring systems on the surface of SCDM fill and environmental monitoring mechanism such as borehole for collection of leachate were instrumented prior to preloading. The fill area was preloaded with selected gravel material (Figure 3). The first phase of preloading involved the application of 18 kPa, followed by additional load of 37 kPa after 30 days of curing under the first phase of preloading weight. The field settlements of SCDM were continuously recorded at F1, F2, F3 and F4 starting from February 6, 2011 (Figure 3 and Figure 5). Figure 4 presents measured field settlements from February 6, 2011 to June 1, 2011 in time scale. No significant additional settlements were recorded after this period, for the two phases of preloading. CPTs were done at different locations

within the field after 28d (P1, P2, P3, P4, P5 and P6), 91d (P11-01, P11-02, P21-01 and P21-02) and 150d (P11-03, P11-04, P21-03 and P21-04) of curing. Detailed CPT locations are shown in Figure 5.

Figure 1: Geographical location of the Gävle Municipality, Port of Gävle and Granudden terminal (Photo: Courtesy of Port of Gävle; map: http://www.umsl.edu/services/govdocs/wofact2001/geos/sw.html)

Figure 2: On-site pugmill mixing freshly dredged materials with binders (right); the mix was discharged underwater into a reclaimed area (left) (Photo: Courtesy of Port of Gävle)

Figure 3: Monitoring instruments and preloading layer of selected gravel on finished SCDM fill (Photo: Courtesy of Port of Gävle)

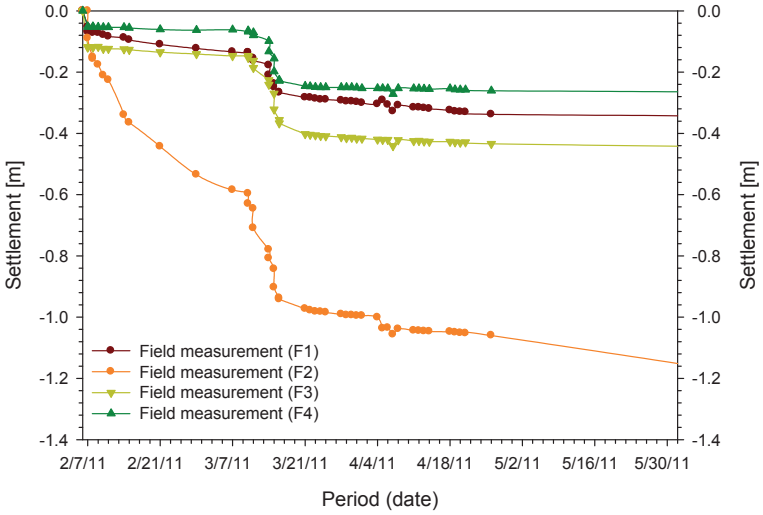

Figure 4: Progressive settlement measurement (Data: Courtesy of Göran Holm at SGI, WSP and PEAB)

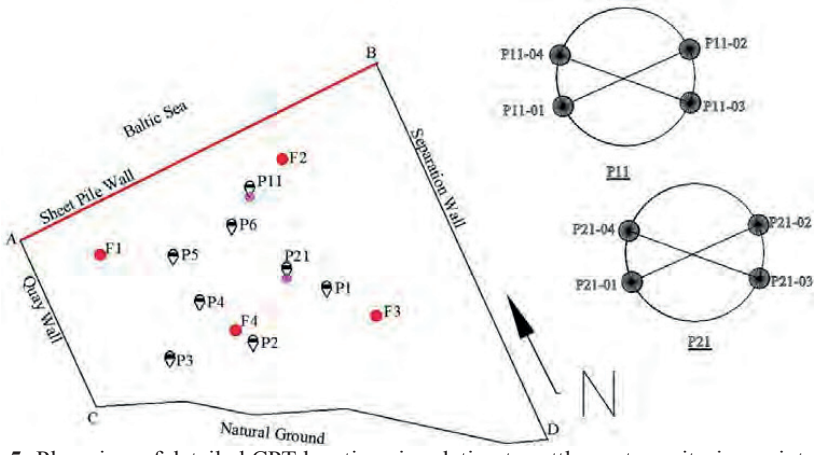

Figure 5: Plan view of detailed CPT locations in relation to settlement monitoring points (Data: Courtesy of WSP and PEAB)

SETTLEMENT ANALYSIS

The verification of field settlements involved simulation of field backfill operations in the finite element method (FEM). The finite element software 'PLAXIS 2D' (Brinkgreve *et al.*, 2010) was utilized in one-dimensional consolidation settlement analyses for the SCDM fill. During the computations, plane strain conditions were assumed and 15 nodes triangular elements were used in a fine mesh with refined SCDM clusters, which gave enough accuracy in reasonable time. The analyses utilized the Mohr-Coulomb (MC) material model under undrained condition case (B) (Brinkgreve *et al.*, 2010). This constitutive model assumes the material isotropic, homogeneous and elastic perfectly plastic, obeying the MC failure criteria. The MC model requires two stiffness parameters and one strength parameter. The primary stiffness parameters include; effective Young's modulus, E' and effective Poisson's ratio, ν' while, the secondary (alternative) stiffness parameters include oedometer modulus, E_{oed} and shear modulus, G. These stiffness parameters relates to each other by

$$E_{oed} = \frac{E'(1-\nu')}{(1+\nu')(1-2\nu')} \tag{1}$$

$$G = \frac{E'}{2(1+\nu')} = \frac{E_u}{2(1+\nu_u)} \tag{2}$$

where E_u and ν_u are the undrained Young's modulus and Poisson's ratio respectively. The shear modulus is independent of drainage conditions (i.e. the undrained shear modulus is equal to the effective shear modulus) and therefore, the effective and undrained Young's moduli are not the same (Muir Wood, 1990). The undrained Poisson's ratio for saturated clay soil normally ranges between 0.4 and 0.5 (Chua and Tenison, 2003; Muir Wood, 1990). The SCDM fill layers utilized the value of ν_u of 0.4 for all layers and all CPT points. PLAXIS also recommends this value of ν_u in MC model under undrained condition case (B). For the SCDM layers the undrained shear

strength was utilized as the only strength parameter in MC model under undrained condition case (B).

In-situ constrained modulus

In terms of CPT data, the relationship between the in-situ constrained modulus and measured CPT quantities has been empirically established (Robertson, 2009; Larsson and Mulabdic, 1991; Lunne *et al.*, 1997). The correlation is presented as

$$M = \alpha_M (q_t - \sigma_{v0}) \tag{3}$$

where q_t is the corrected cone resistance, σ_{v0} is the total vertical stress and α_M is the constrained modulus cone factor. Robertson (2009) suggested the following correlations for selection of the constrained modulus cone factor

If $I_c \geq 2$

$$\alpha_M = Q_{t1} \qquad when\ Q_{t1} \leq 14 \tag{4}$$

$$\alpha_M = 14 \qquad when\ Q_{t1} > 14 \tag{5}$$

If $I_c < 2$

$$\alpha_M = 0.03\left(10^{0.55 I_c + 1.68}\right) \tag{6}$$

where Q_{t1} is the normalized cone resistance for clay soil and I_c is the soil behavior type index. The normalized cone resistance, Q_{t1} for clay is given by

$$Q_{t1} = \left(\frac{q_t - \sigma_{v0}}{\sigma'_{v0}} \right) \tag{7}$$

where σ'_{v0} is the effective vertical stress whereas the soil behavior type index, I_c can be calculated from

$$I_c = \left[(3.47 - \log Q_{t1})^2 + (\log F_r + 1.22)^2 \right]^{0.5} \tag{8}$$

where F_r is the normalized friction ratio. The calculated I_c of the SCDM from the Port of Gävle had values between 2.8 and 4.7, with an average value of 3.6. These values classify the SCDM from Port of Gävle as normally consolidated soil in accordance with Robertson (2009) chart.

Undrained shear strength

The in-situ undrained shear strength, S_u can be estimated from CPT data (Robertson, 2009; Robertson *et al.*, 1986; Abu-Farsakh *et al.*, 2003; Houlsby and Teh, 1991, Kulhway and Mayne, 1990) by the following correlation

$$S_u = \frac{q_t - \sigma_{v0}}{N_k} \tag{9}$$

where N_k is the cone tip factor. Lunne *et al.* (1986) reported the N_k values for Scandinavian clays in the range of 15 to 21. Robertson (2009) suggested the average N_k value of 14 for insensitive fine-grained soils. The SCDM from the Port of Gävle had an average sensitivity value of 1, which according to Robertson (2009) can be regarded as insensitive NC clay. Thus, the N_k value of 14 was adopted in equation (9) for the SCDM fill from Port of Gävle.

Computations

The evaluated input parameters of the SCDM fill showed significant variations in stiffness and strength parameters along the entire depth and across the field. Thus, depending on the observed variations in measured CPT quantities, the SCDM fill was subdivided into layers of thickness between 0.23 and 0.30 m. These thicknesses were considered in close interval with CPT sampling and sufficient to capture the variations of stiffness along the entire depth. **Table 1** presents an example of the input parameters E_{oed} and S_u for SCDM fill layers based on CPT data at point P3 only. All layers at this CPT point were assigned an average unit weight of 13.85 kN/m^3 and the hydraulic conductivity of 5.5 x 10^{-7} m/s in vertical direction.

PLAXIS input parameters in MC model involved the use of secondary stiffness parameters, where oedometer modulus evaluated as in-situ constrained modulus in equation (3) and an assumed undrained Poisson's ratio of 0.4 were utilized. The plastic calculation type was used during layer placement and preloading. After completion of backfill operations, preloading weight was placed and all initial displacements were reset to zero. This was done in order to mimic field operation, where recording of the field settlements stated after preloading the SCDM fill. Since it is customary to preload the stabilized mass in phases, PLAXIS consolidation analyses for the SCDM fill were carried out in two phases of preloading.

In the first phase, the SCDM fill was preloaded with 18 kPa. However, due to partial submergence into the ground water of the placed gravels, which resulted into reduced effective vertical stress, the average effective preloading weight of 10 kPa was utilized during simulations. Consolidation analyses followed for the period of 30 days.

The second phase of preloading started after 30 days, with an application of an average additional effective load of 37 kPa, followed by consolidation analysis to minimum excess pore pressure (EPP). Note that, due to differences in maximum depths of the SCDM fill (**Table 2**), the consolidation period to minimum EPP varied between CPT points. Simulations of the field settlements involved the use of stiffness evaluated after 28, 91 and 150 days of curing. For simplicity in PLAXIS 2D simulations, the evaluated stiffness and strength parameters were assumed to be homogenous across the CPT section of the SCDM fill; therefore, the SCDM fill were modeled with maximum depth of the fill at a particular CPT point.

An example of computation is presented for CPT data from point P3 for which the curing time was 28d. Figure 6 presents the numerical model showing boundary conditions. The Anchor rod shown is for illustration purpose only; the length of the anchor rod is equal to the width of the model in the actual simulations. Figure 7 displays one-dimensional deformed mesh at the end of consolidation and, Figure 8 shows the maximum vertical deformation of 0.20 m of the SCDM fill for a settlement analysis performed on the section at CPT point P3. Similar computations were carried out for the other CPT points.

Table 1: Input parameters for PLAXIS simulation of SCDM fill at CPT point P3

Layer ID	1	2	3	4	5	6	7	8	9	10	11	12	13	14
E_{oed} (kN/m^2)	849	2387	1083	1189	2924	1493	4376	6603	2728	1545	1250	383	589	407
S_u (kN/m^2)	16	27	18	19	29	21	35	43	27	20	18	10	12	10

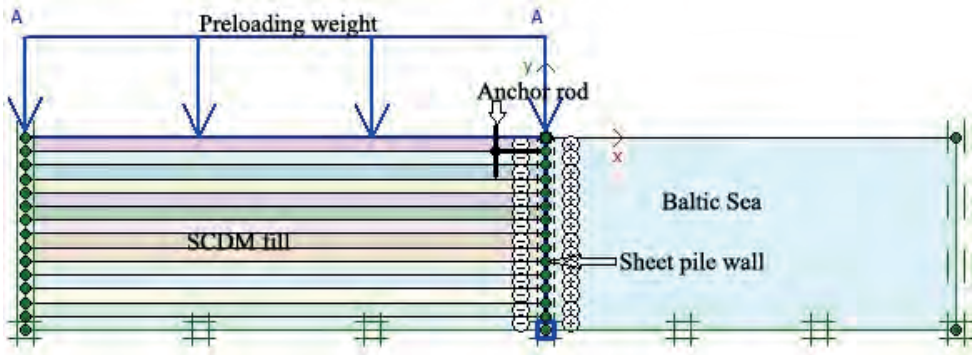

Figure 6: Section model showing boundary conditions for the SCDM fill (based on the CPT data at P3)

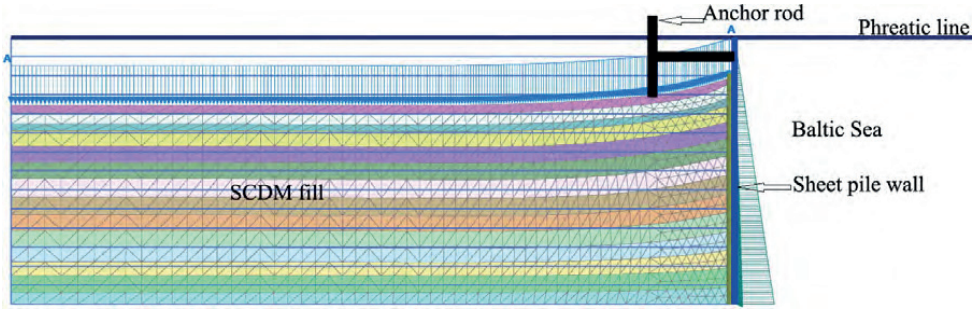

Figure 7: Section model showing exaggerated (scaled up five times) deformed mesh at the end of consolidation of the SCDM fill (based on the CPT data at P3)

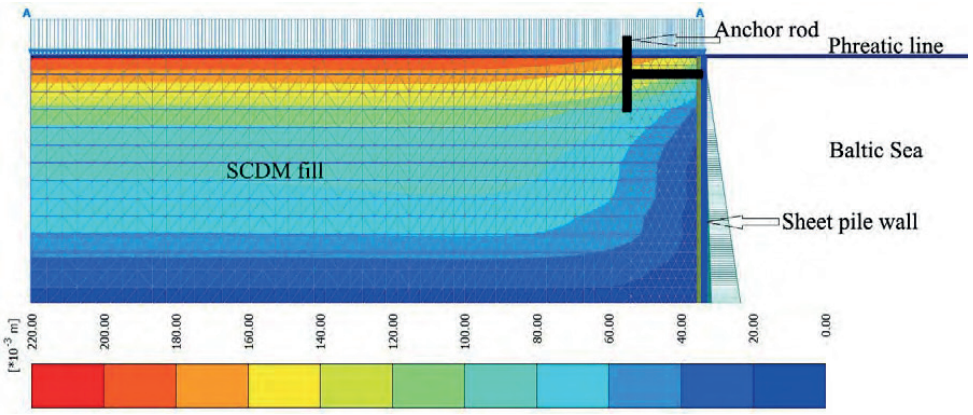

Figure 8: Section model showing the maximum vertical deformation of 0.21 m in the SCDM fill (Based on CPT data at P3)

RESULTS

Verification against field settlement

Figure 4 presents the measured field settlement values from Port of Gävle in time scale. In order to validate the applicability of the evaluated oedometer modulus for estimation of settlement, the computed settlement values were compared with measured settlement values by cumulative settlement curves (Figure 9 to Figure 12). Note that, due to the lack of CPT repetitive data, spread of CPT points and variations in depths of the SCDM fill (**Table 2**), comparisons of the measured settlement values against computed settlement values were not restricted to the CPT points, which were located nearby the monitoring points. Thus, the comparisons aimed at finding out the evaluated stiffness and curing period corresponding to the field stiffness, which resulted into the measured settlement values during the two phases of preloading. Results show that, measured settlement values at F1 corresponded well with computed settlement values from CPT point P21-03 during the first phase and CPT points P1 and P11-01 during the second phase of preloading (Figure 9). The measured settlement values at F2 correlated with the computed settlement values from CPT point P21-01 (Figure 10). The measured settlement values at F3 matched quite well with computed settlement values from CPT points P1 and P11-01 during the first phase and CPT points P4 and P11-02 during the second phase of preloading (Figure 11). While, the measured settlement values at F4 showed comparable correlations with the computed settlement values from CPT point P5 during the first phase, and CPT points P2 and P21-03 during the second phase of preloading (Figure 12).

Table 2: The magnitude of computed final settlement values for all CPT data

CPT Point	Maximum Depth (m)	Curing period (days, d)	Settlement (v_u = 0.4) (m)
P1	7.25	28	-0.35
P2	6.09	28	-0.24
P3	4.06	28	-0.20
P4	8.12	28	-0.42
P5	8.70	28	-0.12
P6	8.12	28	-0.88
P11-01	6.44	91	-0.33
P11-02	6.21	91	-0.43
P11-03	6.44	150	-0.45
P11-04	6.90	150	-0.32
P21-01	6.44	91	-1.09
P21-02	7.72	91	-1.64
P21-03	7.25	150	-0.25
P21-04	7.44	150	-0.88

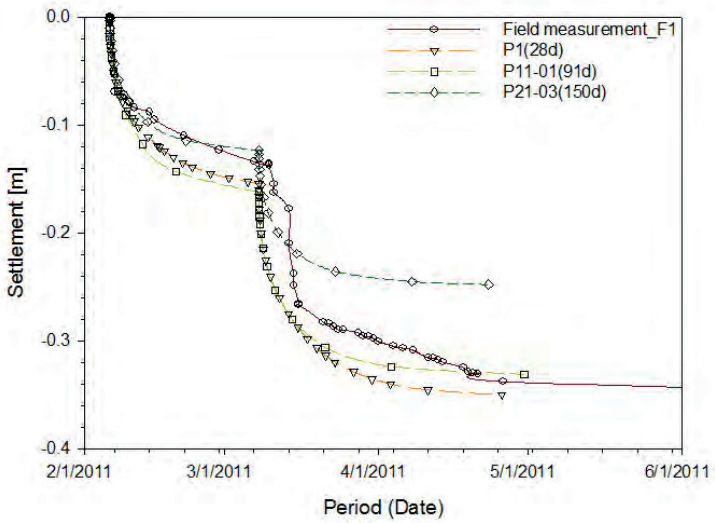

Figure 9: Comparison between measured values at F1 and computed settlement values from CPT point P1 (28d), P11-01 (91d) and P21-03 (150d) versus time

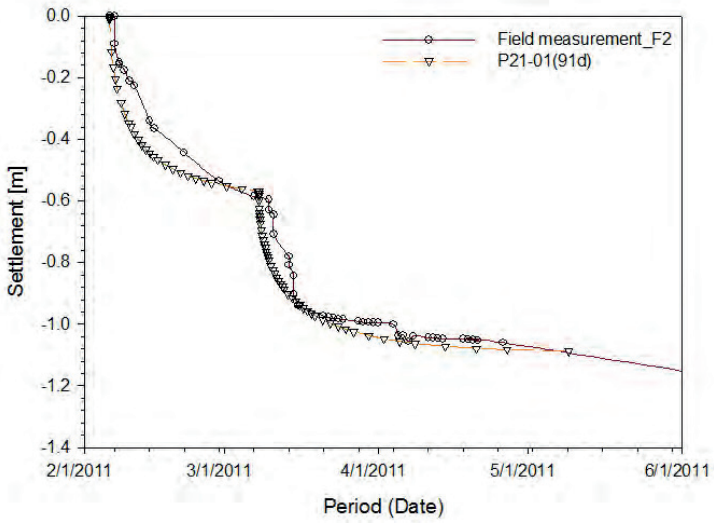

Figure 10: Comparison between measured values at F2 and computed settlement values from CPT point P21-01 (91d) versus time

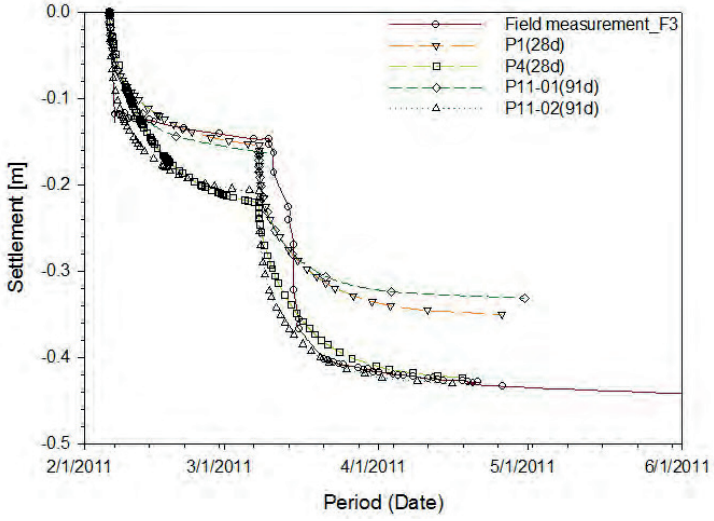

Figure 11: Comparison between measured values at F3 and computed settlement values from CPT point P1 (28d), P4 (28d), P11-01 (91d) and P11-02 (91d) versus time

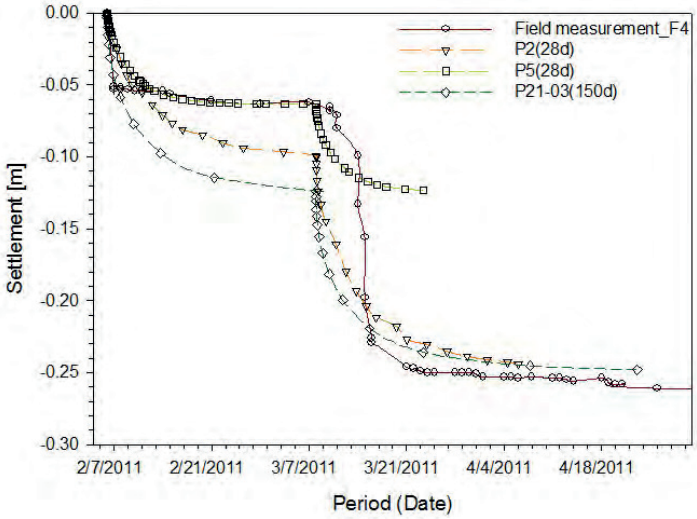

Figure 12: Comparison between measured values at F4 and computed settlement values from CPT point P2 (28d), P5 (28d) and P21-03 (150d) versus time

DISCUSSION

The field settlements of stabilized dredged material due to preloading weight were analyzed using finite element software, PLAXIS 2D. The computed settlement values suggests that, most of measured settlement values were due to stiffness evaluated following 28 days of curing under the first phase or second phase of preloading weight. With exception to Figure 10, computed settlement utilizing the SCDM stiffness obtained after 91 or 150 days of curing resulted into decreased or same magnitudes of settlement as computed magnitudes of settlement using the SCDM stiffness evaluated following 28 days of curing. Both field and computed settlement showed inconsistency and variations in magnitudes of settlement within the same field under the same preloading weight. These variations suggest that, the SCDM fill exhibited different stiffness and strength parameters within a short distance across the field and along the entire depth of the fill. The authors postulate uneven distribution of preloading weight and curing air temperature as contributing factors for the absence of CPT repetitive data and discrepancies in both measured and computed settlement values.

Effect of preloading weight

Preloading weight applied on stabilized soils helps to remove air pockets and bring soil particles closer together for effective hydration reaction, which results into homogenous stabilized mass and increased vertical stresses (Åhnberg, 2007). During stabilization solidification process at the Port of Gävle, the first stabilized layer was placed approximately 90 days prior to the final layer. Because of three months interval of placement, layers placed earlier had probably gained enough strength (and presumably with large volume of locked water) to

resist further compression. Thus, preload weight applied after placement of the final layer had little or no compression effect on the first layers. In addition to that, at a certain period of curing, water may become lodged in between solid particles by cementation effect. This may result into pore blockage, preventing inflow or out flow of water; this may subsequently impede any development or dissipation of excess pore pressure (EPP) under applied load. The essence of EPP is to receive and gradually transfer the load into soil skeleton as water dissipates, giving enough time for soil particles to smoothly reorient and compact uniformly. In the absence or presence of disproportional EPP, the preloading weight may induce uneven jagged stress causing collapse of water voids. Consequently, layers with larger water voids become prone to compression on application of preloading weight. Thus, uneven effective vertical stress from preloading weight across the field, which ranged from 39kN/m^2 to 49kN/m^2 as evaluated from CPT data contributed to variations in stiffness across the field. For instance, compared to measured field settlement values, the computed settlement values from CPT points P1 and P11-01 (Figure 9), CPT points P4 and P11-02 (Figure 11) and CPT points P2 and P21-03 (Figure 12) suggest that, at these locations the SCDM fill was initially preloaded with weight lower than the presumed effective value of 10 kPa. According to Åhnberg *et al.* (2001), in order to avoid uneven quality in different sections of a stabilized area, it is important to apply preloading weight in a uniform manner, that is, the same height of the fill should be placed at the same time after stabilization in the entire working area.

Effect of curing temperature

The hydration process occurs immediately upon mixing cement with soil and other additives in the presence of water. The reaction results into hardened and aggregated soil particles (EuroSoilStab, 2002). This process is slow, proceeding from the surface of cement grains and the center may remain unhydrated. Furthermore, at low temperature (below 4°C) the process can be impaired considerably (Sherwood, 1993; Maher *et al.*, 2004). Therefore, the hydration process requires sufficient moisture at a favorable temperature to proceed. Underwater discharge assured sufficient moisture at minimum variation of temperature. However, the mixing and placement of SCDM at the Port of Gävle commenced in the end of October 2010 through the end of January 2011, during which, the average air temperature in Gävle may reach -5°C. Thus, the entire fill operation was carried out during unfavorable temperature for effective hydration reactions to proceed. This contributed to irregularity and variations in stiffness and strength along the entire depth of the SCDM fill. The CPT data revealed very soft layers at the bottom of the SCDM fill at CPT points P6 and P21. These layers were prone to compression upon application of preloading weight, this explains the reason for higher computed and measured magnitudes of settlement (Figure 10 and **Table 2**).

CONCLUSIONS

Verification of one-dimensional field settlement of stabilized contaminated sediments in finite element method (FEM) was presented. The finite element analysis in PLAXIS 2D software, utilized in-situ constrained modulus evaluated from CPT empirical correlations. The computed settlement values gave quite comparable results with measured ones. These findings conclude that, CPT data and CPT empirical correlations established for conventional soils can be utilized in stabilized soils as well.

With regard to trend and magnitude of settlement of the SCDM fill from the large-scale field test at the Port of Gävle, the following conclusions are drawn:

- Repeatability of CPT data in stabilized material was unlikely; thus, variations in computed magnitudes of settlement within the same field were inevitable.
- The representative stiffness for settlement computations of SCDM fill in structural backfill was achieved during 28 days of curing. However, several CPTs are required to give suitable representative of in-situ mechanical parameters in the SCDM fill.
- The mechanical parameters evaluated from the CPT data before the end of hydration reaction should be regarded as valid at that particular time and location of CPT point.
- As a result of mixing and placing the materials at very low temperature (below 4°C), inadequate hydration reactions occurred, this caused variations in stiffness and strength properties between layers along the entire depth.

ACKNOWLEDGEMENTS

The authors would like to acknowledge SMOCS (The Sustainable Management Of Contaminated Sediments) project, an EU funded project within the Baltic Sea regional program for period 2007 – 2013 for the useful data and contribution to the accomplishment of this work. SMOCS project leader Mr. Göran Holm at Swedish Geotechnical Institute is acknowledged for the analysis of field measurements and laboratory test results in addition to overall project management. Tech. Lic. Bo Svedberg is hereby recognized for coordination activities. Within the SMOCS frameworks, special thanks remain to the management of the Port of Gävle and in particular to Mr. Jonas Rahm and Ms. Linda Astner for facilitation of large-scale field test. Construction companies, WSP and PEAB are hereby appreciated for undertaking field operations including CPT testing and measuring field settlements.

REFERENCES

1. Abu-Farsakhi, M., Tumay, M., and Voyiadjis, G (2003) “Numerical Parametric Study of Piezocone Penetration Test in Clays”, *International Journal of Geomechanics*, Vol. 3, 170-181.
2. Brinkgreve, R.B.J, Swolfs, W.M and Engin, E. (2010) “PLAXIS 2D 2010 User Manual”, Plaxis bv. Deft, the Netherland. ISBN-13: 978-90-76016-08-5.
3. Chua, K.M. and Tenison, J. (2003) “Explaining the Hveem Stabilometer Test: Relating R-value, S-value and the Elastic Modulus,” Journal of Testing and Evaluation, Vol.31, No.4. Available online at: www.astm.org.
4. EuroSoilStab (2002) “Development of Design and Construction Methods to Stabilize Soft Organic Soils: Design Guide for soft soil stabilization:” CT97-0351, Project No. BE-96-3177, European Commission, Industrial and Materials Technologies Programme (Rite-EuRam III) Bryssel.
5. Fossenstrand, I. (2009) “Stabilisering och solidifiering av muddermassor i Gävle hamn”, MSc Thesis. Luleå University of Technology, Luleå, Sweden (In Swedish).
6. Houlsby, G.T. and Teh, C.I. (1991) “An analytical study of the Cone Penetration Test in Clay”, Géotechnique, Vol. 41, No. 1, 17-34.
7. Kulhawy, F.H. and Mayne, P.W. (1990) “Manual on Estimating Soil Properties for Foundation Design”, RePort EL-6800, Electric Power Research Inst., Palo alto, 308p.

8. Larsson, R. and Mulabdic, M. (1991) “Piezocone Tests in Clay”, Swedish Geotechnical Institute, Linköping. RePort 42. 240p.

9. Lunne, T., Andersen, H.K., Low, E.H., Randolph, F.M., and Sjursen, M (1986) “Guidelines for Offshore In-situ Testing and Interpretation in Deep water Soft Clays”, Canadian Geotechnical Journal. 48. 543-556.

10. Lunne, T., Robertson, P.K., and Powell, J.J.M. (1997) “Cone penetration testing in geotechnical practice”. Blackie Academic, EFSpon/Routledge; New York.

11. Maher, A., Bennert, T., Jafari, F., Douglas, W. and Gucunski S. N. (2004), “Geotechnical Properties of Stabilized Dredged Material from New York-New Jersey Harbor”, Journal of Transportation Research Board, In Geology and Properties of Earth Materials, 2004, 86-96.

12. Muir Wood, D. (1990) “Soil Behavior and Critical State Soil Mechanics”, Cambridge University Press. ISBN: 978-0-52-33249-1.

13. Robertson, P.K (2009) “Interpretation of Cone Penetration Tests-A Unified Approach”, Canadian Geotechnical Journal. 46. 1337-1355.

14. Sherwood, P (1993) “Soil Stabilization with Cement and Lime. State of the Art Review”. Transport Research Laboratory. HMSO. London.

15. SMOCS (2010) “Demonstration of the Stabilization and Solidification Technology in a Field Test at Port of Gävle, Sweden”. Available at http://smocs.eu/?page_id=5, retrieved [2012, 10, 30].

16. Swedish EPA (2001) “Swedish Environmental protection agency”, Dumping wastes at Sea SFS 2001:1063.

17. Åhnberg, H (2007) “On yield stresses and the influence of curing stresses on stress paths and strength measured in triaxial testing of stabilized soils”, Canadian Geotechnical Journal, Vol. 44: 54-66.

18. Åhnberg, H., Bengtsson, P.-E., and Holm, G (2001) “Effect of initial loading on the strength of stabilized peat”, *Proceeding of ICE-Ground improvement*, Vol. 5, 35-40.

Paper VII

Makusa, G.P., Mattsson, H., and Knusson, S. (2014). Shear strength evaluation of preloaded stabilized dredged sediments using CPT. *3rd International symposium on cone penetration testing, Las Vegas, Nevada, USA-2014*.

3rd International Symposium on Cone Penetration Testing, Las Vegas, Nevada, USA - 2014

Shear strength evaluation of preloaded stabilized dredged sediments using CPT

G.P. Makusa, H. Mattsson & S. Knutsson
Department of Civil, Environmental and N atural Resources Engineering, Luleå University of Technology, Luleå, Sweden.

ABSTRACT: The undrained shear strength of preloaded stabilized dredged sediments increases with curing time. Evaluation of in-situ undrained shear strength using cone penetration test (CPT) data normally requires calibration of the CPT data with known undrained shear strength from vane shear test to obtain the cone factor, which is normally utilized in CPT empirical correlation to estimate the undrained shear strength. In this study, a new CPT empirical correlation for evaluation of in-situ undrained shear strength is presented. The proposed empirical correlation utilizes the effective vertical stress characteristic ratio to estimate the CPT induced stress, which was correlated to the in-situ undrained shear stress. The undrained shear strength computed using the proposed empirical correlation agrees reasonably well with the undrained shear strength estimated using the established empirical correlation at a large-scale field test.

1 INTRODUCTION

Soft soil deposits have normally sufficient strength to support their own weight and other limited loadings. Shear stresses within the soil deposits, which are also subjected to their own weight, can be regarded as relatively low compared to the available shear strength to support self-weight and other loadings. It is well known that failure of soil will occur when the induced shear stress becomes larger than the available shear strength. According to researchers (e.g. Lunne et al., 1997; Robertson, 2009), the undrained shear strength s_u from cone penetration test (CPT) data can be estimated from

$$s_u = \left(q_t - \sigma_{v0}\right)/N_{kt} \qquad (1)$$

where q_t is the total cone resistance, σ_{v0} is the total vertical stress and N_{kt} is the tip cone factor. The tip cone factor N_{kt} is obtained by calibrating the CPT data with known undrained shear strength from vane shear test (Kulhawy and Mayne, 1990). According to Robertson (2009) the values of N_{kt} ranges between 10 and 20 with an average value of 14 for insensitive soils. However, in stabilized soft soils and sediments, the undrained shear strength increases as the curing process progresses, which may require repeated calibration of CPT data to obtain the new value for N_{kt} with curing time. This can be time consuming and costly.

The present work seeks to address the use of CPT induced stress to evaluate the undrained shear strength of a preloaded stabilized contaminated dredged material (SCDM) utilized as structural backfill at a large-scale field test at the Port of Gävle.

2 LARGE-SCALE FIELD TEST AT PORT OF GÄVLE

Contaminated dredged fine sediments at high initial water contents can be amended with binders for reuse in structural backfill. In order to assess the mechanical properties of in-situ stabilized dredged sediments, a large-scale field test was carried out at the Port of Gävle in Sweden (Holm et al., 2012; Makusa et al., 2012; Makusa, 2013). Mixing and backfill operations at the large-scale field test started at the end of October 2010 and continued through the end of December 2010. The dredged sediments at initial water content between 250% and 1000% were mixed with cement 40%, fly ash 40% and blast furnace slag (also known as GGBS) 20% using the on-site pugmill to produce stabilized contaminated dredged material (SCDM). The total amount of binders was 150 kg per cubic meter of freshly dredged sediments. The SCDM was discharged in a reclaimed area by using underwater tubes connected to the pugmill as shown in Figure 1. A total of about 8,000 m^3 of the SCDM was utilized in a reclaimed area as a structural backfill material. It is customary required to preload the stabilized mass immediately after mixing and placing in a designated area for curing. According to Holm et al. (2012), the application of preloading weight was delayed because the immediate strength of the SCDM was too low to support the preloading weight. Thus, the SCDM was preloaded with selected gravel on February 6, 2011 after gaining enough strength to support the first phase of preloading weight. For quality assurance and classification of soil behavior type, several cone penetration tests (CPT) were carried out after several days (d) of curing. For the purpose of this study, CPTs data from 16 test points at the large-scale field test were considered; the cone penetration tests were as follows: six tests were carried out on February 23, 2011 after about 17d of curing following the first day of preloading, four tests were carried out on April 15, 2011 after about 67d of curing, four tests were carried out on June 20, 2011 after about 135d of curing and two tests were carried out on October 4, 2011 after about 250d of curing under preloading weight.

The first phase of preloading utilized selected gravel of about 1.0 m height (equivalent to an average value of 18 kN/m^2) applied in 4 days consecutively, which was approximately equal to 4.5 kN/m^2/day. The second phase of preloading, which was carried out after about 28d (March 7-16, 2011) utilized the same selected gravel of about 1.5 m height (equivalent to an average value of 27 kN/m^2) applied in 9 days consecutively, which was equivalent to 3.0 kN/m^2/day. No significant excess pore pressure was recorded during the period of preloading (Holm et al., 2012). This study, evaluates the undrained shear strength of the SCDM utilizing vertical stress characteristic ratio.

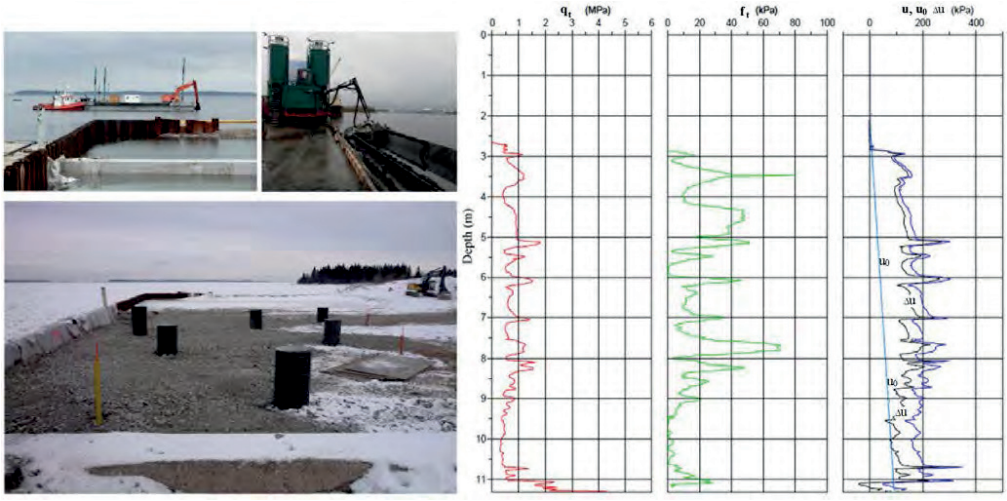

Figure 1. Stabilization of contaminated dredged sediments for use as structural backfill material (Makusa, 2013).

3 INITIAL VERTICAL STRESS AND STRESS CHARACTERISTICS

3.1 *Initial vertical stress*

Vertical stresses in a soil deposit can be described in terms of total vertical stress and effective vertical stress. Conventionally, initial effective vertical stress σ'_{v0} is normally given by

$$\sigma'_{v0} = \sigma_{v0} - u_0 \tag{2}$$

where u_0 is the hydrostatic pore water pressure (Terzaghi et al. 1996).

3.2 *Initial stress characteristics*

According to Lunne et al (1997), the compression index C_c can be given by

$$C_c = \frac{2.3(1+e_0)\sigma'_{v0}}{M} \tag{3}$$

where e_0 is the initial void ratio and M is the constrained modulus. By rearranging Eq. (3), the compression ratio C_r can be obtained from

$$\frac{C_c}{1+e_0} = \frac{2.3\sigma'_{v0}}{M} = C_r \tag{4}$$

Thus, by Eq. (4), the initial effective vertical stress and compression ratio are interrelated by

$$2.3\sigma'_{v0} = MC_r \tag{5}$$

The expression above was hereby referred to as effective vertical stress-characteristics. The term to the left side of Eq. (5) contains no void ratio, which means that there is also a link to the total vertical stress-characteristic (e.g. for soil above the phreatic surface where, the total vertical stress is normally regarded as equal to the effective vertical stress). As a result, Eq. (5) can also be written in terms of total vertical stress-characteristic in form of

$$2.3\sigma'_{v0} = k_0\sigma_{v0} \tag{6}$$

where k_0 is the effective vertical stress-characteristic ratio given by $k_0 = 2.3\sigma'_{v0}/\sigma_{v0}$. The value of k_0 depends on the unit weight of the soil and not on the depth of the deposit. For soils below the phreatic surface, the value of k_0 can be utilized to estimate the initial effective vertical stress using hydrostatic pore water pressure as described below.

3.3 *Initial effective vertical stress in terms of stress characteristic ratio*

By Eq. (2) and Eq. (6) the initial effective vertical stress can be estimated from

$$\sigma'_{v0} = k_0 u_0 / (2.3 - k_0) \tag{7}$$

Consequently, by Eq. (7), the effective vertical stress induced by cone penetration and the undrained shear strength can be estimated as discussed hereafter.

4 ESTIMATING INDUCED EFFECTIVE VERTICAL STRESS

During a cone penetration test (CPT), shear stress is induced in the soil as the cone advances. The induced shear stress results in failure of the surrounding soil. The resistance of the soil to the CPT penetration is

normally recorded at the tip of the cone and reported as total cone resistance q_t. Thus, the CPT measures the total vertical stress. By Eq. (7) the initial effective vertical stress was estimated using hydrostatic pore water pressure u_0 and the effective vertical stress-characteristic ratio k_0; it follows by intuition that the increase in effective vertical stress due to applied CPT pressure will also be influenced by k_0 in a similar way as hydrostatic pore pressure u_0. Consequently, resistance of CPT to penetration will be affected by k_0 as well such that, for the cone to advance, the increased effective vertical stress must overcome the initial effective vertical stress given by Eq. (7) at a controlled rate of penetration. As a result, the effective vertical stress induced by CPT to overcome the initial effective vertical stress and result in failure of the stabilized mass was empirically given by

$$\sigma'_{CPT} = k_0 \left(q_t - u_0\right)/\left(2.3 - k_0\right) \tag{8}$$

The CPT induced stress was found to be proportional to the undrained shear strength of preloaded stabilized contaminated dredged material (SCDM). Consequently, in this study the undrained shear strength s_u of the SCDM at the large-scale field test was estimated using

$$s_u = 0.1\sigma'_{CPT} \tag{9}$$

where 0.1 is a proportionality constant. Notice that the value of the constant is equal to the penetration length. According to Sandven (2010) for sampling interval of 20 mm and 50 mm, the penetration length is equal to 0.1 m and 0.2 m, respectively. The sampling interval of 20 mm was utilized during the cone penetration tests at the large-scale field test at the Port of Gävle. In this study, the undrained shear strength from the large-scale field test obtained from Eq. (1) were compared with those obtained using the proposed CPT empirical correlation presented by Eq. (9).

5 RESULTS

Figure 2 presents the effect of curing period on the average effective vertical stress-characteristic ratio k_0, CPT induced vertical stress σ'_{CPT}, tip cone factor N_{kt} obtained by calibrating the CPT data using estimated undrained shear strength from Eq. (9) and the undrained shear strength s_u of the SCDM at the large-scale field test at Port of Gävle. Figure 3 shows comparison for undrained shear strength evaluated using Eq. (1) with N_{kt} of 17 relative to Eq. (9) versus depth.

6 DISCUSSION

The influence of curing period on the strength of stabilized contaminated dredged material (SCDM) was presented. Results of the study show that the effective vertical stress characteristic ratio k_0 increased with curing time as shown in Figure 2(a). As a result of increase in k_0, the CPT induced stress also increased as it can be seen in Figure 2(b). Calibration of the CPT data to obtain N_{kt} for Eq. (1) using the undrained shear strength obtained from Eq. (9) indicated that the value of tip cone factor N_{kt} decreased from 24.8 at the time of preloading to 14.5 after about 250 days of curing as presented by Figure 2(c). According to Göran Holm (personal communication, May 16, 2013), a value of N_{kt} equal to 17 was utilized to evaluate the undrained shear strength s_u at the large-scale field test. Figure 2(d) shows that the undrained shear strength, which were obtained by Eq. (1) using N_{kt} = 17, and Eq. (9) were found to be within the same range and trend of increase except for the values at the time of preloading (0d). Authors postulate the discrepancies between the average values of undrained shear strength obtained by Eq. (1) relative to Eq. (9) that can be seen in Figure 2(d) could probably be due to the use of a constant value of N_{kt} of 17 in Eq. (1) compared to the use of the value of k_0 in Eq. (9). Nonetheless, Figure 3 shows reasonable agreement for evaluated undrained shear strength versus depth beyond 0d of curing.

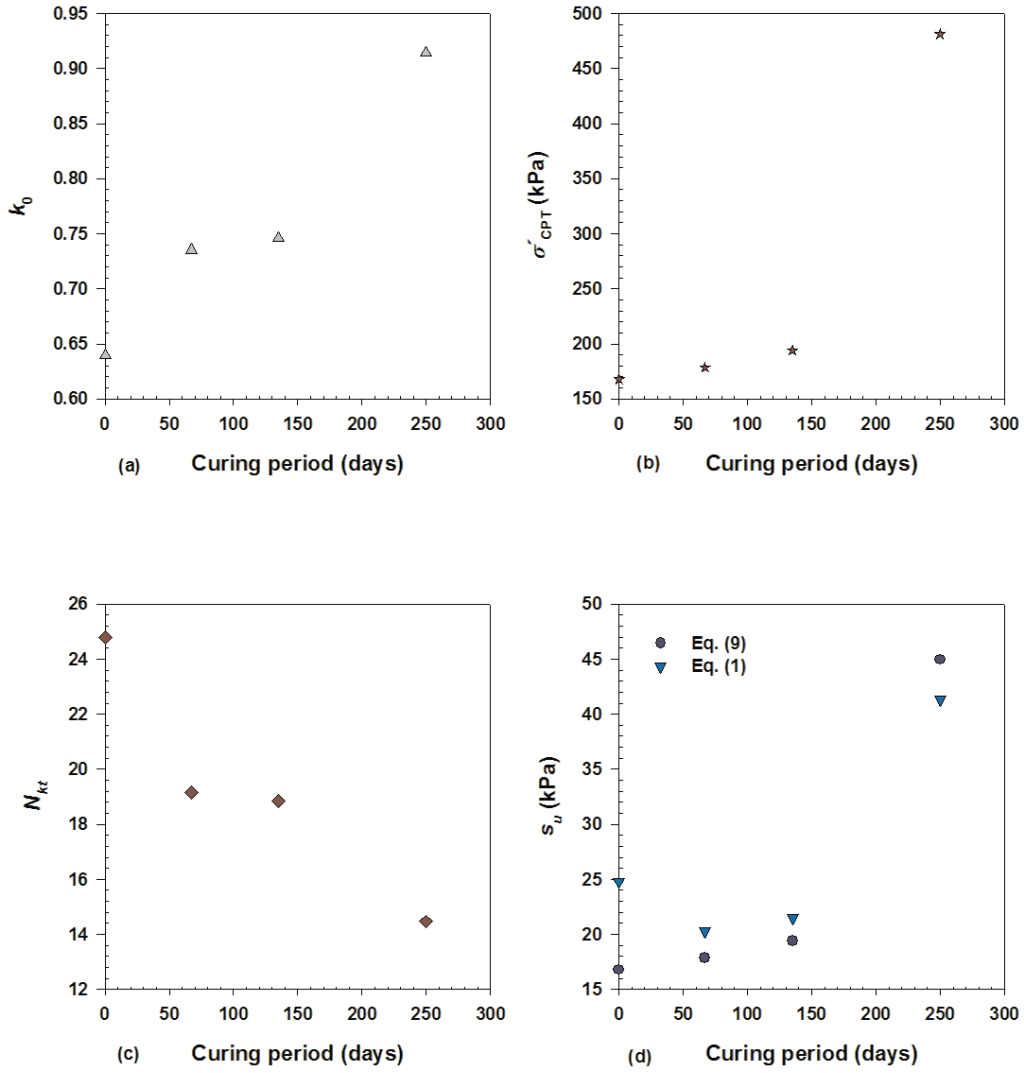

Figure 2. Effect of curing period on (a) effective vertical stress-characteristic ratio k_0 (b) CPT induced stress σ'_{CPT} (c) tip cone factor N_{kt} (d) undrained shear strength s_u evaluated with N_{kt} factor of 17 in Eq. (1) relative to Eq.(9).

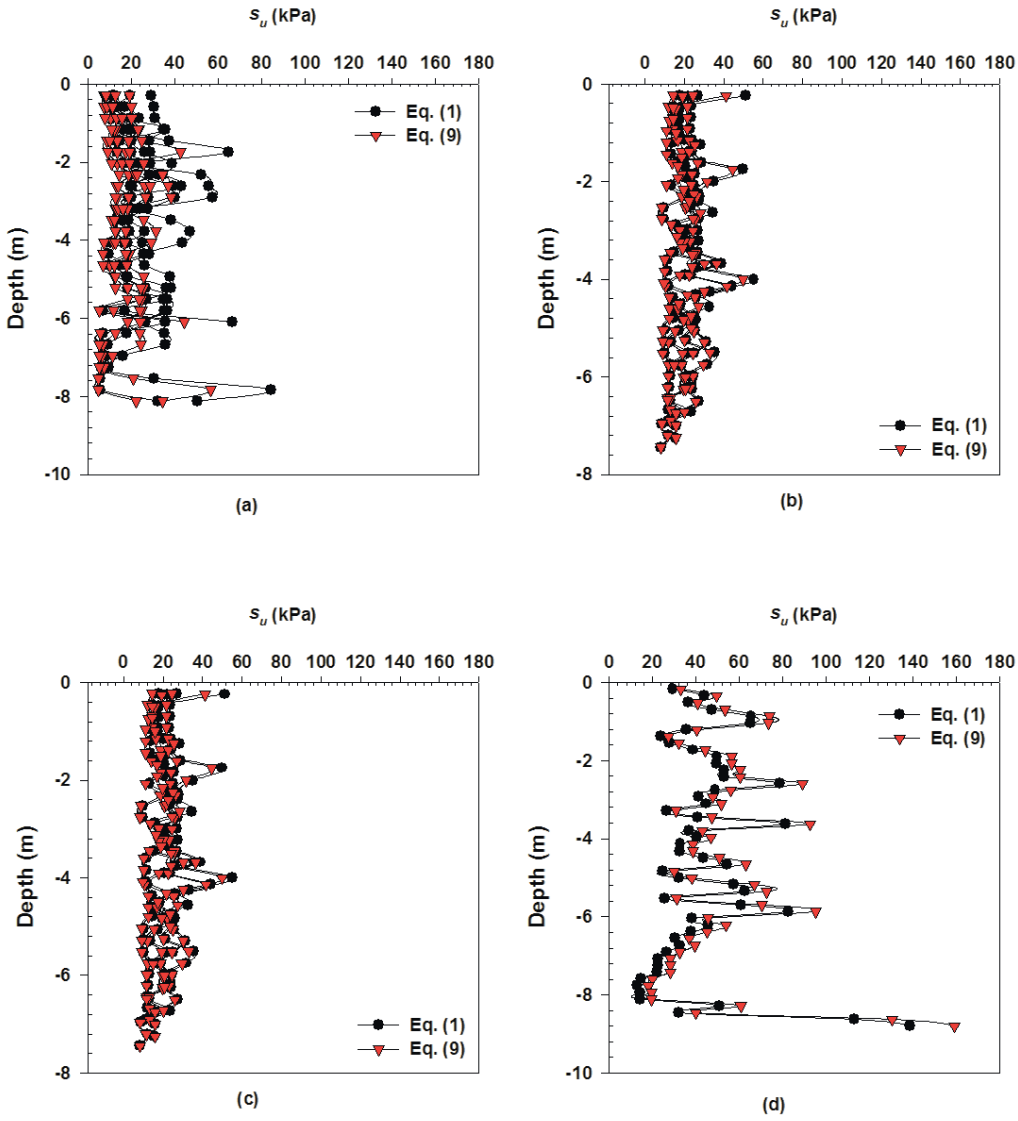

Figure 3. Evaluated undrained shear strength versus depth at the large-scale field test (a) at the time of preloading (b) after 67 days of curing (c) after 135 days of curing (d) after 250 days of curing (Eq.(1) used $N_{kt} = 17$).

7 CONCLUSIONS

Evaluation of undrained shear strength of preloaded stabilized contaminated dredged material (SCDM) using cone penetration test (CPT) data was presented. Based on the findings of this study, the following concluding remarks were drawn:

- The stress characteristic ratio k_0 is indeed a parameter representing in-situ strength.
- The induced shear stress due to CPT can be utilized to estimate the undrained shear strength of preloaded stabilized material with reasonable accuracy during the period of curing without the need for repeated calibration of the CPT data.

ACKNOWLEDGEMENT

The author would like to acknowledge sustainable management of contaminated sediments (SMOCS) project and EU Baltic Sea region programme for financial support along with the Port of Gävle in collaboration with Luleå University of Technology and Swedish Geotechnical Institute (SGI). Special acknowledgments remain to Mr. Jonas Rahm and Ms. Linda Astner at the Port of Gävle, as well as, all participants in the SMOCS project, especially, Mr. Göran Holm and Tekn. Lic. Bo Svedberg for continuous support and encouragement. Mr. Per-Evert Bengstsson at SGI is hereby acknowledged for valuable assistance with all field data from the large-scale field test. In addition, we would like to recognize the work done by the consultancy company WSP and construction company PEAB for undertaking the large-scale field operations including in-situ tests.

REFERENCES

Holm, G., Bengtsson, P. and Larsson, L. (2012). *Field test at Port of Gävle*, Sweden. Linköping: Swedish Geotechnical Institute.

Kulhawy, F.H. and Mayne, P.W. (1990). *Manual on estimating soil properties for foundation design*. Palo Alto: Electrical Power Research Inst.

Lunne, T., Robertson, P.K., and Powell, J.J.M. (1997). *Cone penetration testing in geotechnical practice*. New York: Blackie Academic, EF Spon/Routledge.

Makusa, G. (2013). *Mechanical properties of stabilized dredged sediments for sustainable geotechnical structures*. Luleå, Sweden: Luleå University of Technology.

Makusa, G.P., Mattsson, H., and Knutsson, S. (2012). Verification of field settlement of in-situ stabilized dredged sediments using cone penetration test data. *Electronic journal of Geotechnical Engineering*, 17/Y, 3365-3680.

Robertson, P. (2009). Interpretation of cone penetration tests - a unified approach. *Canadian Geotechnical Journal*, Vol. 46(11), 1337-1355.

Sandven, R. (2010). Influence of test procedures on obtained accuracy in CPTU. *Proc. 2nd Int. Symp. on Cone Penetration Testing*, . Huntington Beach, CA: Int. Society for Soil Mechanics and Geotechnical Engineering.

Terzaghi, K., Peck, R.B. and Mesri, G. (1996). *Soil mechanics in engineering practise* (3rd ed.). New York: John Wiley and Sons.